Wavelet analysis in the field of coastal engineering

Applications in time-series analysis

T.J.P. de Rooij

Delft University of Technology, Deltares

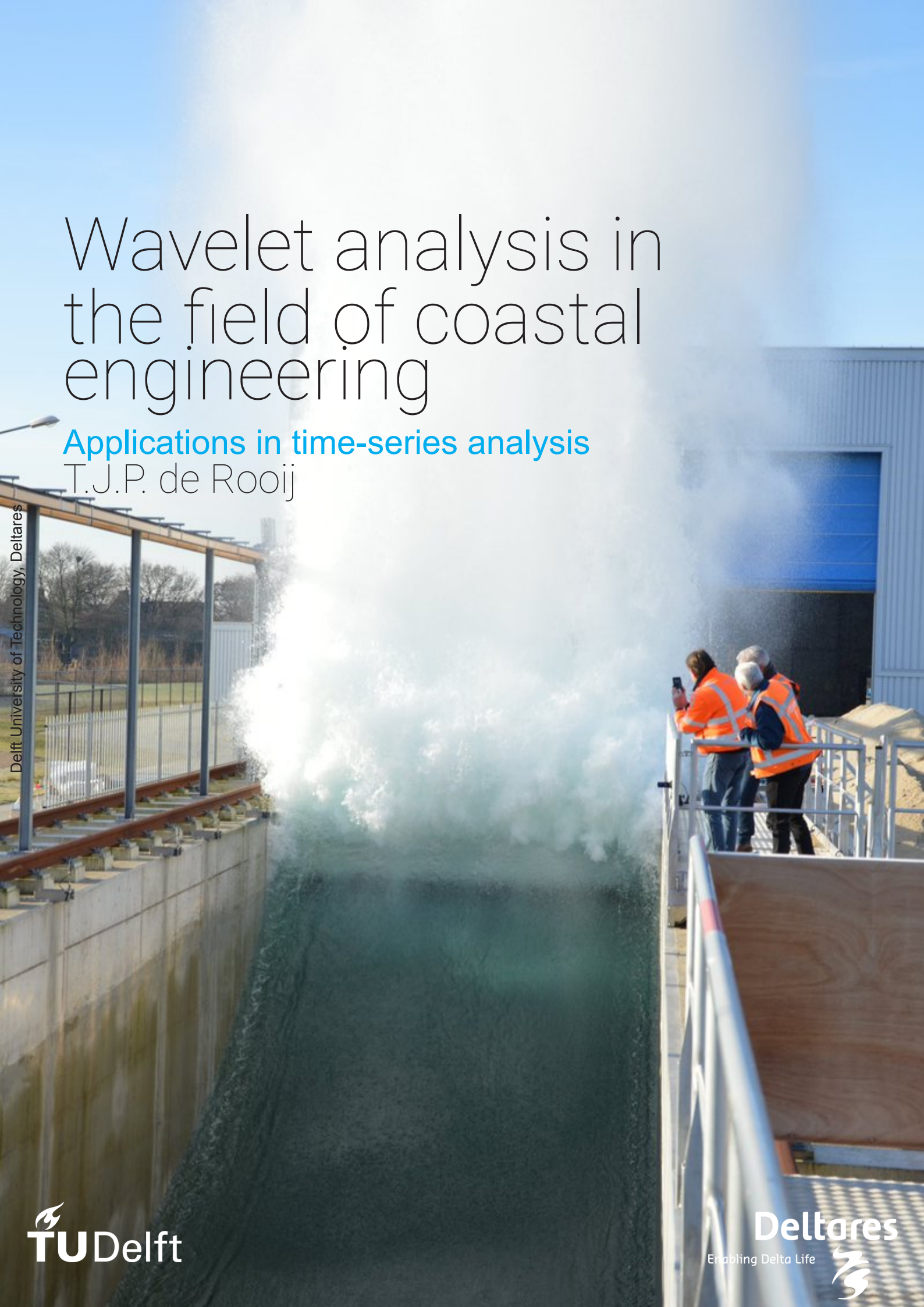

TU Delft

Deltares
Enabling Delta Life

Wavelet analysis in the field of coastal engineering

Applications in time-series analysis

by

T.J.P. de Rooij

A master thesis submitted in partial fulfilment
of the requirements for the degree of

Master of Science

in Applied Mathematics
at the Delft University of Technology,
to be defended publicly on Monday October 30, 2017 at 16:15.

Student number	4077903
Specialisation	Computational Science and Engineering
Project duration	February 1, 2017 – October 31, 2017

Thesis committee	Prof. dr. ir. C. Vuik,	TU Delft, Professor of Numerical Analysis, supervisor
	Prof. dr. ir. A.W. Heemink	TU Delft, Professor of Mathematical Physics
	Ir. J. Kramer,	Deltares, dep. of Coastal Structures and Waves, supervisor
	Ir. A. Capel,	Deltares, dep. of Coastal Structures and Waves

An electronic version of this thesis is available at *http://repository.tudelft.nl/*

TU Delft Delft University of Technology

Deltares Enabling Delta Life

Abstract

Time-frequency analysis and digital signal processing are important tools in the field of coastal engineering. Both can be done using techniques like Fourier or wavelet analysis, however, analysts from this field experience a threshold to use wavelet analysis instead of their current methods, often Fourier-based. This is due to the lack of guidelines in the many choices accompanied by applying wavelets [29]. This thesis investigates the added value of wavelet analysis in the field of coastal engineering. There are two wavelet transform types: continuous and discrete. The first one is most often used for time-frequency analysis. The range of signals that can be analysed more accurately has been increased by adding different signal extension methods and a method to quantify the effect of missing data points, based on the wavelets energy distribution. This allows a more accurate time-frequency analysis of time-series that cannot be assessed in the Fourier domain. The continuous wavelet coefficients can also be used for separating incident and reflected waves. Because the wave number of a wave is dependent on its frequency, the wavelet-based method performs equally well or worse for stationary signals than the current Fourier coefficient based method [38, 63]. For coastal engineering time-series with a changing mean water level, the time-dependency of the wavelet transform results in better separation than the Fourier coefficient based case. The discrete wavelet transform is mostly deployed in digital signal processing. Filtering in the discrete wavelet domain allows for better justification of the filtering of different signal elements such as noise and transients for signals that behave non-stationary, like measurements of impacts. The difference with the standard time or frequency domain methods lies within this justification, instead of a 'gut feeling' often used. Different algorithms to determine thresholds for use in noise filters have been tested. The soft applied universal threshold was the most effective of the compared algorithms in filtering noise from a non-stationary signal. In stationary signal cases, the low-pass filter showed better performance. The discrete wavelet decomposition offers many signal processing opportunities due to the wide range of wavelets that can be chosen.

Preface

This thesis explores the applications of wavelet analysis in the field of coastal engineering. Coastal engineering is a branch of civil engineering, mostly concerned with the challenges of building in coastal areas. The subject of this thesis was commissioned by Deltares[1], an independent research institute for applied research in the field of water and subsurface. The main areas of expertise of this institute are flood risk, delta planning, infrastructure, environment, and water and subsoil resources. Deltares has a large number of experimental facilities which allow them to do scaled and full-scale experiments. The department of Coastal Structures and Waves, concerned with the effects of waves on coastal structures, has supervised me during the research. They conduct a lot of experiments to quantify the effects of waves on structures, by using various measurement techniques among other a point measurements resulting in time series of a particular quantity, e.g. surface elevation.

In coastal engineering in general and at Deltares in specific most time-series are analysed using the Fourier transform, to investigate frequency behaviour. Wavelet analysis is a time-frequency analysis, which adds the notion of time to frequency analysis. Instead of studying only time or frequency behaviour, the coupling of the two can be studied as well. This characteristic allows the analysis and processing of non-stationary signals, where Fourier analysis in theory is only applicable to stationary signals. This thesis explores, improves and applies the two different branches of wavelet analysis, i.e. continuous and discrete, to many coastal engineering challenges.

The three main subjects of this thesis are the expansion of the use of the wavelet power spectrum to common coastal engineering time-series, the application of wavelet coefficients in separating waves and the application of discrete wavelet filters to coastal engineering experimental signals. The added value of wavelet analysis lies in the addition of the notion of time. Non-stationary time-series are best analysed using wavelet analysis, although this is mostly qualitative and not quantitative. Problems like missing data points can be analysed with a certain reliability in the wavelet domain, which is not possible in the frequency domain. The separation of waves based on wavelet coefficients is much more effective in non-stationary wave situations than the Fourier-based method. Filtering in the discrete wavelet domain has many advantages concerning non-stationary time-series as well. However, in coastal engineering, these are sometimes hard to exploit due to the wide range of scales in the time-series.

The thesis committee consists of four members. Prof.dr.ir. C. Vuik, professor of numerical analysis and also my daily supervisor, and prof.dr.ir. A.W. Heemink, professor of mathematical physics, are both from the department of Applied Mathematics at the Delft University of Technology. Ir. J. Kramer is a project engineer in the department of Coastal Structures and Waves at Deltares and ir. A. Capel is a senior advisor and researcher in that same department. Both conduct a lot of experiments in the Deltares facilities.

Acknowledgements

First I would like to thank Jan and Alex for the research proposal and their supervision during this project. They were always willing to help and shine their light on challenges or results. The same holds for my daily supervisor, Kees, whom I have visited approximately twice a month to discuss my progress. He never let the mathematical background go out of sight.

Working at Deltares meant being surrounded by a lot of experts from the field, special thanks to Martijn and Tim, who have delivered much input for my research. Next to experts, there are also a lot of students from the field doing an internship or graduation project at Deltares. Thanks to all of you (Anne, Ana, Bas, Cleo, Kamilla, Marlies, Menno, Jelmer, Menno, Tim, Tim, Toon and the others) for the nice coffee (tea) breaks and lunches in the sun (if it wasn't raining and the temperatures were okay). Also, thanks for the advise, tips and explanations regarding coastal engineering processes and jargon. And of course, I thank my parents, sisters and friends for their support during this project. At last special thanks to my housemate Stella, who was often there to distract me from my thesis so that I could distract her from hers.

T.J.P. de Rooij
Delft, October 20, 2017

[1] *https://www.deltares.nl/*

Contents

List of Tables

List of Figures

Abbreviations, symbols and maths

List of abbreviations

Abbreviation	Definition	Explanation
CFT	Continuous Fourier Transform	Section 2.2.1
CWT	Continuous Wavelet Transform	Section 2.3.1
COI	Cone of Influence	Page 28
DCWT	Discretised Continuous Wavelet Transform	Equation 2.22
DFT	Discrete Fourier Transform	Section 2.2.2
DTFT	Discrete Time Fourier Transform	Section 2.2.2
DTWT	Discrete Time Wavelet Transform	Equation 2.21
DSP	Digital Signal Processing	Page 19
DWD	Discrete Wavelet Decomposition	Page 11
DWT	Discrete Wavelet Transform	Page 11
ESD	Energy Spectral Density	Equation 2.27
FA	Fourier Analysis	Section 2.2
FFT	Fast Fourier Transform	Page 8
flop	Floating Point OPeration	Section 5.3
FT	Fourier Transform	Section 2.2.1
FWT	Fast Wavelet Transform	Section 2.3.2
GWN	Gaussian White Noise	Section 2.5
GWS	Global Wavelet Spectrum	Section 2.4.2
ICWT	Inverse Continuous Wavelet Transform	Section 2.3.1
IDWT	Inverse Discrete Wavelet Transform	Section 2.3.2
IFFT	Inverse Fast Fourier Transform	Section 2.2.3
ISTFT	Inverse Short-term Fourier Transform	Section 2.2.3
MAD	Median of Absolute Deviation	Page 12
MRA	Multi Resolution Analysis	Appendix B
NaN	Not any Number	
PDS	Power density spectrum	Equation 2.28
PSR	Peak-to-Sum Ratio	Equation 4.1
RGWS	Rectified Global Wavelet Spectrum	Equation 2.30
RWPS	Rectified Wavelet Power Spectrum	Equation 2.29
RMSE	Root Mean Square Error	Equation 2
SAWP	Scale Averaged Wavelet Power	Section 2.4.2
SNR	Signal-to-Noise Ratio	Equation 2.36
std	Standard deviation	Equation 4
STFT	Short-term Fourier Transform	Equation 2.17
VDS	Variance density spectrum	Equation 2.28
WA	Wavelet Analysis	Section 2.3
WC	Wavelet Coherence	Section 2.4.5
WFT	Windowed Fourier Transform	Section 2.2.3
WPS	Wavelet Power Spectrum	Equation 2.29
XWT	Cross-Wavelet Transform	Section 2.4.4
ZOI	Zones of Influence	Section 3.1.4

List of symbols

Symbol	Explanation
Capital	Fourier or Wavelet Transform of signal, e.g. $X(\omega)$, $X(a,b)$
Bold	A vector, e.g. $\boldsymbol{x} = \{x_j\}_{j=0,\ldots,N-1}$
a	Scale parameter in continuous wavelet domain
a_i	i^{th} level of approximation coefficients (Discrete Wavelet Transform)
A	Set of scales for the DCWT
b	Translation parameter in continuous wavelet domain
$C_{a,j}$	Separation coefficient at scale a and gauge j
d_i	i^{th} level of detail coefficients (Discrete Wavelet Transform)
dB	Decibel: $10\log_{10}(\cdot)$
f	Frequency variable $\left[\text{Hz} = \text{s}^{-1}\right]$
f_s	Sampling frequency [Hz]
f_N	Nyquist frequency [Hz], i.e. $f_N = f_s/2$
f_ψ	Wavelets centre frequency [Hz], $f_\psi = 1/\lambda_\psi$
g	Gravitational acceleration parameter $\left[\text{m/s}^2\right]$, 9.81 m/s^2 on earth
h	Water depth parameter [m]
$H(x)$	Heaviside Step function, see equation 13
i	$i^2 = -1$, imaginary unit
k	Wave number [rad/m], see Section D.1
N	Length of discrete signal
m	Unit for meters
rad	radians
t	Time variable [s]
s	Unit for seconds
S	Sparsity based on PSR
$S()$	Smoothing operator
$S^f_{xx}(\omega)$	Energy spectral density (ESD) of $x(t)$ [$\cdot^2$/Hz]
$S^w_{xx}(a,b)$	Rectified wavelet power spectrum (RWPS) of $x(t)$
w	Wavelet coefficient in discrete wavelet domain
$W(a,b)$	Wavelet coefficient in continuous wavelet domain
W^{xy}	Cross-wavelet transform (XWT) of signals x and y
$x(t)$	Signal function in continuous time
$x[n]$	Signal function in discrete time
Z	Complex waveform
$\delta(x)$	Delta Dirac function, see equation 11
δ_{ij}	Kronecker delta function, see equation 12
γ^2_{xy}	Coherence between signal x and y, see equation 2.33
Δt	Sampling interval [s]
Δx	Spacing difference [m]
ϵ	Residual
$\zeta(t)$	Analytic wave function, i.e. $\text{Re}(\zeta(t)) = \eta(t)$
$\eta(t)$	Real wave function
$\theta(t)$	Phase, can be function or constant [rad]
θ_{xy}	Phase difference between signal x and y (see Section 2.4.3)
$\kappa(t)$	Scale Averaged Wavelet Power, SAWP
λ	Wave length [m]
λ_ψ	Equivalent wavelength of wavelet [s], $\lambda_\psi = 1/f_\psi$; linear relationship scale a: $\lambda_{\psi_a} = a\lambda_\psi$
μ	Mean
σ	Standard deviation
σ^2	Variance
$\phi(t)$	Refinable function
$\psi(t)$	Wavelet
$\psi_{ab}(t)$	Continuous wavelet at scale a, with translation b

Symbol	Explanation
τ_a	e-folding time of a wavelet, see Section 3.1.3
ω	Radial frequency variable [rad/sec], $\omega = 2\pi f$
Ω	Sum of weighting factors

Mathematics

Complex Numbers

The imaginary number i is defined as $i^2 = -1$. A complex number $z = x + iy$ consists of a real part $\mathrm{Re}(z) = x$ and an imaginary part $\mathrm{Im}(z) = y$. The modulus of this complex number z is defined by $|z| = \sqrt{x^2 + y^2}$ and the argument $\theta = \arg(z)$ by

$$\arg(z) = \arctan\left(\frac{\mathrm{Im}(z)}{\mathrm{Re}(z)}\right). \tag{1}$$

Complex number can be written in polar form as $z = |z|e^{i\theta}$. The complex conjugate of a complex number is defined as $z^* = \mathrm{Re}(z) - i\mathrm{Im}(z) = |z|e^{-i\theta}$.

Mathematical operators

Operator	Operation
$(\cdot)^*$	Complex conjugate
$\langle x_1, x_2 \rangle$	Inner product operation $\int_{-\infty}^{\infty} x_1(t)(x_2(t))^* \ \mathrm{d}t$
$*$	Convolution
$\circledast$	Circular convolution
$\arg(\cdot)$	Argument function
$\tilde{\cdot}$	Estimator of $(\cdot)$
$\bar{\cdot}$	Mean value; $\overline{x} = \frac{1}{N}\sum_{j=0}^{N-1} x_j$
$\mathrm{Re}(\cdot)$	Real part of $\cdot$
$\mathrm{Im}(\cdot)$	Imaginary part of $\cdot$
$\mathcal{F}\{\cdot\}(\omega)$	Continuous Fourier Transform
$\mathcal{F}^{-1}\{\cdot\}(t)$	Inverse Continuous Fourier Transform
$\mathcal{G}\{\cdot\}(\omega)$	Windowed Fourier Transform
$\mathcal{O}(\cdot)$	Landau's $\mathcal{O}$-symbol
$\mathcal{W}\{\cdot\}(a,b)$	Continuous Wavelet Transform
$\mathcal{W}^{-1}\{\cdot\}(t)$	Inverse Continuous Wavelet Transform

Functions

Root Mean Square Error

The root mean square error (RMSE) of two vectors discrete signals $x[n]$ and $y[n]$ is defined as

$$\sqrt{\frac{1}{N}\sum_{n=0}^{N-1}(x[n] - y[n])^2}. \tag{2}$$

Expected Value

$$\mathrm{E}[x] = \lim_{N\to\infty}\frac{1}{N}\sum_{i=1}^{N} x_i \tag{3}$$

Variance

$$\mathrm{Var}(x) = \sigma^2 = \mathrm{E}\left[(x - \mathrm{E}[x])^2\right] = \mathrm{E}\left[x^2\right] - \mathrm{E}[x]^2 \tag{4}$$

Median of Absolute Deviation (MAD)

The *median of absolute deviation* (MAD) of a time-series $x[n]$ is defined as the median of the time-series $|x[n] - \mathrm{E}[x]|$.

Convolution

The convolution of two signals $x(t)$, $y(t)$ is defined by

$$(x * y)(t) := \int_{-\infty}^{\infty} x(\tau)y(t-\tau)\,\mathrm{d}\tau = \int_{-\infty}^{\infty} x(t-\tau)y(\tau)\,\mathrm{d}\tau = (y * x)(t). \tag{5}$$

It is important to note that the convolution of two signals in the time domain is equivalent to the multiplication of their transforms in the frequency domain [42]. This is known as the *convolution property*:

$$\mathcal{F}(x * y)(\omega) = X(\omega) \cdot Y(\omega). \tag{6}$$

The (discrete) convolution of two discrete time signals $x[n]$ and $y[n]$ (assume both length N) is given by:

$$(x * y)[n] = \sum_{k=-\infty}^{\infty} x[k]\,y[n-k], \qquad \text{for } 0 \leq n < N. \tag{7}$$

To compute the discrete convolution, information from $x[n]$, $n \geq N$ is needed, but the signal does not exist there. The *circular convolution* considers these two signals as periodic, such that $x[N] = x[0]$, $x[N+1] = x[1]$ etc. The computation (7) is abbreviated to

$$(x \circledast y)[n] = \sum_{k=0}^{N-1} x[k]\,y[n-k], \tag{8}$$

where the $\circledast$ denotes the *circular* or *cyclic* convolution.

Cross Correlation

The *cross correlation* of two complex signals $x(t)$ and $y(t)$ is defined by [20]

$$(x \star y)(t) := \int_{-\infty}^{\infty} x(\tau)^* \cdot y(t+\tau)\,\mathrm{d}\tau = x(-t)^* * y(t). \tag{9}$$

The *auto correlation* of a function $x(t)$ is the cross correlation of this function with itself; $(x \star x)(t)$.

In the Fourier domain the cross correlation satisfies $\mathcal{F}\{x \star y\}(\omega) = X(\omega)^* \cdot Y(\omega)$. The autocorrelation thus satisfies $\mathcal{F}\{x \star x\}(\omega) = X(\omega)^* \cdot X(\omega) = |X(\omega)|^2$.
In statistics the autocorrelation expressed as the expected value of two signals, i.e.

$$\mathrm{E}[x(t_1)x(t_2)]. \tag{10}$$

Delta Dirac function

The Delta (Dirac) function is a theoretical function with a support reduced to $t = 0$, but with an integral of 1. This theoretical function simplifies computations, leaving convergence issues aside [37]. The Delta function $\delta(t)$ associates any continuous function $f(t)$ to its value at $t = 0$:

$$\int_{-\infty}^{\infty} \delta(t - t_0) f(t)\,\mathrm{d}t = f(t_0). \tag{11}$$

Note that by this property that

$$f(t) * \delta(t) = f(t).$$

The Kronecker delta function is the discrete counterpart of the Delta Dirac function. It is defined by:

$$\delta_{ij} = \begin{cases} 1 & \text{if } i = j \\ 0 & \text{elsewhere} \end{cases}. \tag{12}$$

Heaviside Step function

$$H(x) = \begin{cases} 0 & x < 0 \\ 1/2 & x = 0 \\ 1 & x > 0 \end{cases} \tag{13}$$

1 Introduction

Time-frequency analysis is the study of the behaviour of signals in the time-frequency space. Knowledge of this behaviour allows researchers to characterise it and filter unwanted elements. Time-frequency analysis was introduced in 1946 by Dennis Gabor. He came up with the idea to place a window over the signal and apply the Fourier transform to the windowed signal, to provide insight into the time-frequency behaviour of a signal [18]. Fourier analysis, along with its transform, was introduced in the early 1800's, which allowed the study of signals in the frequency domain. From the 1960's researchers from different disciplines started to adjust the window that was introduced by Gabor, by changing its size depending on the frequency of interest. Meyer[1], Daubechies and Mallat unified this work in the mid-eighties, marking the birth of wavelet analysis [13, 36].

Wavelet analysis has strong similarities with Fourier analysis. The advantage of wavelet analysis over Fourier analysis is that there is not one base as in Fourier analysis (i.e. a base sines and cosines), but there are many bases to choose from, called wavelets, hence the name wavelet analysis [29, 30, 57]. This offers a broader range of applications, and therefore wavelet analysis is adopted in many different fields, such as electrical engineering, ecology, finance, etc. [2, 9, 42]. In civil engineering, the wavelet transform became more and more popular since the turn of the century. However, guidelines are missing for the application of wavelet analysis in different fields of civil engineering [29]. One such field is the field of coastal engineering.

Bosboom and Stive [7, p.1], experts from the field, describe coastal engineering as: "[...] the branch of civil engineering concerned with the planning, design, construction and maintenance of works in the coastal zone." These works are divided into soft and hard measures. Soft measures make use of natural coastal material, such as beach nourishments, while hard measures consist of man-made structures, for instance, breakwaters. The purposes of these measures are plentiful: from the development of harbours to the control of shoreline erosion. The most important ones are defence structures against floodings [7]. These floodings can be caused by natural effects such as storms, tides and tsunamis. Above all the long-term sea-level rise is a thread for low-lying areas all over the world. Thus coastal engineering deals with relevant social-economic problems.

In the field of coastal engineering different kinds of signals are investigated, e.g. pressures, forces and elevations. These signals are always digital, i.e. they are sampled with a certain frequency and stored on a computer. These signals can be the result of experiments on (scaled) hard measures, such as collected in the facilities at Deltares. Furthermore, they can be the result of in situ measurements or simulations of both soft and hard measures [15, 34]. This results in a wide variety of challenges: ranging from time-frequency analysis for measurements with missing data points to filtering pressure sensor measurement data plagued by noise. The filtering of (digital) signals is one of many components of digital signal processing. Digital signal processing is the application of a wide variety of signal processing operations by digital means, for instance, a computer [46]. Time-series concerning hard measures often have some unique characteristics, such as large amplitude differences in a short amount of time, that are a better fit to analyse and process using wavelet analysis than current methods. Wavelets are not applied much in the area of coastal engineering. The abundance of choices in wavelet analysis, such as a choice of base, creates a threshold to apply it in this field. Guidelines regarding the use of wavelet analysis in the field of coastal engineering are needed, to decrease this experienced threshold.

[1] This years Abel Prize is appointed to Yves Meyer for his work in wavelet analysis [5].

1.1. Research

The goal of this thesis is to derive guidelines for practical applications of wavelet analysis in the field of coastal engineering. Application of these guidelines by coastal engineers could contribute in the knowledge to cope with the unique characteristics of signals seen in the field of coastal engineering and thus could assist in the future creation of coastal infrastructure. Because there is such a wide range of signals, the scope of this thesis is limited to time-series. Hence, the main research question of this thesis is:

How can wavelet analysis improve time-series analysis and processing in the field of coastal engineering?

It is important to note that wavelet analysis is divided into two categories. The first category uses continuous wavelet coefficients to do time-frequency analysis and some basic signal processing [29, 55]. Time-frequency analysis based on the continuous wavelet transform has already been applied much in coastal engineering, often based on the guidelines from other research fields [15, 16, 22, 29, 55]. An interesting feature of the continuous wavelet coefficients is that they can be used in digital signal processing instead of Fourier coefficients [21, 34]. This offers opportunities for problems where the behaviour in the frequency domain depends on time.

The second category is the discrete wavelet transform, which is applied in digital signal processing only [28, 42]. An example of the application of the discrete wavelet transform is the JPEG-format [14, 42]. The coefficients in the discrete wavelet decomposition have many applications in digital signal processing, from denoising and compression to filtering specific signal elements. The focus of this thesis lies in the application of wavelet analysis in general. Therefore the sub-questions are divided into the application of the discrete and the continuous branch. Another sub-question will address the added value of wavelet analysis onto coastal engineering signals. These questions are presented at the end of the next chapter, Background.

1.2. Overview

The next chapter will provide background with respect to coastal engineering time-series, Fourier and wavelet analysis. It is concluded with four research questions. The first and second sub-question concern the application of the continuous wavelet transform and are addressed in Chapter 3. The third sub-question considers the application of the discrete wavelet transform and is discussed in Chapter 4. In Chapter 5 the added value of wavelet analysis with respect to current methods for signals from the field of coastal engineering is addressed. Lastly, the research questions will be answered in Chapter 6, followed by recommendations for future research. The appendices contain some theoretical additions and results that could not be presented in the main part of this thesis. The content of the appendices is summarised on page 78.

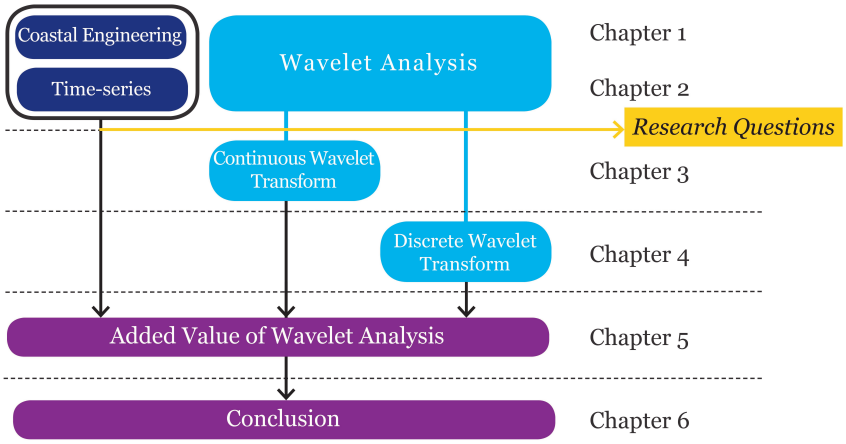

Figure 1.1: A schematic overview of the content of this thesis.

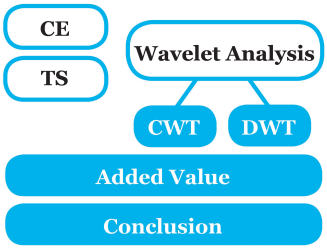

2 Background

As addressed in the introduction, the aim of this research is to derive the guidelines with respect to the application of wavelet analysis in the field of coastal engineering. This chapter provides the background for these guidelines. Therefore it starts with the definition of a time-series and which different analyses there are. Two types of analysis will be explained more elaborate: Fourier Analysis in Section 2.2 and Wavelet Analysis in Section 2.3. These analyses are applied in both (time-)frequency analysis and digital signal processing, which is discussed in respectively Section 2.4 and 2.5. At the end of this chapter, the research questions supporting the main research question will be presented.

2.1. Time-series and Signal Analysis

In the field of coastal engineering, many different time-series are analysed and processed. These time-series are the result of simulations and measurements, which are conducted in the field or an experimental environment. The most common measured quantities in coastal engineering are distances, forces and pressures. The measurements are often analysed, processed, or a combination of these two. In Section 2.1.1 some general characteristics of time-series are discussed. This is followed by different types of signal analysis, which are elucidated in Section 2.2 and 2.3. At the end of this chapter, in Section 2.6, the challenges with respect to coastal engineering time-series are discussed.

2.1.1. Time-series

Time-series are generally divided into two categories: deterministic and random signals. *Deterministic signals* can be modelled completely as a function of a variable, for instance time. A deterministic signal has a known and unambiguous value at every point in time [11, 20]. These signals are composed of additions, subtractions, delays, derivations and integrals of deterministic parts. *Random* or *stochastic signals* are non-deterministic signals [20]. These are modelled using probability theory.

Most signals in coastal engineering are considered random; they are the result of a so-called *random process*. Such a process can produce an entirety of random signals, which is called an *ensemble*. One signal from such an ensemble is known as a *sample function* in mathematics or as a *realisation* in signal analysis. Random signals cannot be described deterministically. They are characterised by characteristics that are valid for the whole ensemble [20]. The whole ensemble is the set of realisations $\{x_i(t)\}$, consisting of the individual random signals $x_1(t)$, $x_2(t)$, etc.

Two important properties of ensembles are the expected value and the variance (or its square root: the standard derivation) at one moment in time. E.g. for the ensemble $x = \{x_i\}$ the expected value is defined as:

$$\mathrm{E}[x(t_0)] = \lim_{N\to\infty} \frac{1}{N} \sum_{i=1}^{N} x_i(t_0).$$

. These characteristics are called time-dependent if they change in time. It should be noted that the *time average* of a signal is the average over the whole time domain, which can be computed for every ensemble member individually. The quadratic average of an ensemble, $\mathrm{E}\left[x^2(t)\right]$, is used to describe the average power of a random process. The expected value and variance often suffice to describe common random signals. The

more general formulation of the expected value and the variance of an ensemble at a certain time t_0 is given by [11]:

$$\mathrm{E}\left[f(x(t_0))\right]. \tag{2.1}$$

The expected value is thus expressed by $f(x) = x$ and the variance by $f(x) = (x - \mathrm{E}[x])^2$. A probability density function is a description of a characteristic (2.1) for the whole time t. Advanced models of random processes can become very complicated, using *higher-order statistics*, such as $f(x) = x^3$ in (2.1) [20].

Random processes, which result in random signals, have a lot of different classifications. Two important classes are stationary processes and linear processes. Often, such a process always relates two (or more) signals to each other. An example of a process is 'a megaphone': one or more people talk into one end, the process in the megaphone amplifies the voices and the horn will broadcast the amplified combination of voices.

Stationary and ergodic random processes

A random process is called *stationary* if its statistical properties do not change over time. In the example of the megaphone, your voice is amplified with the same factor at all times. This is considered a stationary process. An ensemble can be stationary as well, implying that the statistical properties of the ensemble do not change over time. For instance, its mean and variance are the same for all times. An ensemble is *stationary to the order N* if [11]:

$$\mathrm{E}[f(x(t_1), x(t_2), \ldots, x(t_N))] = \mathrm{E}[f(x(t_1 + \Delta t), x(t_2 + \Delta t), \ldots, x(t_N + \Delta t))] \tag{2.2}$$

for all Δt. All signals from this ensemble are stationary as well. This expression is difficult to use, therefore a random process is often called stationary if its second-order expected values only depend on the difference of observed time points $t_1 - t_2$ [20]. This can be checked using the autocorrelation function (9). Note that this mathematical description excludes finite random signals and deterministic functions other than constant functions as stationary [20]. A random process is called *weak stationary* if only the autocorrelation and the expected value of a signal are stationary [8, 11], respectively if for all Δt

$$\mathrm{E}[x(t_1)x(t_2)] = \mathrm{E}[x(t_1 + \Delta t)x(t_2 + \Delta t)], \text{ and} \qquad \mathrm{E}[x(t_1)] = \mathrm{E}[x(t_1 + \Delta t)].$$

For a stationary random process for which all time averages are the same as all ensemble averages, the process is an *ergodic* random process [11, 20]. This holds for all function $f(\boldsymbol{x})$ from (2.2). A signal is again called *weak ergodic* if the autocorrelation and expected value of the signal are the same as their time averages [20].

Linearity

A process or function $f(\boldsymbol{x})$ is a *linear process* if the following relationship holds [11]:

$$f(A\boldsymbol{x} + B\boldsymbol{y}) = Af(\boldsymbol{x}) + Bf(\boldsymbol{y}). \tag{2.3}$$

For instance if two people talk into the same megaphone at the same time, both their voices are equally amplified. If one of them starts to talk louder, the result will be louder as well. However, if the megaphone is limited to a certain maximum output volume, it could be that this louder person is amplified less then the other person. Then the process is classified as *non-linear*. Important is that a signal can be the result of a non-linear process, but cannot be non-linear on its own. If a signal is the result of a non-linear process, it is often referred to as non-linear as well.

Time invariance

The last important characteristic of a system is its *time invariance*. This means that *the response to a delayed input signal results in a corresponding delayed output signal* [20]. Systems that are both linear and time-invariant are abbreviated to *LTI* systems.

2.1.2. Signal Analysis

There are different methods to analyse the time-frequency behaviour of a signal. This section will present different 'observation options' of temporal information. These 'data types' could also be applied to spatial information, but that is outside the scope of this thesis. The goal is to find an easy retrieval of both temporal and frequency information of a signal $x : \mathbb{R} \to \mathbb{C}$, a function of time t. An important theme in analysis is the representation of a known or unknown function (or signal, time-series) $x(t)$ by special known functions [6].

Often the function is referred to as *(time) signal* or *time-series*, which is a broader concept of *a function or sequence that represents information* [20].

For the representation of the function, a set of functions is chosen. This set always has a mathematical correspondence. The analytical properties of a set tend to show the evident or hidden symmetries of the considered function $x(t)$. This family is known as the *basis functions*. In general, the set is given by

$$\{e_\alpha | \alpha \in I\} \qquad \text{with the basis functions } t \mapsto e_\alpha(t). \tag{2.4}$$

The index set I can be discrete, but also continuous. An arbitrary function $x(t)$ can thus be represented in the form

$$x(t) = \sum_{\alpha \in I} c_\alpha e_\alpha(t) \tag{2.5}$$

in the discrete case. This expression (2.5) is called a *representation*. In the continuous case the representation is expressed as an integral:

$$x(t) = \int_I c(\alpha) e_\alpha(t)\, \mathrm{d}\alpha.$$

Here the c_α, or $c(\alpha)$, is the coefficient belonging to the basis function $e_\alpha(t)$. The set of coefficients $\{c_\alpha | \alpha \in I\}$ is called the *analysis* of x with respect to the family $\{e_\alpha | \alpha \in I\}$. The inverse operation that takes a given set of coefficients as input and returns the function itself as output is called the *synthesis* of x by means of e_α. There are tons of different families of basis functions to choose from. The Taylor polynomial for instance uses higher and higher derivatives of the function $x(t)$. In this thesis two different families will be addressed. These are known respectively as the complex exponentials in Fourier analysis (FA, Section 2.2) and wavelets in wavelet analysis (WA, Section 2.3). First a brief overview of these techniques is presented, using an example comprehensible for readers with different backgrounds: a guitar player striking three strings separately. After that these techniques will be elaborated more.

Time Domain

The receiver of a time signal, for instance, an ear receiving sound waves, a cellphone receiving the 4G signals or laser equipment measuring wave heights at Deltares, always receives an amplitude at a given time. Mathematically this is seen as a function: $x(t)$, mostly being referred to as a *(time) signal* in signal analysis. From this signal, many properties of the transmitter, transmission and receiver can be derived using the right techniques. However, in transmission the signal $x(t)$ can be disturbed, making it hard to draw the right conclusions based on the time signal.

Fourier Transform

The signal $x(t)$ does contain more information than just the amplitude at a given time. With the right mathematical transformations, an insight into the different frequencies of the signal can be given. The *Fourier transform* (FT) is a common and much-used transformation to derive the energy density per frequency of a signal. This transformation represents the signal in the Fourier or frequency domain. Remember the guitar player? If only the time domain signal of the sound is considered, one cannot know which notes were played. However, we do know at what times the strings were struck, by observing the amplitude differences in time. If only the Fourier transform of the signal is considered, the representation of the signal in the frequency domain, one can tell exactly which notes were played, but not in which order.

Short-term Fourier Transform

A (practised) listener, however, can tell both the notes and the order in which these notes were played! This is impossible when only the time domain or the frequency domain of the signal is reviewed. A visual representation of these domains is shown in Figure 2.1(a-b). In the early twentieth century, Gabor [6] was the first to act on this shortcoming, developing the Gabor transform. He used the combination of a window function and the Fourier transform to derive a coupling of the temporal and frequency domain. Hence, this method gives insight into the occurrence of frequencies in distinct time intervals as depicted in Figure 2.1c. Later his work was placed in the framework of the *short-term Fourier transform* (STFT, Section 2.2.3). A disadvantage of this method is the relatively large loss of both temporal and frequency information, which is explained by the uncertainty principle (see Section A.2.1).

Wavelet Analysis

The introduction of wavelet analysis minimises these losses. Wavelet analysis is a tool that cuts the function $x(t)$ up into different frequency components, studying each component with a resolution matching its scale [14]. So it is like the STFT, but more optimised. In the 1960's the basis of the wavelet transform was developed in both mathematics and physics. In the late 1980's the approaches from different disciplines were combined, which led to the theory of wavelet analysis as it is known today. As shown in Figure 2.1d, for different frequencies the time spacings are different, this again finds its explanation in the uncertainty principle. The simpler explanation is that it takes longer for a low-frequency wave to complete a full cycle. Therefore one will have to 'listen longer' to detect it. A high frequent wave can be detected in much less time. However, in this case, it is harder to determine which frequency it is.

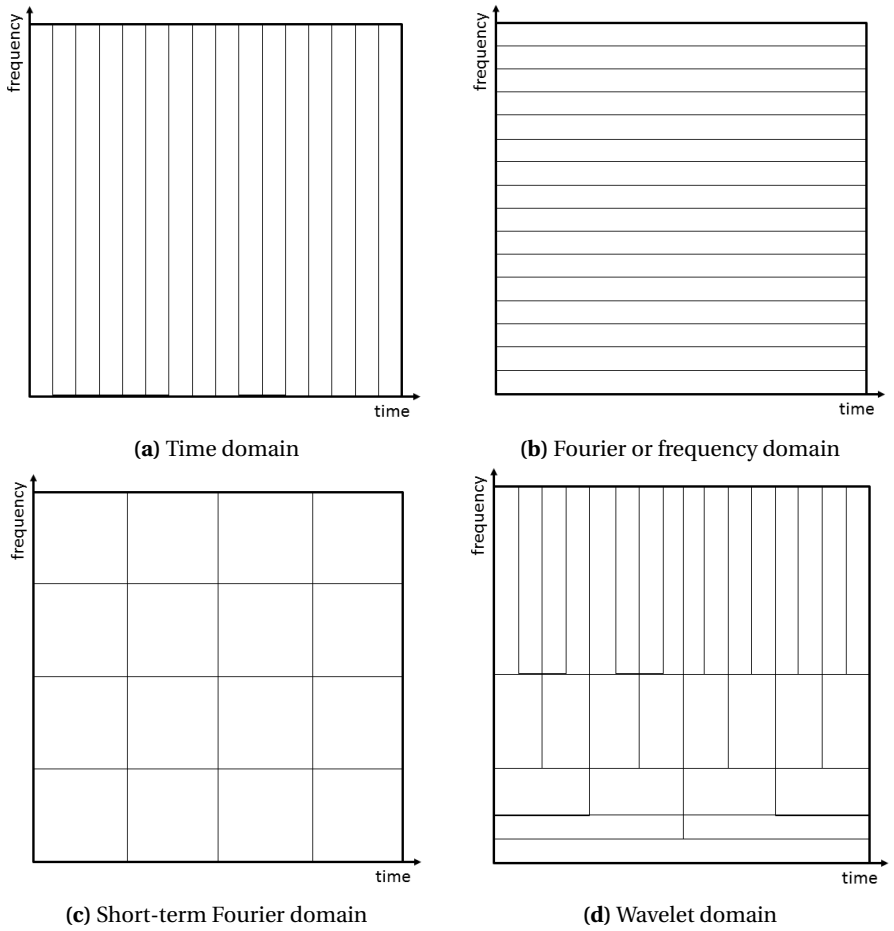

(a) Time domain

(b) Fourier or frequency domain

(c) Short-term Fourier domain

(d) Wavelet domain

Figure 2.1: Schematic representation of the four different analyses of a signal.

2.2. Fourier Analysis

In the last section, four different kinds of signal analysis were discussed. This section will explain Fourier analysis and the short-term Fourier transform. The next section addresses wavelet analysis. In the formal Fourier analysis, the basis functions as described in equation 2.4 are from the family of complex exponentials:

$$t \mapsto e^{ikt} = \cos(kt) + i\sin(kt), \qquad k \in \mathbb{Z}. \tag{2.6}$$

This is a family of 2π-periodic, orthonormal functions. For any $f \in L^2(\mathbb{R}/2\pi)$, measurable functions $f : \mathbb{R} \to \mathbb{C}$, the formal definition of the Fourier transform can be applied. This theory was expanded to cover not only these specific functions, but all functions on $\mathbb{R}$. This results in the Fourier series representation of $x(t)$:

$$x(t) := \sum_{k=-\infty}^{\infty} c_k e^{ikt}. \tag{2.7}$$

2.2.1. Continuous Fourier Transform

The Fourier transform (abbreviated to FT) of a time signal, or function, $x \in L^1$ is defined by the integral [11]

$$\mathcal{F}\{x(t)\}(\omega) = \mathcal{F}x(\omega) = X(\omega) := \int_{-\infty}^{\infty} x(t)e^{-i\omega t}\,\mathrm{d}t, \qquad \omega \in \mathbb{R}. \tag{2.8}$$

Here ω denotes the angular frequency in rad/s, i.e. $2\pi f$. This transform gives a representation in the complex domain of the frequency content of the time signal $x(t)$. Often the modulus of the Fourier transform is displayed against the frequency ω to indicate the energy density over the spectrum. As discussed before, information concerning time-localisation cannot be read off from $X(\omega)$. Therefore it is impossible to determine at what time, which frequencies are present in the signal. However, when one is looking out for one frequency, like radars which respond to very specific frequencies, this characteristic of the Fourier transform is very convenient.

$X(\omega)$ is also known as the two-sided spectrum of $x(t)$. The original time signal can be reconstructed from this spectrum by using the inverse Fourier transform (IFT)

$$x(t) = \frac{1}{2\pi}\int_{-\infty}^{\infty} X(\omega)e^{i\omega t}\,\mathrm{d}\omega, \tag{2.9}$$

the linear combination of the pure oscillations of all frequencies $\omega \in \mathbb{R}$. Note that for a periodic, continuous time signal the CFT is discrete in frequencies because the CFT will exist of a finite set of basis coefficients. However, for a general non-periodic signal this will not hold. An important characteristic of a stationary signal is that its frequency content does not change over time, i.e. its Fourier coefficients are time-invariant [42]. This implies that both the power spectral density and the autocorrelation of the signal are time-invariant too.

The Fourier transform of a signal consists of a real and an imaginary part. The decomposition $\mathcal{F}\{x\}(\omega) = X(\omega) = Y(\omega) + iZ(\omega)$ is known as the *Cartesian* or *quadrature form* [11]. An other well known form is the *polar form*: $X(\omega) = |X(\omega)|e^{i\arg(X(\omega))}$. This is also known as the *magnitude-phase form*, in which the real functions $|X(\omega)|$ and $\arg(X(\omega))$ denote the magnitude and the phase of the signal. The quadrature Fourier series uses the property that the complex exponential can be written as a sum of a sine and a cosine, which leads to another representation of any physical waveform $x(t)$ (over the interval $a < t < a+T$) [11]:

$$x(t) = \sum_{n=-\infty}^{\infty} a_n \cos n\omega_0 t + b_n \sin n\omega_0 t \tag{2.10}$$

$$\text{where } a_n = \begin{cases} \dfrac{1}{T}\displaystyle\int_a^{a+T} x(t)\,\mathrm{d}t & n = 0 \\ \dfrac{2}{T}\displaystyle\int_a^{a+T} x(t)\cos n\omega_0 t\,\mathrm{d}t & n \geq 1 \end{cases} \quad \text{and } b_n = \begin{cases} 0 & n = 0 \\ \dfrac{2}{T}\displaystyle\int_a^{a+T} x(t)\sin n\omega_0 t\,\mathrm{d}t & n \geq 1 \end{cases}.$$

2.2.2. From Continuous to Discrete

As stated before, most signals in the field of coastal engineering are discrete. The continuous Fourier transform is therefore not applicable to these signals. The sampling theory describes how these so-called *sampled signals* can be transformed using the discrete Fourier transform (DFT). In Appendix A this theory and some advantages and disadvantages are discussed more elaborate.

A sampled signal can be represented as a sum of delta functions. For this we assume a *uniform sampling*, sampled with the *sampling frequency* $f_s = \Delta t^{-1}$ [Hz]. Assume a continuous signal $x(t)$ is being sampled, then the uniform sampling of this signal is described as

$$x_{\text{sampled}}(t) = \sum_{k=-\infty}^{\infty} x(t)\delta(t - k\Delta t) = \sum_{k=-\infty}^{\infty} x(k\Delta t)\delta(t - k\Delta t).$$

Now determine the Fourier transform of $x_{\text{sampled}}(t)$, using the linearity property (G.1) of the Fourier transform and the Fourier transform of the Delta function (G.9) to derive the *discrete time Fourier transform* (DTFT, discrete in time, continuous in frequency):

$$\mathcal{F}\left\{x_{\text{sampled}}\right\}(\omega) = X_{\text{sampled}}(\omega) = \sum_{k=-\infty}^{\infty} x(k\Delta t)e^{-i\omega k\Delta t}.$$

Most sampled signals $x(k\Delta t) = x[k]$ are finite. For now, we will work with the abbreviated expression for a signal of length N

$$X(\omega) = \sum_{k=0}^{N-1} x(k\Delta t)e^{-i\omega k\Delta t}. \tag{2.11}$$

Discrete Fourier Transform

Expression (2.11) can be simplified further, by discretisation of the frequency domain. In the discrete Fourier transform (DFT) the following set of orthogonal basis functions is used [37]:

$$\left\{e_n[k] = \exp\left(\frac{i2\pi nk}{N}\right)\right\}_{0\leq n\leq N}. \tag{2.12}$$

Using this basis, the *discrete Fourier transform* (DFT) is defined. This transform is discrete in both time and frequency. Now again consider a discrete time signal, given by $x[k]$, with $k \in \mathbb{N}$ and finite with a duration of time T, then the DFT becomes

$$\mathcal{F}\{x[k]\}[n] := X[n] = \sum_{k=0}^{k=N-1} x[k]e^{-i2\pi nk/N}, \qquad \text{where } n = 0,1,2,\ldots,N-1, \tag{2.13}$$

and the inverse operation is given by

$$\mathcal{F}^{-1}\{X[n]\}[k] := x[k] = \frac{1}{N}\sum_{n=0}^{N-1} X[n]e^{i2\pi nk/N}, \qquad \text{where } k = 0,1,2,\ldots,N-1. \tag{2.14}$$

Note that the basis functions (2.12) are independent of the sampling frequency or the total duration of the signal $x[n]$. The resulting DFT has domain $[-f_{\text{sample}}/2, f_{\text{sample}}/2]$.

Fast Fourier Transform

The fast Fourier transform (FFT) is a faster implementation of the DFT algorithm. The direct computation of the DFT is of $\mathcal{O}(N^2)$ arithmetic operations [46]. The FFT algorithm brings this number down to $\mathcal{O}(N\log N)$ operations by breaking the large convolution from equation 2.13 into shorter convolutions, lowering the number of operations [46]. The terms are interchangeable because the DFT and FFT algorithm both result in the same Fourier coefficients.

2.2.3. Short-term Fourier Transform

To apply time-frequency analysis, a connection between time and frequency information has to be extracted from a time signal. The WFT makes use of a so-called *window function* $g : \mathbb{R} \to \mathbb{R}_{\geq 0}$ to connect time and frequency [6]. This window function should have the property of compact support, containing $t = 0$, or at least a maximum at $t = 0$, and decaying fast for $|t| \to \infty$ and $\int_{-\infty}^{\infty} g(t)\,\mathrm{d}t = 1$. A widely used window is the *Gabor window*, named after the physicist mentioned in the introduction. He remarked that the window $\mathcal{N}_{\sigma,0}$ is optimal to extract time-frequency information using the Fourier transform. This Gabor transform window is given by

$$g(t) = \mathcal{N}_{\sigma,0}(t) := \frac{1}{\sqrt{2\pi}\sigma}e^{-t^2/2\sigma^2}, \qquad \text{with } \sigma \text{ constant.} \tag{2.15}$$

The choice for a window like (2.15) instead of a rectangular pulse for instance is obvious to the reader familiar with Fourier transform properties. The sharp cut off by a rectangular window will lead to rippling effects, described in Section A.1. These contributions will disturb the results. The WFT is the CFT of the signal $x(t)$ multiplied with the window function $g(t)$.

The chosen window g will be slid over the signal $x(t)$ not to select the full signal, only parts of it. Therefore the *window transform* is defined as

$$g_s : \quad t \mapsto g(t-s), \tag{2.16}$$

a translation by $s \in \mathbb{R}$ of the window g. Note that for $s > 0$ the window is translated to the right. Now define:

$$\mathcal{G}\{x\}(\omega, s) := \int_{-\infty}^{\infty} x(t)g(t-s)e^{-i\omega t}\,\mathrm{d}t = \int_{-\infty}^{\infty} x(t)g_s(t)e^{-i\omega t}\,\mathrm{d}t. \tag{2.17}$$

This use of the translated window transform is widely known as the *short-term Fourier transform* (STFT) because the multiplication by $g(t-s)$ localises the Fourier integral in the neighbourhood of $t = s$ [37]. The

value of $\mathcal{G}\{x\}(\omega, s)$ represents again the complex amplitude by which the pure harmonic $e^{i\omega t}$ is present in the signal $x(t)g_s(t)$ for that particular s. By the redundancy of information of the signal $x(t)$ in the STFT $\mathcal{G}\{x\}(\omega, s)$, there are many inverse transformations defined [6]. The representation of this transformation is often given by a *spectrogram*. The spectrogram is a measure of the energy of $x(t)$ in the time-frequency neighbourhood of (ω, s). This neighborhood is specified by its so-called Heisenberg box $h_{\omega,s}$ (see Section A.2.1). For large signals, the spectrogram can become quite hard to read. The two most applied enhancers are window overlapping and bin averaging. This last one, however, decreases time-frequency resolution even further.

Discrete Short-term Fourier Transform

The derivation of the discrete short-term Fourier transform (DSTFT) is following the same steps as the derivation from the continuous Fourier transform to the discrete Fourier transform. In the discrete case a *discrete window* or *window sequence* $g[n]$ is chosen. Most of the time this is a symmetric discrete signal of period N, with unit norm $\|g\| = 1$ [37]. The discrete signal $x[n]$ is multiplied with the shifted *window sequence* $g[n-k]$, resulting in the expression

$$X(\omega, k) = \sum_{n=-\infty}^{\infty} x[n]g[n-k]e^{-i\omega n} = x[n]e^{i\omega n} * g[n].$$

The same step as for the DFT (Section 2.2.2) is done, leading to the expression for the DSTFT [37]:

$$X[n, k] = \sum_{\ell=0}^{N-1} x[n]g[n-k]\exp\left(\frac{-i2\pi n\ell}{N}\right).$$

2.3. Wavelet Analysis

In wavelet analysis, a different set of basis functions is chosen. Instead of using the complex polynomials, a so-called wavelet $\psi(t)$ is used. The wavelet transform of a continuous time signal $x(t)$ is defined by [64]

$$\mathcal{W}\{x\}(a, b) = W(a, b) = \int_{-\infty}^{\infty} x(t)\psi^*_{ab}(t)\ \mathrm{d}t, \tag{2.18}$$

where ψ^*_{ab} is the complex conjugate of a *daughter wavelet*. This expression denotes the autocorrelation (9) of the signal $x(t)$ with this daughter wavelet, which is derived by scaling and translating the wavelet $\psi(t)$ by respectively a *scaling factor* a and a *translation* b:

$$\psi_{ab}(t) = \frac{1}{\sqrt{a}}\psi\left(\frac{t-b}{a}\right). \tag{2.19}$$

This scaling ensures energy conservation, i.e. all wavelets have the same unit energy (2.20b). A wavelet function is characterised by a finite support and a zero mean value. This is where the term *wavelet* originates from; a function with these two characteristics will be of a short wavelike shape. The formal definition of a wavelet is: a function $\psi : \mathbb{R} \to \mathbb{C}$ satisfying the conditions [6]:

$$\psi \in L^2, \tag{2.20a}$$

$$\|\psi\| = 1, \text{ and} \tag{2.20b}$$

$$C_\psi := \int_{\mathbb{R}\setminus\{\}} \frac{|\mathcal{F}\psi(\omega)|^2}{|\omega|}\ \mathrm{d}\omega < \infty. \tag{2.20c}$$

Wavelets can be both real or complex valued. This leads to respectively real or complex-valued coefficients. It is important to note that a continuous wavelet is often a composition of a wave and a window. Different continuous wavelets are presented in Section C.2. Observe the Complex Morlet wavelet as an example (see Table C.1). It is the product of a wave described by $e^{i\omega_0 t}$ and a Gaussian window, $e^{-t^2/2}$. The wavelet transform is therefore very similar to the STFT. However, due to the scaling, the size of the window changes per frequency, as is depicted in Figure 2.1d. This allows the investigation of a larger range of frequencies than in the STFT.

2.3.1. Continuous Wavelet Transform for Discrete Signals

For the discrete case we consider signals that are samples with a constant sampling interval Δt. To compute the wavelet transform of a discrete signal, the integral has to be discretised. This discretisation can be written as a sum:

$$W^{\mathrm{DT}}(a,b) = \sum_{m=0}^{N-1} x[m] \cdot \sqrt{\frac{\Delta t}{a}} \psi^* \left(\frac{t-b}{a} \right). \tag{2.21}$$

The factor $\sqrt{\Delta t}$ has been added to assure that $\left|W^{\mathrm{DT}}(a,b)\right| \approx |W(a,b)|$, so that the discrete coefficients are a good approximation of the continuous ones. By maintaining a continuous translation, this transformation has much abundant information. By discretising b with the sampling frequency f_s we find the discretised continuous wavelet transform as

$$W(a, n\Delta t) = W[a,n] = \sum_{m=0}^{N-1} x[m] \cdot \sqrt{\frac{\Delta t}{a}} \psi^* \left(\frac{(m-n)\Delta t}{a} \right) = x[n] * \sqrt{\frac{\Delta t}{a}} \psi^* \left[\frac{n\Delta t}{a} \right]. \tag{2.22}$$

This discretised expression approaches the continuous wavelet transform very well and is therefore referred to as the continuous wavelet transform in most modern literature [1, 15, 34, 55]. In this thesis, however, the term *discretised continuous wavelet transform* (DCWT) is preferred.

The fastest way to compute the coefficients is through the Fourier domain [55]. This is divided into four steps. It starts with a discrete signal $x[n]$.

1. Compute the Fourier transform $X = \mathcal{F}\{x\}$ using the FFT.
2. Choose a (discretised) wavelet function $\psi[n]$ (with $\Psi = \mathcal{F}\{\psi\}$) and a set of scales to analyse.
3. For each scale, construct the normalised wavelet function using

$$\Psi(a\omega_k) = \sqrt{\frac{2\pi a}{\Delta t}} \Psi_0[a\omega_k], \quad \omega_k = \begin{cases} \dfrac{2\pi k}{N\Delta t} & : \quad k \le N/2 \\ \dfrac{2\pi k}{N\Delta t} & : \quad k > N/2 \end{cases}. \tag{2.23}$$

4. Find the wavelet transform at all scales a using the inverse FFT:

$$W(a, n\Delta t) = W[a,n] = \mathcal{F}^{-1}\left\{ X[\omega_k] \cdot \Psi^*[a\omega_k] \right\} = \sum_{k=0}^{N-1} X[\omega_k] \Psi^*[a\omega_k] e^{i\omega_k n \Delta t}. \tag{2.24}$$

Reconstruction

By the redundancy of the DCWT coefficients in time and scale the reconstruction is less arbitrary than the reconstruction of a signal from the Fourier domain. However, it is possible to reconstruct the time-series with a completely different wavelet function [55]. The easiest function possible would be the Delta function $\delta(t)$. Assume a discrete number of scales $A = \{a_1, a_2, \ldots\}$, logarithmically scaled with distance $a_{i+1} - a_i = \log(\Delta a)$. In that case the reconstructed real valued time-series becomes [55]:

$$x[n] = \frac{\Delta a \sqrt{\Delta t}}{C_\delta \psi(0,0)} \sum_{j=0}^{J} \frac{\mathrm{Re}(W[a_j, n])}{a_j^{1/2}}, \tag{2.25}$$

with C_δ a constant defined by:

$$C_\delta = \frac{\Delta a \sqrt{\Delta t}}{\psi(0,0)} \sum_{j=0}^{J} \frac{\mathrm{Re}([W_\delta[a_j])}{a_j^{1/2}}, \qquad \text{where } W_\delta[a] = \frac{1}{N} \sum_{k=0}^{N-1} \Psi^*[a\omega_k].$$

The result $x[n]$ in (2.25) is known as an analytical signal. When the decomposed signal was real, the real value of this analytical signal represents the reconstruction of the original signal.

2.3.2. Discrete Wavelet Transform

The *discrete wavelet transform* (DWT) is a powerful tool to decompose a signal. Discrete signals can be decomposed into the same number of elements as the original signal. Therefore it is much less abundant than the continuous wavelet transform. The DWT theory can be approached from the definition of the CWT, with the addition of the notion of frames in Hilbert spaces [6, 14, 37]. Here, however, the definition of the DWT through a *multi resolution analysis* (MRA) is presented, which has two main advantages. The first advantage is that the MRA theory is discrete to begin with, resulting in a more natural derivation of the DWT, easier to implement as a computer algorithm [6, 28, 42]. Secondly, the MRA structure allows for a convenient, fast and exact calculation of wavelet coefficients by providing a recursion relation.

In a nutshell: a multi resolution analysis[1] of the L^2 space consists of a set of nested subspaces V_n, that comply with six conditions. These conditions ensure that the analysis can represent all functions in the L^2 space in a unique way. A function is projected on the subspace V_n using the refinable function ϕ_n. This function is called orthogonal if $\langle \phi(x), \phi(x-k) \rangle = \delta_{0k}\ \forall k \in \mathbb{Z} \setminus \{0\}$. The difference of the projection onto two consecutive subspaces, V_{n+1} and V_n, can be described by the projection using the wavelet ψ_n and is known as the fine detail. The discrete wavelet transform describes a function as the sum of the projection on space V_ℓ and a summation of all fine details above. This summation is finite for discrete signals. Important to know is that the daughter wavelets are not used for an arbitrary set of scales and all translations, but as a fixed set:

$$\psi_{nk}(t) = 2^{n/2}\psi(2^n t - k). \tag{2.26}$$

This fixed set leads to a number of N discrete wavelet coefficients for a signal of length N.

Fast Wavelet Transform

The *fast wavelet transform* (FWT) is the fast implementation of the DWT. The algorithm is based on filters, first described in the late 1980's by Daubechies [13]. The signal at level n, s_n, is filtered using a wavelet, which results in d'_{n+1}, the detail 'signal' at the next level. The approximation 'signal' at that same level can be determined by subtracting: $a'_{n+1} = s_n - d'_{n-1}$, however, in the FWT case a filter implementation is used as well. Both the detail and approximation signal are then down-sampled by a factor 2 to determine the detail and approximation coefficients at level $n+1$: d_{n+1} and a_{n+1}. By combining the information in these two sets of coefficients, the original signal can be reconstructed (see Figure 2.2a). By cascading the algorithm; using the approximation coefficients as input for the next step, more levels of coefficients are determined. To reconstruct the original input the last set of approximation coefficients and all detail coefficients are used (see Figure 2.2b).

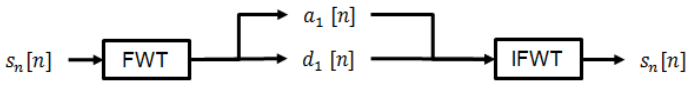

(a) One decomposition and reconstruction of the fast wavelet transform

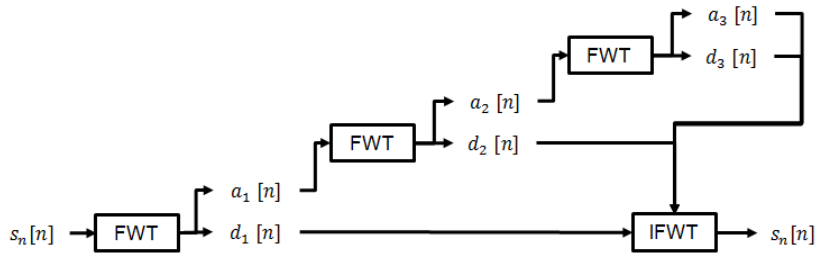

(b) Three decomposition steps and one reconstruction of the cascaded fast wavelet transform.

Figure 2.2: Fast Wavelet Transform, the a_i are the approximation coefficients, the d_i the detailed coefficients at level i.

2.3.3. Wavelets

In the previous sections both the continuous and discrete wavelet transform are presented. As explained earlier, there are many different wavelets available. An overview of these different wavelets is presented here.

[1] More background concerning the MRA and an example of the Haar wavelet is presented in Appendix B.

In Appendix C a more elaborate description of a lot of different wavelets is given, in Appendix B the Haar wavelet is derived from the definition of the multi resolution analysis..

In this section, a little overview of the different wavelets is given. The realm of wavelets is divided into two types of wavelets: continuous and discrete wavelets. This difference is because both transforms discretise scale differently. The discrete wavelet transform generally uses an exponential scale with base 2 (see (2.26)), whereas the continuous wavelet transform uses a much smaller base ($\sim 2^{-10}$). Moreover, different wavelet characteristics are preferred in the different transforms. Wavelets that result in a good time-frequency representation of a signal are not suitable to create a sparse representation that is created by the DWT.[2] Vice versa, wavelets that create sparse representations result in poor time-frequency analyses. Wavelets have many characteristics of which the most important ones are listed here.

Orthogonality As mentioned in Section 2.3.2 wavelet decomposition is characterised by a refinable function $\phi(x)$ and a wavelet $\psi(x)$. In the bi-orthogonal case there is a set of two refinable functions ϕ and $\tilde{\phi}$, such that $\langle \phi(x), \tilde{\phi}(x-k) \rangle = \delta_{0k}$. An orthogonal wavelet family is also bi-orthogonal, i.e. the family is its dual.

Symmetry A family is known as symmetric if the wavelet function is a symmetric function. Note that an orthogonal family of real wavelets cannot be symmetric.

Moments The number of vanishing moments influences the support in time and frequency space of the wavelet and the scaling function. If there is a larger support in the time domain a smaller support in frequency domain can be achieved and vice versa. The definition of the discrete and continuous moments is presented in respectively Section B.6 and C.1.1.

Filter Most discrete wavelets have the advantage that they can be written as a filter, i.e. they can be implemented using the FWT. This is beneficial in computations, these can be done by low-level electronics. The filter length ℓ_f of the wavelet determines the size of the wavelet and the maximum decomposition level: $2^{\text{max.level}} \cdot \ell_f = N$, where N is the length of the signal. To ensure max.level $\in \mathbb{N}$ different signal extension modes can be applied, which will be discussed later.

Continuous Wavelets

There are many continuous wavelets, of which only a hand full are often used in time-frequency analysis. They are divided into complex and real wavelets, as presented in Figure 2.3. Real wavelets in combination with real signals lead to real coefficients, so they do not convey phase information. Edges in signals are often detected by using wavelets with a relatively short time support. This has all to do with the time-frequency distribution of the wavelet. For a wavelet to be applicable in time-frequency analysis, it has to have a relative short bandwidth in the frequency domain [30]. This is a characteristic that a lot of discrete wavelets lack and therefore are not used much in the continuous wavelet transform.

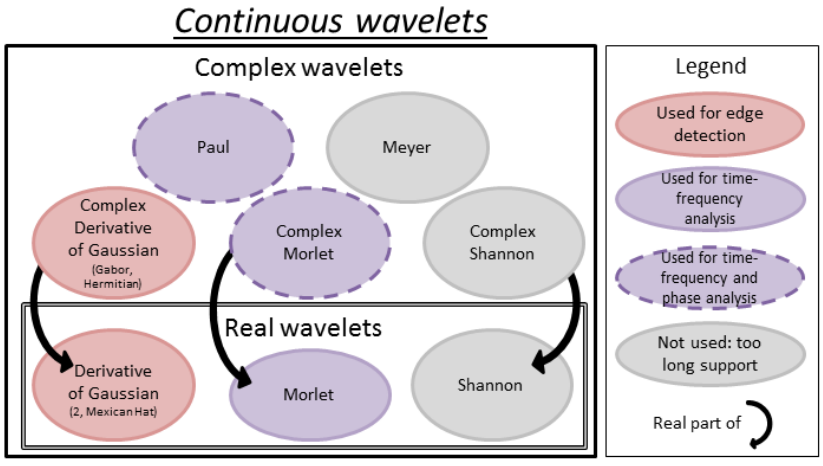

Figure 2.3: An overview of the most used continuous wavelets. More elaborate description of these wavelets in Section C.2.

[2] Only the discretised Meyer wavelet is sometimes used in the DWT, see Table C.2.

The continuous wavelets are dependent on t, whereas the discrete wavelets are defined dimensionless. Continuous wavelets are characterised by a centre frequency, f_ψ in Hz. Its centre frequency is of course inversely proportional to its equivalent wavelength $\lambda_\psi = 1/f_\psi$ in seconds. The equivalent wavelength of a wavelet is proportional to the scale a: $\lambda_{\psi_a} = a \cdot \lambda_\psi$. The e-folding time of a wavelet, τ_a, is based on the drop of power for a discontinuity at the edge by a factor e^{-2} [55]. This time is used to determine edge effects, which are more elaborately addressed in Section 3.1.3. The e-folding time at a certain scale is proportional to the scale, i.e. $\tau_a \cdot a$. A more elaborate description of the different continuous wavelets is presented in Section C.2. An example of two different Morlet wavelets is shown in Figure 2.4.

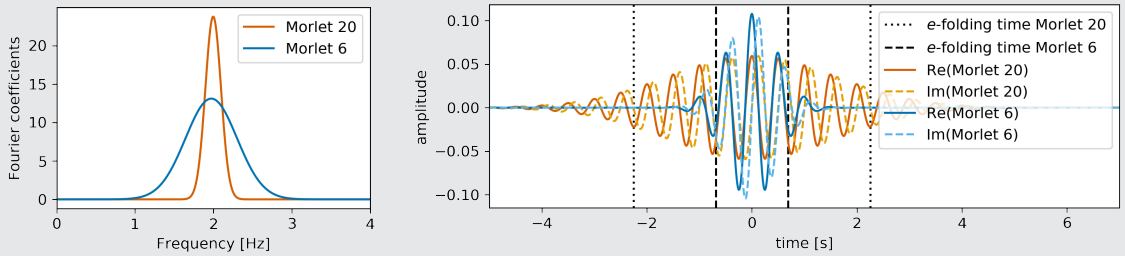

(a) Fourier coefficients **(b)** Function in time

Figure 2.4: The Fourier coefficients and functions in time for two different Morlet wavelets with the same centre frequency $f_\psi = 2$.

Discrete Wavelets

In the discrete wavelet transform much more wavelets are employed than in the continuous wavelet transform. In Figure 2.5 an overview of the most commonly used wavelets is presented. If one would want to merge the continuous and discrete wavelets shown in Figure 2.3 and Figure 2.5[3], the continuous wavelets would be addressed as 'non-orthogonal'. The lack of orthogonality makes them less suited for discrete wavelet transformation. Techniques such as lifting can be used to create an unlimited amount of new discrete wavelets based on these wavelets [28]. How to pick the right discrete wavelet for your signal is discussed later.

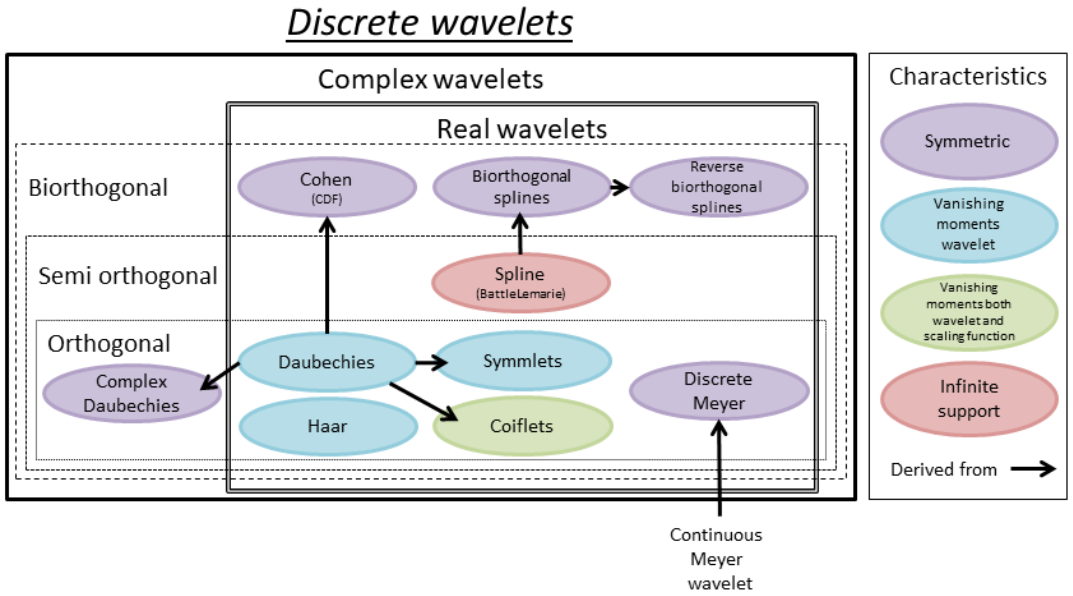

Figure 2.5: An overview of the most used discrete wavelets. More elaborate description of these wavelets in Section C.3.

[3] Both figures are based on the work of van Berkel [57] and expanded with some extra information.

2.4. Time-frequency Analysis using Fourier and Wavelet Coefficients

Fourier and wavelet coefficients are applied in many engineering fields. The magnitude of the coefficients is often used as a measure of the energy density of a signal. The argument of the coefficients can be employed in many different ways, which is addressed after that. At the end, some different time-frequency analysis tools are discussed.

2.4.1. Amplitude

To determine which (time-)frequency components are present in a signal, often the *magnitude spectrum* is analysed. Expressed by $|X(\omega)|$ in the continuous Fourier domain and by $|W(a,b)|$ in the continuous wavelet domain.

Spectral Densities

The energy spectral density of a signal describes the distribution of the energy of a signal over the frequencies. Assume a discrete signal $x[n]$ with the Fourier coefficients $X[k]$, then the *energy* E of a discrete signal $x[n]$ is defined as [46]

$$E_x = \sum_{n=0}^{N-1} |x[n]|^2 = N \sum_{k=0}^{N-1} |X[k]|^2, \tag{2.27}$$

which is known as Parseval's relation. The expression $|X[k]|^2$ is therefore known as the energy density spectrum (EDS). The variance density spectrum (or *power density spectrum* (PSD) in most engineering fields [46]) has the property that the integral over the frequencies equals the variance (or average power) of the signal. The *variance density spectrum* (VDS) for discrete signals is thus defined by

$$S_{xx}^{f}[k] = \frac{f_s}{N^2} |X[k]|^2. \tag{2.28}$$

The variance density spectrum in coastal engineering is denoted as $E(f)$, which has the units m^2/Hz for time-series containing water elevations [24]. If the VDS of only one ensemble member is assessed, the error of the raw spectrum is around 100%. This poor reliability is not acceptable and is often improved by dividing the signal into p segments and averaging the spectra of these different segments. The error then reduces by a factor $\sqrt{p}$ and the frequency resolution decreases from $\Delta f (= f_s/N)$ to $p\Delta f$ Hz [24]. The segmenting will only integrate to the variance of the signal for stationary signals.

Wavelet Power Spectrum

The *scalogram* or *wavelet power spectrum* (WPS) is often defined as the square of the modulus of the wavelet coefficients [19, 55]. In the same manner as the energy density spectrum for Fourier coefficients:

$$S_{xx}^{w}(a,b) = |W(a,b)|^2. \tag{2.29}$$

For a white noise time-series the expected value of these WPS values is equal to the variance of that signal for all a and b [55]. Therefore, the WPS presents a measure of the power relative to a white noise signal with the same variance as the signal. Liu et al. [32] show that this definition is not a physically consistent definition of energy, in an average sense. It should be the transformation coefficient squared divided by the scale it is associated to, i.e.

$$S_{xx}^{w\ \mathrm{R}}(a,b) = \frac{\left|W(a,b)^2\right|}{a}. \tag{2.30}$$

This quantity is denotes as the *rectified* wavelet power spectrum (RWPS). Note the behaviour of noise, however, becomes dependent on the scale. An example of these effects are given in Demonstration 2.1

2.4.2. Averaging Wavelet Coefficients

By averaging the wavelet power spectrum in time the so-called *global wavelet spectrum* (GWS) is created. The rectified global wavelet spectrum (RGWS) is the time average of the RWPS. This global wavelet spectrum provides a consistent and unbiased estimation of the true power spectrum of a time-series [55]. The addition of the scale in the rectified one leads to a bias. Furthermore, it could provide a useful measure to base the background spectrum for significance testing. Examples of these measures are presented in Demonstration 2.1.

The *scale averaged wavelet power* (SAWP) is used to examine fluctuations in power over a range of scales, also referred to as a band. The SAWP between two scales a_0 and a_1 is defined by [55]

$$\kappa(t) = \frac{\Delta a \Delta t}{C_\delta} \sum_{a=a_0}^{a_1} \frac{|W_a(t)|^2}{a}. \tag{2.31}$$

This results in a time-series containing the average variance of the wavelet coefficients in a certain frequency band. It can, therefore, be used to examine modulation of one time-series by another. When further examination is needed, the cross-wavelet spectrum is often used.

Demonstration 2.1 (Energy density) In this demonstration, an example is given of the different measures of energy density presented in Section 2.4. Four waves with an amplitude of 1 m and periods of 2^{-3}, 1/2, 2, and 8 seconds are summed. To show the difference of the effect of noise on the variance density spectrum and the (rectified) global wavelet spectra, white Gaussian noise with a variance of the signal has been added to the signal. The VDS of the signal and the noisy signal are presented in Figure 2.6a. This representation indeed is rather grassy; a more reliable VDS of the signal is presented in Figure 2.6b. The effects of the segmenting are very clear: the frequency resolution and maximum period have decreased.

In the spectrum of the signal without noise, four peaks of equal size are present at the periods of the waves: all waves contain equal energy. The WPS and RWPS of the noiseless signal are presented in Figure 2.6c and 2.6d. The difference between these two if clear. The rectified WPS shows four 'peaks' of equal height, whereas the normal one does not; the peaks increase in intensity. This effect is also shown in the time-averaged (R)WPS, the (rectified) global wavelet spectra, shown in Figure 2.6g and 2.6h. This difference is due to the scaling of the wavelet: a high scale (thus large period) wavelet has a smaller amplitude compared to a lower scale wavelet. Assume these wavelets have an equivalent wavelength of respectively $\lambda_{\psi_1} > \lambda_{\psi_2}$. The correlation of the wavelet ψ_1 with a sine (amplitude 1, period of λ_{ψ_1}), results in a smaller value than the correlation between ψ_2 a sine with the same amplitude but period λ_{ψ_2}. By dividing the results by the corresponding scales, this 'problem' is solved.

However, if we add noise to the signal, the RWPS and RGWS are disturbed differently than the WPS and the EDS. The WPS and GWPS of the noisy signal are shown in Figure 2.6e and 2.6f. The power of white Gaussian noise is equally distributed over all frequencies [55], which is clear in from EDS and the GWS (Figure 2.6a, 2.6g). When applying the rectification as proposed by Liu et al. [32], the energy of the wavelet becomes dependent on the scale of the wavelet. The energy in the low scale wavelet is larger than the energy in the high scale wavelet, which leads to the linear decrease in noise power as shown in the RGWS in Figure 2.6h.

Scaling of energy

The heart of the problem described in Demonstration 2.1 lies in the definition of the Fourier and wavelet analysis. The discrete coefficients do not contain information for one specific frequency (at a specific time), but information over the neighbourhood [32]. These neighbourhoods are graphically shown in Figure 2.1. To define a physically consistent energy, the coefficients have to be multiplied by a factor. In a global analysis as Fourier analysis, this factor is independent of the scale, which therefore does not affect the analysis. In wavelet analysis, a localised analysis, this factor is dependent on the scale, and therefore these effects appear [32]. For an orthonormal wavelets basis, the derivation in (2.30) is correct. However, all popular wavelets used in time-frequency analysis lack this characteristic[4] and thus this introduced scaling is not correct.

This difference between the energy scaling in the Fourier spectrum and the wavelet power spectrum is a threshold for analysts to use this method. An often used solution is to scale the WPS values logarithmically, which decreases the difference in peak height (optically). The other problem that arises it that the units of the energy expressed by the WPS are not in terms of the regular m^2/Hz for instance. The WPS, however, can be expressed in relation to energy in white Gaussian noise, because that is equal over all coefficients [55]. All in all the WPS and RWPS are effective in qualitative time-frequency analysis and not in quantitative time-frequency analysis. For quantitative analysis, it is better to use the Fourier transform or the short-term Fourier

[4] Most orthonormal discrete wavelets are for instance not symmetric, which makes them unsuitable for time-frequency analysis.

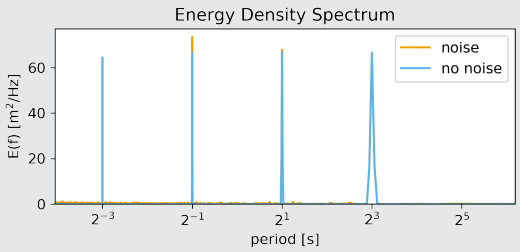

(a) VDS of the signal with and without noise

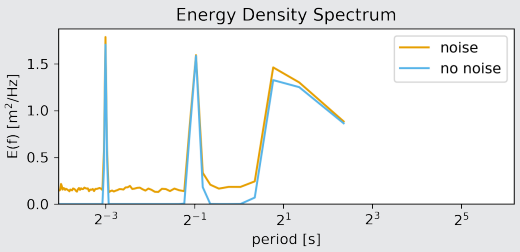

(b) Same VDS, based on 40 segments

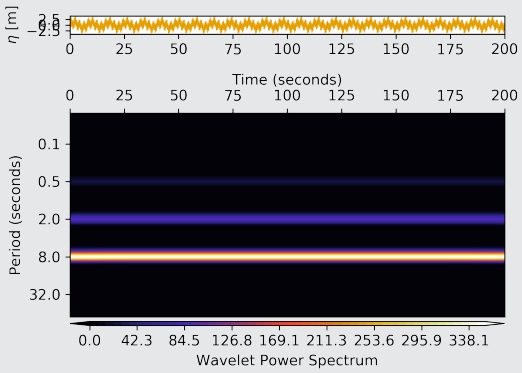

(c) WPS - no noise

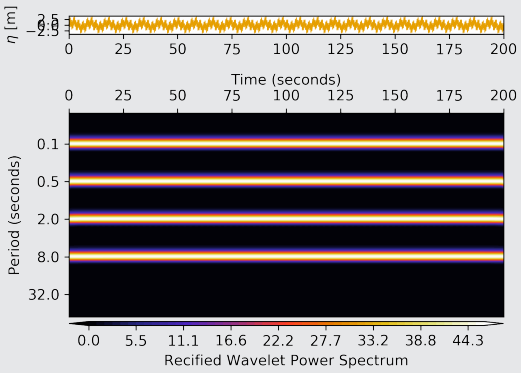

(d) RWPS - no noise

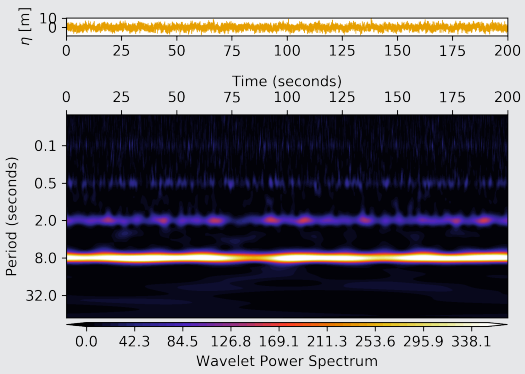

(e) WPS - noise

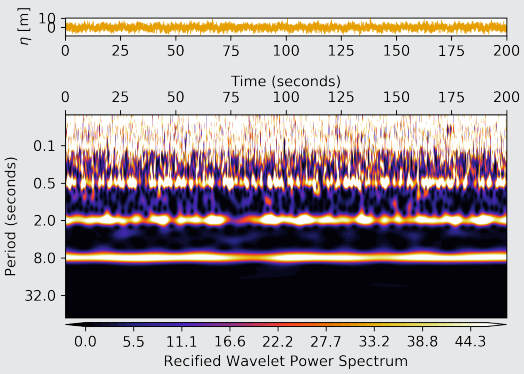

(f) RWPS - noise

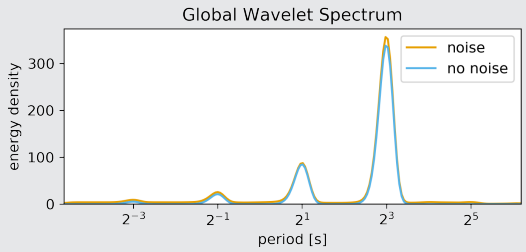

(g) GWS of both signals

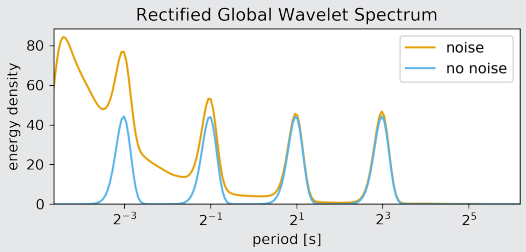

(h) RGWS of both signals

Figure 2.6: Different energy spectral densities discussed in Section 2.4. The used wavelet is the Morlet 10 wavelet.

transform. Often a quantitative analysis is about the significance of events. The theoretical noise behaviour in the wavelet domain is effective in determining the significance of time-frequency behaviour [19, 55, 64].

2.4.3. Phase

The argument (1) of both the Fourier and Wavelet coefficient, respectively $\arg(X(\omega))$ and $\arg(W(a,b))$, contains the phase difference of the complex waveform with respect to the signal. In the Fourier transform this is the complex exponential $e^{i\omega t}$ and for the wavelet transform it is the wavelet $\psi(a,b)$. Note that this wavelet has to be complex to determine the argument. The phase difference between two signals is often assessed in cross-spectral form.

2.4.4. Cross Spectral Information

The relation between different time-series is also often of interest of data analysts. Both in the Fourier as the wavelet domain this can be studied. The continuous wavelet coefficients are therefore employed in the cross-wavelet tools. The three best known are the cross-wavelet power spectrum, the wavelet phase difference and the wavelet coherency [2]. These know different applications in for instance ecology [9, 10, 48], finance [2] and meteorology [55]. Al three tools will be discussed shortly. Significance testing for these cross-wavelet tools is almost always done via Monte Carlo simulations [2].

The *cross-wavelet transform* (XWT) of two time-series $x(t)$ and $y(t)$ is defined as [2, 55]

$$S_{xy}^{w} = W\{x\}W^{*}\{y\}. \tag{2.32}$$

The XWT exposes region with high common power and reveals information about the phase relationship [22]. The quantity S_{xy}^{w} can be divided by the scale it is associated with, to produce the Rectified Cross-wavelet Spectrum (RXWS). The cross-wavelet power spectrum is defined by the modulus of the given product, $|S_{xy}^{w}|$, and illustrates the local correlation between the two time-series at each scale. The complex argument $\arg(W^{xy})$ can be interpreted as the local relative phase between x and y. Normalisation of both time-series will result in a different cross-wavelet spectrum if they are of different magnitudes. By normalising both series, the regions of high power correlation are not dominated by the time-series with the larger variance anymore. This will not have any effect on the phase behaviour that can be extracted from the XWT. The *cross-power spectral density*, the equivalent of the XWT in the Fourier domain, is defined as the Fourier transform of the cross-correlation (2.32) of two signals and denoted by S_{xy}^{f}. This quantity is always real and therefore only indicates frequencies of common high power [46].

The phase difference of two wavelet transforms indicates the delay of the oscillations between two time-series as a function of time and scale and is defined as the argument of the XWT (1) [2, 55]. Different values point to lagging or leading phase of the function x or y as:

$$\arg(S_{xy}^{w}) \in \begin{cases} (0,\pi/2) & \text{series are in phase, } y \text{ is leading with phase } \phi_{x,y}, \\ (-\pi/2,0) & \text{series are in phase, } x \text{ is leading with phase } -\phi_{x,y}, \\ \{-\pi,\pi\} & x \text{ and } y \text{ are in anti phase}, \\ (\pi/2,\pi) & x \text{ is leading}, \\ (-\pi,-\pi/2) & y \text{ is leading}. \end{cases}$$

2.4.5. Coherence

Another measure for correlation between two time-series is the *coherence*. Two waves are said to be coherent if they have the same wavelength and there is a constant phase difference between them [41]. Where the cross-spectra correlates regions of high power, the coherence correlates regions of constant phase difference. The term coherence is used in the Fourier domain as well, which is called coherence. Coherence in the wavelet domain will be referred to as wavelet coherence. The coherence (in the Fourier domain) between two continuous functions $x(t)$ and $y(t)$ is defined as [50]

$$\gamma_{xy}^{2}(\omega) = \frac{|S_{xy}^{f}(\omega)|^{2}}{S_{xx}^{f}(\omega)S_{yy}^{f}(\omega)}. \tag{2.33}$$

For this value holds $0 \leq \gamma_{xy}^{2}(\omega) \leq 1$.

This value can be read as the fractional portion of the output power that is (linearly) contributed by the input power. So if $x(t) = y(t)$ the coherence equals 1. This value of 1 implies that the two signals are linearly

related. If the signals are uncorrelated, then $S_{xy}(\omega) = 0$ and so will the coherence be. Any value in between 0 and 1 indicates a partially linear relationship. This difference has three main contributors [22]:

1. In both signals noise can be present;
2. The two signals are not completely linearly related, there is some non-linear relation between the two;
3. The signal $y(t)$ is determined not only by $x(t)$ but also by other input signals.

When this coherence function is directly implemented in the discrete functions, all values are equal to 1 even if the signals are uncorrelated. So when sampled signals are used, the estimates of the smoothed power and cross-spectral density functions should be used [50], using a smoothing function $S()$:

$$\tilde{\gamma}^2_{xy}(\omega) = \frac{\left|S\left(S^f{}_{xy}(\omega)\right)\right|^2}{S\left(S^f{}_{xx}(\omega)\right) S\left(S^f{}_{yy}(\omega)\right)}. \tag{2.34}$$

If no smoothing is applied the sampled coherence function $\hat{\gamma}^2_{xy}$ will be one for all ω [50], this even holds for unrelated signals. By smoothing the three different variables of the sampled coherence function $\tilde{\gamma}^2_{xy}$, the coherence will be close to the real coherence γ^2_{xy}. The smoothing, however, will result in a reduced frequency resolution. For more considerations regarding this smoothing, the reader is referred to Shin and Hammond [50].

Wavelet Coherence

The described coherence functions results are only valid for stationary signal cases [61]. When non-stationary signals need to be addressed, the wavelet coherence is used. The continuous wavelet coherence (WC) of functions x and y for scale a and translation b is defined as [22]

$$\gamma^2_{xy}(a,b) = \frac{\left|S\left(a^{-1}S^w_{xy}(a,b)\right)\right|^2}{S\left(a^{-1}\left|S^w_y(a,b)\right|^2\right) \cdot S\left(a^{-1}\left|S^w_y(a,b)\right|^2\right)}, \tag{2.35}$$

where $S()$ is again a smoothing operator. This time the smoothing operator consists of a smoothing in time and in scale: $S(W) = S_{\text{time}}(S_{\text{scale}}(W))$. Again, without smoothing operator, the wavelet coherence will be one everywhere, just as in the Fourier case [55]. The wavelet coherence can be seen as a localised correlation coefficient in the time-frequency space, i.e. when there is little power in the XWT coherence can still be detected. However, to find this relation, some time and frequency information is lost due to the smoothing process. For further considerations of this wavelet coherence smoothing and a suitable smoothing operator for the Morlet wavelet, the reader is referred to Grinsted et al. [22]. There are two main advantages of the wavelet coherence (WC) over the cross-wavelet transform (XWT): the first is that the WC is a normalised value, the second one is that the WC is less disturbed by spurious coincidences compared to the XWT. Though there are some redundancies between the XWT and WC, they do complement each other [22].

2.4.6. Stationarity Signals and Linear Representation

The definition of a stationary signal as presented in (2.2) is difficult to understand. The other explanation comes from the time-frequency domain. Assume a simple non-stationary signal: a recording of length $2T$ seconds, the first T seconds are filled with no signal, followed by a sine wave with amplitude 1 for the next T seconds. If this signal is Fourier transformed and the power per wave is expressed in the ESD, this signal will be interpreted as the presence of wave with an amplitude of $1/2$ over the whole time domain. This is not true, and therefore the Fourier transform is unsuited to apply to non-stationary signals, i.e. the wrong conclusions may be drawn. However, if the wavelet transform is applied, there will be a clear difference in the first and last part of the signal, which may result in better conclusions. This is why the stationarity of a signal can also be recognised on its time-frequency behaviour, i.e. if the frequency content of a signal does not change over time, it is often referred to as stationary.

The Fourier and wavelet transform do share an important characteristic: when a signal is transformed (either Fourier or wavelet), the signal is represented as a linear combination of basis functions ($e_\alpha(t)$ in equation 2.5, respectively complex exponentials or wavelets). The description of a non-linear signal by means of a linear combination of basis functions does have a mathematical meaning. However, this does often not have a physical meaning [25]. This means that a non-linear signal is 'identified' as a sum of harmonics (mathematical), but physically it can be something else, for instance, one wave with a changing harmonic. This is a

characteristic that should be kept in mind when analysing signals; non-linear signals are not recognised as such in both methods.

2.5. Digital Signal Processing

All presented methods have a decomposition and a reconstruction formula, i.e. the transformations can be reversed. The application of the reconstruction allows for signal processing in these domains, by decomposing, adjusting the coefficients and reconstructing. Signal processing using the DCWT is not addressed much because filtering in the discrete wavelet domain is more efficient. On the one hand due to the faster FWT implementation and on the other hand due to the relative large reconstruction error of the DCWT. The reconstruction error of the FFT or DWT, which are often only affected by the rounding error of the computer, is normally in the absolute range of 10^{-15}.

2.5.1. Elements of a Signal

When applying digital signal processing, filters are often used. They are used to separate different elements in the signal from the rest of the signal. A signal is therefore assumed to be a linear combination of different signal elements. A number of these elements is therefore addressed here shortly. In Section 2.5.2 the use of filters in frequency and wavelet domain are explained.

Noise

A received waveform $x(t) = s(t) + v(t)$ usually consists of two parts: a desired part $s(t)$, containing the information, and the undesired part $v(t)$ [11]. The desired part is referred to as the *signal*, the undesired part as *noise*. The sum of these parts $s(t)$ is then referred to as the *noisy signal* or *received signal*. This is noise in the broadest sense of the word, and it has all kinds of shapes and sizes: it can be 'added' to the desired signal by the sender, the measurement equipment or other processes. Often noise is assumed to be of constant power in all frequencies, *white noise*, but could also be contained in specific frequencies, which is known as *coloured noise*. These names are in convention with light; white light contains photons of all frequencies and coloured light only those of specific frequencies. Noise does not always have to be of constant power, but can, for instance, fade out or build up. This is known as *non-stationary noise*. The amount of noise on a signal is often described using the signal-to-noise ratio, SNR for short [11]. It is the ratio between the power of the signal and the power of the noise:

$$\text{SNR} = \frac{P_{\text{signal}}}{P_{\text{noise}}}, \tag{2.36}$$

often expressed in decibels. If the variance of the signal and noise are known and the signal is of zero-mean, the SNR is also expressed by

$$\text{SNR} = \frac{\sigma^2_{\text{signal}}}{\sigma^2_{\text{noise}}}. \tag{2.37}$$

Transients and Discontinuities

The detection of transients and discontinuities (or edges in signal analysis) is very important in most engineering fields. Any discontinuity measured by a sensor may characterise an event [42]. *Transients* are always of short duration and unpredictable nature, changing frequency over time and often decay fast: the parameters of the transient and its arrival time are unknown. In the Fourier domain the STFT is used to determine the location of the transient. The trade-off between time and frequency chosen beforehand influences the detection of a certain transient. The time-frequency representation of the WT, on the other hand, enables exact localisation of any abrupt change, impossible for the STFT. This is not only applicable to transients, but also to discontinuities. Transients usually only appear in the lower scales of the discrete wavelet transform, whereas the higher scales represent the low-frequency basis of the signal. The choice of wavelet is very important in the detection of transients; since the wavelet coefficients represent the correlation between the transient and the wavelet function used. The detection will improve when the shape of the transient and wavelet are similar [42]. Discontinuities are recognizable by their high detail coefficients over a lot of decomposition levels in the discrete wavelet case. Especially the Haar wavelet had good discontinuity recognising properties because it is a discontinuous wavelet.

Amplification or delay

The noise theory discussed until now concerns noise as an addition to the signal: additional noise. Often a large share of the mutation of a signal consists of this additional noise [11]. However, noise can also adjust or adapt the signal in other ways: noise can also be a distortion of the amplification or delay of (parts of) the signal. Amplification (or damping) and the delay of parts of the signal may have different causes. Note that if the whole signal has been amplified or delayed with the same factor, this does not affect the signal analysis that much. These two noise effects are often modelled as filters. Damping is often a result of the range of the measurement equipment. For instance, the detection of sounds by the human ear rapidly decays under 50 Hz, which can be modelled as a damping. In a spectrum or WPS, this can be noted from the amplification or damping of specific frequencies or detail coefficients.

Delays can have a lot of different causes, also often modelled as a filter. As addressed before, a delay is modelled as a phase change in the Fourier domain (G.2). Therefore it is also known as *phase noise*. Phase noise is hard to detect because it is a non-linear effect. E.g. $\sin(\omega_0 t + \theta(t))$ has a basis frequency of $\omega_0 = 2\pi f_0$, however, this might be altered by the phase change $\theta(t)$. Because both the wavelet and Fourier transform are linear transforms, some phase changes $\theta(t)$ might be hard to detect: by the linearity they are modelled as different frequencies instead of one phase changing frequency.

2.5.2. Filters

These different signal elements are often filtered from the signal. For instance, noise filtering or denoising is a much applied in signal processing. The goal of denoising is to filter the noise present in the measurement without distorting the underlying signal. In the Fourier domain, a filter removes energy from some frequency bands. Generally speaking, there are two types of filters in this domain: low-pass filters and high-pass filters, respectively filtering out high and low frequencies from the signal. Combinations of these filters lead to band-pass, band-stop and more kinds of filters [46].

As discussed before, discrete wavelet coefficients are mainly used in signal processing, especially filtering. The difference with the filters in the Fourier domain is that the discrete wavelet filters can filter out some elements in a frequency band, while other elements pass. This is impossible for a Fourier filter: all elements in a frequency band are damped with the same factor.

The first level of the discrete wavelet approximation coefficients addresses the highest frequencies present in the signal. As the levels of decomposition rise, the addressed frequencies are lower; in the low scale detail levels, a lot of high-frequency components of the signal are caught. Noise can be present in all decomposition levels, however, often there is much noise in the high frequencies (low levels), with respect to the signal power in the higher levels. Only some of the coefficients are important in supporting discontinuities or other high-frequency signal components. This assumption lies at the basis of FWT filtering: by applying a threshold to the coefficients in the low scales, noise is reduced.

The two most used ways of thresholding are hard and soft thresholding, though there are a lot of 'intermediate' thresholding possibilities [3], as shown in Figure 2.7. Hard thresholding for a threshold T is defined by (w is the discrete wavelet coefficient):

$$w_{\text{new}} = \begin{cases} 0 & |w| < T \\ w & \text{else} \end{cases}, \tag{2.38}$$

and soft thresholding by

$$w_{\text{new}} = \begin{cases} 0 & |w| < T \\ w - T & w \geq T \\ w + T & w \leq -T \end{cases}. \tag{2.39}$$

Applying the thresholds is a simple process, the crux lies in determining the thresholds. The most used threshold is the so-called universal threshold [51]:

$$T = \sigma_1^{\text{noise}} \sqrt{2\log(N_1)}. \tag{2.40}$$

This universal threshold is based on the standard deviation of the noise of the first detail level σ_1^{noise}. N_1 is the number of elements of the first detail level. The standard deviation of the noise is often replaced by an estimator based on the Median of Absolute Derivation (MAD) of the detail level d_i, $\tilde{\sigma}_i{}^{\text{noise}} = \text{MAD}(d_i)/0.675$ [42] based on a Gaussian White Noise (GWN) assumption.

By using different thresholds, different types of signal elements can be taken out. The results of filtering in the wavelet domain can be even further improved by using techniques like:

1. Shifting [28] uses the not shift invariant characteristic of the FWT. By shifting the original signal and averaging the denoised copies, a better approximation of the underlying signal can be reached.
2. Cycle spinning [28] is a process that shifts the approximation coefficients at every step.
3. A combination of different algorithms, or cascading different algorithms by using the output of one algorithm as input for another.

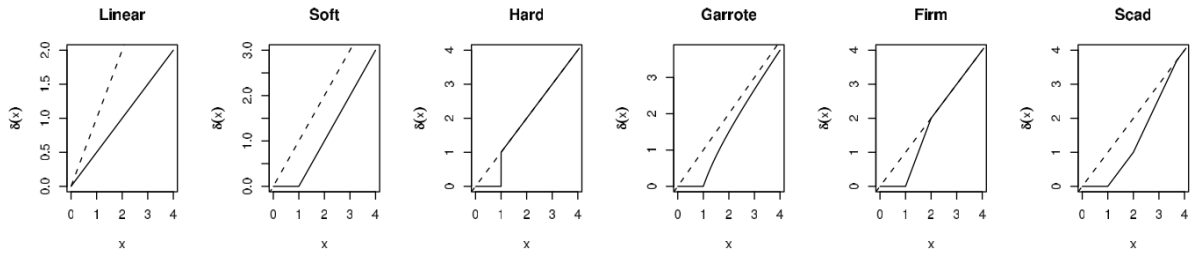

Figure 2.7: Different types of discrete wavelet thresholding. From Antoniadis [3, Figure 1].

Linearity and Stationarity

Linearity and stationary are characteristics of a signal. Both Fourier and wavelet analysis are linear analyses; they decompose the signal into a sum of linear combinations. Elements that can be filtered have to be elements in this sum. Non-linear elements thus are hard to filter by either the Fourier or wavelet transform, because they are not described by a linear combination.

Fourier analysis is only suited for stationary signals; the frequency content of a signal cannot change over time. The magnitude of a Fourier coefficient $|X(\omega)|$ is either 0 or larger than that, i.e. the frequency is present in the signal or not. So if a frequency component is filtered out, it is filtered from the signal at all times. In the wavelet transform the magnitude of a wavelet with scale a_1 and translation b_1 can be larger than zero, while at another time b_2 $|X(a_1, b_2)| = 0$. Signals with a changing frequency content, are better filtered using the wavelet transform. One can decide to not address a certain frequency at a certain time, but at another time it can be filtered.

2.5.3. Other Techniques

Time-frequency analysis and (digital) signal processes are not only implemented in the Fourier and wavelet domain. Of course the behaviour of the signal in the time domain gives information about the signal as well. Filtering signals without transformations is also applied, i.e. filtering in the time domain. The advantage of this type of filtering is that fewer calculations are needed because the signal does not have to be transformed (twice). These filters are often referred to as signal smoothing filters, for they optically make the signal smoother. The most used filters are [39]: the (weighted) moving average filter and the Savitsky-Golay filter. Another type of filter is the Kalman filter, which is much more computationally intensive. This filter filters signals based on a model prediction of the signal and the signal itself [62]. It can be applied on temporal information, but also in the Fourier or wavelet domain.

Multi-channel Approach

The focus of this thesis lies in *single-channel* noise reduction methods. In this method, it is assumed that there is only one sensor available. In *multi-channel* noise reduction methods, the input of different sensors is used to suppress noise. A good example is a modern mobile phone, which often has two or more microphones to record a voice when calling, to be able to suppress noise better. This method is most used in speech enhancement, however, multi-channel noise reduction can have some application in the field of coastal engineering as well. The multi-channel approach can be applied in al different kinds of domains, among which the wavelet domain.

Hilbert-Huang Transform

In time-frequency analysis there are more options than the STFT or the wavelet transform. The Hilbert Huang transform has been developed by NASA in the late 90s, to specifically analyse non-linear, non-stationary data [27]. Applications of this transform emerged around 2005 [26, 44]. This method combines an empirical mode decomposition with Hilbert spectral analysis [25]. The signal is first decomposed in so-called empirical

modes: simple harmonic components which can have variable amplitude and frequency in time. These modes are then analysed using Hilbert spectral analysis, which computes instantaneous frequencies easily. The Hilbert transform of a signal $x(t)$, $\mathcal{H}\{x\}(i\omega)$ is defined by[20]:

$$\mathcal{H}\{x\}(\omega) := \frac{1}{\pi}\mathcal{F}\{x(t)\}(\omega) * \frac{1}{\omega} = \frac{1}{\pi}\int_{-\infty}^{\infty} \frac{X(\eta)}{\omega-\eta}\ \mathrm{d}\eta.$$

In contrary to the Fourier and wavelet transform, the basis of this decomposition, the empirical modes, is adaptive. The instantaneous frequency is a controversial definition, and inceptive: when something is instantaneous, it is localised in time. However, time and frequency are inverse quantities, resulting in the ambiguity [17]. The resulting algorithm, the called the Hilbert-Huang transform has a lot of empirical support [25, 26, 44]. An overview of the comparison of the three methods is given in Table 2.1. The most important improvement of the Hilbert-Huang transform with respect to the Fourier and wavelet transform is that it is a non-linear transform, allowing better analyse of non-linear systems.

This all sounds very promising, however, the great drawback of this method is the lack of theoretical base. Due to its adaptive base, one element of the basis could counteract another element, resulting in a false energy distribution in time-frequency. This is in contrast with Fourier and wavelet analysis, which both have an elegant mathematical framework, very suitable for model building [17].

Table 2.1: Comparative summary of the Fourier, wavelet and HH transform. From [25, Tab. 1].

	Fourier	**Wavelet**	**Hilbert-Huang**
Basis	a priori: $e^{i\omega t}$	a priori: $\psi(t)$	adaptive
Frequency	convolution: global uncertainty	convolution: regional uncertainty	differentiation: local, certainty
Presentation	energy frequency STFT: energy-time-frequency	energy-time-frequency	energy-time-frequency
Non-linear	no	no	yes
Non-stationary	no	yes	yes
Feature extraction	no	discrete: no, continuous: yes	yes
Theoretical base	theory complete	theory complete	empirical base
Computation time	FFT: $\mathcal{O}(N\log_2 N)$ STFT: $\mathcal{O}(N^2\log N)$	CWT: no fast algorithm DWT (all scales): $\mathcal{O}(N^2\log N)$	$\mathcal{O}(N\log N)$

2.6. Coastal Engineering Challenges

This chapter started with the description of time-series of which some important characteristics were discussed, such as stationarity and linearity. Thereafter the field of signal analysis was explored. The different domains, to know the time, frequency and wavelet domain are summarised in Figure 2.1.

Fourier analysis and wavelet analysis are elaborately explored in respectively Section 2.2 and 2.3. The main difference between the two methods is that Fourier analysis correlates the signal with infinite complex exponentials with a certain specific frequency, whereas wavelet analysis correlates the signal with finite supported functions, that can be real or complex. This allows time-frequency analysis through wavelet coefficients. In the Fourier domain only frequencies can be studied. The discrete wavelet transform is a 'compact form' of the continuous wavelet transform, which gives other insights into signals.

In Section 2.4 different applications of both the continuous and discrete wavelet coefficients are addressed. Moreover, a clear overview of the different continuous and discrete wavelets and their different characteristics is given (in respectively Figure 2.3 and 2.5). In this last section, different coastal engineering challenges are coupled with possible solutions based on wavelets. Based on this outline, the sub-questions to answer the research question are presented.

In the field of coastal engineering, many time-series are recorded. These measurements concern both soft or hard measures. Measurements on hard measures (structures) are often conducted in an experimental setting. This often results in time-series containing pressures and forces. Soft measures are measured both in the field and in experimental settings, resulting in pressures, surface elevations, velocities and temperatures. Furthermore, wind speeds, water temperature etcetera are recorded and often used as input for models.

Time-frequency Analysis

Time-frequency analysis allows analysts to get an overview of the behaviour of a signal, which sometimes is not directly observed from the time-series or the spectrum. Especially when signals are non-stationary, i.e. some frequency components can dominate a time-series at some time, while at another time they are not present, the Fourier spectrum is not worth much. Missing data points or other (known) disturbances often appear in long-term soft measure measurements, for instance, due to deterioration of the equipment or power failure. A lot of experience with these signals is needed to correctly analyse them. Wavelet analysis might provide solutions concerning these problems.

A threshold in the use of wavelet analysis in many fields is the different concept of 'energy', expressed in the wavelet power spectrum. The correction per scale by Liu et al. [32] presented in Section 2.4.1 addresses this problem for small bandwidth phenomena, but has some drawbacks as well. In time-frequency analysis, wavelet analysis will serve better as a qualitative than a quantitative method. It is especially useful when very high and very low scale processes are in play, if the scales differ less, the short-term Fourier Transform will offer a more quantitative alternative.

Separating Waves

Time-frequency analysis is often based on the energy distribution, which is based on the magnitudes of the coefficients. An example of the use of phase information (Section 2.4.3) in coastal engineering is the separation of incident and reflected waves. Measurements record a superposition of the two, and therefore they have to be separated. This information is important for testing constructions. Constructions, or scale models of them, are tested on different characteristics such as stability and overtopping. To determine these characteristics, the reconstruction of the wave pattern (as close to the construction as possible) is indispensable. The reconstruction of the incident wave is used to determine whether the imposed spectrum is met. Based on the reflected wave a measure of absorption is determined.

The most often used method to separate these waves is based on Fourier coefficients and was proposed by Mansard and Funke [38]. Their method uses information of three gauges, which is an expansion of the analysis of Goda and Suzuki [21], who solved the problem using two measurement gauges. The expansion to N gauges was done in the early 1990's by Zelt and Skjelbreia [63]. The use of wavelet coefficients in this application is rather new. In 2010 a method was proposed by Ma et al. [34] using two gauges to separate waves. An expansion to multiple gauges is indispensable to show comparable results to the Fourier coefficients based methods. This subject will be treated more elaborate in Section 3.2.

Noise Reduction

The testing of constructions often includes the effect of impacts on these structures. These impacts are measured through force and pressure sensors. The impacts result in non-stationary elements in the recordings.

Examples of recordings of impacts are shown in Section F.1.3. These signals are subject to a lot of noise. Due to their non-stationary nature, it is expected that filters that apply thresholding in the discrete wavelet domain would perform better than filters in the time or frequency domain.

2.6.1. Research Questions

All in all, it can be concluded that there is a lot of potential for wavelet analysis in the field of coastal engineering. The main research question of this thesis is:

How can wavelet analysis improve time-series analysis and processing in the field of coastal engineering?

Four research questions have been drafted to answer this question. They concern the application of both amplitude and phase determined in the continuous wavelet transform, the application of the discrete wavelet transform in denoising and the added value over the current methods.

1. What improvements are necessary for the (discretised) continuous wavelet transform to improve time-frequency analysis for time-series in the field of coastal engineering?
2. Does the separation of incident and reflected waves based on wavelet coefficients for N gauges perform better than the separation based on Fourier coefficients?
3. Which discrete wavelet-based algorithm is best suited to remove noise from coastal engineering signals?
4. What is the added value of wavelet analysis over current time-series analysis methods in coastal engineering?

The thesis overview in Figure 1.1 has been expanded with these research questions in Figure 2.8. To answer the first two sub-questions, the next chapter focusses on the continuous wavelet transform. In Chapter 4 different wavelet-based noise filter algorithms are compared. The added value of both continuous and discrete wavelet transform is discussed for some coastal engineering time-series in Chapter 5. The conclusions and the answer to the main research question are presented in Chapter 6.

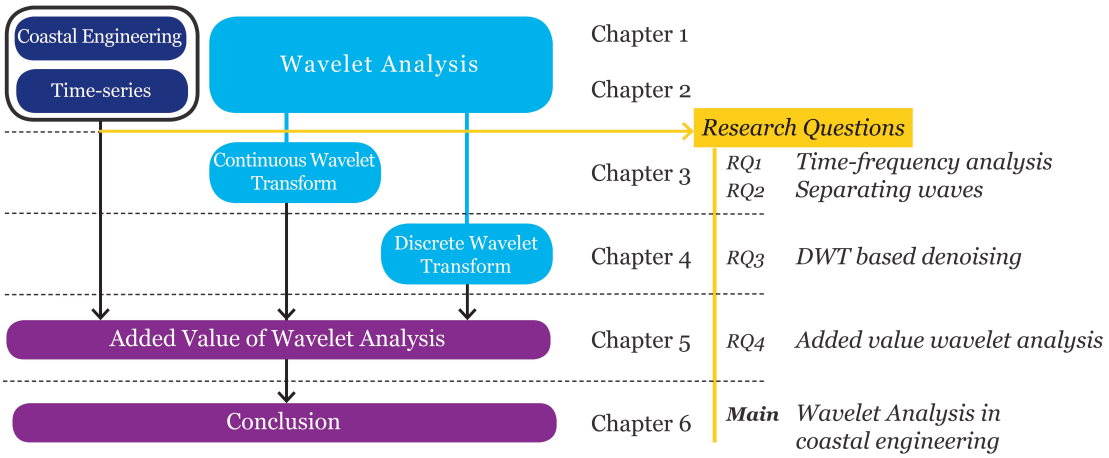

Figure 2.8: The schematic overview of the contents of this thesis expanded with the four research questions.

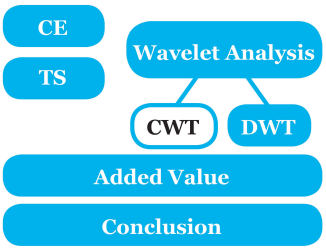

3

Continuous Wavelet Coefficients

This chapter focusses on applications of the continuous wavelet coefficients, computed using the the discretised continuous wavelet transform, DCWT, see equation 2.22. As explained in the last chapter, these coefficients are used in time-frequency analysis and to separate waves. In this chapter the wavelet coefficients based methods are compared to the Fourier coefficients based methods. First, the most used and freely available protocol to determine the DCWT of a signal by Torrence and Compo [55, 56] is presented. Their algorithm is the basis for over 5800 scientific publications (Scopus, 9 May 2017), among which some of Deltares [15, 16]. This algorithm is expanded to allow better analysis of time-series, with special interest in challenges in coastal engineering time-series (Section 3.1). This section is followed by a section with an important coastal engineering application of the continuous wavelet coefficients: the separation of 2D waves. The errors of this algorithm can be analysed using both traditional and wavelet-based measures. The added value of these expansions and improvements will be discussed in Chapter 5.

To calculate the coefficient via the DCWT (2.22) it is most efficient to utilise the convolution property (6). Torrence and Compo [55] have proposed a protocol around the algorithm to determine the reliability of the coefficients as well. The protocol is given below. To the reader unknown terms are discussed after the protocol. Furthermore, expansions and improvements are discussed per step as well.

1. Apply signal extension, by padding zeros, if necessary, this results in the signal x.
2. Compute the Fourier transform $X = \mathcal{F}\{x\}$ using the FFT.
3. Choose a wavelet function ψ (with $\Psi = \mathcal{F}\{\psi\}$) and a set of scales $\left(A = \{a_1, \ldots, a_{N_A}\}\right)$ to analyse.
4. For each scale, construct the normalised wavelet function using equation 2.23.
5. Find the wavelet transform at all scales a_j using the inverse FFT (2.24).
6. Determine the cone of influence and the Fourier wavelength at that scale. The cone of influence shows which coefficients are effected because the wavelet crosses the edge of the signal.
7. Remove any padding and contour plot the wavelet power spectrum.
8. Determine the confidence contour of the scalogram. Plot this contour and the cone of influence on top of the scalogram.

3.1. Expansion

Some steps of the presented protocol can be expanded to improve analysis of the DCWT results, specifically for time-series from the field of coastal engineering. These expansions of the original protocol are discussed in this section. The computational resources are discussed later, in Section 5.3.

1. Extending the discrete signal over its boundaries is has two reasons. The first one is the circularity assumption made in the convolution through the FFT. The convolution (5) is an infinite sum. The signal is not infinite because of its discrete nature. In the circular convolution (8) the signal is assumed to be periodic. This will lead to edge effects in the wavelet coefficients.

   Furthermore, the FFT algorithm is most effective for signals of length 2^k, $k \in \mathbb{N}$. If signal extension is applied, it is best to pad a signal with a length $2^{k-1} < L \leq 2^k$ to a length of 2^{k+1} instead of 2^k ($k \in \mathbb{N}$). In

Section 3.1.3 different extension methods are added to the just one method discussed by Torrence and Compo [55], zero padding.

2. The computation of the Fourier transform of a function in general is not hard, but when data points are missing, it is impossible to compute the Fourier transform. By adding dummy values at the missing data points, the effects on the spectrum are hard to predict. Missing data points is a frequent defect in coastal engineering time-series. In Section 3.1.4 a solution is proposed, together with two methods to access the reliability of the calculated wavelet coefficients. For cyclic time-series there will not be a cone of influence and extending is therefore not needed.
3. The choice of wavelet and set of scales influences one's analysis. Different types of continuous wavelets are already addressed in Section 2.3.3. For long signals or a large set of scales, the number of wavelet coefficients can become very large. Some considerations regarding these problems are discussed in Section 3.1.1 and 3.1.2.
5. Whether the FFT algorithm is still the best way to go for signals with missing data points is addressed in Section 3.1.4.
6. The cone of influence is based on the e-folding time of the wavelet Section 3.1.3. In Section 3.1.4 other reliability measures are addressed, that do not only address the edges of the signal, but also the missing data points.
8. The significance contour is not addressed in this research. The significance can be determined analytically or by applying Monte Carlo methods [55].

3.1.1. Choice of Wavelet, Number of Scales

The wavelets generally used in time-frequency analysis are shown in Figure 2.3. Choosing a wavelet depends on the objective of the analysis: edge detection, time-frequency analysis or phase analysis. Then there is the choice for a complex of real wavelet. Imagine a simple oscillation (a sine) and a simple wavelet. When a real wavelet and an oscillation are out of phase, the wavelet coefficient becomes very small, due to the low correlation. A complex wavelet consists of a real and a complex part. This complex part is phase shifted with respect to the real part of the complex wavelet, which allows it to express both the positive and negative parts of an oscillation in one coefficient, i.e. if the real part has a low correlation, the imaginary part has a high correlation and vice versa.

The continuous wavelets often possess a parameter which can be tweaked. This parameter influences both the centre frequency f_ψ and the bandwidth of the wavelet at scale 1, not its time support. Tweaking this parameter changes the time-frequency distribution of the wavelet. Often the higher this parameter, the smaller its bandwidth and thus the larger its time support for a specific equivalent wavelength. The parameters for different wavelets are presented in Section C.2.

Because the bandwidth of the wavelet increases as the scale increases, often a logarithmic scaling is chosen for the scales. The inverse CWT operation as defined in (2.25), assumes the use of a logarithmic scaling. This bandwidth on his term influences the number of scales that needed to cover the whole frequency domain. It is safe to assume that most wavelets cover the domain if a choice of 10 scales per octave (doubling of scales) is used [32].

3.1.2. Down-sampling

For long signals the discrete wavelet transform might become too large to store in memory, or takes much time to compute the continuous wavelet coefficients. When there is only an interest in relatively low frequencies, down-sampling can be applied to speed up the process. Down-sampling is the process of reducing the sampling rate of a time-series. A down-sampled time-series contains fewer data points, which reduces the CWT computation time and the memory needed to store the result. Down-sampling is a sampling rate conversion process [46]. The focus here lies on the sampling rate conversion in the digital domain and how this effects the CWT coefficients. Consider a signal $x[n]$ with a sampling frequency $f_x = 1/\Delta t_x$ which is down-sampled to signal $y[m]$ with $f_x > f_y = 1/\Delta t_y$. Only rational sampling rate conversion will be addressed, i.e. $f_x/f_y \in \mathbb{Q}$. First, an integer conversion factor is addressed, followed by a more general rational factor.

Down-sampling with an integer factor d, can be done by simply selecting every d^{th} value of the time-series. This is known as decimating and will lead to major aliasing effects[1]. To avoid aliasing, the bandwidth

[1] For more information about aliasing see Section A.1

of the signal $x[n]$ has to be reduced to $f_{\max} = f_x/d$. The signal can be decimated after applying the low pass filter $h[n]$, to cut off the high frequencies inducing the aliasing, i.e.

$$y[m] = \sum_{k=0}^{\infty} h[k]x[md-k]. \tag{3.1}$$

This combination of filtering and decimating is called down-sampling and it results in a time-variant system: if $x[n]$ produces $y[m]$, then $x[n-n_0]$ does only result in $y[n-n_0]$ if n_0 is a multiple of d. For the spectra of the original signal $x[n]$ ($X[k]$) and the resulting spectrum of $y[n]$ ($Y[k]$) the following relationship holds:

$$Y[k] = \frac{1}{d} X\left[\frac{k}{d}\right].$$

From this relationship can be concluded that the resulting spectrum is a scaled variant of the original spectrum. Note that this scaling does not preserve energy. The energy in the time-series is reduced with a factor $1/\sqrt{d}$. From the definition of energy given in equation 2.27 it is directly clear why there is less energy after than before: the number of data points decreases, which results in less energy.

When a signals sampling rate is converted by a rational factor i/d, it first has to be interpolated by a factor i, and then decimated by a factor d. The interpolation process by a natural factor i converts the signal $x[n]$ to the signal $w[m]$, where $f_w = if_x$. This is obtained by first adding $i-1$ zeros between successive values of $x[n]$ to obtain $v[m]$:

$$v[m] = \begin{cases} x[m/i] & m \in \{i\ell \mid \ell \in \mathbb{N}\}, \\ 0 & \text{elsewhere.} \end{cases}.$$

The spectrum of the new signal $v[m]$ has the same shape as the spectrum of $x[n]$: $V[\omega] = X[\omega i]$. The spectrum is an i-fold periodic repetition of the original spectrum. These repetitions, however, are non-unique. Thus the signal $v[m]$ has to be passed through a low pass filter $g[m]$. This filter ideally cuts off all repetitions and scales the result by a factor i so that $w[m] = x[m/i]$ for $m \in \{i\ell \mid \ell \in \mathbb{N}\}$. This results in the interpolation

$$w[m] = \sum_{k=-\infty}^{\infty} g[m-k]v[k] = \sum_{k=-\infty}^{\infty} g[m-ki]x[k].$$

When the sampling rate by a factor i/d is considered, first the signal has to be interpolated by a factor i, because this keeps the original spectral shape in tact. Then the signal can be decimated to find the signal with a new sampling rate of $f_y = f_x i/d$. The interpolation term already has a normalization term, thus the energy of the signal is conserved. However, the decimation process does not. Therefore a signal that has been resampled with a rate of i/d, will have an energy reduction of $1/\sqrt{d}$ as well. For other non-rational sampling rate conversions, different techniques can be used; those are not within the scope of this study.

Down-sampling affects the frequency content of the signal by filtering high-frequencies and preserving low frequencies. This operation, therefore, does not affect the mean of the signal, but the standard deviation of the signal will decay as the new sampling frequency increases. The discrete wavelet coefficients of a down-sampled signal have to be scaled with a factor $\sqrt{d}$ to ensure that the coefficients are equal to the original coefficients. This can be shown by substituting the original signal spectrum $X[\omega]$ for the down-sampled signals spectrum $Y[\omega]$ into equation 2.24. For $\ell = n/d$ holds:

$$W(\ell, a) = \mathcal{F}^{-1}\left\{Y(\omega_k)\Psi^*(a\omega_k)\right\} = \mathcal{F}^{-1}\left\{\sqrt{d}\frac{1}{d}X\left(\frac{\omega_k}{d}\right)\Psi^*(a\omega_k)\right\}. \tag{3.2}$$

The spectrum $\frac{1}{\sqrt{d}}X\left(\frac{\omega_k}{d}\right)$ is a scaled version of the original spectrum $X(\omega)$, with the energy preserved. Note that this is not the spectrum belonging to the down-sampled signal, but it is only used to not change the wavelet coefficients due to down-sampling. The smaller number of samples in the time-series due to down-sampling will result in a smaller number of samples in the wavelet approximation. In Figure 3.1 two different signals are compared.

Demonstration 3.1 (Down-sampling) In Figure 3.1a the wavelet power spectrum of a random signal is presented. The wavelet power spectrum of the down-sampled signal multiplied by a factor $\sqrt{50}$ is found in Figure 3.1b. From the signal at the top it is clear that the down-sampling has influenced a lot of high frequencies. These are therefore not shown; both wavelet power spectra are based on the same set of scales.

In Figure 3.1c and 3.1d, the argument of the wavelet coefficient for both signals is given. Again

the same pattern arises as before, however, note the arguments of the down-sampled signal is much coarser. This is especially clear for small periods. This is due to the decrease in resolution. The signal has 9500 data points and the down-sampled signal has less than 200. This leads to a resolution difference visible in the figures.

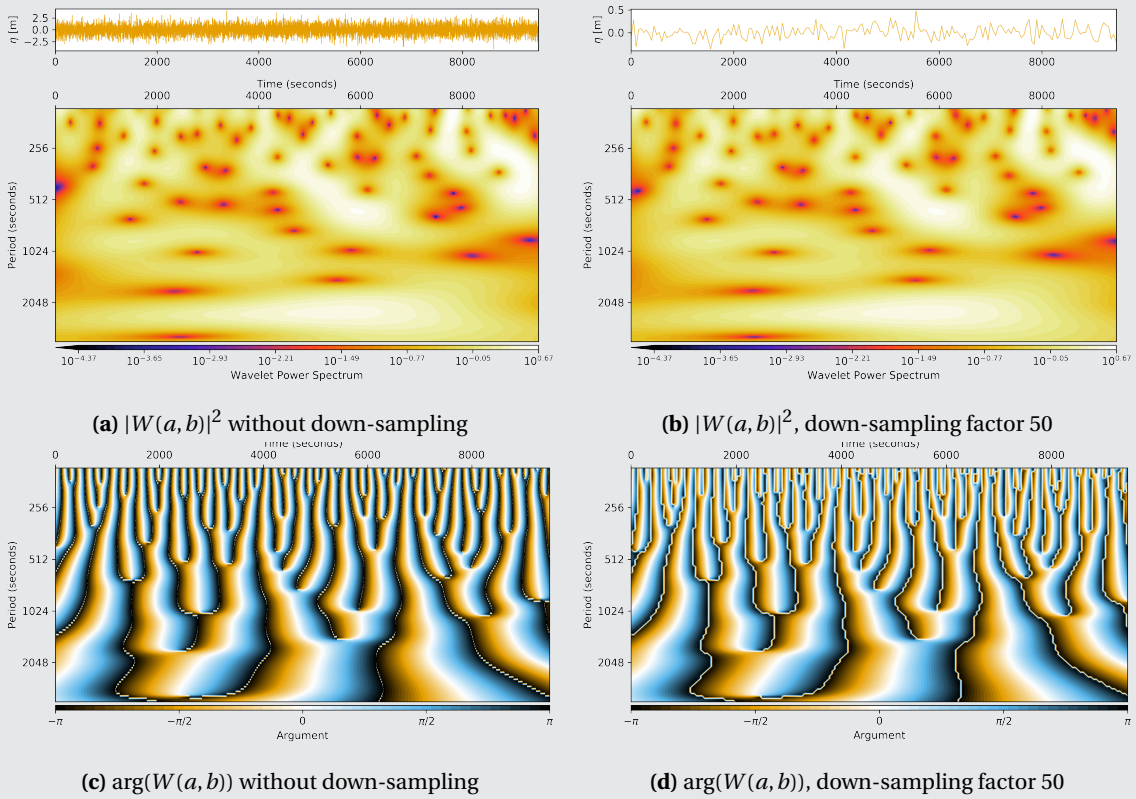

(a) $|W(a,b)|^2$ without down-sampling

(b) $|W(a,b)|^2$, down-sampling factor 50

(c) $\arg(W(a,b))$ without down-sampling

(d) $\arg(W(a,b))$, down-sampling factor 50

Figure 3.1: A random generated noise signal is down-sampled with a factor 50. Boundaries are padded with zeros.

3.1.3. Wavelet Coefficients near the Boundaries

As explained in Section 3.1, the signal is extended to prevent edge effect from distorting the time-frequency analysis near the edges of the signal. At low scales, wavelets have a small support in the time domain, so the number of affected wavelet coefficients will be small. The higher the scale, the larger the support of the wavelet in the time domain and the more wavelet coefficients are affected.

Cone of Influence

The cone of influence (COI) is the name of a line that shows which wavelet coefficients are and are not influenced by the boundaries, in theory. Outside the cone, the coefficients are expected to be influenced by the boundary. In general holds: the closer to the boundary, the more affected a coefficient will be. This cone is based the e-folding time τ_a of the used wavelet [55]. This is the time in which the wavelet power of a Delta Dirac peak at the edge of a signal has decreased by a factor e^{-2}. This time is proportional to the used scale: the higher the scale, the larger the e-folding time. The cone of influence is a guideline and not a strict border. There will still be coefficients affected by the signal extension within the cone. Strictly speaking, all coefficients within the compact support of the wavelet are influenced by the signal extension. This compact support is larger than the e-folding time. In the following paragraphs, the cone will be expanded, and the effect of missing data points on the wavelet coefficients will be added to the cone of influence.

Signal Extension

The reliability of wavelet coefficients near the edges of the signal depends on the choice of signal extension. So what are the options to pad the time-series and which ones are the best? In DWT practice a number

of paddings are proposed and implemented [54]. Some of these have also been implemented in the CWT algorithm. After itemising these different extensions, including some advantages and disadvantages, some recommendation for different kinds of signals are presented in Figure 3.2.

- No padding:

$$\left| \; x_0 \quad x_1 \quad \cdots \quad x_{N-2} \quad x_{N-1} \; \right|$$

  No padding is the most obvious and easy choice to make. As mentioned before, some FFT algorithms perform optimal when a signal of length $\ell_{\text{optimal}} \in \{2^k \mid k \in \mathbb{N}\}$ is used. So when padding has to be applied, it makes sense to lengthen the signal up to a length in $\{2^k \mid k \in \mathbb{N}\}$. For the signals we use, the time efficiency is negligible. The FFT algorithm has the circular convolution property [11]; when a convolution is computed through the Fourier transform, the signal is treated as a periodic signal. This could lead to unexpected behaviour at the beginning and end of the signal. When padding is applied, it is convenient to make sure that the signal is not extended with just a few data points, but with many, that way the circularity will have little influence on the result. Of course, padding is superfluous when handling a cyclic signal.

- Zero padding:

$$\cdots \quad 0 \quad 0 \; \left| \; x_0 \quad x_1 \quad \cdots \quad x_{N-2} \quad x_{N-1} \; \right| \; 0 \quad 0 \quad \cdots$$

  This type of padding is never advised. At first glance the zeros do not contribute anything to the coefficients near the edge. This is true, however, this can create large jumps in the signal, which leads to unwanted high and low scale behaviour near the edges of the signal.

- Constant padding: repeating the values x_0 and x_{N-1} at the edges of the signal

$$\cdots \quad x_0 \quad x_0 \; \left| \; x_0 \quad x_1 \quad \cdots \quad x_{N-2} \quad x_{N-1} \; \right| \; x_{N-1} \quad x_{N-1} \quad \cdots$$

  This type of padding will not lead to high coefficients at low scales, but might lead to high coefficients in the high scales. Advised to use when $|x_{N-1} - x_0|$ is relatively large.

- Symmetric padding: the series is mirrored in the edges

$$\cdots \quad x_1 \quad x_0 \; \left| \; x_0 \quad x_1 \quad \cdots \quad x_{N-2} \quad x_{N-1} \; \right| \; x_{N-1} \quad x_{N-2} \quad \cdots$$

- Reflect padding: the series is mirrored in the points x_0 and x_{N-1}

$$\cdots \quad x_2 \quad x_1 \; \left| \; x_0 \quad x_1 \quad \cdots \quad x_{N-2} \quad x_{N-1} \; \right| \; x_{N-2} \quad x_{N-3} \quad \cdots$$

- Periodic padding: the signal is assumed periodic

$$\cdots \quad x_{N-2} \quad x_{N-1} \; \left| \; x_0 \quad x_1 \quad \cdots \quad x_{N-2} \quad x_{N-1} \; \right| \; x_0 \quad x_1 \quad \cdots$$

  Periodic padding would lead to almost the same scalogram as when no padding is applied. The padded signal is longer than the original signal, which allows higher scale wavelets (with a long time support) in the analysis. For high scales, the support of the wavelet can be important to improve the analysis.

  Symmetric, reflect and periodic padding all are best applicable to periodic signals. The difference between symmetric or reflect padding is the repetition of the value at the edge of the signal. This will mostly affect the low scale coefficient behaviour. When $|x_{N-1} - x_0|$ is relatively large, reflect and symmetric padding are chosen above periodic padding. E.g. periodic padding will then lead to high coefficients in the low scales.

- Linear padding: the end points of the signal are connected linearly:
  ($\Delta = x_{N-1} - x_0$, h is the number of data points to add)

$$\cdots \quad \left(x_0 - 2\frac{\Delta}{h}\right) \quad \left(x_0 - \frac{\Delta}{h}\right) \; \left| \; x_0 \quad x_1 \quad \cdots \quad x_{N-2} \quad x_{N-1} \; \right| \; \left(x_{N-1} + \frac{\Delta}{h}\right) \quad \left(x_{N-1} + 2\frac{\Delta}{h}\right) \quad \cdots$$

  This type of padding may result in high low scale coefficients, because of the abrupt change of derivative at the edges. For a relatively large value of Δ also high scale coefficients will increase.

- Linear continuation: the ends are extended using the first derivatives in the ends ($d_1 = x_0 - x_1$, $d_N = x_{N-1} - x_{N-2}$)

$$\cdots \quad (x_0 - 2d_1) \quad (x_0 - d_1) \mid x_0 \quad x_1 \quad \cdots \quad x_{N-2} \quad x_{N-1} \mid (x_{N-1} + d_N) \quad (x_{N-1} + 2d_N) \quad \cdots$$

  This type of padding is not advised to use. The derivative based on two neighbouring points can be very large due to the erratic behaviour of (noisy) measurements.

- Smooth padding: instead of using the first order derivative (linear continuation), higher order derivatives are used.
- Smooth padding: in stead of using the derivative based on the edge values, the derivative is based on the difference over the whole signal, i.e. $x_0 - x_{N-1}$. For signals with a trend (i.e. non-stationary) this might be very effective.
- Mean value padding: $\bar{x} = \frac{1}{N} \sum_{i=0}^{N-1} x_i$

$$\cdots \quad \bar{x} \quad \bar{x} \mid x_0 \quad x_1 \quad \cdots \quad x_{N-2} \quad x_{N-1} \mid \bar{x} \quad \bar{x} \quad \cdots$$

  This type of padding has the same effect as zero-padding on a normalised signal. It might lead to some spurious low scale coefficients, but for the high scales, it will be an effective estimator of the signal. Do not use when the signal has a trend.

- Noise padding: add noise to both ends, this could be from a Gaussian distribution or a random walk.

$$\cdots \quad \mathcal{N}(\bar{x}, \text{var}) \quad \mathcal{N}(\bar{x}, \text{var}) \mid x_0 \quad x_1 \quad \cdots \quad x_{N-2} \quad x_{N-1} \mid \mathcal{N}(\bar{x}, \text{var}) \quad \mathcal{N}(\bar{x}, \text{var}) \quad \cdots$$

  On high scale coefficients the effects will be more or less the same as for the mean value padding. The noisy behaviour will result a unpredictable effect at all scales and is not implemented therefore.

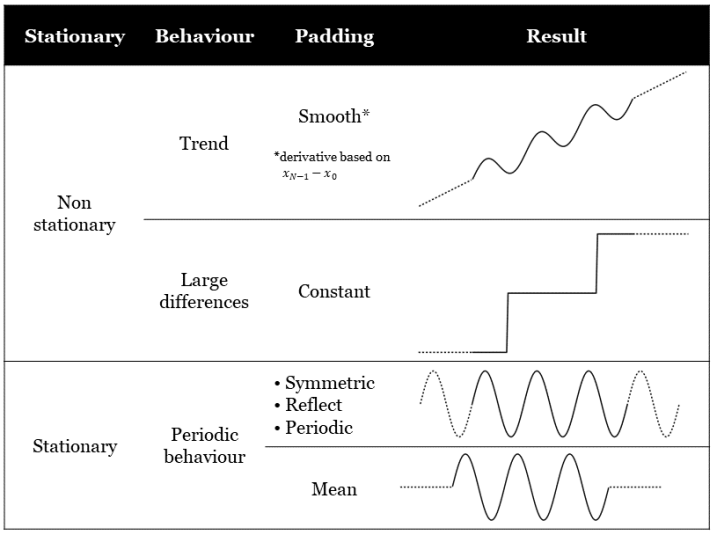

Figure 3.2: Different signals and the preferred signal extension method. For more explanation of the pro's and con's of a method, consult the more elaborate overview above.

3.1.4. Missing Data Points

Time-series in coastal engineering often have some missing data points. These defects are caused by many different causes, for instance, an equipment-damaging storm or power failure at sea. When the equipment has been restarted, the measurements are often continued. When applying Fourier analysis, it is only valid to asses the spectrum when the signal is stationary. Missing data points cannot be part of a stationary signal. When these missing data points are replaced by values to apply the Fourier Transform, the signal stays non-stationary. The spectrum, therefore, does not reflect the frequencies of uninterrupted signal. A set of consecutive missing data points is called a gap. Often, a gap is filled with NaN's[2]. When there is a NaN in a time-series, many computations return NaN's as well, resulting in a large disturbance in the analysis. Therefore these have to be addressed; there are two relatively simple ways:

- Implement the convolution form of the DCWT algorithm. When a NaN appears in the computation, the coefficient will become a NaN as well, which will lead to a scalogram with blank spots. However, the most efficient convolution algorithms will result in all NaN coefficients, even if the NaN is not in the time support of the wavelet. Moreover, blank spots do not have any indication of reliability or whatsoever. It is just a yes or no: a NaN has or has not been part of the computation.
- When using the FFT form of the DCWT algorithm, there cannot be any NaN's in the signal, because this will lead to a full NaN FFT. To use this implementation of the algorithm, missing data points have to be filled in. This will lead to a full scalogram, however, the cone of influence has to be adapted in such a way that it shows the influence of not only the boundary but also of the NaN's.

The second option has been implemented and tested with coastal engineering data. There are different ways to fill the 'blank' spaces. We will consider two cases; the NaN values are depicted with a dash (−):

- NaN('s) at the edge of the signal:
  $\boldsymbol{x} = \begin{bmatrix} - & \cdots & - & x_k & x_{k+1} & \cdots & x_{N-1} \end{bmatrix}$ or $\boldsymbol{x} = \begin{bmatrix} x_0 & x_1 & \cdots & x_k & - & \cdots & - \end{bmatrix}$.
  These are best addressed by the different signal extension modes discussed before; i.e. omit the missing data points near the edges before applying signal extension.
- NaN('s) not at the edge of the signal: $\boldsymbol{x} = \begin{bmatrix} x_0 & \cdots & x_k & - & \cdots & - & x_\ell & \cdots & x_{N-1} \end{bmatrix}$, which cannot be addressed by the different signal extension modes.

Of course multiple gaps can occur in a signal. Again there are many ways to replace the missing data points:

- Zero filling: replace the missing values by 0's.
- Linear filling: fill the gap with a linear interpolation between the values adjacent to the gap.
- Noise filling: replace the missing values with random noise.
- Mean value filling: replace the missing values by the mean value of the time-series.
- Median filling: replace the missing values by the median of the time-series.
- Higher order interpolation methods can be used to fill values within gaps. However, for these methods to work, there have to be enough values at the edges of the gap. This cannot be assured for field data, where effects like $\begin{bmatrix} \cdots & - & x_i & - & \cdots \end{bmatrix}$ can occur.

Note that the Fourier transform can be applied to time-series where the missing data points are filled as well. The filled data points are non-stationary signal elements, which cause unwanted effects in the resulting spectrum. For a signal with constant frequency content over the whole time, a decrease in power over the whole spectrum is expected when some data points are eliminated, plus some effects of the jumps at the edges of the filling. The effect on a signal with a changing frequency content is addressed in Demonstration 3.2.

Demonstration 3.2 (Effect of missing data points on spectrum) In Figure 3.3a two signals are plotted. The original signal consists of 100 random real waves plus a non-linear element: a waveform with a linearly increasing frequency from 0 to 500 Hz over the whole duration. In the other signal, 10% of the data points are swapped for zeros. If the spectra are compared, we note that for many frequencies the energy indeed is approximately 10% less than the energy of the original signal. However, in the band 200 - 350 Hz this is not true. The non-linear element loses more power than the waves and thus the spectrum is affected. This effect cannot be predicted when the underlying signal

[2] NaN is short for 'not any number'

element is unknown.

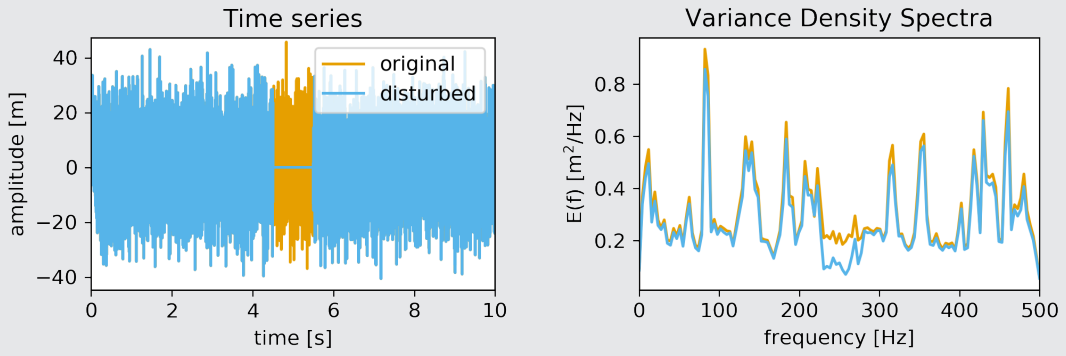

(a) A non-stationary signal and 10% of its data points missing, filled with zeros.

(b) The variance density spectra of both signals.

Figure 3.3: A signal, its power spectral density and the effect if 10% of the data points are missing.

Expanding the Cone of Influence

In the case of the wavelet power spectrum, some of the coefficients near the gap will be affected, but not all coefficients as is the case for the spectrum. This is due to the finite support of the wavelet. Some coefficients, such as low scale, with a time support within the gap, will be affected severely. The same wavelet with a time support completely outside the gap will not be affected at all. So, a lot of coefficients are affected a bit, and therefore an expression for the degree of affectedness will be derived. If the edges of the gaps are interpreted as beginnings and ends of signals, the cone of influence can be divided into multiple cones of influence.

Demonstration 3.3 (Cones of influence) For the coming demonstrations, gaps are made into a signal with zeros. This signal is shown in Figure 3.4a. It contains only zeros and some gaps. The gaps from left to right have a length of 100, 10, 50, 217, 1 data point(s). The sampling frequency of this signal is 1 Hz.

In that same Figure, the expansion based on the cone of influence is shown. Expected is that the missing of one data point (last gap) should influence a little number of wavelet coefficients. However, in the figure is shown that the effect of one missing data point is enormous. Therefore, a different solution has to be found.

Zones of Influence

Consider a wavelet at scale a. The cone of influence is based on the fact that a certain part of the wavelet extends over the border, based on the e-folding time. Assume this part to be q. If one data point is missing from the signal, the wavelet at scale a is affected less than this part q, however, by the expansion of the cone of influence, it is ruled out. Therefore a better measure can be developed. This measure is expressed in the fraction g, determined per translation n and scale a:

$$g_{an} = \frac{\text{number of known data points in time-series for } t \in [n - \tau_a \cdot a, n + \tau_a \cdot a]}{\text{total number of data points in } t \in [n - \tau_a \cdot a, n + \tau_a \cdot a]}. \tag{3.3}$$

If this fraction g is 1, there are no missing data points in the 'significant' time support of the wavelet. If this fraction is 0, all data points within this time support are missing. The values that are padded at the boundaries are considered as NaNs as well. The example presented in Demonstration 3.3 is expanded using this method and presented in Demonstration 3.4. Note that the shapes are not cones anymore and therefore the term 'Zones of Influence' will be used from now on (abbreviated to ZOI).

Demonstration 3.4 (Zones of influence 1.0) In Figure 3.4b the contours based on a value of $g = 0.9$ are shown. If the value of g is equal to 1, the cones of influence from Figure 3.4a are retrieved. As the period increases, the time support of the influence increases until there is a horizontal line and the influence stops. Even a non-connected area is created at about (5000, 1000). The horizontal line is the result of the increasing time support of the wavelet. The fraction g crosses the limit (0.9 in this case) from one to the other scale. For the non-connected area holds the same, where the combination of the two gaps left and right from the $t = 5000$ seconds influence the number of known data points in g (3.3). The solid horizontal lines are remarkable and do not seem very natural. A different path, therefore, is explored in the next section.

3.1.5. Wavelet Energy Distribution

This approach does not address the place of the gap with respect to the translation of the wavelet. Wavelets have finite support, their amplitude decays to zero and most have the characteristic $|\psi(0)| \geq |\psi(t)| \ \forall t$. The fraction g presented in (3.3) does not take these characteristics in account. So a better approximation can be used to determine the effect of missing data points. Therefore the wavelets energy is employed, defined in equation 2.27. For the discrete time-series $x[j]$ of length N with sampling interval Δt and the daughter wavelet $\psi_{an} = \psi(a, n\Delta t)$ the fraction g_{an} is defined as

$$g_{an} = \frac{\sum_{j=0}^{N} x^{\text{NaN}}[j] \cdot \left|\psi_{an}[j]\right|^2}{\sum_{j=0}^{N} \left|\psi_{an}[j]\right|^2}, \qquad \text{with } x^{\text{NaN}}[j] = \begin{cases} 0 & \text{if } x[j] \text{ is a NaN,} \\ 1 & \text{elsewhere} \end{cases}. \tag{3.4}$$

This fraction is the amount of energy of the wavelet that is correlated with non-missing data-points divided by the total energy of the wavelet within the discrete domain of the signal.

The convolution operation can be used to efficiently compute this fraction at one scale for all translations. When the compact support of the wavelet is completely within a gap, the resulting fraction will be 0. When it is completely outside a gap, the result is 1. Other values are within this range. The value represents the relative amount of energy of the wavelet used in computing the coefficient. To take the boundary effects into account, the signal $x^{\text{NaN}}[j]$ is padded with zeros on both sides. Which results in values of 0.5 at the edges of the signal, because half the wavelet is within the support of the discrete signal $x[j]$ and half the wavelet is outside. The zones of influence derived from this wavelet energy distribution are expected to be more of a droplet shape because a general continuous wavelets energy is highest in the centre and decays fast. The example from Demonstration 3.3 is discussed in Demonstration 3.5. In Demonstration 3.6 the accuracy of the determined values are compared to the real change of the coefficients.

Demonstration 3.5 (Zones of influence 2.0) In Figure 3.4c and 3.4d two contours based on the wavelet energy distribution are presented. The first is based on a significance value of 0.9, the second of 0.95. By comparing the first one with the first attempt from Figure 3.4b, some clear improvements are visible. The horizontal stops are not there, and more droplet like shapes are presented. The significance of 0.95 (Figure 3.4d) clearly decreased the number of reliable coefficients. However, compared to the expansion of the cone of influence in Figure 3.4a, below the short gaps there is much improvement.

Demonstration 3.6 (Accuracy of the zones) The most important question regarding the zones of influence is whether the estimate of this influence is correct. I.e. consider a zone of influence of 95%: the coefficients within this zone should be disturbed at most 5%, but are they?

To find out, an artificial signal is created. The signal consists of some sines, cosines and a small noise contribution. First the clean wavelet power spectrum (WPS) is created, denoted by S^{signal} (Figure 3.5a). The signal extension method used is the zero padding. Then a number of NaN's are introduced, which results in the WPS S^{NaN} in Figure 3.5b. This WPS is extended using the smooth signal extension method, based on the first derivative at the edge of the signal.

First have a look at the computed significance levels of the zones of influence of the signal with gaps in Figure 3.5c. As expected the influence of the gaps decreases as the scales increase (as do the periods). The WPS of the disturbed signal S^{NaN} shows that the gaps and the different signal

extension method have major effects on the wavelet coefficients. At the borders, the coefficients increase, due to the extreme boundary condition. The coefficients in the gaps have not uniformly increased or decreased with respect to the coefficients in Figure 3.5a. We note that the white line, the 0.9999 significance border contains most of the changes. Now we compute the relative change of the WPSs: $|S^{\text{signal}} - S^{\text{NaN}}|/|S^{\text{signal}}|$. To compare this to the computed zones of influence in Figure 3.5c, the value $1 - |S^{\text{signal}} - S^{\text{NaN}}|/|S^{\text{signal}}|$ is shown in Figure 3.5d. This way the value 1 denotes a 100% match between the original and adjusted coefficient and the 0 a complete mismatch. The predicted zones of influence are close to the real zones of influence but do differ at some points.

The influence can be split into contributions of the boundary and the gap. First, consider the contribution of the boundary. Here the most striking feature is that the wavelet coefficient is affected severely by the signal extension method, although a small part of the wavelet is expected to be determined by the signal extension. The effect of the gaps is a lot closer to the computed zones of influence, however, still there is some unwanted behaviour. In the low scale range, the highly disturbed wavelet coefficients are well predicted. For the larger scales, there are many spots where the difference is much larger than expected. For instance around the period of 512 seconds, under the second gap at 5800 seconds, large differences are present. Compare these spots in the WPSs in Figure 3.5a and 3.5b and note that these spots occur mostly where the wavelet coefficients are relatively low. The absolute difference (figure not included) shows that the absolute change of the high and low valued coefficients around this point is very close. Therefore the relative change is much worse for coefficients with a small modulus.

At the lowest scales an interesting effect arises: wavelet coefficients of the lowest scales at the edges of the signal and the gaps, belonging to wavelets that theoretically should not be influenced by the gaps are inside the computed 0.9999 zone of influence in Figure 3.5c. In Figure 3.5d this affection of low scale coefficients can be noted, although it is hard to see. These figures are created using the Morlet wavelet, but this effect also shows for other wavelets. This effect is independent of the gaps in the signal, or with the signal extension method: it is the result of the discretisation of the low-scale wavelets Fourier distribution used in the Torrence and Compo code [56]. At $\omega = 0$ a small value is assigned, which leads to the addition of a constant in the time domain. This results in a contribution of time-series values outside the theoretical low-scale wavelets support to its coefficient.

The definition of the cone of influence is based on the effect of a discontinuity at the edge of the signal [55], and therefore cannot be applied to gaps. The wavelets energy distribution has been used to quantify the effect of gaps and the boundaries of the signal onto the resulting wavelet power spectrum. In Demonstration 3.6 the real disturbance and the disturbance based on the wavelets energy distribution have been compared. Two important things are shown. Firstly, the old cone and new zones of influence have to be interpreted with great care, they do give a general insight into changes of the coefficients by gaps and the boundaries, but they do not predict the exact influence. Moreover, secondly, the choice of signal extension method has a large influence on the wavelet power spectrum. It is important to choose a suitable signal extension method. From these effects of the extensions, we may conclude that better filling methods may reduce the influence of the gaps on the WPS enormously. When the filling of the gap is close to the original signal, the theoretical zones of influence are a much better approximation of the real influence. For instance, when a single NaN is replaced by an average of the two neighbouring values, it is very hard to spot the differences between the original and the signal with gaps.

Better estimates of wavelet coefficients can be reached by filling the data points using data at other moments, or data from other measurement points (in combination with a model). Fourier analysis can then also be applied again. However, there will not be a cone of influence to show the analyst which coefficients are expected to be affected by the filling because all coefficients are.

Finally, the minimum equivalent wavelet period of $2\Delta t/\lambda_\psi$ as advised by Torrence and Compo [55] is not sufficient. The low scale coefficients are affected by the signal values outside the theoretical time support of the wavelet. This is due to discretisation effects and can, therefore, be worse for some wavelets than for others. By using a minimum scale of $3\Delta t/\lambda_\psi$ the problem is solved for all wavelets currently available in the package.

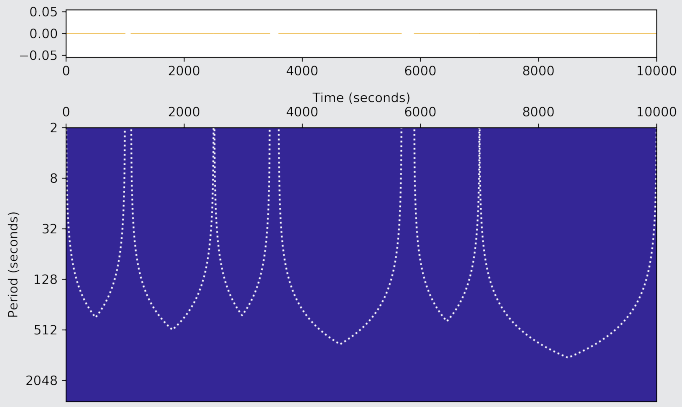

(a) On top: zero signal filled with gaps, below: multiple cones of influence: the beginning and end of gaps are interpreted as respectively the end and beginning of a signal.

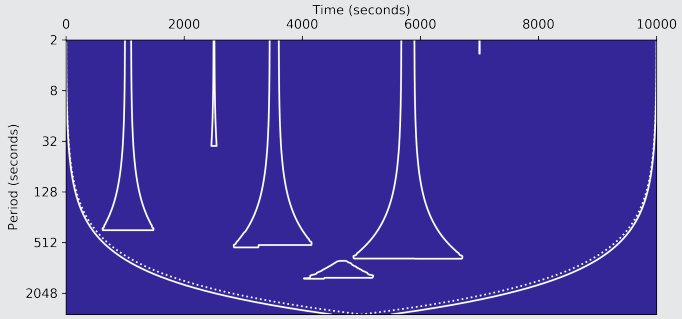

(b) Zones of influence based on the fraction g from (3.3). Solid contour shows $g = 0.9$.

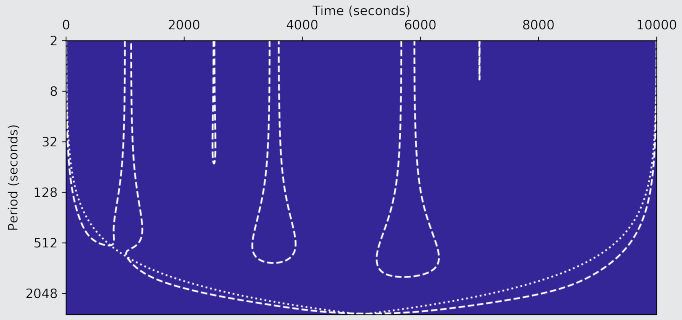

(c) Zones of influence based on the wavelets energy distribution (3.4). Dashed contour shows significance 0.9 based on wavelet energy distribution.

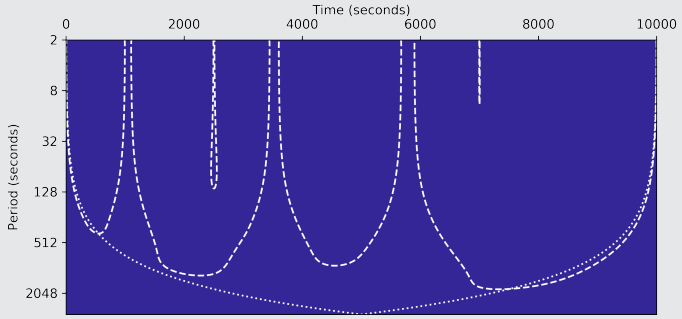

(d) Zones of influence based on the wavelets energy distribution (3.4). Dashed contour shows significance 0.95 based on wavelet energy distribution.

Figure 3.4: From cone of influence to zones of influence, in three steps. All figures are based on the Morlet 6 wavelet. The dotted line in **(b)**-**(d)** shows the cone of influence of the boundaries based on the e-folding time.

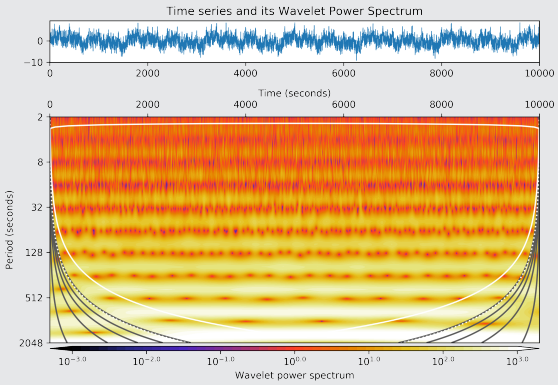

(a) The WPS of the signal without gaps S^{signal}. Zones of influence given by lines, significance of lines from bottom to top: 0.6, 0.8, 0.9, 0.95, 0.98, 0.9999 (white line)

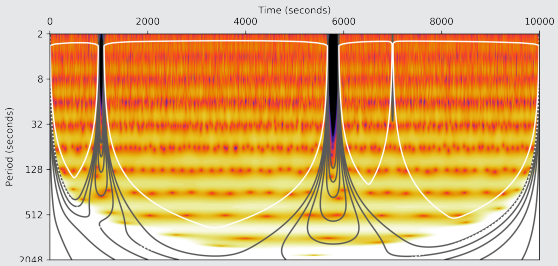

(b) The WPS of the disturbed signal S^{NaN}, with the significance lines from **(b)**. Signal extension mode 'smooth' results in very high coefficients at the boundary. This is therefore an extreme example. Using a more suitable signal extension method results in boundary values close to those in **(a)**.

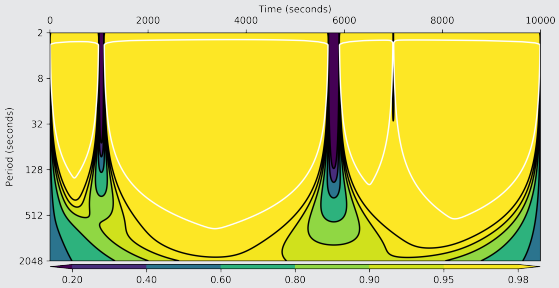

(c) The expected zones of influence based on two large gaps and one single NaN. Colors represent the relative amount of the wavelets energy used in computation of the coefficient. The black lines correspond with the colorbar, the white line represents the 0.9999 significance value.

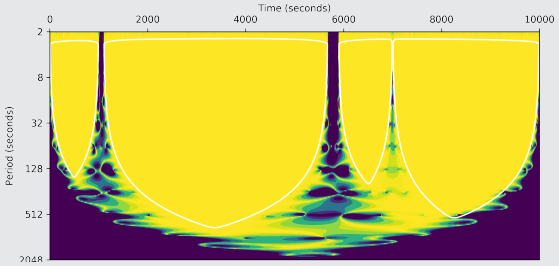

(d) The computed influence based on wavelet power presented in **(a)** and **(c)**. The values represents $1 - |S^{\text{NaN}} - S^{\text{signal}}|/|S^{\text{signal}}|$. White line is same as in **(b)**.

Figure 3.5: The zones of influence: comparison of computed zones in **(b)** and real influence in **(d)**.

3.2. Separation of Incident and Reflected Waves (2D)

In Section 2.4.3 is explained why the separation of incident and reflected waves is of special interest in the field of coastal engineering. A much-used solution to this problem was published by Mansard and Funke [38], who recover the separated waves in the Fourier domain based on three points of measurement. This method was generalised to N points by Zelt and Skjelbreia [63]. Both these methods use amplitude and phase information in Fourier coefficients to separate these waves. Throughout the rest of this chapter, the method of Zelt and Skjelbreia [63] will be referred to, because for two or three gauges in the system, their solution is equal to the solution as published by respectively Goda and Suzuki [21] and Mansard and Funke [38]. This section starts with the general theory about how to separate incident from reflected waves, based on the analytic solution by Ma et al. [34]. They proposed a wavelet coefficient based method using two gauges. An expansion of this method will be presented in Section 3.2.3, followed by all kinds of factors influencing the results of the separation.

Let us first start with the theory. A general experimental set-up in which incident and reflected waves are to be separated is shown in Figure 3.6. On the left, there is a wave maker which creates waves. These waves propagate through the flume and bump onto the construction at the right end of the flume. For simplicity assume that they are being (partially) reflected or absorbed at this point. So there are waves travelling from left to right, and from right to left, i.e. in one dimension. Let us assume that the mean water level is h meters above the floor. If this mean water level changes (over time or over space) this problem becomes a two dimensional problem.

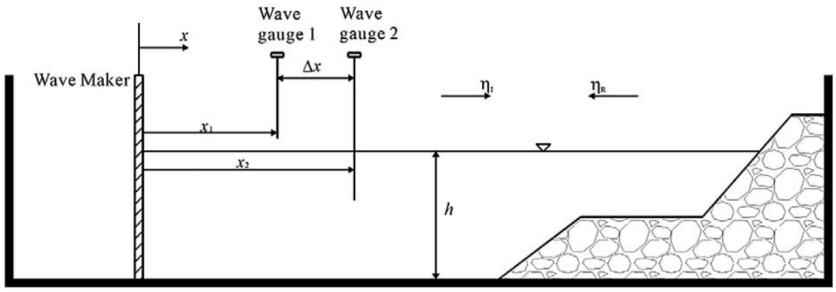

Figure 3.6: Measurement set-up in a flume for separating incident and reflected waves, two gauges are depicted [34, fig.1].

Throughout the flume wave gauges are placed, measuring the water level that is constantly changing due to the waves travelling back and forth. In the sketch in Figure 3.6 two gauges are depicted, later a scenario with more than two gauges will be addressed. The waves created by the wave maker are assumed to be a linear combination of harmonics. A wave gauge at location x will therefore also measure a linear combination of harmonics, i.e. the wave gauges measures a water level deviation of

$$\eta(x,t) = \sum_{\ell=-\infty}^{\infty} a_\ell \cos(\omega_\ell t + \theta_\ell). \tag{3.5}$$

All these waves have an individual amplitude a_ℓ, frequency ω_ℓ and phase θ_ℓ. The measurement is divided into its different harmonics (ω_ℓ), for which the incident and reflected waves can be separated [34, 63]. The solutions per harmonic can be summed to recover the total incident and reflected wave.

So, from now on consider one single wave (with a fixed frequency ω) propagating from left to right through the channel. This wave is called the incident wave:

$$\eta_{\text{incident}}(t) = W^I \cos\omega t + \theta_I. \tag{3.6a}$$

This is the wave created by the wave maker at the left of the channel. This point, i.e. $x = 0$, will be the point of reference for now. This wave has amplitude W^I, radial frequency ω and phase θ_I. At the end of the channel, the wave is being partially reflected or absorbed. The reflected wave as observed from the reference point (wave maker) is described by

$$\eta_{\text{reflected}}(t) = W^R \cos(\omega t + \theta_R). \tag{3.6b}$$

Typically $W^R \leq W^I$ holds for the amplitude of the reflected wave. However, this is not a necessary condition. The phase of the reflected wave, θ_R, depends among others on the length of the channel, the original phase θ_I and the reflection properties of the construction.

Now, assume there are two gauges in the channel, one on a distance of x_1 from the wave maker and the second one at a distance $x_2 > x_1$. Define $x_2 - x_1 = \Delta x$, as depicted in Figure 3.6. The surface elevation as recorded at point x_1 is measured as one wave with amplitude a_1 and phase θ_1. However, it is the sum of the incident and reflected wave at that point:

$$\begin{aligned}\eta(x_1,t) &= \xi_1 \cos(\omega t + \theta_1) \\ &= W^I \cos(\omega t - kx_1 + \theta_I) + W^R \cos(\omega t + kx_1 + \theta_R).\end{aligned} \tag{3.7a}$$

The incident and reflected wave were defined at the reference point, so at the point x_1 a phase shift is introduced with respect to that point $x = 0$. This phase shift is expressed in $-kx_1$, for the reflected wave it is $+kx_1$ because it is travelling in the other direction. This phase shift depends on the wave number k, a measure of the number of oscillations per distance for waves of different frequencies. More theory about this number is presented in Section D.1. It is important to know that the wave number depends on the depth of the water the wave is travelling in (d), the frequency of the wave (ω) and the gravitational acceleration (g).At point x_2, the measured water level is thus described by

$$\begin{aligned}\eta(x_2,t) &= \xi_2 \cos(\omega t + \theta_2) \\ &= W^I \cos(\omega t - kx_2 + \theta_I) + W^R \cos(\omega t + kx_2 + \theta_R) \\ &= W^I \cos(\omega t - kx_1 - k\Delta x + \theta_I) + W^R \cos(\omega t + kx_1 + k\Delta x + \theta_R).\end{aligned} \tag{3.7b}$$

Reconstructing the incident and reflected waves through the equations (3.7) directly is hard. Therefore their analytic forms are being used. The real part of these analytic wave descriptions are the waves described by (3.7):

$$\begin{aligned}\zeta(x_1,t) &= \xi_1 e^{i(\omega t+\theta_1)} \\ &= W^I e^{i(\omega t - kx_1 + \theta_I)} \quad + \quad W^R e^{i(\omega t + kx_1 + \theta_R)},\end{aligned} \tag{3.8a}$$

$$\begin{aligned}\zeta(x_2,t) &= \xi_2 e^{i(\omega t+\theta_2)} \\ &= W^I e^{i(\omega t - kx_1 - k\Delta x + \theta_I)} \quad + \quad W^R e^{i(\omega t + kx_2 + k\Delta x + \theta_R)} \\ &= W^I e^{i(\omega t - kx_1 + \theta_I)} e^{-ik\Delta x} \quad + \quad W^R e^{i(\omega t + kx_2 + \theta_R)} e^{ik\Delta x}.\end{aligned} \tag{3.8b}$$

The incident and reflected analytic waves can be reconstructed from these equations through the following relationship[3] [34]:

$$W^I e^{i(\omega t - kx_1 + \theta_I)} = \frac{\zeta(x_1,t)e^{ik\Delta x} - \zeta(x_2,t)}{2i\sin(k\Delta x)}, \tag{3.9a}$$

$$W^R e^{i(\omega t - kx_1 + \theta_R)} = \frac{\zeta(x_1,t)e^{-ik\Delta x} - \zeta(x_2,t)}{-2i\sin(k\Delta x)}. \tag{3.9b}$$

This are two complex equations for two complex amplitudes $W^I e^{i(\omega t - kx_1 + \theta_I)}$ and $W^R e^{i(\omega t - kx_1 + \theta_R)}$. The real parts of these analytic separated waves result in the separated waves that were present at the gauge. Note that this is the solution at the distance x_1 from the wave maker. These equations can be extended to a sloping bathymetry and obliquely incident waves [34, 35].

3.2.1. The Coefficients

The analytical expressions of the waves in (3.8) can be based on Fourier or wavelet coefficients. To explain this, go back to the definition of a discrete representation (2.5) from Chapter 2:

$$x(t) = \sum_{\alpha \in I} c_\alpha e_\alpha(t).$$

In the case of Fourier and wavelet analysis, the coefficients c_α are based on the correlation between the chosen basis functions $e_\alpha(t)$ and the function $x(t)$. This results in complex coefficients[4], which on their term can

[3] In Section D.2 the derivation of this result is given.
[4] If complex wavelets are used in the decomposition.

be used as the analytic signal, i.e. the analytic form of a measurement at a general location x for the frequency ω can be represented as

$$\zeta(x,t) = \xi e^{i(\omega t+\theta)} = \underbrace{\xi}_{|c_\alpha|} \cdot \underbrace{e^{i\theta}}_{\arg(c_\alpha)} \cdot \underbrace{e^{i\omega t}}_{e_\alpha(t)} = c_\alpha e_\alpha(t).$$

The equations 3.9 are solved by using the coefficients c_α and thus without basis function $e_\alpha(t)$, which is the term $e^{i\omega t}$ in (3.9). The time-series of the incident and reflected waves are reconstructed by 'adding' the basis functions, i.e. by applying the inverse transformation.

Goda and Suzuki [21] use Fourier coefficients for c_α, which is a good match with the given derivation because in Fourier analysis the basis functions are complex exponentials. Ma et al. [34] uses continuous wavelet coefficients for the analytic form, where the basis functions $e_\alpha(t)$ consist of scaled and translated versions of a wavelet $\psi(t)$. The linear representation (2.5) in both Fourier and continuous wavelet transform results in a linear representation in respectively frequencies and scales. Using these transforms on a measured waveform already applies the linear decomposition as expressed in (3.5). Ma et al. [34] use numerical examples, simulations with large numbers of waves in stationary and non-stationary situations, to show that their method is independent of the length of the channel. They find an average reflection coefficient error of 3.3%. A comparable error is found in the verification presented in Figure D.1.

3.2.2. Dependency of Gauge Distance Δx and Wave Number k

The largest influence on the correctness of the recovered separate waves is the distance between the gauges. The reconstruction formulas (3.9a) and (3.9b) both depend on the factor $1/\sin(k\Delta x)$. Remember that the wave number k actually depends on the frequency ω and thus scale a (see equation D.1). Figure 3.7 shows the effect of the distance between the gauges on that factor $\sin(k\Delta x)$. The value of this factor sometimes is zero or a value very close to zero. Computational errors are caused by values of $\sin(k\Delta x)$ close to 0. These errors result in the wrong estimation of the separate waves. For values where $\sin(k\Delta x) = 0$, the solution cannot be derived at all.

The best solution is to place the gauges in such a way that the factor $\sin(k\Delta x) > 0$ for all frequencies of interest. This can, however, be impossible for a large frequency bandwidth. This problem can be solved by combining measurements from gauges at multiple distances. The Fourier counterpart of this algorithm, developed by Goda and Suzuki [21], has this same shortcoming. This algorithm has been expanded twice, once to three gauges by Mansard and Funke [38] and finally to N gauges by Zelt and Skjelbreia [63]. This expansion is applied to the wavelet coefficients in Section 3.2.3. The other solution would be to carefully choose the spacing of the scales to avoid these critical points. This option, however, is not explored in this thesis.

Another important assumption has been made in the derivation process. That assumption is that the wave number based on the centre frequency of the wavelet at scale a, $f_c = f_\psi \cdot a$, is representable for all frequencies in the bandwidth of the wavelet $\psi_a(t)$. This is not true, and this assumption cannot be without side effects. This and a comparison to the method using the Fourier transform by Zelt and Skjelbreia [63] will be addressed after expanding the method to N gauges.

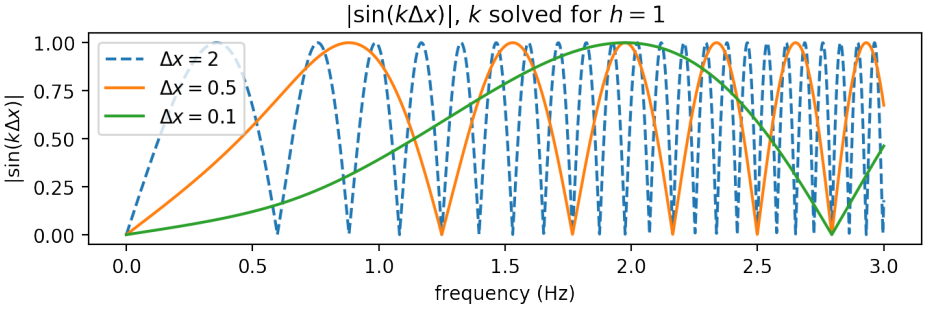

Figure 3.7: The effect of the placement of the gauges on the factor $\sin(k\Delta x)$. The wave number is based on the solution of the dispersion equation for a water depth of 1 meter.

3.2.3. Expanding to N Gauges

As described in the last section, the information of multiple gauges can be used to separate the incident and reflected wave more accurately over larger bandwidths. This section starts with a mathematical derivation for a number of $N \geq 2$ gauges. This derivation is followed by a verification that shows that the $N = 2$ case results in the same equations as derived by Ma et al. [34]. Then the error of the solution is analysed.

So now assume that, instead of two, there are N gauges in the system: at different distances $x_1 < x_j < x_N$. Again assume the incident and reflected wave are described by (3.6). Define the distance between gauge m and n as $\Delta x_{mn} = x_n - x_m$. Gauge m is used as as reference point, then the analytical form of the wave at scale a of the wave height measured at gauge j becomes

$$\zeta_{a,j}(t) = W^I_{a,j} e^{i(\omega_a t - k_a x_m + \theta^I_a)} e^{-ik_a \Delta x_{mj}} + W^R_{a,j} e^{i(\omega_a t + k_a x_m + \theta^R_a)} e^{ik_a \Delta x_{mj}}, \qquad j = 1, \ldots, N. \tag{3.10}$$

This is a generalisation of the step from (3.8a) to (3.8b). $W^I_{a,j}$ denotes the modulus of the wavelet coefficient of the incident wave at scale a, $W^R_{a,j}$ idem for the reflected wave. k_a is the wave number for the centre frequency of the wavelet at scale a. First we substitute the analytical representation of the incident and reflected wave at the reference point m for

$$W^I_{a,j} e^{i(\omega_a t - k_a x_m + \theta^I_a)} = Z^I_a, \qquad\qquad W^R_{a,j} e^{i(\omega_a t + k_a x_m + \theta^R_a)} = Z^R_a.$$

For $N = 2$ this system of equations from (3.10) is solved by (3.9), as will be shown later. For larger N, this system becomes overdetermined. The linear least squares method is applied to solve this. Instead of solving Z^I_a and Z^R_a, equations for the estimates, respectively $\widetilde{Z^I_a}$ and $\widetilde{Z^R_a}$, will be solved. Therefore the residual $\epsilon_{a,j}$ is defined as the difference between the estimated water level at gauge j minus the measured water level at gauge j (both for scale a):

$$\epsilon_{a,j} = \left(\widetilde{Z^I_a} e^{-ik_a \Delta x_{mj}} + \widetilde{Z^R_a} e^{ik_a \Delta x_{mj}}\right) - \zeta_{a,j}. \tag{3.11}$$

The system is solved for $\widetilde{Z^I_a}$ and $\widetilde{Z^R_a}$ by minimising the sum of the moduli of the residuals. For reasons discussed later, a weighting factor $w_{a,j} > 0$ is added per gauge. Define the sum of the weighting factors as $\Omega_a = \sum_j w_{a,j}$. The objective is to determine the minimum of

$$\sum_{j=1}^{N} w_{a,j} |\epsilon_{a,j}|^2 = \sum_{j=1}^{N} w_{a,j} \epsilon_{a,j} {\epsilon_{a,j}}^*. \tag{3.12}$$

If the derivative of this sum with respect to the real and imaginary parts of $\widetilde{Z^I_a}$ and $\widetilde{Z^R_a}$ equals zero, the minimum occurs. The following relationship holds at that point [63]:

$$\sum_{j=1}^{N} w_{a,j} \epsilon_{a,j} e^{ik_a \Delta x_{mj}} = \sum_{j=1}^{N} w_{a,j} \epsilon_{a,j} e^{-ik_a \Delta x_{mj}} = 0. \tag{3.13}$$

Again we have two complex equations for two complex amplitudes. Substituting (3.11) into (3.13) yields the two equations:

$$\sum_{j=1}^{N} w_{a,j} \left(\widetilde{Z^I_a} e^{-ik_a \Delta x_{mj}} + \widetilde{Z^R_a} e^{ik_a \Delta x_{mj}} - \zeta_{a,j}\right) e^{ik_a \Delta x_{mj}} = 0 \quad \Rightarrow \quad \sum_{j=1}^{N} w_{a,j} \zeta_{a,j} e^{ik_a \Delta x_{mj}} = \widetilde{Z^I_a} \Omega_a + \widetilde{Z^R_a} \sum_{j=1}^{N} w_{a,j} e^{2ik_a \Delta x_{mj}},$$

$$\sum_{j=1}^{N} w_{a,j} \left(\widetilde{Z^I_a} e^{-ik_a \Delta x_{mj}} + \widetilde{Z^R_a} e^{ik_a \Delta x_{mj}} - \zeta_{a,j}\right) e^{-ik_a \Delta x_{mj}} = 0 \quad \Rightarrow \quad \sum_{j=1}^{N} w_{a,j} \zeta_{a,j} e^{-ik_a \Delta x_{mj}} = \widetilde{Z^I_a} \sum_{j=1}^{N} w_{a,j} e^{-2ik_a \Delta x_{mj}} + \widetilde{Z^R_a} \Omega_a.$$

This can be written as a matrix-vector product:

$$\begin{bmatrix} \Omega_a & \sum_{j=1}^{N} w_{a,j} e^{2ik_a \Delta x_{mj}} \\ \sum_{j=1}^{N} w_{a,j} e^{-2ik_a \Delta x_{mj}} & \Omega_a \end{bmatrix} \widetilde{\begin{bmatrix} Z^I_a \\ Z^R_a \end{bmatrix}} = \begin{bmatrix} \sum_{j=1}^{N} w_{a,j} \zeta_{a,j} e^{ik_a \Delta x_{mj}} \\ \sum_{j=1}^{N} w_{a,j} \zeta_{a,j} e^{-ik_a \Delta x_{mj}} \end{bmatrix}. \tag{3.14}$$

This matrix-vector product has a unique solution if the matrix is non-singular. Singularity should thus be avoided, this will be addressed later. $\widetilde{Z^I_a}$ and $\widetilde{Z^R_a}$ are solved as:

$$\widetilde{Z^I_a} = \frac{1}{D}\left(\Omega_a \sum_{j=1}^{N} w_{a,j} \zeta_{a,j} e^{ik_a \Delta x_{mj}} - \sum_{j=1}^{N} w_{a,j} e^{2ik_a \Delta x_{mj}} \sum_{j=1}^{N} w_{a,j} \zeta_{a,j} e^{-ik_a \Delta x_{mj}}\right), \tag{3.15a}$$

$$\widetilde{Z_a^R} = \frac{1}{D}\left(\Omega_a \sum_{j=1}^{N} w_{a,j}\zeta_{a,j} e^{-ik_a\Delta x_{mj}} - \sum_{j=1}^{N} w_{a,j} e^{-2ik_a\Delta x_{mj}} \sum_{j=1}^{N} w_{a,j}\zeta_{a,j} e^{ik_a\Delta x_{mj}}\right), \tag{3.15b}$$

with the discriminant

$$D = \Omega_a^2 - \sum_{j=1}^{N} w_{a,j} e^{-2ik_a\Delta x_{mj}} \sum_{j=1}^{N} w_{a,j} e^{2ik_a\Delta x_{mj}}. \tag{3.15c}$$

Note that the discriminant D is a real quantity and can be rewritten to [63]:

$$D = \Omega_a^2 - \left(\sum_{j=1}^{N} w_{a,j}\cos(2k_a\Delta x_{mj})\right)^2 - \left(\sum_{j=1}^{N} w_{a,j}\sin(2k_a\Delta x_{mj})\right)^2 = 4\sum_{j=1}^{N}\sum_{\ell<j} w_{a,j}^2 \sin^2(k_a\Delta x_{\ell j}). \tag{3.16}$$

Verification for Two Gauges

First is shown that the N gauge expression for $N = 2$ is equal to the method of Ma et al. [34]. By manipulating (3.15a), we can express the separation coefficient at scale a, $C_{a,j}$, as

$$\widetilde{Z_a^I} = \sum_{j=1}^{N} C_{a,j}\zeta_{a,j} = \sum_{j=1}^{N} \zeta_{a,j} \underbrace{\frac{w_{a,j}}{D}\left(\Omega_a e^{ik_a\Delta x_{mj}} - e^{-ik_a\Delta x_{mj}} \sum_{\ell=1}^{N} w_\ell e^{2ik_a\Delta x_{m\ell}}\right)}_{=C_{a,j}}. \tag{3.17}$$

The coefficient $C_{a,j}$ can be simplified to:

$$\begin{aligned}
C_{a,j} &= \frac{w_{a,j}}{D}\left(\Omega_a e^{ik_a\Delta x_{mj}} - e^{-ik_a\Delta x_{mj}} \sum_{\ell=1}^{N} w_\ell e^{2ik_a\Delta x_{m\ell}}\right) \\
&= \frac{w_{a,j}}{D}\left(\sum_{\ell=1}^{N} w_\ell e^{ik_a\Delta x_{mj}} - e^{-ik_a\Delta x_{mj}} \sum_{\ell=1}^{N} w_\ell e^{2ik_a\Delta x_{m\ell}}\right) \\
&= \frac{w_{a,j}}{D} \sum_{\ell=1}^{N} w_\ell \left(e^{ik_a\Delta(x_j - x_m)} - e^{ik_a\Delta(2x_\ell - 2x_m)} e^{-ik_a\Delta(x_j - x_m)}\right) \\
&= \frac{w_{a,j}}{D} \sum_{\ell=1}^{N} w_\ell e^{-ik_a(x_m - x_\ell)} 2i\sin(k_a(x_j - x_\ell)) \qquad \left[\text{use } e^{i(a-b)} - e^{-i(a-b)} e^{i(2c-2b)} = e^{-i(b-c)} 2i\sin(a-c)\right] \\
c_{a,j} &= 2i\frac{w_{a,j}}{D} e^{-ik_a x_m} \sum_{\ell=1}^{N} w_\ell e^{ik_a x_\ell} \sin(k_a\Delta x_{\ell j})
\end{aligned}$$

Now assume there are two gauges at a distance $x_1 < x_2$, and the equations are solved at x_1 (thus $m = 1$). The weights of the two gauges are both equal to 1, i.e. $w_1 = w_2 = 1$. Then the discriminant (3.16) simplifies to:

$$D = 4\sin^2(k_a\Delta x_{12}).$$

$C_{a,1}$ and $C_{a,2}$ are then solved as:

$$\begin{aligned}
C_{a,1} &= 2i\frac{1}{D} e^{-ik_a x_1} \sum_{\ell=1}^{2} e^{ik_a x_\ell} \sin(k_a\Delta x_{\ell 1}) = 2i\frac{1}{D} e^{-ik_a x_1}\left(e^{ik_a x_1}\sin(k_a\Delta x_{11}) + e^{ik_a x_2}\sin(k_a\Delta x_{21})\right) \\
&= 2i\frac{1}{D} e^{-ik_a x_1}\left(-e^{ik_a x_2}\sin(k_a\Delta x_{12})\right) = -2i\frac{1}{4\sin^2(k_a\Delta x_{12})} e^{-ik_a x_1} e^{ik_a x_2}\sin(k_a\Delta x_{12}) \\
&= \frac{e^{ik_a\Delta x_{12}}}{2i\sin(k_a\Delta x_{12})}
\end{aligned}$$

and

$$\begin{aligned}
C_{a,2} &= 2i\frac{1}{D} e^{-ik_a x_1} \sum_{\ell=1}^{2} e^{ik_a x_\ell} \sin(k_a\Delta x_{\ell 2}) = \frac{2i}{D} e^{-ik_a x_1}\left(e^{ik_a x_1}\sin(k_a\Delta x_{12}) + e^{ik_a x_2}\sin(k_a\Delta x_{22})\right) \\
&= \frac{2i}{4\sin^2(k_a\Delta x_{12})}\sin(k_a\Delta x_{12}) = \frac{-1}{2i\sin(k_a\Delta x_{12})}.
\end{aligned}$$

When these values for $C_{a,1}$ and $C_{a,2}$ are substituted into (3.17) equation 3.9a is recovered. For the reflected wave, the same similarity with (3.9b) can be shown, using the relationship [63]

$$\widetilde{Z_a^R} = \sum_{j=1}^{N} C_{a,j}^* \zeta_{a,j}. \tag{3.18}$$

Numerical test show the same results when the analytic solution (3.9) or the least squares approximation (3.15) for $N = 2$.

3.2.4. Error Analysis and Reduction

The residual at scale a is defined by (3.11). This can be rewritten such that

$$\zeta_{a,j} = \widetilde{Z_a^I} e^{-ik_a \Delta x_{mj}} + \widetilde{Z_a^R} e^{ik_a \Delta x_{mj}} - \epsilon_{a,j}.$$

If this expression is filled into (3.17) and (3.18) an expression of the error for both the incident and reflected wave is found as

$$\widetilde{Z_a^I} = Z_a^I - \sum_{j=1}^{n} C_{a,j} \epsilon_{a,j}, \qquad \widetilde{Z_a^R} = Z_a^R - \sum_{j=1}^{n} C_{a,j}^* \epsilon_{a,j}.$$

If the residual signal is zero the 'exact' coefficients are obtained[5]. This is the case for $N = 2$. Otherwise the error at gauge j for scale a, $\epsilon_{a,j}$, is amplified by the coefficient $C_{a,j}$. This amplification of the error is represented by the factor

$$|C_{a,j}| = \left| \frac{\partial \widetilde{Z_a^I}}{\partial \epsilon_{a,j}} \right| = \left| \frac{\partial \widetilde{Z_a^R}}{\partial \epsilon_{a,j}} \right| = 2 \frac{w_{a,j}}{D} \left| \sum_{\ell=1}^{N} w_{a,\ell} e^{ik_a x_\ell} \sin(k_a \Delta x_{\ell j}) \right|. \tag{3.19}$$

The error is worst when $D = 0$. For N arbitrarily placed gauges, this occurs if $k_a \Delta x_{mn} = \ell\pi$ ($\ell \in \mathbb{Z}$). The error can be reduced by influencing the weight $w_{a,n}$, $n \in \{1, \ldots N\}$. Zelt and Skjelbreia [63] have introduced a weighting that should reduce the error, which is discussed in Demonstration 3.13.

In numerical experiments without noise and with a constant wave number the residual signal will contain mainly errors due to discretisation. These will be present near the boundaries of the signal due to signal extension and the circularity of the convolution. In real experiments the residual signal also accounts for effects like [63]

- Noise;
- Discretisation errors;
- Non-linear hydrodynamic effects;
- Deviations from the linear dispersion relation (D.1);
- Wave motions in the third dimension, i.e. over de width of the channel (also known as cross modes);
- Viscous effects;
- Energy dissipation (for instance by friction or wave breaking).

In this section factors such as gauge placement and weighting and how they affect the error will be discussed. The next section explores the effect of the characteristics of the signals on the result. This will all be based on numerical experiments. Chapter 5 present an example of the separation of a time-series from the field of coastal engineering. These numerical examples are based on the signals described in Demonstration 3.7.

Demonstration 3.7 (Separate coastal engineering time-series) Numerically simulated waves will be separated using wavelet coefficients. These results will be compared to the results from the Fourier algorithm from Zelt and Skjelbreia [63]. Note that this algorithm for $N = 2$ is equal to Goda and Suzuki [21] and for $N = 3$ to Mansard and Funke [38] [63]. The signals are based on a general measurement set-up in a flume at Deltares. On one end there is a wave maker, on the other end, there is some structure that is being tested. The gauge placement is given in Table 3.1. This is the

[5] These coefficients are not necessarily the exact coefficients, but the relationship $\widetilde{Z_a^I} + \widetilde{Z_a^R} = \zeta_{a,j}$ will hold when the residual at scale a is zero. By assuming $Z_a^I + Z_a^R = \zeta_{a,j}$, the relationship $\widetilde{Z_a^I} + \widetilde{Z_a^R} = Z_a^I + Z_a^R$ holds as well.

standard set-up at Deltares, based on the optimal criterion from Zelt and Skjelbreia [63]. In the comparison is worked with the deviation of the mean water level, because the frequency $\omega = 0$ can not be separated (i.e. for all scales $k = 0$).

The wave spectrum is based on a much-used spectrum in coastal engineering, a JONSWAP spectrum [24]. The peak frequency lies at 0.8 Hz. Random frequencies in the range $[0.01, f_N]$ are picked. The sample frequency $f_s = 12$ Hz is used, so the Nyquist frequency is 6 Hz. The assumed water depth is 0.7 meter, and the wave numbers are based on the solution of the linear dispersion equation (D.1).

Number of gauges	Distances from wave maker
2	39.382, 40.1
3	39.382, 39.83, 40.1
4	35.742, 39.382, 39.83, 40.1
5	35.742, 38.726, 39.382, 39.83, 40.1

Table 3.1: Distance of gauges used in the demonstrations

Gauge Placement

As mentioned the determinant is non-zero if for all gauges m and $n(\neq m)$ holds: $k_a \Delta x_{mn} = \ell\pi$ $(\ell \in \mathbb{Z})$. This is the same as $2|\Delta x_{mn}|/a\lambda_\psi \in \mathbb{Z}$ for each combination of $m, n \in \{1, \ldots, N\}$. This is observed most easily by checking the behaviour of $\sin(k\Delta x)$ as shown in Figure 3.7. Wave gauge positions should be chosen carefully to ensure that this criterion is not approached near frequencies of interest.

Demonstration 3.8 (Wave number) Before considering different numbers of gauges, the wave number is shortly addressed. When the wave number is set equal to all frequencies, an almost perfect reconstruction of the incident and reflected wave is achieved, shown in Figure D.3. The error in the reconstruction of the incident and reflected wave is in the order of magnitude of the error of the reconstruction of the signal from the wavelet coefficients. When the wave number is based on the solution of the linear dispersion equation (D.1), the error of the reflection coefficient based on the wavelet coefficients is approximately 5% (see Figure D.2).

This error is mostly due to the very low frequencies and the frequencies above 1.5 Hz. The error in the low frequencies and at the spikes visible in the Fourier spectrum is due to the critical gauge placement, which will be addressed in Demonstration 3.9. Note that in the frequencies above 3.5 Hz the recovered spectrum based on the wavelet coefficients is worse than the one based on the Fourier coefficients. This is discussed more elaborate in Demonstration 3.10.

Demonstration 3.9 (Critical gauge placement, number of gauges) It is known from the mathematics that the gauge placement is very important for the results. A combination of the right distance and number of gauges ensures the best result. The improvement between the case using two gauges (Figure D.2) and three gauges (Figure D.4) is very large. The estimate of the reflection coefficient in the Fourier case decrease from 79% to 6% and for the wavelets from 5% to 0.2%. The addition of more gauges (five: Figure D.5) does improve the result for the Fourier-based method to 0.5%. The reconstruction of the separated waves based on the wavelet coefficients shows an underestimation of energy in the incident and reflected waves, which was not the case for three gauges, which showed overestimation. The estimate of the reflection coefficients is comparable to the three gauges case. The Fourier-based methods over-estimates the waves in both cases, due to low-frequency behaviour.

The Fourier method is more plagued by low frequencies when a little number of gauges is used. The higher number of gauges suppresses the distortion by low frequencies in both methods. For the wavelet-based method, the high-frequency errors increase when more gauges are used: for five gauges the reconstructed incident and reflected wave both contain almost 5% less energy the original separate waves. The addition of the fourth and fifth gauge introduced a relatively large distance with respect to the distances when only three gauges are used (see Table 3.1). The introduction of

this large distance results in a larger error.

Different Wavelets, Number of Scales

On the first eye changing wavelets would not effect the results of the separation. That is does, is shown in Demonstration 3.10.

Demonstration 3.10 (Different wavelets) For the results shown in Figure D.2 the Morlet 60 wavelet has been used, and in Figure D.9 the Morlet 6 wavelet. The difference between the Morlet 6 and Morlet 10 wavelet is depicted in Figure 2.4. By increasing the parameter to 60, the wavelet becomes even more localised in frequency, but more spread out in time. The Morlet 6 wavelet is performing over 15 times worse than the Morlet 60 wavelet. Increasing the number of gauges does not change this fact, as can be observed in Figure D.5 and D.10. Note that for low frequencies, they both reconstruct the same spectra, but for higher frequencies, this does not hold. If the wave number is again assumed equal, there is little to no difference between the separation using these two wavelets, as can be seen in Figure D.3 and D.11.

So answer to this problem consists of three factors: the wavelet, the frequency of the wave and the wave number. As mentioned before in Section 3.2.2, the separation depends on the assumption that the wave number is valid for all frequencies within the band of the wavelet. Because the Morlet 60 wavelet has a much smaller bandwidth than the Morlet 6 wavelet, this assumption is valid for more frequencies. This problem increases when higher frequencies are studied. In coastal engineering, these higher frequencies do not occur frequent, which allows this method to be used. Other wavelets with smaller bandwidth can be implemented to avoid this problem for higher frequencies.

Another influencer is the number of scales. For a too small number, the reconstruction will start deviating more from the original signal: the combined bandwidth of the wavelets of all scales do not cover the bandwidth of the signal as described before. For good results it is important to take the guidelines in Section 3.1.2 into account. By increasing the number of scales, the errors due to the estimate of the wave number are not expected to decrease drastically. The error might even increase because a higher number of scales results in a more dense set of frequencies. A more dense set of frequencies results in more solutions with a determinant close to zero.

Demonstration 3.11 (Number of scales) The general setting of 200 scales (Figure D.5) is compared to two other numbers of scales. By decreasing the number of scales, the reconstruction error of the separated waves increases much (Figure D.12): from 0.001% to about 12%. This results in estimates of m_0 of the incident and reflected wave that are off with over 170%. Notable is that, although the reconstruction error is large, the estimate of the reflection coefficient is still quite accurate. Increasing the number of scales to 1000 does not decrease the reconstruction error (Figure D.13), it is also around 0.001%, and therefore the estimates of the values are comparable to the estimates using 200 scales.

Determinant Limiter

Finding the right gauge placement is one way to ensure that the results are less disturbed by a close-to-zero valued determinant. However, this is not always possible. In measurements, it may happen that the gauges are wrongly placed, or that there is just a limited amount of gauges available. By introducing a limiter based on the determinant, the frequencies or scales (in respectively the Fourier or wavelet-based solutions) for which the determinant is under a certain limit are eliminated. The reconstructed wave values are set to 0.[6]

This has the opposite effect as dividing by close-to-zero values. As could be observed, this often resulted in more energy in both separated waves. The disposal of energy by using the determinant limiter is expected to result in a bit weaker resulting signal: some energy is left out of the reconstruction that is in both original signals. In wavelet analysis, another option is to limit the maximum period used in determining the wavelet coefficients. For low frequencies, this results in the same effect as omitting the frequencies for which the determinant is under the limit.

[6] This is already used in practice at Deltares.

Demonstration 3.12 (Determinant limiter, $p_{\max}$) A determinant limiter has been added, and the results are improved very much. Both algorithms without determinant limiter do overestimate the reflection coefficient quite severely in the two gauges case (Figure D.2). However, by adding a determinant limiter of 0.1, the estimation of the reflection coefficient for both algorithms is around 1% off, instead of 80% and 5% in respectively the Fourier and wavelet cases. This is shown in Figure D.6. From the recovered spectra it is clear that the spikes at the erroneous frequencies are not present anymore.

If the determinant limiter is increased more, more energy is taken from the separated waves. The results of the use of a determinant limit of 0.5 is shown in Figure D.14. For estimating the reflection coefficient, this is not that big of a problem if the relative energy change in the reconstructed incident and reflected wave is approximately the same. However, the introduction of this determinant limiter may lead to other underestimation problems when other wave characteristics are studied. So, this limiter has to be used with care.

More or less the same results are found in the wavelet algorithm by limiting the maximum period $p_{\max}$ of the decomposition. This, however, does only effect the low frequencies and not the high frequencies for which the determinant is close to 0. The limitation of $p_{\max}$ can be used to suppress the effect discussed in Demonstration 3.8.

Weighting

As mentioned before, the error can be reduced by introducing the weighting factor into the equations. Zelt and Skjelbreia [63] propose a weighting coefficient based on two characteristics. The first characteristic is the quantification of the phase difference associated with the spacing between gauge j and the other gauges. Multiples of one-half the wavelength associated with scale a are undesirable. The second characteristic is the spacing relative to the wavelength: a large spacing is undesirable. Especially for wavelets, where for large distances the factor $k\Delta x$ is much more off. The resulting weighting coefficients of Zelt and Skjelbreia [63] are defined as:

$$w_{a,j} = \sum_{\ell=1}^{n} G(k_a \Delta x_{\ell j}) \qquad \text{with } G\left(k_a \Delta x_{\ell j}\right) = \frac{\sin^2\left(k_a \Delta x_{\ell j}\right)}{1 + \left(k_a \Delta x_{\ell j}/\pi\right)^2}. \tag{3.20}$$

This weighting will result in an estimate for the incident and reflected wave that is the same (aside from a phase shift) for all reference points.

Demonstration 3.13 (Weighting factors) The effects of the addition of the weights from (3.20) is higher when the number of gauges is little. The higher the number of gauges, the less need there is for the weights. For three gauges, the error of the Fourier case reduces from 6% to about 3%, in the wavelet case there is little difference observed (see Figure D.4 and D.15).

3.2.5. Linearity, Stationarity and Noise

As both the Fourier and wavelet transform are linear operations, they are not fit to analyse non-linear signals with. The separation of waves is a perfect example of where this analysis would fail. Again assume two gauges for simplicity. The assumption on which the whole analysis is built is that both gauges measure the same linear combination of waves, different by only a phase shift. If for instance, a wave changes frequencies between two points (i.e. a non-linear relationship), this assumption is not valid. Non-linear effects will, therefore, result in a larger residual signal and thus an underestimation of both separated waves. Linear relations, such as a sloping bathymetries [34] and oblique incident waves [35] can be added to the separation algorithms.

Furthermore Ma et al. [34] note that this method is not suitable for breaking waves because energy is dissipated in the wave breaking. This loss of energy due to breaking reduces the energy measured at the gauges, for both incident and reflected waves. This will cause wrong estimates for the reflection behaviour of the structure. Whether the estimate increases or decreases depends on whether the incident or reflected waves lose more energy in this process. This, however, will be a problem for every method that determines the energy in the wave at a certain distance from the reflecting area.

Stationarity

Fourier analysis, in theory, is not applicable to non-stationary waves, and wavelet analysis is. Remember that a signal is non-stationary if the statistical properties of the ensemble it belongs to change over time (see page 4), which in one of the members of the ensemble often translates to a changing frequency content over time. For the demonstrations above this is not true, the statistical properties of the ensemble used are constant in time. To create a non-stationary signal, it is most easy to change the mean or the variance of the signal.

Changing the mean has a nasty side-effect: the wave number is dependent on the water level and this becomes a variable of time. This causes the following time dependencies in (3.15) as follows:

$$\widetilde{Z_a^I}(t) = \frac{1}{D(t)}\left(\Omega_a(t)\sum_{j=1}^{N} w_{a,j}(t)\zeta_{a,j}(t)e^{ik_a(t)\Delta x_{mj}} - \sum_{j=1}^{N} w_{a,j}(t)e^{2ik_a(t)\Delta x_{mj}}\sum_{j=1}^{N} w_{a,j}(t)\zeta_{a,j}(t)e^{-ik_a(t)\Delta x_{mj}}\right), \tag{3.21a}$$

$$\widetilde{Z_a^R}(t) = \frac{1}{D(t)}\left(\Omega_a\sum_{j=1}^{N} w_{a,j}(t)\zeta_{a,j}(t)e^{-ik_a(t)\Delta x_{mj}} - \sum_{j=1}^{N} w_{a,j}(t)e^{-2ik_a(t)\Delta x_{mj}}\sum_{j=1}^{N} w_{a,j}(t)\zeta_{a,j}(t)e^{ik_a(t)\Delta x_{mj}}\right), \tag{3.21b}$$

with discrimant

$$D(t) = \Omega_a(t)^2 - \sum_{j=1}^{N} w_{a,j}(t)e^{-2ik_a(t)\Delta x_{mj}}\sum_{j=1}^{N} w_{a,j}(t)e^{2k_a\Delta x_{mj}}. \tag{3.21c}$$

The effect of non-stationary signals on the algorithm is discussed in Demonstration 3.14, 3.15 and 3.16.

Demonstration 3.14 (Change reflection coefficient over time) By changing the reflection coefficient over time, the variance of the signal changes over time. Because the water level remains equal, this problem can be solved using (3.15). The results are presented in Figure D.16. Clearly, the changing variance has little effects on both algorithms. Their performance is comparable to the stationary reflection coefficient case (Figure D.5).

Demonstration 3.15 (Sloping signal) In this demonstration, a water level variation of 0.5 meters over 8 minutes has been added to the signal. The water depth, therefore, changes from 1 meter to 1.5 meters. The effect of this slope on both methods is directly clear from the results presented in Figure D.17.

The Fourier method is disturbed by two effects. The first effect is the changing water depth, which effects the wave number through time. As the water level rises, the error of the Fourier separated waves becomes more variable. The other effect is the presence of low frequencies that are the result of the non-stationarity.

The result is that the wavelet separated waves are much closer to the original incident and reflected wave than the Fourier separated waves. The deviations of the wavelet separated important values are in the same order of magnitude as the case without slope (Figure D.5).

Demonstration 3.16 (Jumps) For this example the wave number was assumed to be for the depth of 1 meter, jumps of 0.5 meter were added as non-stationary elements. As known from Fourier analysis a jump is build of all frequencies (see equation G.10). However, the CWT is limited both at the lower frequencies because of boundary effects and on the higher end due to discretisation. The Fourier transform in general has a lower lowest frequency and a higher highest frequency. The results can be observed in Figure D.18. Both the separation in Fourier and wavelet domain cannot (fully) reconstruct the jump. When the signal is extended, it becomes clear from the error of the wavelet reconstruction that both the high and low frequencies close to the jump are missing to reconstruct the jump. The shape of the used wavelet, the Morlet 60 wavelet, is visible in the plot. In the Fourier case, there are also some expected Gibbs ripples at the edges of the jump.

Noise

The last signal element to discuss is noise. Noise can be present in the measurement, but can also be the result of for processes in the flume. Assume on both measurements uncorrelated noise is present. In this

ideal case it is expected that the noise does not affect the separation, i.e. it will all be directed to the residual signal. This type of noise is addressed in Demonstration 3.17. By filtering the signal before separating the waves, the effects of the noise on the signal is decreased.

Correlated noise, on the other hand, can be the result of processes in the flume for instance resonance of the structure or due to the digital processing of the signals. When there is a correlation between the noise of the gauges, this will not end up in the residual, but in the separated waves.

Demonstration 3.17 (Noise) In this demonstration different amounts of noise have been added to the simulated measurements. White Gaussian noise has been added with powers of 1/100, 1/10, 1, 10 and 100 times the power of the incident wave. The determinant limiter is set to 0.1. Both the two and five gauges cases are discussed here. In the case of where noise powers of 1/100, 1/10 and 1 times the power of the incident wave are added, the resulting separated waves for both methods are very close to the cases without additional noise. This is because the noise is spread over the whole spectrum, whereas the main power of the signal is in the frequency band $[0.5, 2]$ Hz. In the frequencies outside this band some disturbance is detected, but this does not significantly affect the results (i.e. reflection coefficient, m_0 etc.).

As the noise power increases, the separation is disturbed more; but there is a significant difference between the two and five gauges cases. In the extreme case of noise that has the power of 100 times the power of the incident wave, both results based on Fourier or wavelet coefficients are nowhere near the original incident and reflected wave. Both, however, perform better in the five gauges case than in the two gauges case: the energy in the separated waves is much less in the five gauges case than in the two gauges case. This is due to the lesser random correlations between five different noise signals than between two. Therefore more noise is filtered when there are more gauges in the system.

The results are shown in the appendix for a noise power of 10 times the incident wave power in both the three and five gauges case (respectively Figure D.19 and D.20). They are compared with the no noise cases in Figure D.7 and Figure D.8. By observing the spectra, it is clear that the noise in the high frequencies disturbs the resulting separation: noise on the signal is added to both incident and reflected wave. The main power bandwidth (0.5-2 Hz) of the separated waves is recovered well: the noise has little effect on the separated waves in this bandwidth.

In the five gauges case, the same random noise signal has been added to all gauges, which shows no difference at all with the uncorrelated noise case. This effect can be subscribed to the lack of phase difference between the noise. To distort the analysis, the noise has to have a correlation with the phase difference $k\Delta x$. Noise present in the flume, such as resonance behaviour, will be correlated with the right phase difference, which will affect the results.

From this demonstration may be concluded that filtering is not necessary for high SNR signals. The least squares method can filter low power noise very well. The more gauges there are in the system, the better the noise can be filtered. Signals with an SNR<0 dB will distort the algorithm and filtering on beforehand is advised.

3.2.6. Residual Signal Analysis

For real signals, the separated signals cannot be compared to a 'known' original incident and reflected wave. How well the estimate is, has to be based on the residuals. These can be computed by subtracting the sum of the recovered incident and reflected wave from the original signal. The residuals can be investigated in three different domains. These are the time domain, the frequency (Fourier) domain and the wavelet (time-frequency) domain.

If waves are compared in the time domain, the difference between the crest and trough height per wave is often analysed [24]. A wave is then defined as the signal between two up or down-crossings. Characteristics such as the height of the 1% highest waves of a set of waves are often based on these values. These values can be used to investigate the error over time.

In the frequency domain, the error per frequency is investigated. Moreover, the reflection coefficient often depends on the frequency. Therefore the frequency domain is the most common domain to analyse the separated waves in.

The residual coefficients in the wavelet domain can be analysed as well. These are defined by (3.11). Averaging the wavelet coefficients in scale is an estimator for the spectrum of the error, which can also be computed using the Fourier transform. The global wavelet spectrum thus has no added value over the Fourier

method.

The time domain method based on the crossings has the disadvantage that the residual wave often contains a different amount of zero-crossings than the original wave, which makes it hard to determine the (relative) error 'per wave'. A solution is to determine the maximum difference between the zero (up or down) crossings of the other wave. Here the scale averaged wavelet power spectrum (2.31) is used. A measure for the error over time can be made by dividing the SAWP of the original signal by the SAWP of the residual signal, resulting in:

$$\epsilon_{\text{rel}}(t) = \frac{\sum_a \frac{\left|\mathcal{W}\left\{\eta_j - \widetilde{\eta_j^I} - \widetilde{\eta_j^R}\right\}(a,t)\right|^2}{a}}{\sum_a \frac{\left|\mathcal{W}\{\eta_j\}(a,t)\right|^2}{a}}. \tag{3.22}$$

Residual analysis using this measure is applied in Chapter 5.

3.3. Guidelines

In this chapter two main subjects were discussed. The first subject was the improvement of time-frequency analysis through the continuous wavelet coefficients. The second subject was the application of continuous wavelet coefficients to separate incident and reflected waves travelling over one axis. The guidelines with respect to the WPS are best summarised in the form of the algorithm as presented at the beginning of this chapter.

Continuous Wavelet Coefficients

1. Apply signal extension to the signal. This results in the signal x. There are many different signal extensions possible (see Section 3.1.3) of which the most important ones are summarised in Figure 3.2.
2. Compute the Fourier transform $x = \mathcal{F}\{x\}$ using the FFT. Missing data points disturb the FFT and therefore have to be filled; different methods are presented in Section 3.1.4. The better the filling complies to the underlying data points, the less errors there will be in the coefficients based on a transformation with these points.
3. Choose a wavelet function ψ and a set of scales to analyse the signal as described in Section 3.1.1. The most used continuous wavelets are summarised in Figure 2.3. When the objective is to separate waves, it is important to pick a complex wavelet, with a small bandwidth.
4. For each scale, construct the normalised wavelet function using (2.23).
5. Find the wavelet transform at all scales a using the inverse FFT, see equation 2.24.
6. Determine the zones of influence. For a signal without missing data points, the cone of influence based on the e-folding time suffices. However, if a signal has missing data points, the zones of influence allows for more insight into the time-frequency behaviour of the signal. It is important to remember that the coefficients depend on the signal, the signal extension and the filling used. Different choices will lead to different coefficients. The COI and ZOI are only guidelines for the reliability of the coefficients, not strict borders.
7. The last two steps remain unchanged, i.e. remove any padding and contour plot the wavelet power spectrum;
8. and determine the confidence contour of the scalogram. Plot this contour and the cone of influence on top of the scalogram.

When averaging in time or scale is applied to the resulting coefficients, the effects of the signal extension on the coefficients have to be taken into account. Especially for high scales, the global wavelet spectrum may be underestimated. The scale averaged wavelet power is less trustworthy closer to the edges of the signal.

Separating Waves

The second main subject of this chapter was the separation of incident and reflected waves. Ma et al. [34] separates waves based on wavelet coefficients for two gauges. Zelt and Skjelbreia [63] use Fourier coefficients to separate the waves for N gauges. In this chapter a combination of these methods is presented: wavelet

coefficients of measurements from N gauges are used to separate waves. In Section 3.2.4 all influencing factors on the error of the separation are discussed. Numerical demonstrations of the influence of these factors are shown as well. A summary of the effects of these factors for the two methods is presented in Table 3.2.

Separation based on wavelets does not perform better than separation based on Fourier coefficients, except for non-stationary signals (as described in Demonstration 3.15). For these cases wavelet analysis shows its added value, by correctly separating the waves without effects of the slope. The wavelet-based method is affected much by the combination of the wave number k, the bandwidth of the wavelet and the distance between the gauges Δx. Because the wave number cannot be changed, it is important to minimise the distances between the gauges and the bandwidth of the wavelet used. Analysing the residual using the relative error in time based on the SAWP (3.22) allows analysis of the error over time.

For both method the error between the reconstruction and the original signals is rather high when using two gauges, and much less when more than two are taken into account. By adding more gauges the solutions improve a more and more, but the largest step is made from two to three gauges. Therefore the use of three well-spaced wave gauges is advised to solve the separation problem. More would lead to unnecessary costs (gauges) and data. Applying the weightings proposed by Zelt and Skjelbreia [63] does not seem to improve the results much.

The added value of these two subjects is addressed in Section 5.1. First, the noise filtering application of the discrete wavelet transform to signals in the field of coastal engineering is discussed.

Table 3.2: Summary of the influence of the different factors on the incident and reflected waves, for both Fourier (Zelt and Skjelbreia [63]) and wavelet coefficients.

Factor	**Zelt and Skjelbreia [63]**	**Wavelet-coefficient based**
Wave number	No influence	High frequency distortion
Number of gauges	Two: poor separation, three: increased performance, more: improvement if the determinant limiter is not used, else little difference. Distance between gauges influences the power loss in the separated signals using De Rooij, place gauges close together for less power loss	
Gauge placement	Important: $2\lvert\Delta x_{mn}\rvert / a\lambda_\psi \in \mathbb{Z}$ for each combination of $m, n \in \{1, \ldots, N\}$ [63]	
Determinant limiter	Corrects the results	Improves results, but also omits energy which leads to underestimation
Weightings	No influence of the proposed weightings by Zelt and Skjelbreia [63]	
Low frequency limit	Still large error for higher frequencies with determinant limiter close to 0	Results close to solution with determinant limiter, less energy is omitted
Wavelet	-	Wave number: short bandwidth wavelet important
Non-stationarity	Distortion for changing mean for low frequencies	No distortion for changing mean; time-dependent wave number can be applied
Noise	For high SNR, most noise goes to the residual, for low SNR, first filter the measurements before separating. More noise is reduced when a larger number of gauges is used.	

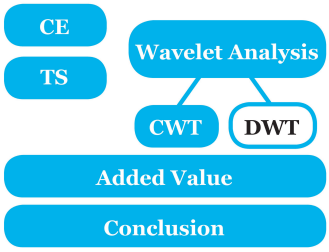

4

Denoising in the Discrete Wavelet Domain

In the previous chapter the computation and application of the continuous wavelet transform is discussed. This chapter concentrates on the application of the discrete wavelet transform (DWT) in noise filtering. Other applications of the applicability of the DWT are discussed in Chapter 5. In Section 2.3.2 the computation of the discrete wavelet transform was addressed and the basics of filtering using these discrete wavelet coefficients in Section 2.5.2. This chapter starts with a more elaborate overview of the different noise filter algorithms, followed by a description of the test cases. After that, the performance of the different filters is presented in Section 4.3, concluded with a discussion of the results.

4.1. Filter Algorithms

In Section 2.5.2 the basics of wavelet filtering are addressed: a signal is filtered by applying a threshold to (some) levels of detail coefficients. In Figure 4.1(a-d) some different discrete wavelet-based noise filter algorithms are shown in a more detailed scheme. A traditional wavelet filter algorithm is shown in Figure 4.1a. At the start of the filtering protocol a choice for a decomposition level k is made, resulting in k sets of detail coefficients and one set of approximation coefficients after applying the DWT. To filter the signal, thresholds have to be picked. This threshold is often based on the standard deviation (equation 4) of the first detail level, d_1. The universal threshold presented in (2.40) is an example of such a threshold. Thresholds at a certain level can also be based on the coefficients in that level, instead of the coefficients in the first level. When the thresholds are determined, they can be applied using hard, soft or other types of thresholding methods (more are shown in Figure 2.7). The thresholded coefficients are then inverse transformed, resulting in a filtered signal.

A disadvantage of this traditional filtering is the choice of decomposition level selection before applying

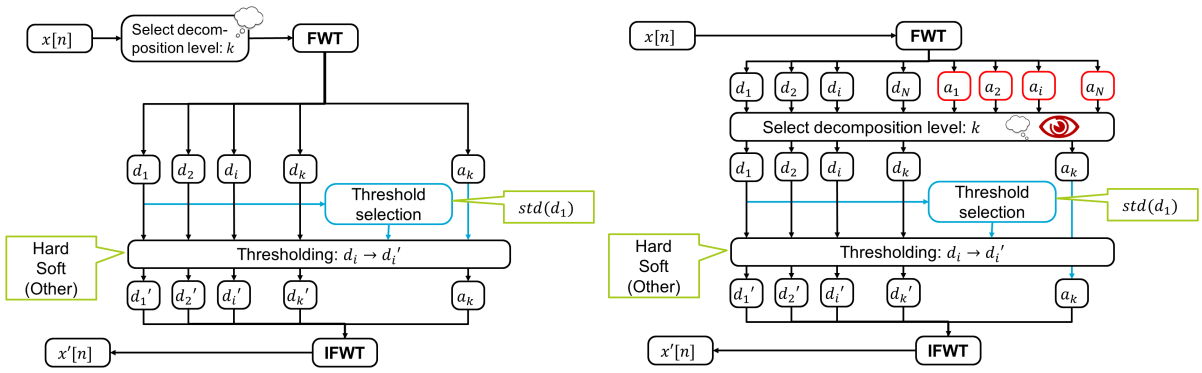

(a) Traditional wavelet filtering. Thresholds are often based on the standard deviation (std) of the first level. Another possibility is a per level threshold.

(b) Subjective wavelet filtering, changes with respect to traditional wavelet filtering (see **(a)**) in red.

Figure 4.1: Different filter algorithms

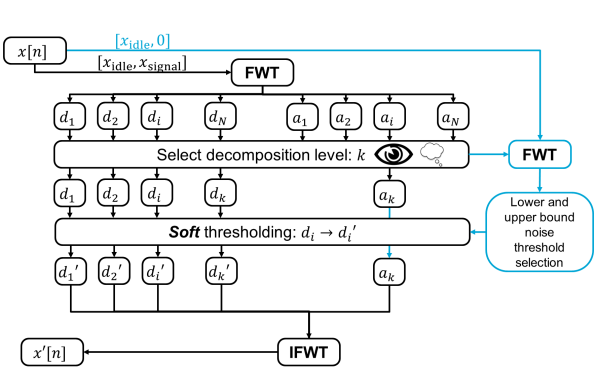

(c) Wavelet filtering based on a signal free period in the signal; threshold selection based on this period.

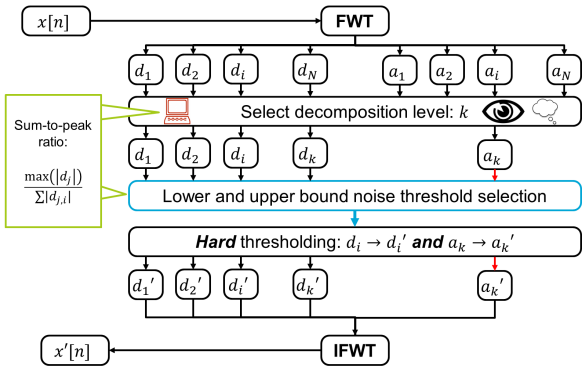

(d) Wavelet filtering by Srivastava [51], level selection possible via subjective and objective methods.

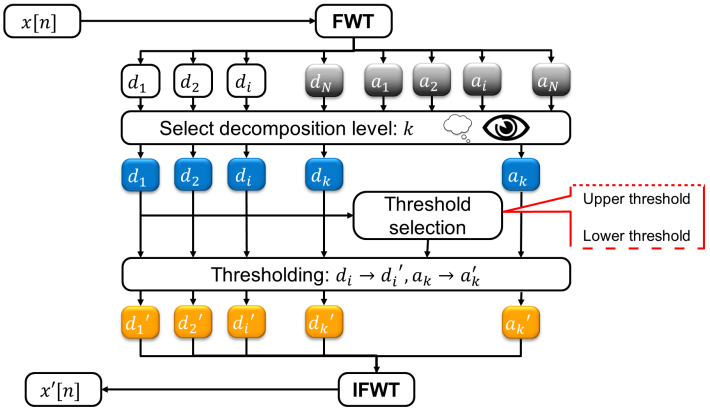

(e) Colours of the coefficients match colours in the plots containing the filters.

Figure 4.1: Filtering algorithms and implementation. The d_i denote the detail coefficients in level i, the a_i the approximation coefficients. By thresholding they are adjusted to d_i' and a_i' respectively.

the filter. This is a very subjective method that will lead to trial-and-error experiments to determine the correct levels. To improve the accessibility of subjective level selection, the decomposition level k is selected after all detail and approximation levels are visually judged. The judgement is discussed in Demonstration 4.1. This visual (subjective) level selection is shown in Figure 4.1b.

In this chapter, the results of this traditional filtering method, using both soft and hard thresholding, is compared to the results of two other threshold determination methods. Both these methods were presented by Srivastava et al. [51]. The first method is based on the fact that there is a period in the signal where there is no underlying signal: the measurement equipment is already turned on, but the experiment has not started yet. The recordings should therefore only contain noise. The discrete signal $x[n]$ is assumed to consist of two parts: a part in which is known there is no signal present, $x_{\text{idle}}[n]$ and a part in which the signal is present, $x_{\text{signal}}[n]$. First, the whole signal is decomposed to select a decomposition level. The signal $x_{\text{idle}}[n]$ is then padded with zeros until it has the same size as $x[n]$. This padded signal is decomposed, and the detail coefficient thresholds are based on the maximum and minimum values in this decomposition. These thresholds are applied by soft thresholding, (2.39). The support of the choice for soft thresholding follows from the question: what if hard thresholding is used? Then noise just a bit above the threshold will have a large impact on the filtered result, which is an unwanted effect. Therefore soft thresholding is used. This algorithm is denoted as the 'signal-free' algorithm.

The last algorithm is named after Srivastava [51]. There are three main differences between this algorithm and the more traditional ones. All three differences are highlighted in Figure 4.1d. The first one is the use of an objective measure to select the decomposition level. This measure is based on the peak-to-sum ratio

(PSR) of the coefficients. The peak-to-sum ratio for a vector $\boldsymbol{x}$ is defined as

$$\text{PSR}(x) = \frac{\max_n(|x_n|)}{\sum_n |x_n|}. \tag{4.1}$$

This ratio is not only used to select the decomposition level, but also to determine the lower and upper thresholds, which is the second difference. In the original thresholding, there is one threshold for the absolute value of the coefficients, not one for coefficients above and below zero. This change has also been applied to the signal free based filter. The last one is the use of hard filtering of the approximation coefficients at level k, where normally only detail levels are filtered, to also address the low-frequency noise in the signal.

It has been discussed before that most of the algorithms rely on a subjective level selection to denoise the signal. Only the Srivastava et al. [51] algorithm has an objective level selection method. To be able to subjectively select a level a clear overview of all approximation and detail levels have to be presented. In Figure 4.1e the different colours refer to the different colours used for lines in plots discussed in the demonstrations in this chapter. Blue lines represent the original detail and approximation coefficients up to k levels, the grey signals represent the computed coefficients that are not used in the filtered reconstruction, and the orange signals are the filtered coefficients. The thresholds are shown by dashed red lines; long dashes show the lower threshold, short dashes the upper.

4.2. Test Signals

In the last section, the different algorithms that are being tested were discussed. In this section, the signals on which they are tested are presented. For this the discrete signal $s[n]$ is defined as the sum of three signals:

$$s[n] = x[n] + w[n] + v[n].$$

Here x is the basis signal, this can be a stationary or a non-stationary signal. The non-stationary signal is based on the impacts present in the force measurement presented in Section F.1.3. w denotes the measurement noise, such as resonance behaviour, only added in the non-stationary signal case. It has a contribution around the 48 Hz and 120 Hz, like the force signal presented in Section F.1.3. At last v contains environmental noise, this can be white noise, red noise and noise at very specific frequencies, for instance originating from the power supply. However, from real data an SNR of over 200 dB was detected for the power supply noise (and its mirrors), it has been added to some test signals, but much effect is not expected because of its low contribution. Moreover, non-stationary environmental noise, such as nearby cellphone calls, are not simulated. The noise will be scaled with different signal-to-noise ratios (SNR, (2.36)). The test signals have a duration of 2 minutes, with a sampling frequency of 3 kHz. All test signals are filtered once, to compare the results of the different algorithms on the same case.

Demonstration 4.1 (Test signal and discrete wavelet coefficients) The three different elements of one of the test signals are depicted in Figure 4.2a. The four signals $s[n]$, $x[n]$, $w[n]$ and $v[n]$ are shown separately in this figure. The Symlets 8 wavelet is applied to decompose the signal s. This wavelet is advised for natural signals [51]. All the approximation and detail levels of this signal are shown in Figure 4.2b. In this demonstration, most noise is contained in the high-frequency range; i.e. the non-stationary signal is of relatively low frequency. This can be seen very clearly in the approximation coefficients; the contribution of the noise drastically decreases as details are omitted. This property is used to choose the maximum level to filter: in levels 1-7 noise is identified in the approximation component, for levels 8 and 9 this becomes harder, for levels 10 and up the noise is not distinguishable in the approximation coefficient. So a subjective choice for decomposition level 9 will be used for all algorithms expect the Srivastava et al. [51] algorithm.

A decomposition level of 9 is chosen for all algorithms except the Srivastava et al. [51] algorithm based on the results presented in Demonstration 4.1. After implementing the algorithms, some fine-tuning can be applied. Often this concerns changing thresholds or threshold methods. This fine-tuning, however, is not applied in this chapter, because the objective is to find the best denoising algorithm, not the best data analyst. As explained before, this algorithm bases some choices on the PSR, (4.1). Srivastava et al. [51] claims that this ratio is a good universal measure, however, after some tests with longer signals, different conclusions have to be drawn. This discrepancy in thresholds is because the Srivastava test signals contain 4096 sampling points,

signals in the field of coastal engineering easily contain over 3 million sampling points, which blows up the sum term in the PSR (4.1). Therefore the adjusted version contains a limited PSR, which is the maximum of the peak-to-sum ratios of segments of 4096 samples of the full-length input.

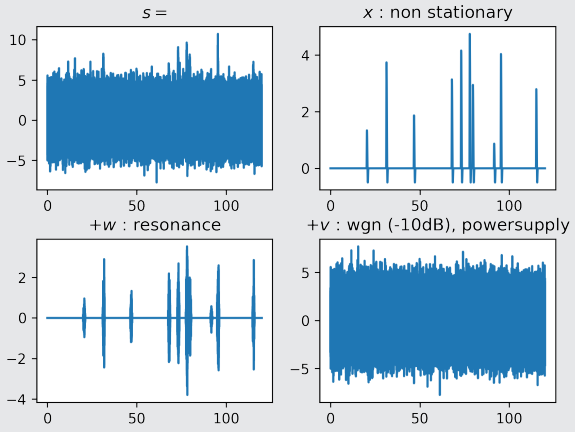

(a) The three signals and their sum

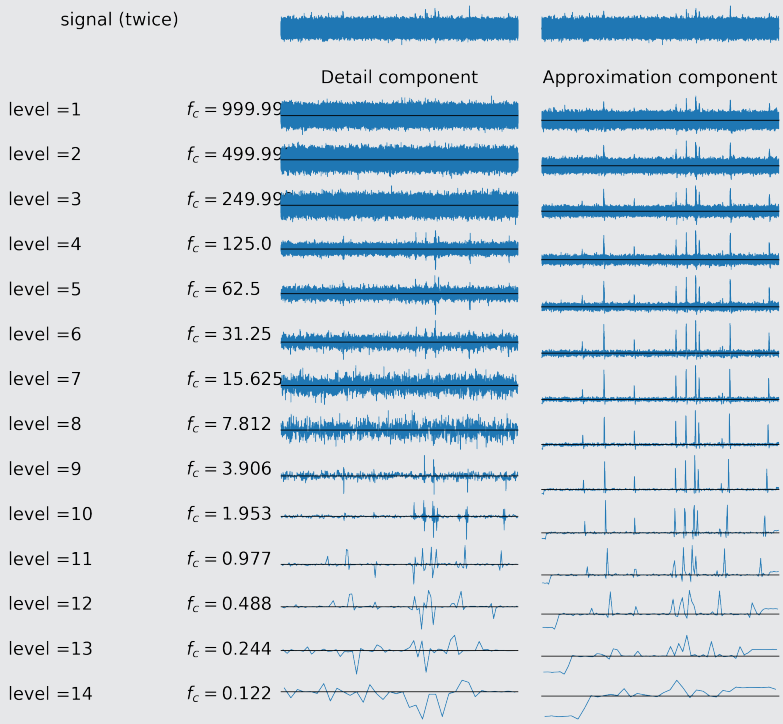

(b) The approximation and detail coefficients for the signal s from Figure 4.2a using the Symlets 8 wavelet. On the left of the coefficients the levels and the centre frequencies f_c of the wavelets are given. Note that all x-scales are the same, the y-scales are different. The black line shows the line $y = 0$.

Figure 4.2: Signal from Demonstration 4.1

Demonstration 4.2 (Srivastava filtering) The result of the Srivastava algorithm using the adjusted PSR is shown in Figure 4.3. The S denotes the PSR of the detail coefficients. For $S < 0.01$ the detail

coefficients are all considered noise, for $0.01 \geq S < 0.2$, there is noise present, but peaks contain information about the signal. For $S \geq 0.2$ there is almost no noise in the detail coefficients, so these are not filtered. Therefore the decomposition level is chosen as the last level with $S < 0.2$. Both these values are empirically based and can be adjusted for different signals. The automated threshold computation shows fairly good results. In level 4-6 the contribution of w in the signal is recognised and filtered out. The upper threshold of this approximation component is too high and will filter too much out. This can be adjusted manually, which will not be applied in this chapter.

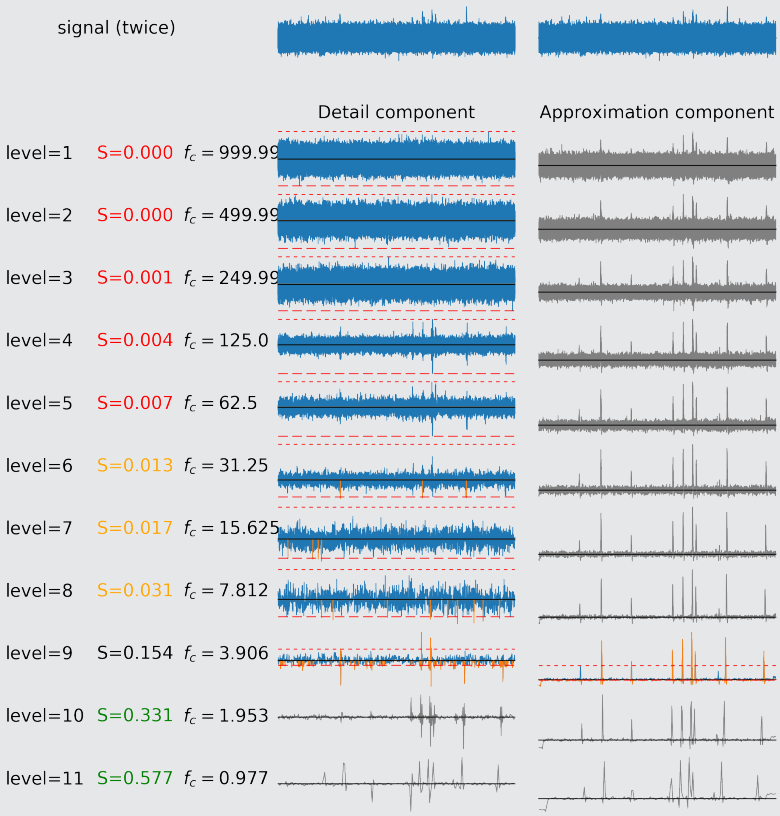

Figure 4.3: The approximation and detail coefficients and their thresholds, as by the Srivastava algorithm. The colours correspond with the colours in Figure 4.1e. The S denotes the PSR (or sparsity) of the detail coefficients at that level.

Let us compare the results from Demonstration 4.2 to the results of the hard thresholding algorithm using the universal threshold in Figure E.4 and to the signal free approach (Figure E.3), where for both a maximum decomposition level of 9 is subjectively selected. The different thresholding algorithms have resulted in different filtered results. The thresholds based on the signal free period let some part of the measurement noise through in the detail levels 4-6, while the universal threshold and the Srivastava based threshold filter it all out. Because there is no approximation coefficient filtering, both the hard and signal free based threshold did not omit any peaks from the stationary basis signal x, in contrast to the Srivastava algorithm. The effects on the reconstruction will be discussed in Section 4.3.

Comparison: Fourier Filtering

The performance of the wavelet filtering algorithms is being compared to the performance of a low pass filter. The filter has not been optimised per signal; neither are the wavelet filters. Some fine-tuning could increase the performance of the Fourier filter, which also holds for the wavelet filters. A low pass filter with a band-pass frequency of 10 Hz and a band stop frequency of 15 Hz is applied in both the stationary and non-stationary basis signal case. When the measurement noise w was not intended to be filtered out, a band-pass frequency

of 100 Hz and a band stop frequency of 150 Hz has been applied. The Fourier filter has been implemented via Matlab. In Chapter 5 some examples using coastal engineering data are discussed.

4.2.1. Different Wavelets

Until thus far the different choices of algorithms have been presented. There are, however, more choices that influence the filter result. The choice of wavelet, for instance, also effects the performance of the algorithms. In the Appendix C, in Table C.2, an overview of the different wavelets available in the PyWavelets package is presented. A total number of 75 wavelets that can be used the PyWavelets package [54]. From these, a set of five wavelets has been chosen to compare. These are:

Haar The Haar wavelet is expected to show poor results: its discontinuous behaviour in time or spectrum do not match any of the signals. This does also result in discontinuous behaviour in the filtered result.

Symmlet 8 Advised by Srivastava [51] for natural signals.

Coiflet 3 Its spectrum is close to the Symmlet 8 wavelet spectrum. So, little difference is expected.

Bior 2.8 A bi-orthogonal, symmetric wavelet. The spectrum of this wavelet has high resemblance with the spectrum of the stationary signal than the others: it has a faster decay toward high frequencies. The numbers denote respectively the number of vanishing moments of the wavelet and scaling function. (For more information see Appendix B.)

Daub 20 The Daubechies 20 wavelet is a wavelet with a long support in comparison to the others. Because of its high number of vanishing moments it has a short support in the frequency space.

These wavelets and their spectra are depicted in Section C.3.1. The choice of wavelet influences the choice of threshold, the reconstruction of the underlying signal and much more. The attentive reader notes that the tested wavelets are all real wavelets. This can be justified by the fact that the test signals are real, just like most signals from the field of coastal engineering. This leads to real coefficients, that can be used in the different algorithms. If a complex wavelet is used, the coefficients contain magnitude and phase information. This phase information is not needed for any of the algorithms, and thus only the magnitude information is of use. The algorithm based on a universal threshold applied with hard thresholding, from level 9 and up, is used to compare the results per wavelet.

4.2.2. Signal Extension Modes

In Section 3.1.3 the importance of the right signal extension method is emphasised. In the discrete wavelet domain, this is as important as in the continuous domain. Signal extension modes have to be applied to most signals; it is very important that the right signal extension mode is chosen before applying a filter. The thresholds are often based on the wavelet coefficients. If these coefficients are distorted by signal extension, this might lead to wrong threshold choices. Especially the thresholds based on a signal-free time are sensitive to poor signal extension mode choices. The PyWavelets packages [54] possesses 6 different signal extension modes:

- Zero-padding;
- Constant-padding;
- Symmetric padding;
- Reflect-padding;
- Periodic: signal is treated periodic, a special mode to compute the least possible number of coefficients is called 'periodization';
- Linear extension.

The standard setting of the PyWavelets decomposition function is the symmetric extension. This setting has been used for all test cases. The coefficients near the boundaries in Figure 4.2b do not show any remarkable behaviour in the detail coefficients, as do the approximation coefficients.

4.2.3. Different Dilation Factor

In the derivation of the DWT through multi resolution analysis (Appendix B) has been done with the dilation factor 2. Generally speaking, the use of this factor 2 results in the wavelet in the next level being twice as long

and the bandwidth of that same wavelet is halved. Another dilation factor can be used as well [28]. With a dilation factor $m > 2$, for one scaling functions, there are $m-1$ different wavelets. The use of different dilation factors may have its advantages [4]. A dilation factor of 2 results in a shift variant transform, with another dilation factor the transform can become more or less shift invariant, and a larger set of smooth wavelet families can be used. These families can posses characteristics like both symmetry and orthogonality, which cannot be in the case of $m = 2$. The use of a larger dilation factor will, however, not necessarily result in better algorithms. It will complicate the filtering steps, because it results in more coefficient levels, leading to more thresholds, which is less user-friendly.

4.3. Results

In this section, the results of the performance of the different filter are compared to the results of the low pass filter. First, the results of the different algorithms are discussed, followed by the effect of the different wavelets. The results are discussed in difference in signal-to-noise ratio (SNR) in dB.

4.3.1. Filters

The result of the comparison of the performance of the different filters on the different signals is presented in Figure E.1. Here, the first thing to note is the lack of improvement in any red noise case. The red noise that is added to the signal has a slope of -6 dB per octave, which originates from sound signal processing. An example of a signal and its red noise can be found in Figure E.11. This has high power for low frequencies, decreasing as the frequency increases. This results in much disturbance of the signal in and below the range of frequencies it consists of (1-10 Hz). Therefore the red noise is not filtered by any of these filters. Moreover, this kind of noise is not present often in coastal engineering time-series. A different filter design is needed to filter this type of noise, which was not a part of this thesis. The red noise cases will therefore not be discussed any further.

In the stationary cases the low-pass filter outperforms all wavelet filter algorithms, although, for the higher SNR, the signal free and universal hard threshold method approach the performance of the low pass filter. This result is to be expected because the low pass filter is very effective in filtering higher frequencies. If we compare the different wavelet filtering algorithms in the stationary cases, the Srivastava algorithm performs the worst, in the high SNR case it even distorts the signal more. The Srivastava algorithm was not to expected to perform well in the stationary signal case; i.e. the PSR is effective to filter peaks from the rest of the signal. In the stationary case, there are no real peaks, therefore this a poor measure.

In the case where the non-stationary signal has to be filtered from the noise, it is the other way around: the wavelet filter algorithms perform better than the low pass filter. In general, it is noted that the filters have more effect when there is more noise on the signal. This is consistent with the low pass filter performance in all cases as well. First, the filtering of both measurement and environmental noise is addressed. The universal threshold (applied hard or soft) performs much worse in the case when there is measurement noise present than in the case where there is no measurement noise. The Srivastava and signal free based algorithms show less difference between these two cases. No conclusion can be drawn on the effect of the power supply based on this data, the results with and without are too close together. To do give a statement about the effect of the power supply, the experiment should be repeated many times.

From the results presented in Figure E.1 it is concluded that in the high SNR cases there is little difference between low pass and wavelet filtering for the stationary case. When the noise increases, especially the universal soft, hard and signal free based algorithms perform much better than the low pass base case. The performance of the Srivastava algorithm stays behind, even with the adapted PSR.

In Figure E.12 the result of different filters is shown. This is for the non-stationary case, with much noise, SNR= -10 dB and measurement noise. From this figure it is clear that the low pass filter leaves too much noise on the signal, the other signals show a nice reconstruction of the jump in the signal. They all show some deviations at different places. From this figure, one cannot derive which of the four algorithms performs the best overall. However, it is clear that the soft and the signal free based best reconstructs the maximum peak. The application of soft or hard thresholding, based on the MAD do have almost the same filter result, this is due too high thresholds. Therefore there is little difference between soft and hard thresholding.

4.3.2. Wavelet Comparison

In the comparison of the five different wavelets, the hard thresholding based on the universal threshold was used. Due to the poor results for filtering red noise, only the white noise cases are compared. The results in

terms of the difference of SNR are presented in Figure E.2. The results per wavelets are addressed here:

Haar Was expected to show the worst results, because of its discontinuous nature. In the stationary basis signal case the Haar wavelet was outperformed by all other wavelets. In the non-stationary, high SNR case it seems to perform slightly better than the others in filtering w. The Haar-wavelet is a relative short wavelet (filter size 2), therefore the addition of an extra decomposition level could increase its performance. The downside of the Haar wavelet is that the reconstruction will shows jumps.

Symmlet 8 In the stationary signal case this wavelet has a comparable performance with the Coiflet 3 and Daubechies 20 wavelet. In the non-stationary case, it performs best in filtering both the measurement noise and the environmental noise from the signal.

Coiflet 3 This wavelet has a spectrum that is very similar to the Symmlet 8 wavelet. This is also directly observed from the results: their performances differ just slightly. It is outperformed by one of the other wavelets in all cases.

Bior 2.8 The bi-orthogonal wavelet can increase the SNR at least 0.5 dB with respect to the other wavelets in the stationary x case. In the non-stationary base case, it performs best in filtering the environmental noise. Other wavelets are better for filtering both the environmental and the measurement noise. The bi-orthogonal wavelet is the only symmetric wavelet in this comparison. The stationary signals and the measurement noise w both have symmetric characteristics. This is why these are addressed best by the bi orthogonal 2.8 wavelet.

Daub 20 The Daubechies 20 wavelet results in comparable noise reduction with respect to the Symmlet 8 and Coiflet 3 wavelets.

4.3.3. Discussion

When dealing with stationary signals and white noise, the use of standard low pass filtered is advised over the use of wavelet filtering. This is consistent with the Fourier theory, which is well-suited to stationary signal situations. For non-stationary signals, especially signals containing peaks and discontinuities, the Fourier theory is not applicable anymore.

Wavelet analysis is better applicable to these non-stationary cases. Filtering in the wavelet domain shows much better results than the use of the low pass filter. However, in this domain, there are much more choices to make than in the frequency filter domain. What wavelet to choose? What signal extension mode to pick? Which decomposition level to use? It is shown that different wavelets result in different outcomes of the algorithms. From theory, it is known that the resemblance of the wavelet in time and frequency domain with the signal is a good estimator of its effectiveness [37]. This theory is consistent with the results of the comparison presented in this chapter. The signal extension mode has to fit the data and has to prevent large jumps or other discontinuous behaviour to affect the coefficients as little as possible. A subjective and objective measure to pick the decomposition level have been presented, a combination of these two will be a good guide for an analyst.

There are many fine-tuning elements that differ per used signal, such as finding a filter that does filter the environmental noise but does not filter the measurement noise. A general objective method does not seem to exist; it is probably easier, faster and more precise to apply some subjective fine-tuning to the thresholds for a whole set of similar signals. The Srivastava conclusions are well-drawn for the short signals they address, but they do not hold for the 30 minutes 3 kHz sampled signals from the coastal engineering field.

4.4. Recommendations Noise Filters

At the end of this thesis some recommendations will be discussed. These are focussed on the application of the discrete wavelet transform in the field of coastal engineering. Therefore some recommendations concerning the compared wavelet-based noise are addressed here. For starters, red noise cases will have to be challenged with different algorithms. The algorithms compared in this chapter are not suitable in these situations.

The signal free algorithm does show high noise reduction, however, there are some improvements to this algorithm. First note that the signal free period is zero-padded, however, we know from DWT theory this might lead to high coefficients at the boundary between the signal free period and the zero-padded part. For instance, a mean value of the signal containing part of the signal could be used as well. However, also other signal extension modes can be evaluated. Furthermore, it is interesting to consider whether approximation level filtering can be part of the signal free based algorithm.

The Srivastava algorithm did not work as well as predicted. The peak-to-signal ratio is a good basis as a measure, but very dependent on the combination of number of peaks in comparison to the length of the signal. Furthermore, the approximation level filtering is not always necessary. It often disturbs the signal more than the same algorithm without the approximation level filtering. The use of the peak-to-signal ratio to select the right decomposition level has proven itself useful and could be used in different algorithms. A separate threshold for coefficients above and below zero is another improvement which can be used in other algorithms.

Most wavelet filter algorithms show great improvements in SNR in stationary noise situations. Non-stationary noise situations have not been addressed, but the performance is predicted to drop. The thresholds are stationary, and when applied to non-stationary noise, this cannot result in non-stationary noise filtering. This also has been seen in the coastal engineering signals, where some non-stationary noise is present. Moreover, a different thresholding technique may show some improvements as well (see Figure 2.7).

On the computational side of the algorithms there are many improvements possible. However, not much time will be gained for the signals discussed. The computers are fast enough to change from time to discrete wavelet domain and back in little time. If there is need for improvements, one can think of the use of the fast Fourier transform instead of the convolution, and to implement a DWT algorithm without down-sampling to speed up the shifting algorithm.

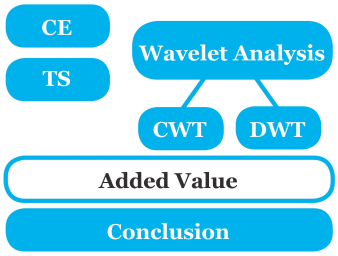

5

Added Value of Wavelet Analysis

Multiple applications of wavelet analysis have been addressed and expanded in the two previous chapters, to improve signal analysis and signal processing in the field of coastal engineering. In Chapter 3 the different applications of the continuous wavelet transform are discussed. The interpretation of coastal engineering data is improved by adding different signal extensions and zones of influence offer guidance for missing data points. Long signals can be down-sampled in to analyse them faster. Furthermore the separation technique for incident and reflected waves in the wavelet domain has been expanded and compared to the current Fourier method by Zelt and Skjelbreia [63]. Section 5.1 addresses the added value of these applications of the continuous wavelet coefficients.

Section 5.2 focusses on applications of the discrete wavelet transform, of which noise filtering is already discussed in Chapter 4. In this chapter, a comparison is made mainly between Fourier and wavelet filters. However, in this chapter, these two will be compared to the filter technique used at Deltares. Furthermore, some other applications of the discrete wavelet transform in digital signal processing will be addressed. At the end of the chapter, the computational intensity of the Fourier and wavelet approaches are compared.

5.1. Spectral Information

In this section, the use of regular (Fourier) spectral information is compared to the spectral information expressed by the continuous wavelet coefficients. These are determined in discretised form using the DCWT, (2.22). In Section 3.1.2 is described that for long or over-sampled signals, down-sampling can be applied. The down-sampling procedure, however, removes energy from the signal. To compare the wavelet coefficients based on down-sampling with the coefficients based on the original signal, they should be multiplied by a factor $\sqrt{d}$, as described in equation 3.2.

In Section 3.1.3 it has been made clear that the continuous wavelet coefficients near the boundaries are sensitive to the signal extension method that is used. In Figure 3.2 the most common signal shapes are tied to preferred signal extension methods. Important is to take the drawbacks of the signal extension method into account. The signal extension method should be chosen with care, based on the objective of the analysis.

5.1.1. Missing Data Points

Missing data points disturb standard frequency analysis. For a stationary signal, the effects of some missing data points are fairly predictable, i.e. the power in the spectrum is expected to reduce with the same factor for all frequencies. Filling gaps could lead to sharp edges in the signal disturbing both low and high frequencies. A comparison of two energy spectra (one disturbed, the other not) is given in Demonstration 3.2. The introduction of sharp edges by filling the data results in disturbance over all frequencies. This is due to the frequency contribution of the sharp edge (see equation G.10). If the signal is non-stationary or contains non-linear signal elements, these effects are even much more unpredictable.

As the wavelet coefficients are dependent on translation (time), the effect of the gap onto the coefficients can be taken into account. This is done by determining the amount of wavelet energy disturbed by the missing data points (see equation 3.4). In Figure 5.1 the so-called zones of influence are depicted with dashed lines. They show the wavelets that are disturbed more than 95%. In the 8 to 16 days area some areas are

marked as significant that are outside the cone of influence based areas (dotted lines). This expansion results in more insight into time-frequency behaviour of the presented signal, that was not available before.

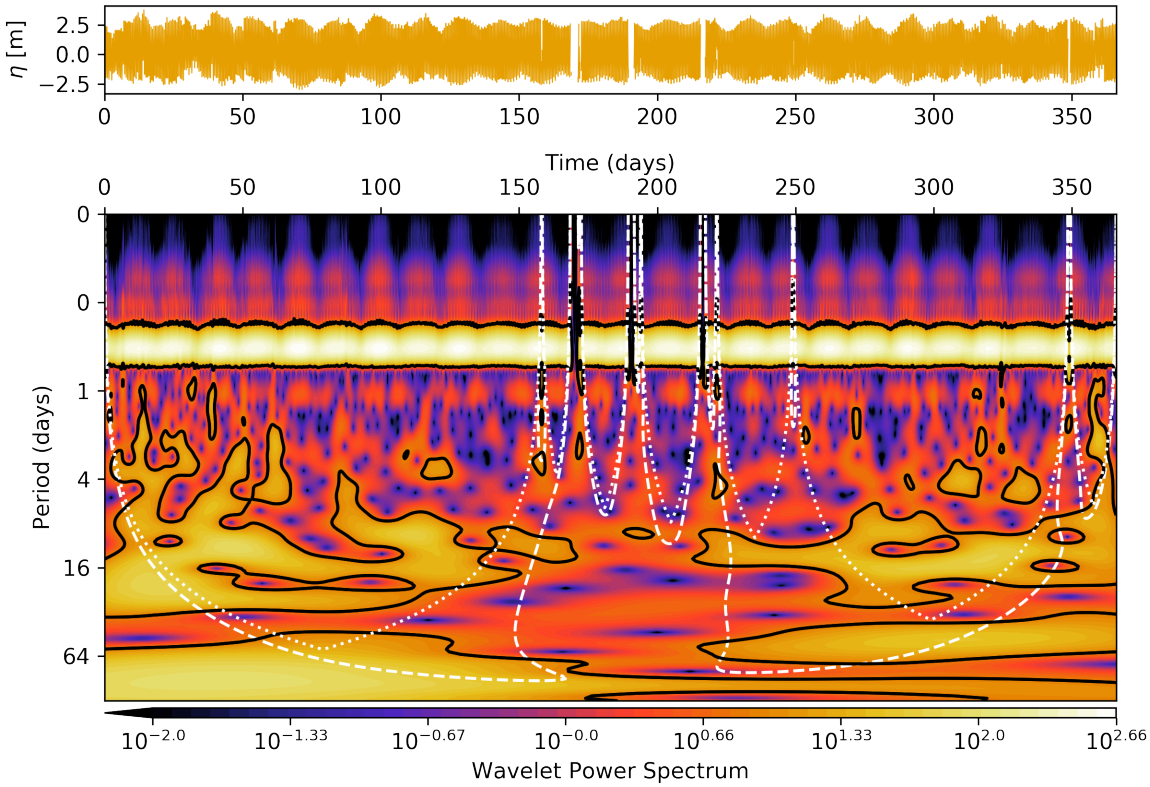

Figure 5.1: Wavelet power spectrum of surface elevation measurements from the Westerschelde (see Section F.1.1). WPS based on Morlet 6 wavelet, mean signal extension and mean NaN filling applied. COI: dotted line; 95% ZOI: dashed line; 95% confidence area based on WGN assumption: black line.

Other Wavelet Applications

Regular coherence and correlation of spectra based on missing data time-series are not used because they are unreliable. The wavelet cross spectrum can be calculated, and its reliability could be determined by multiplying the zones of influence of the two signals. In the wavelet coherence, the smoothing operator has to be taken into account when using the zones of influence to determine reliability. Averaging of the wavelet power spectrum will lead to the same problems as the Fourier transform for filled signals, i.e. the effect of the filling on the result is hard to predict.

5.1.2. Separating Waves

In the standard wave separating techniques, Fourier coefficients are used to separate the incident and reflected wave. In Section 3.2.5 is shown that wavelet coefficients are more effective to use in separating non-stationary signal cases than Fourier coefficients. Fortunately, many signals in coastal engineering have stationary characteristics, which allow analysis through the Fourier coefficients [24]. In the following example, a non-stationary wave from the field of coastal engineering is discussed. Not only the separation of the incident and reflected wave is discussed; other wavelet applications will be addressed as well.

The non-stationary case that is addressed in the following example is an experiment where the water level in the flume is increased by 20 cm over 72 minutes and then decreased again, to mimic the effects of the tide. A more elaborate signal description is given in Section F.1.2. This increase in water level influences the wave number k. There are two options to apply the method of Zelt and Skjelbreia [63] on this signal. The first is to apply the separation to segments of the signal, assuming a constant water level within this interval[1]. This,

[1] Is applied at Deltares at this moment

however, results in separated waves with discontinuities. The other option is to use the mean water level for the whole signal, as is done in Section 3.2. This does result in separated continuous waves. That is the case that is compared with the separation using wavelet coefficients in this section.

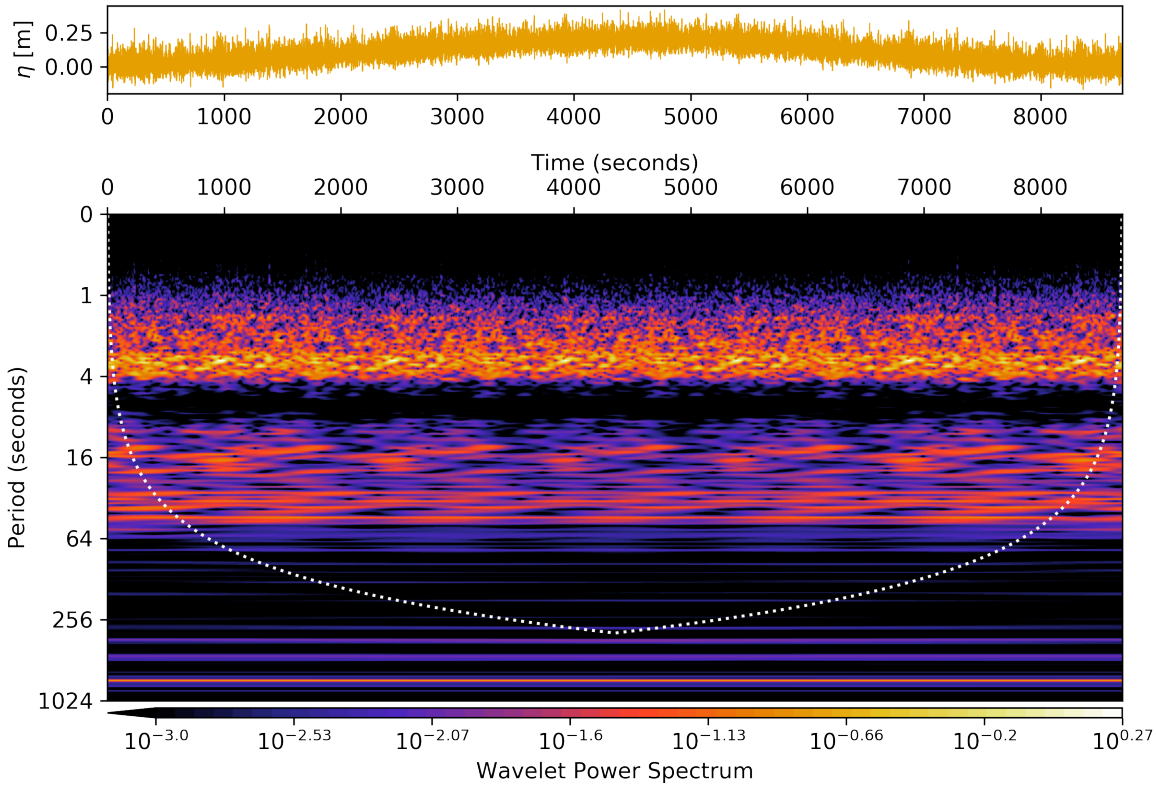

Figure 5.2: Wavelet power spectrum of deviation of water level at first gauge using the Morlet 60 wavelet.

Averaging

The signal used to separate waves is shown in Figure 5.2. The wavelet power spectrum shows high power in the periods of 1-4 and 8-64 seconds. The first band, 1-4 seconds, is dictated by the settings of the wave maker. In the band between 8 to 64 seconds is relative much power compared to the periods between 4 to 8 seconds. This power is assumed to be the result of the pumps that actively regulate the mean water level in the flume during the experiment. These two bands are also distinct in the global wavelet spectrum shown in Figure 5.3a. In this figure, the global wavelet spectrum is compared to the regular Fourier spectrum. In general, the GWS is a good approximation of the underlying Fourier spectrum [55], however, note that in this case the wavelet power decreases after a period of 256 seconds and the Fourier power increases. This discrepancy is the result of the non-stationary water level and will cause low-frequency effects in the separation in the algorithm of Zelt and Skjelbreia [63].

Cross-wavelet Applications

Furthermore, we have a look at the cross-wavelet spectrum and wavelet coherence of two neighbouring measurements. These are shown in Figure 5.3b and Figure 5.3c. It is clear that the power in both period bands is present in both signals. From the wavelet coherence plot, the coherence between the two signals is not directly clear. From the average over scale, it becomes clearer that the coherence in the 4-64 seconds period band is high (Figure 5.3d).

Separated Waves

The waves are separated using both Fourier and wavelet coefficients. In the Fourier case, the mean water level over the whole experiment is used to determine the wave number. Three cases are compared: no determinant

limiter, a determinant limiter of 0.1 and the case without determinant limiter and without all frequencies below 1/10 Hz. The results of these cases are presented in Section F.2.1.

When no determinant limiter is used, the Fourier-based reflection coefficient is 1. As expected, it is plagued by especially low-frequency disturbance. The wavelet-based reflection coefficient is around 0.45. This is pretty high because a reflection coefficient $\leq 1/3$ is expected.

When the determinant limiter of 0.1 is used both methods find a reflection coefficient of about 0.25. The reconstructed waves do not overlap exactly, but their wave characteristics are comparable. When the limiter is used, some energy that is in the waves is not taken into account in the reconstruction. If instead of a limiter, only the frequencies below 1/10 Hz are not taken into account, the Fourier reflection coefficient is about 0.5. The wavelet-based reflection coefficient, however, becomes 0.26, just slightly higher than in the determinant limiter case. This is because the m_0 of the incident wave is slightly lower and the m_0 of the reflected wave slightly higher. The total energy of the sum of the reconstructed waves is comparable.

So the difference between 0.26 and 0.42 can be assigned to the frequencies below 1/10 Hz. These were assumed to be the result of the active water level regulation. Looking back at the cross-wavelet spectrum shown in Figure 5.3b, much energy is present in the periods above 10 seconds. Moreover, the coherence of these periods is large as well, thus on beforehand this effect could have been predicted.

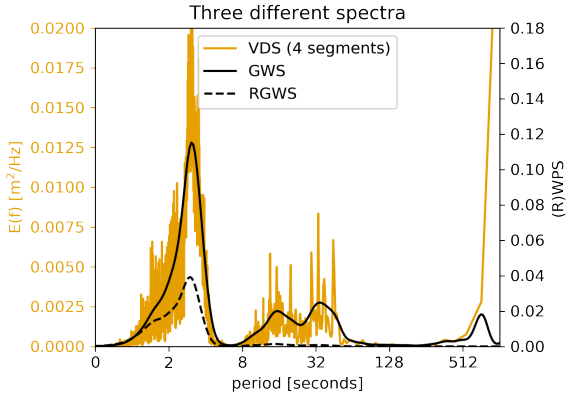

(a) Comparison of Fourier spectrum and GWS using the Morlet 6 wavelet.

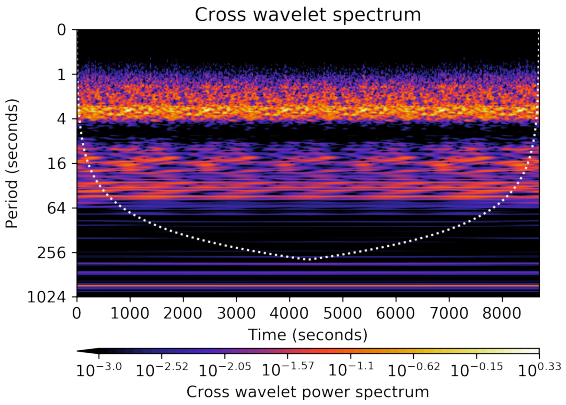

(b) Cross-wavelet spectrum for the first and second water height meter (Morlet 60 wavelet).

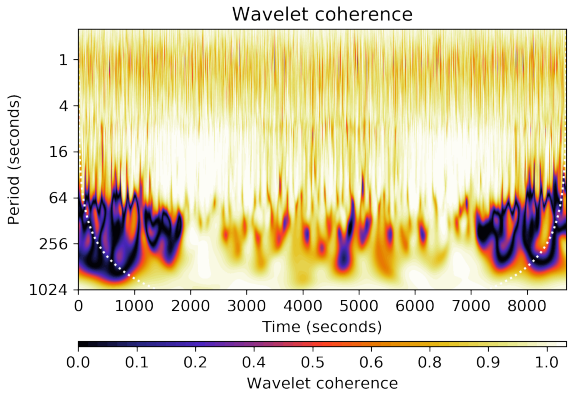

(c) The wavelet coherence for the first and second water height meter (Morlet 6 wavelet, using code of Grinsted et al. [22]).

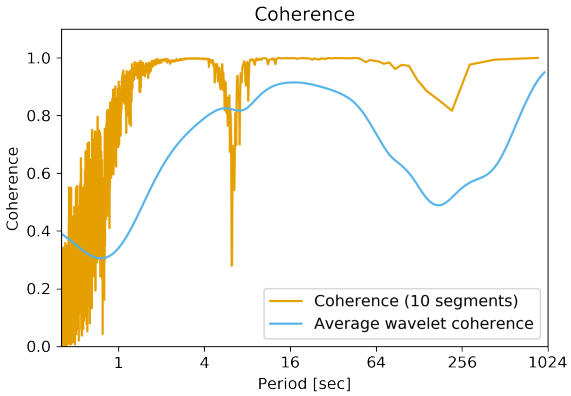

(d) The Fourier coherence and average wavelet coherence

Figure 5.3: Cross-spectral analysis of waves for WL657585e (more information: Section F.1.2)

Residual Analysis

Residual analysis is performed on the case with a minimum frequency of 1/10 Hz, without determinant limiter (Figure F.5). This analysis is done for the separation based on Fourier coefficients and based on wavelet

coefficients. In Figure 5.4a the spectra of the residual for both methods are shown. As is expected from the results in Figure F.5 the relative error per frequency deviates between the wavelet and Fourier-based separation near the frequencies affected by the gauge spacing. Note that this relative error is mostly high at low power frequencies, therefore the contribution to the absolute error is low.

This also becomes clear from the error of the separated waves over time. In Figure 5.4b three different errors are displayed for the first 2000 seconds of the measurement. The error based on the wave height distance between two down-crossings of the original signal minus the water level is plagued by many spikes. This is because the down-crossings of the original signal are not at the same places as the down-crossings of the residual signal. The other two errors are based on the scale averaged wavelet spectrum (SWAP) of the residual signal, as defined in equation 3.22. The error of the Fourier and the wavelet-based solutions are almost equal. Note that this method of analysing the residual error is thus not flawless. From the results (Figure F.5) it is clear that the estimate based on the wavelet coefficients is much better than the one based on the Fourier coefficients. Errors in the incident and reflected wave often cancel each other, resulting in a comparable residual signal.

In Figure 5.4c the error and the wave height are both shown in time. There is a clear correlation visible between a high relative error and high waves, i.e. for larger waves the relative error is larger. Sorting the waves from high to low does indeed show that the correlation is true (see Figure F.6). Thus the absolute error for large waves is even larger. So the separation of waves is less accurate for larger waves, i.e. the largest incident and reflected waves are underestimated or overestimated most. This effect was predicted based on the fact that higher waves are subject to non-linear processes that are not taken into account due to the linearity assumption at the basis of the separation algorithm.

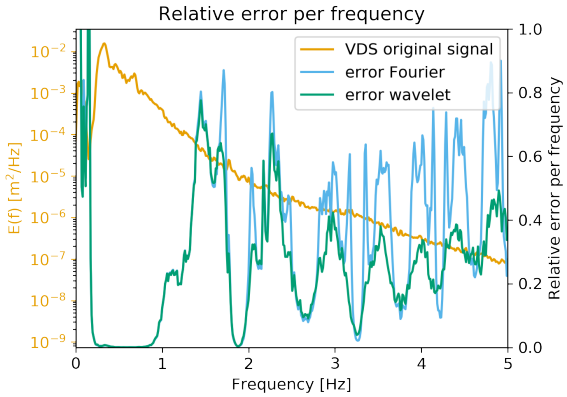

(a) Relative error per frequency of separated waves.

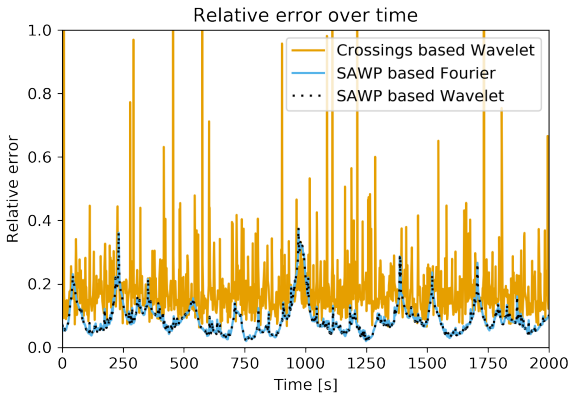

(b) Relative error in time, based on difference between crest and though per wave (on the left) and based on SAWP (on the right).

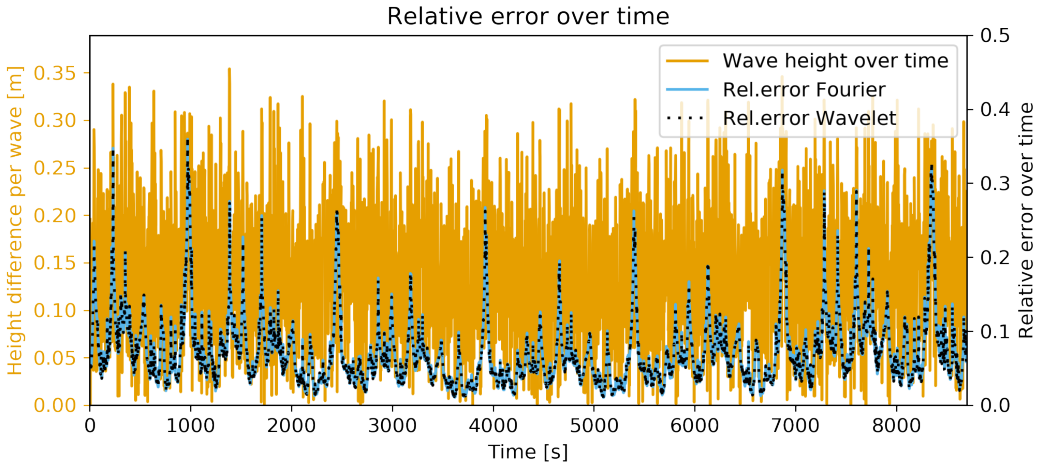

(c) On the left: height difference per wave in time. On the right: $\epsilon_{\text{rel}}(t)$ from (3.22) for both methods.

Figure 5.4: Residual analysis of separated waves case WL657585e (more information: Section F.1.2). The relative errors based on the SAWP are filtered using a moving average filter with a length of an average wave (i.e. 43). The Morlet 6 wavelet is used to determine wavelet power.

5.2. Discrete Wavelet Decomposition Filtering

There are numerous applications of filtering in Coastal Engineering. In Chapter 4 different noise filters are compared. In this section also other applications will be presented. The first one is filtering in general. Often data analyst filter signals based on gut feelings, lacking a justification of the used filter. The first example shows that these gut feelings are correct int his case. However, comparable results can be obtained through reasoning based on the discrete wavelet decomposition. The second example will show the added value of filtering with respect to non-stationary signals and the brought spectrum of discrete wavelets. The last example shows the filtering of a transient from the rest of the signal.

Filter Force

The first example discussed here, is a force measurement from the measurement A3W1T304 (see Section F.1.3). The goal of the filtering is to reconstruct the peak forces in the signal. Due to effects such as resonance and noise, the peak can be over or underestimated. Such an error has its effect on structures that are designed or tested based on these measurements.

These signals are normally filtered using the Savitsky-Golay(x, y) filter. This filter bases the filtered data point on the fitting of a y^{th} order polynomial through x data points [39]. The setting used in this case is based on 'gut feelings' and is set on $x = 201$ and $y = 5$. This will be compared to two wavelet filters and a low-pass filter with a cut off frequency of 16 Hz. The wavelet used in both filters is the Symlets 8 wavelets, based on its result in Chapter 4. The objective of the filtering is to find the peak force of the signal.

The first DWD filter is based on noise in the ten first seconds of the measurement (Figure F.8). The result of this filter is shown in Figure 5.5a. Noise is filtered out, but the resonance frequency is still in the signal. If the moments of impact are studied more carefully (Figure F.7), the approximation coefficients show that the resonance frequency is mainly caught in the sixth and seventh detail levels. The second filter (Figure F.9) therefore omits all detail coefficients from these levels. Resulting the signals shown in Figure 5.5b.

Both wavelet filters have also been applied in shifted mode. The peak values of the different filters are:

- For the Savitsky-Golay(201,5) a peak value of 20.8 is recovered,
- the low-pass filter recovered 20.5 at the peak,
- the wavelet filter (with detail levels 6 and 7 omitted) without shifting 20.9 and
- the shifted one 20.3.

Note that these values are relatively close together, but that the shifted wavelet filter has recovered the lowest value. For many structures, some resonance is expected, but this may be not as much as in the scaled model in the flume. By soft thresholding, the analyst can choose to damp the resonance. This is much easier in wavelet analysis than using other filter types.

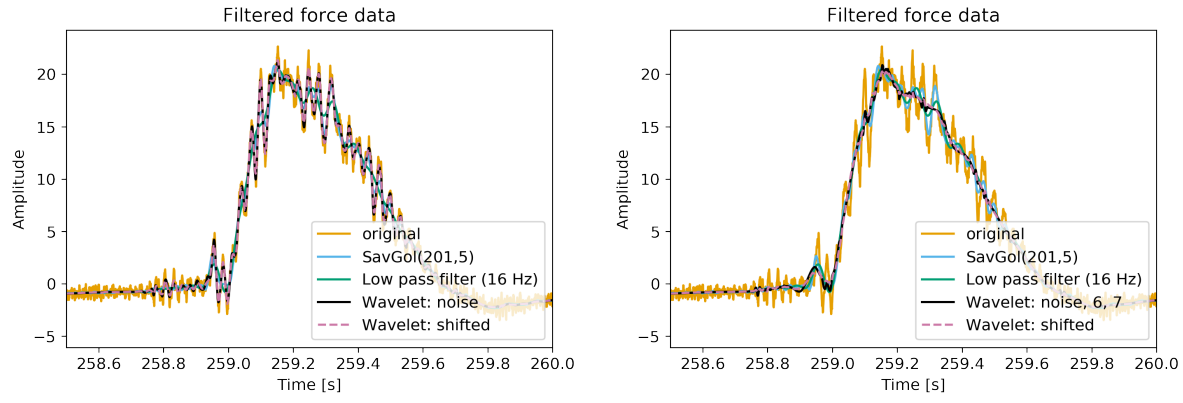

(a) Filtering noise from signal

(b) Filtering noise and resonance from signal

Figure 5.5: Filtering force signal from A3W1T304 (see Section F.1.3).

Over-topping Reservoir

In this second example, we consider a water height measurement from the over-topping reservoir. To learn more about the forces on the structure, the water slamming over the structure is captured in the over-topping reservoir. The goal is to determine the volume of water that is filling this reservoir. This can be done by multiplying the water level difference due to an over-topping with the area of the reservoir. However, due to non-stationary effects such as sloshing this water level is quite hard to read. To reconstruct the underlying signal with jumps and without these vibrations a wavelet filter based on the Haar wavelet can be used (Section C.2). A standard frequency filter would be completely useless because filtering would lead to a smoothing of the jumps.

The Haar wavelet, in general, is not much used, however, for this application it is perfectly fit. There will not be a delicate filter design as discussed above, only the reconstruction of the approximation levels will be used. In Figure 5.6a the reconstruction of a number of different levels is shown. The level 15 and 16 reconstructions appear to be too fine to use as estimator for the surface elevation after a pulse. The level 17 and 18 reconstructions, on the other hand, are too coarse. This is illustrated in Figure 5.6b. The width of the Haar wavelet these levels is too large to catch the jumps on a smaller scale.

Here the level 16 or 17 approximation level would be advised. Jumps are reconstructed very clearly, however, they do not all appear on the time at which the largest difference in the original signal is observed. This is the result of the dyadic structure of the discrete wavelet decomposition. By shifting the signal, the jumps can be shifted so that they occur at the same time as the original jump. By changing the sampling interval the problem cannot be solved, i.e. this problem moves to other scales. For jumps close to each other, lower level approximation coefficients will have to be used to reconstruct the jumps at that scale.

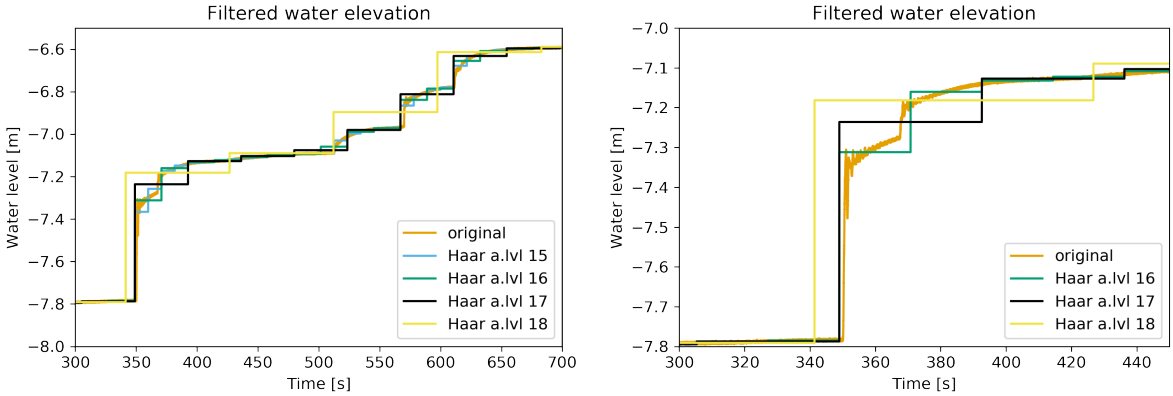

(a) Part of the signal

(b) Smaller part of the signal

Figure 5.6: Reconstructing jumps in signal using the approximation levels of the Haar wavelet decomposition.

Transient

Another useful application of filters in the discrete wavelet domain is the ability to extract transients from a signal. Transients are signal elements of short duration and unpredictable nature. A transient decays fast, has an unknown frequency content, and has an unknown arrival time [42]. For instance when forces on structures in breaking wave conditions are investigated transient-like signal elements appear in coastal engineering research. Such a signal is considered in this final example. Due to the confidentiality of this recording, no background or dimensions regarding this signal are given.

In Figure 5.7 two consecutive wave impact are presented. The first hit is a non-breaking wave; the second one is due to a breaking wave. The force exerted on the structure by such a breaking wave is in general described as the sum of a regular wave force and a 'triangle' on top of it. This signal is filtered using the Symmlet 8 wavelet. The filtering is done in a number of steps; all these steps are presented in Figure 5.7b. This figure presents the result of a shifted algorithm because the filtering without shifting shows less desirable results. First the noise was filtered, followed by the resonance of the structure.

The next step is to filter the transient. This is done by carefully adjusting the filter. The assumption of the sum of a regular wave and a 'triangle' on top was tried to reconstruct. As can be observed in Figure 5.7b, a clear triangular shape is present in the transient at the time of the second wave peak. The peak without

the transient shows some sharp edges; this is due to the shifted filter. The first peak of the 'transient filtered' signal also is decreased in height. This is because the wavelet content of the transient overlaps the wavelet content of the entire signal. This form of transient filtering is a local operation. Especially because the wave heights differ and therefore the shape of the transient. To design a discrete wavelet filter to extract transients from many waves in one time-series is very hard and should use non-stationary thresholds. The final filter (for the 'transient filtered' line in Figure 5.7b) is presented in the Appendix, Figure F.10.

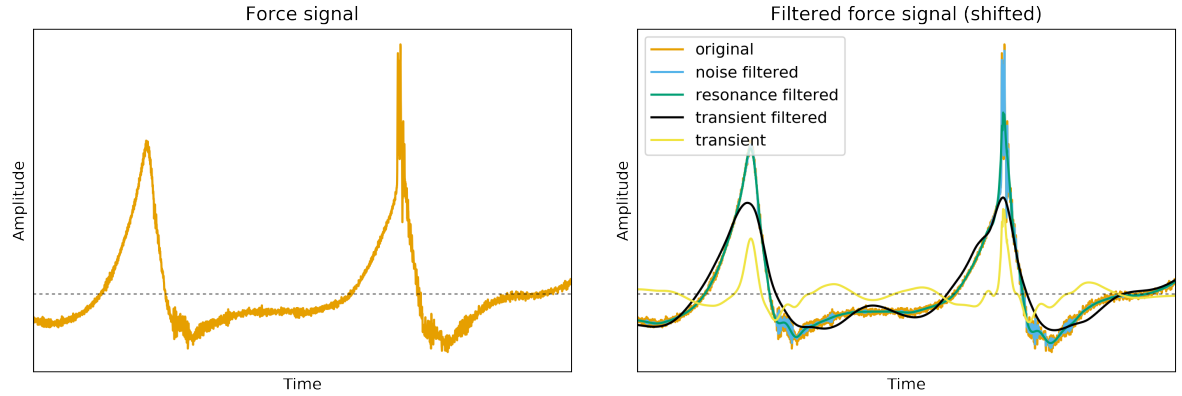

(a) Two hits of waves on the structure. The first hit was a regular wave, the second a breaking wave.

(b) Filtering the transient from the original signal in multiple steps. Final filter in Figure F.10.

Figure 5.7: Filtering transient in a coastal engineering force measurement. Dimensions are left out for confidentiality. The thin dotted line indicated the 0 force level.

5.3. Computation

The last comparison between the two techniques is the difference in computing capacity. In this section, two important facets of the computation will be addressed. The first is the number of floating point operations (flops) needed to perform a given task. The second one is the amount of memory needed to store the results. This is expressed in the number of floats. Assume there are G gauges, recording signals consisting of N data points (i.e. floats). Complex-valued floats need twice as much space to save as real-valued floats. The computation time for the wave number is not taken into account.

Fourier

As discussed on page 8, the Fourier Transform needs $\mathcal{O}(N \log N)$ flops to compute. A multiplication in the Fourier domain with a filter takes N flops. A Fourier transformed signal can be stored in the same amount of floats as the original signal. The wave separation technique by Zelt and Skjelbreia [63] uses four sums that sum over the number of gauges, G. Therefore solving the system of equations uses $\mathcal{O}(G)$ flops per frequency, so to find the solution of the separation problem in the frequency domain, therefore, is of $\mathcal{O}(NG)$ flops. Note that this is without the operations needed to solve for the complex exponentials e^{ikx} and the wave number through the dispersion relationship.

CWT

The CWT (2.22) results cannot be stored in the same amount of floats as the original signal. Assume the CWT is performed over A number of scales, then the resulting wavelet coefficients consist of AN complex floats. The cone of influence needs little space to be saved, A floats. The zones of influence are very costly to store compared to the COI, with AN floats. Due to the computation through the FFT, it only takes $AN \log N$ flops to compute these coefficients. The reconstruction formula (2.25) uses $\mathcal{O}(AN)$ flops if the coefficients C_δ is already known. When it has to be computed the reconstruction is of $\mathcal{O}(AN^2)$ flops.

The separation of the incident and reflected wave based on wavelet coefficients takes $\mathcal{O}(GAN)$ flops for G gauges and A scales and N steps in time. Again the computation of the exponential function and the wave number are not taken into account. However, in the non-stationary case, these have to be computed AN times, instead of just A times in the discrete case.

DWT

The discrete wavelet coefficients can be computed very effectively through the fast wavelet transform algorithm. This algorithm is of $\mathcal{O}(N^2 \log N)$ flops. The result can be stored in $\mathcal{O}(N)$ floats, the same as for amount as for the original signal. Determining thresholds depends on the techniques used. General denoising methods use $\mathcal{O}(N \log N)$ operations [51]. So denoising discrete wavelet coefficients takes $\mathcal{O}(N^2 \log N)$ flops, which is an order N higher than filtering using discrete Fourier coefficients.

Considerations

All work in this thesis has been applied on a 4 GB RAM personal computer. On such a machine the difference in computation time between the FFT and DWT is not noticeable (for time-series containing up to 3 million data points). The PyWavelets [54] package uses the FWT algorithm and computes the results very fast. The continuous wavelet transform, on the other hand, takes more time to compute. The used basis code of Torrence and Compo [56] is less optimised than the FWT based code. Furthermore, there are side processes running, for instance, to calculate the wavelets used in the algorithm and the COI. Often the most time-consuming part of the time-frequency analysis is the creation of figures. The creation of contour plots (WPS) is much more expensive than plotting a line (VDS).

The separation of the incident and reflected wave is not very expensive. The computation time for solving the exponential function and the dispersion relation dominate these two processes, and these were not taken into account because the number of flops for these operations is unknown. This is not a problem for this comparison because both the Fourier and wavelet cases are slowed down by the same factor by these processes. Solving the non-stationary wavelet-based separation problem presented in Section 5.1.2 (about 180.000 data points) took about 1550 seconds, while the stationary separation using Fourier coefficients only takes 8 seconds, which is quite a large difference. It is not too much, and the code can be optimised if faster computation times are desired, or the signal can be down-sampled to decrease N.

5.4. Discussion

The results presented in this chapter offer some opportunities. However, the results are not a major improvement in comparison with the current method. The (discretised) continuous wavelet transform is a powerful tool in time-frequency analysis. By choosing the correct signal extension method and use the zone of influence to cope with the effects of gaps in the data, the effectiveness of the time-frequency analysis has been expanded.

In many applications, the wavelet coefficients can be used instead of Fourier coefficients. The example addressed in Section 5.1.2 discussed many applications of the wavelet coefficients. The signal used has a non-stationary mean, theoretically better suitable for wavelet analysis than Fourier analysis. The global wavelet spectrum does not have added value to the Fourier spectrum for stationary signals. In this non-stationary case, it is clear that the global wavelet spectrum expresses the power distribution of the signal better than the spectrum.

The scale averaged wavelet power, on the other hand, allows insight into the power distribution of a signal in time. This is used to show that the separation algorithms have a larger relative error for large waves than for small waves. The separation of waves using wavelet or Fourier coefficients often results in separated waves that are very similar. Import differences between the solutions are that wavelet transform has a lower density in the frequency domain which results in less disturbance due to critical gauge spacing. The introduction of the determinant limiter improves the result of the Fourier coefficient based algorithm much more. On the other hand, the lower density is a downside, because the wave number is frequency dependent, which results in less accurate reconstruction of waves above certain frequencies.

For waves in the field of coastal engineering, this often is not a problem because high frequencies are of very low power. The near and far shore waves have a more narrow range of wave numbers, so a larger set of frequencies can be separated in these conditions. When a signal has non-stationary elements such as a changing mean water level, the wavelet coefficients are more suitable for separating the waves.

5.4.1. Guidelines Discrete Wavelet Transform

At the end of Chapter 3 some guidelines regarding the use of the continuous wavelet coefficients have been discussed. In Chapter 4 different noise filters have been discussed, and in this chapter some other applications of the discrete wavelet transform with respect to coastal engineering signals were shown. Therefore some guidelines regarding the discrete wavelet transform are summarised here. The discrete wavelet trans-

form gives a whole other insight into the signals behaviour than the discrete Fourier transform and thresholding in this domain leads is a whole different approach to filtering than filtering in the Fourier domain. In the Fourier domain coefficients are changed by the same factor, while in the wavelet domain this is not necessary.

Important in digital signal processing using wavelets is the right choice of wavelet. In Figure 2.5 an overview of the most common available discrete wavelets is given. The resemblance of the wavelet to the signal in time or frequency domain is very important. For instance, is your signal discontinuous, choose a discontinuous wavelet. Does the spectrum of your signal decay fast? Pick a wavelet with the same characteristic. For most signals from natural sources, the Symlet or Coiflet wavelets are preferred [51]. Especially low-level wavelets such as the Haar wavelet or Daubechies < 4 often result in non-fluent filter results. If more time-consuming filter expansions are used, such as shifting (see Section 2.5.2), the choice of wavelet influences the result less. The added value of filtering in the discrete wavelet domain is to apply thresholding; omitting entire sets of coefficients often leads to results that can also be achieved using Fourier filters.

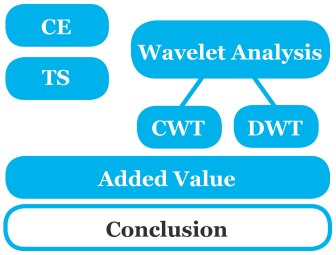

6

Conclusion and Recommendations

The goal of the research was to create guidelines to guide analysts in applying wavelet analysis on time-series from the field of coastal engineering. The wavelet transform is divided into two domains: the continuous wavelet transform and the discrete wavelet transform. Specific guidelines regarding these transforms are discussed at the ends of respectively Chapter 3 and Chapter 5. Moreover, in Chapter 5 the added value is shown of both transforms in time-frequency analysis and digital signal processing in coastal engineering. In this last chapter, the answer to the research questions and the conclusions of this work will be shared, followed by some recommendations and suggestions for future research.

6.1. Conclusions

What improvements are necessary for the (discretised) continuous wavelet transform to improve time-frequency analysis for time-series in the field of coastal engineering?

The discretised continuous wavelet transform based on the work of Torrence and Compo [55] has been expanded by the addition of different signal extension modes. The right choice of extension mode increases the reliability of the wavelet power spectrum outside the cone of influence. In Figure 3.2 some recommendations regarding the right choice are presented. To improve time-frequency analysis of signals with missing data points, the zones of influences have been developed. These zones indicate the disturbance of the wavelet coefficients, based on the wavelets energy distribution. These improvements allow better time-frequency analysis for time-series from the field of coastal engineering.

Does the separation of incident and reflected waves based on wavelet coefficients for N gauges perform better than the separation based on Fourier coefficients?

The results of Ma et al. [34] and Zelt and Skjelbreia [63] have been combined to create an algorithm to separate incident and reflected waves for more than two gauges. These waves do only travel back and forth in one direction. Due to the increasing bandwidth of wavelets for higher frequencies, the algorithm using Fourier coefficients shows better results than the one based on wavelet coefficients for high frequencies. However, this effect can be minimised by choosing a small bandwidth wavelet. The other option is to minimise the distance between different gauges. For relative low frequencies, which frequently occur in coastal engineering problems (< 5 Hz), there is almost no difference between the solution based on wavelet or Fourier coefficients. The determinant limiter that was introduced reduces the amount of energy in the reconstructed signals based on wavelet coefficients more than those based on Fourier coefficients. This is due to the resolution difference in the frequency domain of both methods. Conversely, the wavelet algorithm is less plagued by the close to zero determinant, resulting in more reliable separation without limiter. In the Fourier-based separation, the determinant limiter is indispensable. When wavelet coefficients are used, it is important to limit the higher scales.

When a non-stationary mean is introduced, the Fourier algorithm is plagued by low-frequency noise. Furthermore, the wave number changes over time, which cannot be included in the Fourier algorithm. Because the wavelet coefficients depend on time, the change of the wave number can be incorporated, decreasing the error of the separation with respect to the Fourier separated waves. All in all, it is concluded that the separation based on wavelet coefficient is better applicable to coastal engineering time-series than the one based

on Fourier coefficients. In particular for signals with a changing mean water level, for stationary signals the solutions do not differ significantly. A number of three gauges is enough to correctly separate waves using both methods.

Which discrete wavelet-based algorithm is best suited to remove noise from coastal engineering signals?
The results of four discrete wavelet-based algorithms were compared to the results of a low pass Fourier filter. The low pass filter showed better results in filtering stationary signals. This is also in line with the theory. As is the fact that the wavelet-based algorithms performed better on the non-stationary signal cases. The Srivastava et al. [51] based thresholds did not work out as well as predicted. The threshold based on an idle period is much more effective in suppressing environmental noise, whereas the threshold based on the MAD did show the best results in filtering both environmental and measurement noise.

The choice of wavelet also influences the output of the filter. Comparing five different ones, lead to the conclusion that symmetric wavelets are a better fit to filter stationary signals, than non-symmetric wavelets. Natural non-stationary signals are better denoised if the discrete wavelet decomposition is constructed using wavelets that mimic natural frequency behaviour. The Symmlets 8 and the Coiflet 3 outperformed the Haar, Daubechies and bi-orthogonal wavelet, as predicted by their spectra and literature.

What is the added value of wavelet analysis over current time-series analysis methods in coastal engineering?
The added value of wavelet analysis is the addition of an extra dimension. Instead of observing signal behaviour in time or frequency, the wavelet coefficients are dependent on both time and frequency. Methods allowing similar insights exist, such as the short-term Fourier transform, but are not optimal. The downside of any time-frequency method is that a trade-off has to be made between the resolution in time and frequency. The resolution cannot be the same compared to only the time or frequency domain.

This trade-off is most clear in the separation of waves, where the wavelet-based separation performs worse than the Fourier-based separation for high frequencies. In the field of coastal engineering, however, these high frequencies do not arise very frequent, and therefore the wavelet and Fourier-based separation methods can be used interchangeably. However, when the mean water level changes over time, the wave number in the wavelet-based separation can be adapted in order to separate the waves better. For the Fourier-based method this is impossible; here lies the added value of the wavelet coefficients with respect to the current method based on Fourier coefficients [21, 38, 63]. Solving the non-stationary problem based on wavelets is much more expensive than solving the stationary problem based on Fourier coefficients due to the fact that the dispersion relation and the complex exponent have to be solved many more times.

The limited time support of the wavelets ensures that local signal elements, for instance, a discontinuity, only affects coefficients near that jump. This is in contrast to the Fourier coefficients, which are affected globally by a local event. Filling missing data points leads to discontinuities which affect all Fourier coefficients. The disturbance of the wavelet coefficients can be estimated using the wavelet energy distribution. This allows analysis of frequencies that are not possible in current methods. In coastal engineering long-term measurements are very common and these often show defects like missing data points. The zones of influence allow time-frequency analysis for these signals.

The examples in Section 5.2 show the wide employability of filtering signal elements in the discrete wavelet domain. The best example of this wide applicability is the reconstruction of jumps using the Haar wavelet. This reconstruction is not possible in any other domain than the wavelet domain. The large number of wavelets available (Figure 2.5) leads to many opportunities. If this is not even enough, wavelets can be created to fit the objective better. The filtering in the wavelet domain has most added value in separating non-stationary signal elements from the rest of the signal. It is much more powerful than current time or Fourier-based methods.

How can wavelet analysis improve time-series analysis and processing in the field of coastal engineering?

All in all, wavelet analysis offers many improvements with respect to currently used time and Fourier-based methods. The wavelet power spectrum and cross-wavelet applications can be applied to signals that are disturbed by missing or incorrect data points. The effect of the gaps can be estimated based on the wavelet energy distribution. This allows quantitative analysis of different frequency components in time.

The separation of waves for signals with a changing mean water level can be solved without dividing the signal into parts. A continuous separated solution is a major improvement with respect to the non-continuous solution based on the Fourier separation currently in use. Furthermore, many challenges can

be solved using the discrete wavelet transform. The discrete wavelet decomposition gives more insight into the behaviour of a signal and its noise. This allows analysts to justify the filter applied, which is a major improvement with respect to the empirically based filters that are currently in use.

The use of the wavelet transform, however, often is more time-consuming. On the one hand, the number of arithmetic operations for most applications is an $\mathcal{O}(N)$ more than the Fourier-based analyses. On the other hand, there is more information to process, which also takes more time. However, this quantity of information is what allows wavelet analysis to improve current methods. It provides more information about the signals behaviour and is better able to cope with non-stationary signal elements. This results in a better separation of waves in non-stationary conditions, mathematically justified filters for all sorts of signal elements and better insight into the time-frequency behaviour of a signal.

6.2. Recommendations and Future Research

In this section, some recommendations and suggestions for future research are shared. These are divided into three items. The first concerns the time-frequency analysis based on the results from Section 3.1, the second concerns the separation of waves based on the continuous wavelet coefficients. The third shows some suggestions regarding the added value of the discrete wavelet transform. Some recommendations concerning the noise filter algorithm are already discussed in Section 4.4.

The largest recommendation regarding time-frequency analysis based on the continuous wavelet coefficients is to apply it. Although the physical interpretation of the signals is not expressed in the same quantity as the Fourier transform, wavelet analysis has proven to be an effective analysis tool in other fields of research, especially for signals with non-stationary elements, which also occur frequently in coastal engineering. The extension of the cone of influence to the zones of influence allows time-frequency analysis for signals with missing data points. This extension is based on the wavelet energy distribution. Another measure could be based on the window function that is present in most continuous wavelets. The statistical significance of the wavelet power spectrum was not addressed in this thesis but is important in the time-frequency analysis. Monte Carlo simulations can always offer good results but are very time-consuming. Available analytical descriptions of background spectra can speed up time-frequency analysis using wavelets.

The separation of waves based on wavelet coefficients is as effective as the method based on Fourier coefficients for waves considered in coastal engineering. Future research could focus on the use of the chosen set of scales to evade the critical points where $\sin(k\Delta x)$ is (close to) zero. Therefore the reconstruction (2.25) has to be adjusted. There is more to gain regarding the reconstruction; the used reconstruction equation has quite a large reconstruction error in comparison to the discrete Fourier and wavelet reconstructions. By implementing a reconstruction using the analysing wavelet, this error might be decreased, which affects the separated waves. The design of a wavelet for the specific goal of separating non-linear waveforms (for instance as presented by Lykke Andersen et al. [33]), could improve separation results as well. The error analysis based on the SWAP (3.22) can be used to determine the error for the different wave sizes. Finally, the wavelet-based algorithm can be expanded to sloping bathymetry [34], oblique incident waves [35] and possible even waves travelling in two dimensions.

With respect to the discrete wavelet transform, only the tip of the iceberg has been shown. There are many expansions such as wavelet packets, multi-wavelets and the use of different dilation factors that could improve filter results [28]. This, however, will not benefit the user experience. The thresholding will become much more complicated, especially for those with little background in discrete wavelet theory. To improve the discrete wavelet filtering as applied in this thesis, a wavelet can be designed that complies to the characteristics of the signal to filter. Additionally, a (wavelet-based) filter resulting in the desired filtered signal has not been found yet for the presented coastal engineering signals. The development of such an algorithm is of much added value for the filtering of much repeated measurements. For now manual fine-tuning seems to be indispensable in filtering. For noise that is increasing in power in time, non-stationary thresholds can be explored as well.

List of Demonstrations

Bibliography

[1] Luís Aguiar-Conraria and Maria Joana Soares. The Continuous Wavelet Transform: Moving beyond Uni- and Bivariate analysis. Journal of Economic Surveys, 28(2):344–375, apr 2014. ISSN 09500804. doi: 10.1111/joes.12012. URL *http://doi.wiley.com/10.1111/joes.12012*.

[2] Luís Aguiar-Conraria, Nuno Azevedo, and Maria Joana Soares. Using wavelets to decompose the time-frequency effects of monetary policy. Physica A: Statistical Mechanics and its Applications, 387 (12):2863–2878, 2008. ISSN 03784371. doi: 10.1016/j.physa.2008.01.063.

[3] Anestis Antoniadis. Wavelet methods in statistics: some recent developments and their applications. Statistics Surveys, 1:16–55, 2007. ISSN 1935-7516. doi: 10.1214/07-SS014. URL *http://arxiv.org/abs/0712.0283{%}5Cnhttp://dx.doi.org/10.1214/07-SS014{%}5Cnhttp://projecteuclid.org/euclid.ssu/1196693422*.

[4] Ilker Bayram and Ivan W. Selesnick. Overcomplete Discrete Wavelet Transforms With Rational Dilation Factors. IEEE Transactions on Signal Processing, 57(1):131–145, jan 2009. ISSN 1053-587X. doi: 10.1109/TSP.2008.2007097. URL *http://ieeexplore.ieee.org/document/4663893/*.

[5] Alex Bellos. Abel Prize 2017: Yves Meyer wins 'maths Nobel' for work on wavelets | Science | The Guardian. *https://www.theguardian.com/science/alexs-adventures-in-numberland/2017/mar/21/abel-prize-2017-yves-meyer-wins-maths-nobel-for-work-on-wavelets*, 2017. Date accessed: 24-3-2017.

[6] Christian Blatter. Wavelets: A Primer. A K Peters, Ltd, 1998. ISBN 9781568811956.

[7] Judith Bosboom and Marcel J.F. Stive. Coastal Dynamics I, lecture notes. VSSD, Delft, 2011.

[8] Peter Brockwell and Richard Davis. Introduction to Time Series and Forecasting. Springer, 2002. ISBN 0387953515. doi: 10.2307/1271510. URL *http://scholar.google.com/scholar?hl=en{&}btnG=Search{&}q=intitle:Introduction+to+Time+Series+and+Forecasting{#}0{%}5Cnhttp://www.jstor.org/stable/1271510?origin=crossref*.

[9] B. Cazelles, Kévin Cazelles, and Mario Chavez. Wavelet analysis in ecology and epidemiology: impact of statistical tests. Journal of The Royal Society Interface, 11(91):20130585–20130585, 2013. ISSN 1742-5689. doi: 10.1098/rsif.2013.0585. URL *http://rsif.royalsocietypublishing.org/content/11/91/20130585.abstract{%}5Cnhttp://rsif.royalsocietypublishing.org/cgi/doi/10.1098/rsif.2013.0585*.

[10] Bernard Cazelles, Mario Chavez, Guillaume Constantin de Magny, Jean-Francois Guégan, and Simon Hales. Time-dependent spectral analysis of epidemiological time-series with wavelets. Journal of the Royal Society, Interface / the Royal Society, 4(15):625–36, 2007. ISSN 1742-5689. doi: 10.1098/rsif.2007.0212. URL *http://rsif.royalsocietypublishing.org/content/4/15/625.short*.

[11] Leon W. Couch. Digital and Analog Communication Systems. Pearson Prentice Hall, 7th edition, 2007. ISBN 0-13-203794-7.

[12] creativecommons.org. Time-Frequency Dictionaries. *http://archive.cnx.org/contents/4a47d3df-bfe5-428c-8bb6-e5b738077caa@2/time-frequency-dictionaries*, 2017. Date accessed: 20-2-2017.

[13] Ingrid Daubechies. Orthonormal bases of compactly supported wavelets. Communications on Pure and Applied Mathematics, 41(7):909–996, oct 1988. ISSN 10970312. doi: 10.1002/cpa.3160410705. URL *http://doi.wiley.com/10.1002/cpa.3160410705*.

[14] Ingrid Daubechies. Ten Lectures on Wavelets. Society for Industrial and Applied Mathematics, Pennsylvania, 1992. ISBN 0-89871-274-2.

[15] M.P.C. de Jong. Low-frequency sea waves generated by atmospheric convection cells. Journal of Geophysical Research, 109:1–18, 2004. ISSN 0148-0227. doi: 10.1029/2003JC001931.

[16] M.P.C. de Jong and J.A. Battjes. Seiche characteristics of Rotterdam Harbour. Coastal Engineering, 51 (5-6):373–386, 2004. ISSN 03783839. doi: 10.1016/j.coastaleng.2004.04.002.

[17] Jaidev Deshpande. PyHHT Tutorials – pyhht 0.0.1. documentation. *http://pyhht.readthedocs.io/en/latest/tutorials.html*, 2017. Date accessed: 29-3-2017.

[18] Dennis Gabor. Theory of Communication, 1946. ISSN 09252312. URL *citeulike-article-id:4452465*.

[19] Z. Ge. Significance tests for the wavelet power and the wavelet power spectrum. Annales Geophysicae, 25(11):2259–2269, 2007. ISSN 1432-0576. doi: 10.5194/angeo-25-2259-2007.

[20] Bernd Girod, Rudolf Rabenstein, and Alexander Stenger. Signals and systems. John Wiley & Sons, inc., 2001. ISBN 0-471-98800-6.

[21] Yoshimi Goda and Yasumasa Suzuki. Estimation of Incident and Reflected Waves in Random Wave Experiments. In Coastal Engineering 1976, pages 828–845, New York, NY, nov 1977. American Society of Civil Engineers. ISBN 9780872620834. doi: 10.1061/9780872620834.048. URL *http://ascelibrary.org/doi/10.1061/9780872620834.048*.

[22] A. Grinsted, J. C. Moore, and S. Jevrejeva. Application of the cross wavelet transform and wavelet coherence to geophysical time series. Nonlinear Processes in Geophysics, 11(5/6):561–566, 2004. ISSN 1607-7946. doi: 10.5194/npg-11-561-2004. URL *http://www.nonlin-processes-geophys.net/11/561/2004/*.

[23] S.A.P. Haddad, J.M.H. Karel, R.L.M. Peeters, Ronald L. Westra, and Wouter A. Serdijn. Analog complex wavelet filters. Proceedings - IEEE International Symposium on Circuits and Systems, pages 3287–3290, 2005. ISSN 02714310. doi: 10.1109/ISCAS.2005.1465330.

[24] Leo H. Holthuijsen. Waves in Oceanic and Coastal Waters. Cambridge University Press, New York, 2007. ISBN 978-0-511-27021-5.

[25] Norden E. Huang and Sauuel S. P. Shen. Hilbert Huang Transform and Its Applications, volume 16. World Scientific Publishing Co. Pte. Ltd., second edition, 2014. ISBN 978-9814508230. doi: 10.1007/s13398-014-0173-7.2. URL *http://www.worldscientific.com/worldscibooks/10.1142/8804*.

[26] Norden E. Huang and Zhaohua Wu. A Review on Hilbert-Huang Transform: Method and Its Applications to Geophysical Studies. Reviews of Geophysics, 46(2007):1–23, 2008. ISSN 87551209. doi: 10.1029/2007RG000228. URL *http://rcada.ncu.edu.tw/reference010.pdf*.

[27] Norden E. Huang, Zheng Shen, and Steven R. Long. A new view of nonlinear water waves: The Hilbert Spectrum. Annual Review of Fluid Mechanics, 31(1):417–457, 1999. ISSN 0066-4189. doi: 10.1146/annurev.fluid.31.1.417. URL *http://www.annualreviews.org/doi/abs/10.1146/annurev.fluid.31.1.417{%}5Cnpapers2://publication/doi/10.1146/annurev.fluid.31.1.417*.

[28] Fritz Keinert. Wavelets and Multiwavelets. Chapman & Hall/CRC, 2004. ISBN 1-58488-304-9.

[29] Byungil Kim, Hoyoung Jeong, Hyoungkwan Kim, and Bin Han. Exploring wavelet applications in civil engineering. KSCE Journal of Civil Engineering, 21(4):1076–1086, 2017. ISSN 19763808. doi: 10.1007/s12205-016-0933-3.

[30] J. F. Kirby. Which wavelet best reproduces the Fourier power spectrum? Computers and Geosciences, 31(7):846–864, 2005. ISSN 00983004. doi: 10.1016/j.cageo.2005.01.014.

[31] Chun-Liu Liu. A Tutorial of the Wavelet Transform. National Taiwan University, Department of Electrical Engineering (NTUEE), pages 1–72, 2010. ISSN 0166526X. doi: 10.1111/j.1600-0404.1995.tb01711.x. URL *http://disp.ee.ntu.edu.tw/tutorial/WaveletTutorial.pdf*.

[32] Yonggang Liu, X. San Liang, and Robert H. Weisberg. Rectification of the bias in the wavelet power spectrum. Journal of Atmospheric and Oceanic Technology, 24(12):2093–2102, 2007. ISSN 07390572. doi: 10.1175/2007JTECHO511.1.

[33] Thomas Lykke Andersen, Mads Røge Eldrup, and Peter Frigaard. Estimation of incident and reflected components in highly nonlinear regular waves. Coastal Engineering, 119:51–64, 2017. ISSN 03783839. doi: 10.1016/j.coastaleng.2016.08.013. URL *http://dx.doi.org/10.1016/j.coastaleng.2016.08.013*.

[34] Yuxiang Ma, Guohai Dong, Xiaozhou Ma, and Gang Wang. A new method for separation of 2D incident and reflected waves by the Morlet wavelet transform. Coastal Engineering, 57(6):597–603, 2010. ISSN 03783839. doi: 10.1016/j.coastaleng.2010.01.002. URL *http://dx.doi.org/10.1016/j.coastaleng.2010.01.002*.

[35] Yuxiang Ma, Guohai Dong, and Xiaozhou Ma. Separation of obliquely incident and reflected irregular waves by the Morlet wavelet transform. Coastal Engineering, 58(8):761–766, 2011. ISSN 03783839. doi: 10.1016/j.coastaleng.2011.03.014. URL *http://dx.doi.org/10.1016/j.coastaleng.2011.03.014*.

[36] S.G. Mallat. A theory for multiresolution signal decomposition: the wavelet representation. IEEE Transactions on Pattern Analysis and Machine Intelligence, 11(7):674–693, jul 1989. ISSN 01628828. doi: 10.1109/34.192463. URL *http://ieeexplore.ieee.org/document/192463/*.

[37] Stéphane Mallat. A Wavelet Tour of Signal Processing. Academic Press, 2nd edition, 1999. ISBN 0-12-466606-X.

[38] E.P.D. Mansard and E.R. Funke. The Measurement of Incident and Reflected Spectra Using a Least Squares Method. In Seventeenth coastal engineering conference, pages 154–172, Sydney, Australia, 1980. Am. Soc. Civ. Engrs.

[39] MathWorks Benelux. Signal Smoothing - MATLAB & Simulink Example - MathWorks Benelux. *https://nl.mathworks.com/help/signal/examples/signal-smoothing.html*, 2017. Date accessed: 7-4-2017.

[40] MathWorks Benelux. Wavelet Toolbox - MATLAB. *https://nl.mathworks.com/products/wavelet.html*, 2017. Date accessed: 27-2-2017.

[41] Gene Mosca and Paul A. Tipler. Physics for Scientists and Engineers. W.H. Freeman and Company, New York, sixth edition, 2009. ISBN 978-0-7167-8964-2.

[42] S.V. Narasimhan, N. Basumallick, and S. Veena. Introduction to wavelet transform: a signal processing approach. Alpha Science International Ltd., 2011. ISBN 978-1-84265-629-7.

[43] Radomír Pavlík. Binary PSK/CPFSK and MSK bandpass modulation identifier based on the complex shannon wavelet transform. Journal of Electrical Engineering, 56(3-4):71–77, 2005. ISSN 13353632.

[44] Z. K. Peng, Peter W. Tse, and F. L. Chu. A comparison study of improved Hilbert-Huang transform and wavelet transform: Application to fault diagnosis for rolling bearing. Mechanical Systems and Signal Processing, 19(5):974–988, 2005. ISSN 08883270. doi: 10.1016/j.ymssp.2004.01.006.

[45] Roger Peyret. Spectral Methods for Incompressible Viscous Flow. Springer Science+ Business Media, New York, 2002. ISBN 978-1-4419-2913-6. doi: 10.1007/978-1-4757-6557-1.

[46] John G. Proakis and Dimitri G. Manolakis. Digital Signal Processing. Pearson Prentice Hall, 2007. ISBN 0-13-228731-5.

[47] John A. Rice. Mathematical Statistics and Data Analysis. Thomson Brooks/Cole, third edition, 2007. ISBN 0-534-39942-8.

[48] Tristan Rouyer, Jean Marc Fromentin, Nils Chr. Stenseth, and Bernard Cazelles. Analysing multiple time series and extending significance testing in wavelet analysis. Marine Ecology Progress Series, 359 (Daubechies 1992):11–23, 2008. ISSN 01718630. doi: 10.3354/meps07330.

[49] David K. Ruch and Patrick J. Van Fleet. Wavelet Theory: An Elementary Approach with Application. John Wiley & Sons, inc., 2011. ISBN 9780470388402. doi: 10.1002/9781118165652.

[50] Kinhong Shin and Joseph K. Hammond. Fundamentals of Signal Processing for Sound and Vibration Engineers. John Wiley & Sons, inc., 2007. ISBN 978-0-470-51188-6.

[51] Madhur Srivastava, C. Lindsay Anderson, and Jack H. Freed. A New Wavelet Denoising Method for Selecting Decomposition Levels and Noise Thresholds. IEEE Access, 4:3862–3877, 2016. ISSN 21693536. doi: 10.1109/ACCESS.2016.2587581.

[52] G. Strang and T. Nguyen. Wavelets and Filter Banks. Wellesley-Cambridge Press, 2003. ISBN 0961408871.

[53] W. Sweldens. The Lifting Scheme: A New Philosophy in Biorthogonal Wavelet Constructions. 2007. URL *papers://b6c7d293-c492-48a4-91d5-8fae456be1fa/Paper/p7558*.

[54] The PyWavelet Developers. Wavelets – PyWavelets Documentation. *http://pywavelets.readthedocs.io/en/latest/ref/wavelets.html*, 2017. Date accessed: 17-3-2017.

[55] Christopher Torrence and Gilbert P. Compo. A Practical Guide to Wavelet Analysis. Bulletin of the American Meteorological Society, 79(1):61–78, 1998. ISSN 00030007. doi: 10.1175/1520-0477. URL *http://atoc.colorado.edu/research/wavelets/*.

[56] Compo, Gilbert P. Torrence, C. Wavelet analysis; significance levels; confidence intervals;. *paos.colorado.edu/research/wavelets/*, 2017. Date accessed: 8-5-2017.

[57] M van Berkel. Wavelets for Feature Detection; Theoretical background. Technical report, Eindhoven University of Technology, 2010.

[58] J. van Kan, A. Segal, and F. Vermolen. Numerical methods in scientific computing. Delft Academic Press, second edition, 2014. ISBN 97890-6562-3638. URL *https://scholar.google.nl/scholar?hl=nl{&}q=vermolen+numerical+methods+in+scientific+computing{&}btnG={&}lr=*.

[59] David F. Walnut. An Introduction to Wavelet Analysis. Birkhauser, 2002. ISBN 0-8176-3962-4.

[60] Filip Wasilewski. Discrete Meyer (FIR Approximation) wavelet (dmey) properties, filters and functions - Wavelet Properties Browser. *http://wavelets.pybytes.com/wavelet/dmey/*, 2017. Date accessed: 17-3-2017.

[61] Langford B. White and Boualem Boashash. Cross Spectral Analysis of Nonstationary Processes. IEEE Transactions on Information Theory, 36(4):830–835, 1990. ISSN 15579654. doi: 10.1109/18.53742.

[62] Peter Wilders and W.A. Heemink. Transport Modelling and Data Assimilation - WI4054. Delft University of Technology, 2016.

[63] J.A. Zelt and James E. Skjelbreia. Estimating Incident and Reflected Wave Fields Using an Arbitrary Number of Wave Gauges. Coastal Engineering Proceedings, 1:777–789, 1992. ISSN 2156-1028. doi: 10.9753/icce.v23.%p. URL *http://journals.tdl.org/icce/index.php/icce/article/view/4736*.

[64] Z. Zhang and J. C. Moore. Comment on "significance tests for the wavelet power and the wavelet power spectrum" by Ge (2007). Annales Geophysicae, 30(12):1743–1750, 2012. ISSN 09927689. doi: 10.5194/angeo-30-1743-2012.

Appendices

A

Sampling Theory

This appendix is an expansion of the short summary of the assumption made in sampling theory to step from continuous to discrete wavelet analysis (Section 2.2.2).

A.1. Nyquist-Shannon Sampling Theorem

As mentioned before the sampling of a signal can be seen as multiplying the continuous signal $x(t)$ by a set of Delta impulses (Section 2.2.2). The Nyquist-Shannon theorem relates properties of the signal to the properties of the sampling frequency and vice versa. This theorem mainly has effect in the Fourier approach used in both the Fourier transform as the short-term Fourier transform. The spectrum of the original signal $x(t)$, $X(\omega)$, repeats at every frequency interval of f_s in the spectrum of the sampled signal $X_{\text{sampled}}(\omega)$ [42]. These repetitions are called *images*. However, if the original spectrum $X(\omega)$ is not limited by a maximum frequency (also known as *bandwidth*) so that $f_{\max} \leq f_s/2$, the repetitions of $X(\omega)$ result in overlapping. The high frequency components of $X(\omega)$ are added to its low frequency components, resulting in a distorted $X_{\text{sampled}}(\omega)$. The repetitions of the spectrum can be cut out by using a *low pass* filter. In this case the choice for a filter selecting the domain $[-f_s/2, f_s/2]$ is made. This, however, does not remove the overlapping components.

This distortion of the recovered signal due to insufficient sampling frequency is known as *aliasing* [42]. Signals with sudden transitions or noticeable noise often contain frequency components of which $\omega \to \infty$, these are therefore impossible to catch by any sampling frequency and are always affected by aliasing effects. These might be small, however. To recover an analogue signal properly from the sampled signal, $f_s \geq 2f_{\max}$ [11, 42]. This minimum sampling frequency for a signal is known as the *Nyquist frequency*, defined as $f_N = 2f_{\max}$ [11]. Sampling a signal under the Nyquist frequency is called *under-sampling*, sampling with a frequency over the Nyquist frequency is called *over-sampling*. Is over-sampling a problem? No it is not, but working with an over-sampled signal results in doing computations that are not strictly necessary. However, when the Nyquist rate is based on the bandwidth of the sampled signal, over-sampling could reduce noise, aliasing and improves the resolution of your signal. These effects are all explained by a theorem called the Nyquist-Shannon or Sampling Theorem. A proof of this theorem is given by Couch [11].

A.1.1. Filtering

The images of a spectrum can be taken out of the spectrum using a gate function $G(\omega)$. This function in signal analysis is referred to as a filter. Filters can be applied using computers, but often also *analogue filtering* (in the form of electronics) is used. An audio amplifier for instance often contains a set of analogue filters to determine the audio signals for the low, mid and high speakers. Often measurement equipment apply filtering effects to the measurements. A *low pass filter* is a filter that passes all frequencies under the cutoff frequency ω_m. In this same way, *bandpass* and *high pass* filters are used to respectively pass signals in a certain bandwidth and above a certain cutoff frequency. This filtering can be interpreted as a multiplication in the frequency domain: $X_{\text{filtered}}(\omega) = X_{\text{sampled}}(\omega)G(\omega)$. If Heaviside windows (13) are used, the *Gibbs phenomenon* or *ripple effect* arises [42].

By truncating the spectrum of the signal, a lot of relative large ripples appear in the time domain. Choosing a longer window leads to increased ripple frequency, with no effect on the ripples magnitude [42]. A solution to this problem is choosing smoother windows, however, this results in loss of frequency resolution.

The filter determines the quality of the signal approximation [42]. Because the DFT is done using a computer, the signal is of finite length T. This can be interpreted as multiplying the original infinite signal with a block window $w(t) = \mathbb{1}_{[0,T]}$. By the inversion property of the Fourier transform (G.7), this will result in rippling effects in the spectrum, which is often observed in spectra.

A.1.2. Fourier Transform Requirements

The Fourier transform cannot just be applied to all functions existing. In mathematical terms the Fourier transform only exists for functions in the L^2 space [20]. This ensures the convergence of the integral in equation 2.8. In physical terms one would speak of functions with a finite energy [11]. Discrete signals can be interpreted as truncated signals, which will thus always be of finite energy. For these, the Fourier transform should be restricted to the representation of smooth, 2π-periodic functions [45]. When used to represent non-periodic functions, or functions with discontinuities, the Gibbs-effect will be present in the spectrum, and convergence around the boundaries will be non-uniform. There are efficient ways to weaken this effect [45], but this is a large disadvantage of the Fourier transform. Vice versa, when signals in the Fourier domain are truncated, the Gibbs effect shows in the time domain.

A.2. Regularity and Decay

The regularity of a signal $x(t)$ affects the decay of its Fourier transform $|X(\omega)|$ and vice versa [37]. The decay depends completely on the worst singular behaviour of $x(t)$. If there exists a constant K and $\epsilon > 0$ such that

$$|X(\omega)| \leq \frac{K}{1+|\omega|^{p+1+\epsilon}}, \qquad \text{then } x \in C^p. \tag{A.1}$$

For instance a step function, which is in C^0, results in a decay of $\mathcal{O}(1/|\omega|)$.

A.2.1. Uncertainty Principle

Equation A.1 shows that for a fast decaying spectrum $|X(\omega)|$ the signal $x(t)$ has regular variations in time. The energy of the signal $x(t)$ therefore has to be spread over a relatively large domain. The *uncertainty principle* relates the localization of energy in time with the localization in frequency. This principle is known to many as the *Heisenberg uncertainty principle*, for its implications in quantum mechanics which were discovered by Werner Heisenberg in the late 1920's. Assume a signal $x(t)$ of which the time spread is reduced, but the total energy is kept constant:

$$x_s(t) = \frac{1}{\sqrt{s}} x\left(\frac{t}{s}\right), \tag{A.2}$$

then its Fourier transform (use Appendix G) is $\mathcal{F}\{x_s\}(\omega) = \sqrt{s}X(s\omega)$. So the increased localization in the temporal domain ($s < 1$) has led to a decreased localization in the frequency domain. These concentrations of energy in time and frequency are therefore restricted.

This restriction is mathematically described by the uncertainty principle. The simplest explanation of this principle is that if one wants to detect a frequency, one has to observe at least one period of the signal. So for low frequencies, this takes a lot of time. For high frequencies, very small time ranges have to be considered. The uncertainty principle knows a number of different mathematical formulations [6, 20, 28, 37]. The principle [37] states that the product of the temporal variance σ_t^2 and the frequency variance σ_ω^2 of a signal $x(t)$ and its Fourier transform respectively are restricted by

$$\sigma_t^2 \sigma_\omega^2 \geq \frac{1}{4}. \tag{A.3}$$

The equality only holds for special cases of the signal. In addition, if a function $x(t) \neq 0$ has a compact support (the signal is of finite length), then its Fourier transform $\mathcal{F}\{x\}(\omega)$ cannot have a compact support and vice versa [37].

Heisenberg Boxes

The so-called *Heisenberg box* is the result of this principle. This box limits the temporal and frequency precision of the STFT and the wavelet transform. The temporal and frequency variance are determined by the choice of the window function $g(t)$. Assume $g(t)$ real and symmetric, with $g_{s,\xi}(t) = e^{i\xi t} g(t-s)$. Then the variances are only dependent on time and frequency, and therefore independent of the translation s and

the modulation ξ (see equation A.4). Hence $g_{s,\xi}(t)$ corresponds to a Heisenberg box of area $\sigma_t\sigma_\omega$, centered around (s,ξ) [37], this is illustrated in Figure A.1. Because the window function does not change, the STFT is of identical resolution across the whole time-frequency plane.

$$\sigma_t^2 = \int_{-\infty}^{\infty} t^2 |g(t)|^2 \, \mathrm{d}t, \qquad \sigma_\omega^2 = \int_{-\infty}^{\infty} \omega^2 |\mathcal{F}\{g(t)\}(\omega)|^2 \, \mathrm{d}t. \tag{A.4}$$

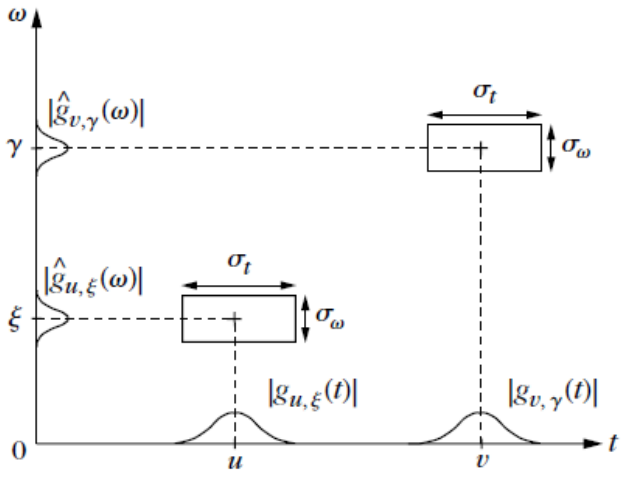

Figure A.1: Heisenberg boxes of two windowed Fourier transforms, where $\widehat{f} := \mathcal{F}f$ [12, 37].

Choice of Windows

From the above, we may conclude that the resolution in time and frequency of the STFT is dependent on the spread of the window in time and frequency. Notice that from the Heisenberg uncertainty principle (A.3) follows that the minimal area of an Heisenberg box is $1/2$. Mallat [37] shows that this can only be reached if g is a Gaussian window function. However, the organization of this box, width vs. height, can be arranged, to match a specific temporal or frequency resolution. This can be done by scaling the window $g(t)$ as in (A.2). The wavelet transform uses this scaling, which results in a changing resolution in the time-frequency plane as depicted in Figure 2.1d.

$g(t)$ finite?

For numerical applications, $g(t)$ must have a compact support, for it is finite. However, this results in an infinite support of the window function in the frequency domain [37]. The frequency resolution of the transform is maximised by concentrating the energy of $\mathcal{F}\{g\}(\omega)$ near $\omega = 0$. Then the temporal and frequency variance σ_t and σ_ω are not to deviating. If we for instance choose to shrink σ_ω to 0 (i.e. by choosing $g(t) = \delta(t)$), this results in the normal Fourier transform: high frequency resolution, but no temporal resolution.

B

Multi Resolution Analysis

The *multi resolution analysis* or *multi resolution approximation* (MRA) is a common way of define the discrete wavelet transform. The *discrete wavelet transform* (DWT) theory can be approached from the definition of the CWT, with addition of the notion of frames in Hilbert spaces [6, 14, 37]. Here however, the MRA approach of the DWT will be followed, which has two main advantages. The first advantage is that the MRA theory is discrete to begin with, resulting in a more natural derivation of the DWT, which is easier to implement as a computer algorithm [6, 28, 42]. Secondly, the MRA structure allows for convenient, fast and exact calculation of wavelet coefficients by providing a recursion relation, for both the discrete and the continuous case. This recursion relation is a relation between scaling coefficients at a given scale 2^{-n-1} and the scaling and wavelet coefficients at the next coarser scale 2^{-n} [59]. This section starts with the definition of a refinable function and an MRA and it ends with the definition of the DWT. This is followed by the covering of bi-orthogonal MRAs, in addition to the orthogonal ones discussed here. Through out this section the example of the Haar wavelet will be used. First we start with a *refinable function*, which is a function $\phi : \mathbb{R} \to \mathbb{C}$ which satisfies a two-scale refinement equation, or *recursion relation* of the form

$$\phi(t) = \sqrt{2} \sum_{k=k_0}^{k_1} h_k \phi(2t-k). \tag{B.1}$$

The $h_k \in \mathbb{C}$ are known as the *recursion coefficients*. A refinable function ϕ is called orthogonal if for $k \in \mathbb{Z}$ [6, 28]

$$\langle \phi(t), \phi(t-k) \rangle = \delta_{0k} \qquad \text{holds.} \tag{B.2}$$

Haar function An example of such an orthogonal refinable function is the *Haar function*, defined as

$$\phi_{\text{Haar}}(t) := \mathbb{1}_{[0,1]} = \begin{cases} 1 & 0 \le t \le 1 \\ 0 & \text{elsewhere} \end{cases}. \tag{B.3}$$

The Haar function is orthogonal and refinable with $h_0 = h_1 = 1/\sqrt{2}$, as shown in Figure C.1.

The set $\{V_j\}_{j\in\mathbb{Z}}$ is called a orthogonal *multi resolution analysis* (MRA) of L^2, where V_j, $j \in \mathbb{Z}$ is a sequence of subspaces of L^2, if it complies to six conditions [28]:

$$V_j \subset V_{j+1} \qquad \text{(nested subsets)} \tag{B.4a}$$

$$\cup_{j\in\mathbb{Z}} V_j = L^2 \qquad \text{(density axiom)} \tag{B.4b}$$

$$\cap_{j\in\mathbb{Z}} V_j = \{0\} \qquad \text{(separation axiom)} \tag{B.4c}$$

$$f(t) \in V_n \iff f(2x) \in f(2t) \in V_{n+1} \ \forall n \in \mathbb{Z} \qquad \text{(scaling property)} \tag{B.4d}$$

$$f(t) \in V_n \iff f(2x) \in f(t-2^{-n}k) \in V_n \ \forall n,k \in \mathbb{Z} \qquad \text{(scaling property)} \tag{B.4e}$$

$$\exists \phi(t) \in L^2 \text{such that } \{\phi(t-k) : k \in \mathbb{Z}\} \text{ forms an orthogonal basis of } V_0 \qquad \text{(scaling function)} \tag{B.4f}$$

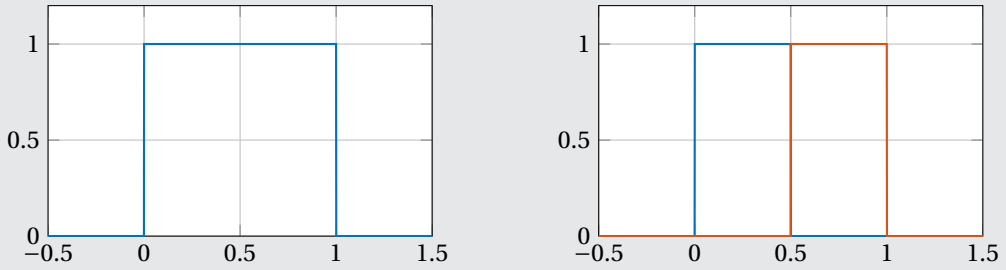

(a) The Haar scaling function $\phi_{\text{Haar}}(t)$

(b) The refined Haar scaling function $\phi_{\text{Haar}}(t) = \sqrt{2}(\phi_{\text{Haar}}(2t)/\sqrt{2} + \phi_{\text{Haar}}(2t-1)/\sqrt{2})$

Figure B.1: Example: the Haar scaling function.

There also exist MRAs built on non orthogonal scaling functions, these will be discussed later (Section B.5). Orthonormalising an existing scaling function is possible, but the resulting new ϕ often does not have compact support anymore, losing its function for practical applications [28]. The fourth condition (B.4d) expresses the main property of an MRA: each subspace V_n consists of the functions in V_0 compressed by a factor 2^n, therefore spanning V_0. From this can be concluded that a stable basis of V_n is given by $\{\phi_{nk}(t) : n \in \mathbb{Z}\}$, where

$$\phi_{nk}(t) = 2^{n/2}\phi(2^n t - k), \qquad k \in \mathbb{N}. \tag{B.5}$$

The last condition (B.4f) implies that any function $f \in V_0$ can be written uniquely as a sum of coefficients f_k multiplied with a scaling function

$$f(t) = \sum_{k\in\mathbb{Z}} f_k{}^* \phi(t-k), \tag{B.6}$$

converging in L^2. The essential characteristic of the MRA is that $\phi(t) \in V_0$ can be written in the terms of the basis of V_1 as

$$\phi(t) = \sum_k h_k \phi_{1k}(t) = \sqrt{2}\sum_k h_k \phi(2t-k), \tag{B.7}$$

for some coefficients h_k. This is called the *refinement equation*. From this follows that ϕ is a refinable function, for ϕ complies to the recursion relation (B.1). This refinement equation can be an infinite sum, but for now we will continue assuming a finite sum. The orthogonality condition (B.2) in this form becomes

$$\sum_k h_k h^*_{k-2\ell} = \delta_{0\ell}. \tag{B.8}$$

The orthogonal projection onto the subspace V_n, denoted with P_n, of an arbitrary function $f \in L^2$ is given by

$$P_n f = \sum_k \langle f, \phi_{nk}\rangle \phi_{nk}. \tag{B.9}$$

Note that the projection $P_n f$ cannot represent details smaller than 2^{-n}. Therefore we say that functions in V_n have *resolution* or *scale* 2^{-n}. An MRA provides a sequence of approximations $P_n f$ of increasing accuracy to a given function f.

Orthogonal projection Lets continue with the Haar example. We are going to approximate the function $\cos(t)$ on the interval $[0, 10]$. We start with the function ϕ_{Haar} (B.3), then

$$P_0 f(t) = \sum_k \langle f, \phi_{0k}\rangle \phi_{0k} = \sum_k \langle \cos t, \phi_{\text{Haar}}(t-k)\rangle \cdot \phi_{\text{Haar}}(t-k).$$

And so the same can be applied to $P_1 f(t)$:

$$P_1 f(t) = \sum_k \langle f, \phi_{1k}\rangle \phi_{1k} = \sum_k \langle \cos t, \sqrt{2}\phi_{\text{Haar}}(2t-k)\rangle \cdot \sqrt{2}\phi_{\text{Haar}}(2t-k).$$

The result of this approximation is given in Figure B.2. Note that the Haar function produces an orthogonal MRA.

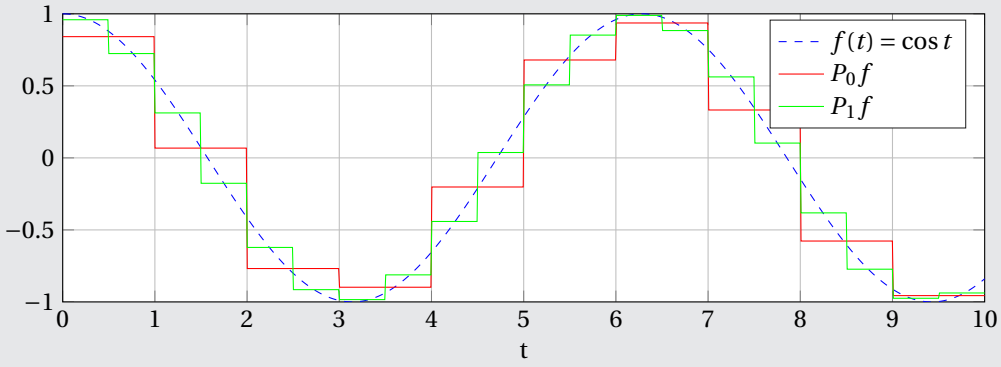

Figure B.2: Orthogonal projection of the function $\cos t$ using the Haar function (B.3).

B.1. Fine Details

Orthogonal components In Example B.2 we have seen that we can approximate a function using the scaling function ϕ. The representation of, for instance, a function $x(t) \in V_1$ can be done by the space V_1, but also by all spaces V_j, $j > 1$ [42]. This representation, however, is not very efficient, because more parameters than necessary are needed. How do you use less parameters? Note we used the functions in V_1 only to represent the part of $x(t)$ which could not be represented by V_0. If we only use the difference between the spaces V_1 and V_0 to describe $x(t)$, less parameters are needed. Therefore the space W_0 will be explicitly designed. This space W_0 is in V_1, but not in V_0 and therefore is called the *orthogonal component* of V_0 in V_1. A more mathematical description follows.

When this difference between two approximations at different levels is considered, the applicability of the MRA rises. The difference between two levels of resolution 2^{-n} and 2^{-n-1} is also called the *fine detail at resolution* 2^{-n}, denoted as Q_n:

$$Q_n f = P_{n+1} f - P_n f. \tag{B.10}$$

Note that Q_n is also an orthogonal projection [28] and that its range W_n is orthogonal to V_n, so the direct sum of the function space V_n and W_n is V_{n+1}:

$$V_n \oplus W_n = V_{n+1}.$$

This is the final step that brings us to another definition of the wavelet, approached discretely instead of continuous. Wavelets are an element of an orthogonal MRA. For any orthogonal MRA with scaling function ϕ [28]

$$\bigoplus_n W_n = L^2 \text{ dense} \tag{B.11a}$$

$$W_k \perp W_n \text{ if } k \neq n \tag{B.11b}$$

$$f(t) \in W_n \iff f(2t) \in W_{n+1} \forall n \in \mathbb{Z} \tag{B.11c}$$

$$f(t) \in W_n \iff f(t - 2^{-n}k) \in W_n \forall n, k \in \mathbb{Z} \tag{B.11d}$$

$$\exists \psi \in L^2, \text{ called a wavelet, such that } \{\phi(t-k) : k \in \mathbb{Z}\} \text{ forms an orthogonal basis of } W_0$$
$$\text{and } \{\psi_{nk} : n, k \in \mathbb{Z}\} \text{ forms a stable basis of } L^2. \tag{B.11e}$$

$$\text{Since } \psi \in V_1, \text{ it can be represented as}$$
$$\psi(t) = \sum_k g_k \phi_{1k} = \sqrt{2} \sum_k g_k \phi(2x-k), \text{ with } g_k = (-1)^k h_{N-k}, \text{ with } N \text{ odd}. \tag{B.11f}$$

Here ψ is known as the *mother wavelet.* In terms of the wavelet function, the projection Q_n is given, in the same way as P_n (B.9):

$$Q_n f = \sum_k \langle f, \psi_{nk} \rangle \psi_{nk}. \tag{B.12}$$

This projection is the final step to the *discrete wavelet transform* DWT.

The Haar wavelet Now we will apply this to the example of the Haar function from Example B.1, to introduce our first wavelet build using MRA: the Haar wavelet (see Figure B.3). The coefficients g_k from (B.11f) to create the Haar wavelet are $\{g_0, g_1\} = \{h_1, -h_0\} = \{1/\sqrt{2}, -1/\sqrt{2}\}$, resulting in the function $\psi_{\text{Haar}}(t) = \mathbb{1}_{[0;0.5)}(t) - \mathbb{1}_{[0.5;1)}(t)$.

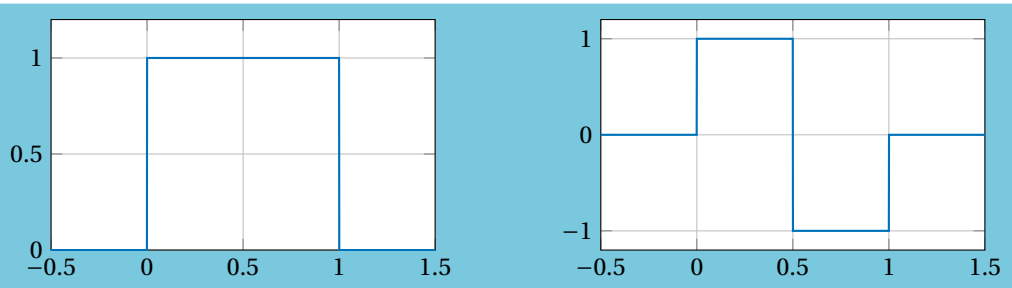

(a) The Haar scaling function $\phi_{\text{Haar}}(t)$ **(b)** The Haar wavelet $\psi_{\text{Haar}}(t)$

Figure B.3: The Haar scaling function and wavelet.

B.2. Discrete Wavelet Transformation

We have seen that given a function $f \in L^2$ we can represent it as a complete decomposition in terms of detail at all levels:

$$f = \sum_{k=-\infty}^{\infty} Q_k f.$$

As an alternative one can choose to start at a level ℓ and use the approximation at resolution $2^{-\ell}$ together with the detail at finer resolution, to decompose f as:

$$f = P_\ell f + \sum_{k=\ell}^{\infty} Q_k f.$$

An infinite sum is not practical applicable, so the sum is reduced to a finite sum: therefore we assume $f \in V_n$ for some $n > \ell$. Then the *discrete wavelet transform* (DWT) is described by

$$f = P_n f = P_\ell f + \sum_{k=\ell}^{n-1} Q_k f. \tag{B.13}$$

The DWT approach is similar to the CWT approach, except of using continuous scale a and translation b, these are chosen discretely as scale n and translation k. The mother wavelet $\psi(t)$ is chosen and the daughter wavelets are

$$\psi_{nk}(t) = 2^{n/2} \psi(2^n t - k). \tag{B.14}$$

The nk Heisenberg box has size $2^{-n}\sigma_t \times 2^n \sigma_\omega$, with different spacings for different frequencies, as for the continuous case. The inverse operation of the DWT will be discussed in Section B.7.

DWT This is the last time the Haar example will be discussed. For the Haar example $P_0 f$ and $P_1 f$ have been computed, following the DWT (B.13) we should find that $P_1 f = P_0 f + Q_0 f$. Therefore we use (B.12) to find

$$Q_0 f = \sum_k \langle f, \psi_{0k} \rangle \psi_{0k} = \sum_k \langle \cos t, \mathbb{1}_{[0;0.5)}(t-k) - \mathbb{1}_{[0.5;1)}(t-k) \rangle \cdot (\mathbb{1}_{[0;0.5)}(t-k) - \mathbb{1}_{[0.5;1)}(t-k)).$$

The result is shown in Figure B.4.

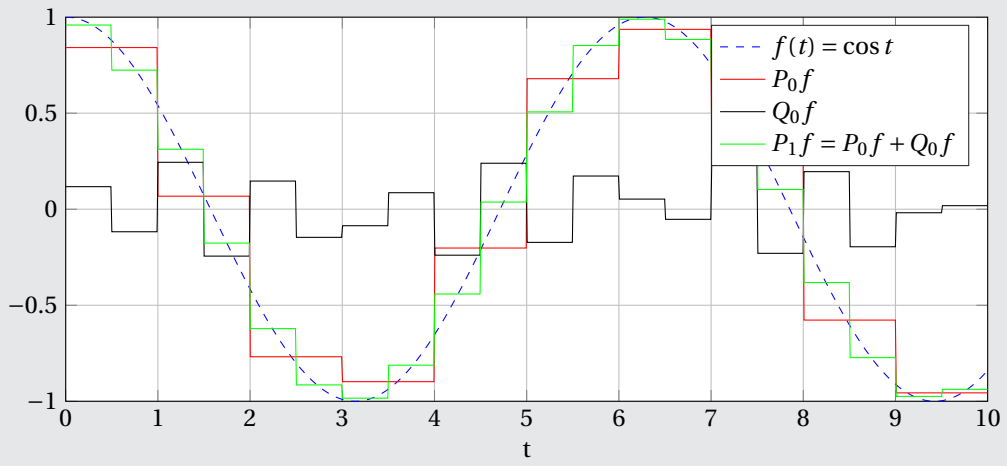

Figure B.4: Discrete wavelet decomposition of $\cos t$ using the Haar function (B.3) and Haar wavelet.

B.3. Requirements for Wavelet Transform

As for the Fourier transform, the integral defining the coefficients should converge. So, just like for the Fourier transform, only functions in the L^2 space are theoretically suitable for wavelet transformation [37]. For discrete signals some requirements will be discussed in Section B.7. However, effects such as the Gibbs effect are not present in the wavelet transform. This makes the wavelet transform much more suitable to use for signals with discontinuities. The Fourier transform can also show unwanted effects in the reconstruction of non periodic functions, for instance a linear function. The reconstruction of the wavelet transform for both non periodic as periodic functions is close to perfect. Because the wavelet transform (up to a certain scale) only catches local effect, the wavelet transform is also better applicable to non-stationary signals.

B.3.1. From CWT to DWT

As mentioned before, there are two ways to derive the DWT. Following the MRA theory, we have found an expression for the (discrete) wavelet coefficient belonging to wavelet ψ_{nk} (from (B.12)): $\langle f, \psi_{nk} \rangle$. The definition of the inner product on L^2 shows the similarity with the continuous wavelet coefficient from (2.18). The CWT and DWT coefficients are defined through the same integral. Therefore a large set of functions is suitable for both continuous and discrete wavelet transform. However, the most are better suited for one or the other; an overview is given in Appendix C. The DWT cannot be derived directly from the CWT expression (2.18), because the set of discrete scales and translations cannot be chosen arbitrarily. The justification of this choice can be made through the notion of frames from the Hilbert space theory, which results in the same expression for the DWT as presented in equation B.13 [6, 14, 37]. A major advantage of the MRA approach is that an efficient algorithm of the DWT is easily derived, for both orthogonal and non orthogonal wavelets (see Section B.5). This algorithm will be explained to the reader in Section B.7.

B.4. The Design Equations

The Fourier transforms of the scaling function and the wavelet are indispensable in the design of wavelets. Here they are shortly reviewed. $H(\omega)$ and $G(\omega)$ are known as the *symbol* of respectively the refinable function and the wavelet[28]:

$$\Phi(\omega) = \mathcal{F}\phi(\omega) = H(\omega/2)\Phi(\omega/2), \qquad \text{with } H(\omega) = \frac{1}{\sqrt{2}} \sum_k h_k e^{-ik\omega}, \tag{B.15}$$

$$\Psi(\omega) = \mathcal{F}\psi(\omega) = G(\omega/2)\Psi(\omega/2), \qquad \text{with } G(\omega) = \frac{1}{\sqrt{2}} \sum_k g_k e^{-ik\omega}. \tag{B.16}$$

The orthogonality condition (B.8) in the Fourier domain becomes

$$|H(\omega)|^2 + |H(\omega+\pi)|^2 = 1. \tag{B.17}$$

Relationship (B.15) can be substituted recursively, to find the formal limit

$$\Phi(\omega) = \left[\prod_{k=1}^{\infty} H(2^{-k}\omega)\right]\Phi(0). \tag{B.18}$$

This approach is effective in the creation of wavelets. This relation can also be used to calculate the refinement equation corresponding to a certain low pass filter [31]. If convergence of this infinite product is assumed, this expression provides a way to compute $\phi(t)$ theoretically. $\Phi(0)$ can be chosen arbitrarily: solutions of the refinement equation (B.7) are only defined up to a constant factor. Choose $\Phi(0) \neq 0$ to find solutions other than $\phi(t) = 0$. Multiples of the solution of the equation are also solutions to the equation.

B.4.1. Cascade Algorithm

The *cascade algorithm* is a more suitable way than (B.18) to approximate point values of $\phi(t)$ [28]. This algorithm applies a fixed point iteration applied to the refinement equation. Starting by choosing a suitable scaling function $\phi^{(0)}(t)$, and define

$$\phi^{(n)}(t) = \sqrt{2}\sum_k h_k \phi^{(n-1)}(2t-k), \tag{B.19}$$

which will converge in many cases.

B.5. bi-orthogonal Wavelets

In the derivation of the DWT we used the existence of orthogonal MRAs. These orthogonal MRAs, however, are not very common [28] and therefore the *bi-orthogonal* MRA will be discussed. We first start with an example from linear algebra, to explain the concept of bi-orthogonality.

bi-orthogonal system Consider two independent vectors $\boldsymbol{b}_1$ and $\boldsymbol{b}_2 \in \mathbb{R}^2$. By independence, $\boldsymbol{b}_1$ and $\boldsymbol{b}_2$ are a basis for $\mathbb{R}$. If $\boldsymbol{b}_1 \perp \boldsymbol{b}_2$, this basis is called orthogonal, if also both vectors are unit vectors, the basis is called orthonormal. Any vector $\boldsymbol{x} \in \mathbb{R}^2$ can be written as $\boldsymbol{x} = \alpha\boldsymbol{b}_1 + \beta\boldsymbol{b}_2$. If we choose $B = [\boldsymbol{b}_1, \boldsymbol{b}_2]$, then we can solve for the coefficients:

$$\boldsymbol{x} = B\begin{bmatrix}\alpha\\ \beta\end{bmatrix} = B\boldsymbol{c} \qquad \Rightarrow \qquad \boldsymbol{c} = B^{-1}\boldsymbol{x}.$$

This, however, is not as easily solved for a nonorthogonal set as for an orthogonal set of basis vectors. Therefore the *dual* base $\{\tilde{\boldsymbol{b}}_1, \tilde{\boldsymbol{b}}_1\}$ is introduced. These vectors comply to [42]

$$\langle \boldsymbol{b}_1, \tilde{\boldsymbol{b}}_1\rangle = 1, \qquad \langle \boldsymbol{b}_2, \tilde{\boldsymbol{b}}_2\rangle = 1, \qquad \langle \boldsymbol{b}_2, \tilde{\boldsymbol{b}}_1\rangle = 0, \qquad \langle \boldsymbol{b}_1, \tilde{\boldsymbol{b}}_2\rangle = 0,$$

such that we can use the relation $\boldsymbol{c} = B^{-1}\boldsymbol{x} = \tilde{B}\boldsymbol{x}$, to determine the coefficients α and β. This matrix $\tilde{B}$ is chosen $\tilde{B} = \left[\tilde{\boldsymbol{b}}_1, \tilde{\boldsymbol{b}}_1\right]^\mathsf{T}$ such that

$$\boldsymbol{x} = \left(\tilde{\boldsymbol{b}}_1^\mathsf{T}\boldsymbol{x}\right)\boldsymbol{b}_1 + \left(\tilde{\boldsymbol{b}}_2^\mathsf{T}\boldsymbol{x}\right)\boldsymbol{b}_2. \tag{B.20}$$

E.g. we choose two non orthogonal vectors, spanning $\mathbb{R}^2$ and a vector $\boldsymbol{x}$:

$$\boldsymbol{b}_1 = \begin{bmatrix}1\\0\end{bmatrix}, \qquad \boldsymbol{b}_2 = \begin{bmatrix}1/2\\ \sqrt{3}/2\end{bmatrix} \qquad \boldsymbol{x} = \begin{bmatrix}1\\1\end{bmatrix}.$$

The dual base for the given $\boldsymbol{b}_1$ and $\boldsymbol{b}_2$ is given by

$$\tilde{\boldsymbol{b}}_1 = \begin{bmatrix}1\\ -1/\sqrt{3}\end{bmatrix} \qquad \text{and } \tilde{\boldsymbol{b}}_2 = \begin{bmatrix}0\\ 2/\sqrt{3}\end{bmatrix}.$$

Then

$$\tilde{\boldsymbol{b}}_1^\intercal \boldsymbol{x} = 1 - 1/\sqrt{3}, \qquad \tilde{\boldsymbol{b}}_2^\intercal \boldsymbol{x} = 2/\sqrt{3}, \qquad \Rightarrow \quad (1-1/\sqrt{3})\begin{bmatrix}1\\0\end{bmatrix} + 2/\sqrt{3}\begin{bmatrix}1/2\\\sqrt{3}/2\end{bmatrix} = \begin{bmatrix}1\\1\end{bmatrix} = \boldsymbol{x}.$$

The sets $\{\boldsymbol{b}_1, \boldsymbol{b}_2\}$ and $\{\tilde{\boldsymbol{b}}_1, \tilde{\boldsymbol{b}}_2\}$ are a bi-orthogonal system of $\mathbb{R}^2$.

As the word *bi* in bi-orthogonal implies, the bi-orthogonal MRA has not one but two refinable functions as a basis. Refinable functions in general are relatively easy to find, but a lot of them do not result in orthogonal MRAs, so the orthogonality conditions will be replaced by milder bi-orthogonality conditions [28]. Two refinable functions ϕ and $\tilde{\phi}$ are called *bi-orthogonal* if

$$\langle \phi(x), \tilde{\phi}(x-k)\rangle = \delta_{0k}.$$

$\tilde{\phi}$ then is referred to as the *dual* of ϕ. This dual, however, is not unique [28], dual lifting, a process discussed later, will produce numerous other duals of the same ϕ. These two scaling functions define two MRAs: $\{V_n\}_{n\in\mathbb{Z}}$ and $\{\tilde{V}_n\}_{n\in\mathbb{Z}}$. Then the construction of the projections follows the same line of reasoning as in Example B.5: there are two projections, P_n (B.21a) and $\tilde{P}_n$ (B.21b) to project a function from L^2 to $\{V_n\}_{n\in\mathbb{Z}}$ and $\{\tilde{V}_n\}_{n\in\mathbb{Z}}$ respectively.

The projections Q_n (B.21c) and $\tilde{Q}_n$ (B.21d) are defined as before, spanning the spaces $\{W_n\}_{n\in\mathbb{Z}}$ and $\{\tilde{W}_n\}_{n\in\mathbb{Z}}$ respectively. The space W_n is now orthogonal to $\tilde{V}_n$, such that the fine detail relation (B.10) still holds. The same hold for $\tilde{W}_n$ and V_n. Now note that $V_n \oplus W_n = V_{n+1}$ still holds, but now as a nonorthogonal direct sum instead of an orthogonal one. Keinert [28] states that finding wavelet functions ψ and $\tilde{\psi}$ which span the spaces W_n and $\tilde{W}_n$ is not that hard, but stability is not guaranteed.

$$P_n f = \sum_k \langle f, \tilde{\phi}_{nk}\rangle \phi_{nk}, \tag{B.21a}$$

$$\tilde{P}_n f = \sum_k \langle f, \phi_{nk}\rangle \tilde{\phi}_{nk}, \tag{B.21b}$$

$$Q_n f = P_{n+1} f - P_n f, \tag{B.21c}$$

$$\tilde{Q}_n f = \tilde{P}_{n+1} f - \tilde{P}_n f. \tag{B.21d}$$

When an orthogonal wavelet is used for decomposition, the representation of the signal is the most compact: the number of convolutions at a scale is proportional to the size of a scale [55]. This will result in a relative sparse representation of the signal. This is characteristic is very desirable in signal compression [28]. An aperiodic shift in time-series produces a different wavelet spectrum, this is often not beneficial in time-series analysis. When a bi-orthogonal wavelet is used, the large scales are highly redundant, the wavelet coefficients at adjacent times are highly correlated. This makes the bi-orthogonal wavelets better applicable to time-series analysis where smooth, continuous variations in wavelet coefficients are expected [55].

B.6. Discrete Moments

In Section C.1 the importance of the number of vanishing moments for the wavelet transform has been addressed. The discrete wavelet do have vanishing moments, just like the continuous case. They, however, can be defined by their coefficients: the kth discrete moment of the refinement function ϕ and the wavelet ψ are defined by their coefficients h_k and g_k. The m denotes the moment of the refinable function, the n the moment of the wavelet [28].

$$m_k = \frac{1}{\sqrt{2}} \sum_\ell \ell^k h_\ell, \qquad n_k = \frac{1}{\sqrt{2}} \sum_\ell \ell^k g_\ell,$$

$$m_k = i^k \frac{\mathrm{d}^k h}{\mathrm{d}\omega^k}(0), \qquad n_k = i^k \frac{\mathrm{d}^k g}{\mathrm{d}\omega^k}(0).$$

If in particular $m_0 = h(0) = 1$, the zeroth moment of a refinement function is 1. These discrete moments are uniquely defined and easy to calculate. They can be computed using the relation between the discrete and continuous moments:

$$\mu_k = 2^{-k} \sum_{p=0}^{k} \binom{k}{t} m_{k-p}\mu_p, \qquad \nu_k = 2^{-k} \sum_{p=0}^{k} \binom{k}{t} n_{k-p}\mu_p.$$

B.7. Discrete Wavelet Transform Algorithmic

In this section of the chapter the two or three steps of the algorithm performing the DWT are explained. Some different formulations of the DWT algorithm are discussed, which are essential to the building of wavelets. The resulting algorithm needs $\mathcal{O}(N \log_2 N)$ operations, which as fast as the DFT„ however, it is asymptotically faster than the STFT algorithm, using $\mathcal{O}(N^2 \log_2 N)$ operations. The two or three steps to do a complete DWT for a 1D signal of finite length are [28]:

1. Optional: preprocessing of the signal (Section B.10);
2. Handling the boundary conditions (Section B.11); and
3. Applying the algorithm (Section B.8).

Finally there are different ways of formulation and implementation of the algorithm. These will be discussed at the end of this section. This section is started with the final step of the DWT: the algorithm. Note we assume the use of bi-orthogonal wavelets, if one uses a orthogonal wavelets the tildes in this explanation can be dropped. The DWT is based on the decomposition of the space V_n:

$$V_n = V_\ell \oplus W_\ell \oplus \ldots \oplus W_{n-1}.$$

B.8. The Algorithm

We start with a function $s \in V_n$ (or signal), which by the theory can be represented by its coefficient vector $\boldsymbol{s}_n = \{s_{nk}\}_{k=1,\ldots,N}$:

$$s(t) = \sum_k s^*_{nk} \phi_{nk}(t). \tag{B.22}$$

The function can also be expanded into two parts:

$$s(t) = \sum_k s^*_{\ell k} \phi_{\ell k}(t) + \sum_{j=\ell}^{n-1} \sum_k d^*_{jk} \psi_{jk}(t).$$

The notations s and d originate from the Haar wavelet, where s denotes the sum and d the difference. For regular wavelets, it is easier to remind s as the smooth part and d as the (fine) detail [28]. The complex conjugate notation of the coefficients comes from the multi-wavelet theory. The DWT and inverse DWT (IDWT) convert the coefficients s_{nk} to $s_{\ell k}$ and d_{jk}, $j = \ell, \ldots, n-1$ and vice versa. Signals consisting of equally spaced samples of the signal s frequently are in the form $s(2^{-n}k)$. The conversion of $s(2^{-n}k)$ to s_{nk} is called *preprocessing*, the reverse processes *post-processing*. Both are explained later. So the signal s is *decomposed* in its components in V_{n-1} and W_{n-1} by

$$\begin{aligned} s = P_{n-1}s + Q_{n-1}s &= \sum_k \langle s, \tilde{\phi}_{n-1,j} \rangle \phi_{n-1,j} + \sum_k \langle s, \tilde{\psi}_{n-1,j} \rangle \psi_{n-1,j} \\ \Rightarrow \boldsymbol{s}_n &= \sum_k s^*_{n-1,j} \phi_{n-1,j} + \sum_k d^*_{n-1,j} \psi_{n-1,j}. \end{aligned}$$

By this the (discrete) signal s, $\boldsymbol{s}_n$ in vector notation, is *decomposed* in two pieces: $\boldsymbol{s}_{n-1}$ (B.23a) and $\boldsymbol{d}_{n-1}$ (B.23b) [28]. From this the signal can be reconstructed following (B.23c).

$$s_{n-1,j} = \sum_k \tilde{h}_{k-2j} s_{nk}, \tag{B.23a}$$

$$d_{n-1,j} = \sum_k \tilde{g}_{k-2j} s_{nk}, \tag{B.23b}$$

$$s_n k = \sum_j (h^*_{k-2j} s_{n-1,j} + g^*_{k-2j} d_{n-1,j}) \tag{B.23c}$$

Where we define

$$\langle \phi_{n-1,j}, \tilde{\phi}_{nk} \rangle = h_{k-2j}, \qquad \langle \phi_{n-1,j}, \tilde{\psi}_{nk} \rangle = g_{k-2j}, \qquad \langle \tilde{\phi}_{n-1,j}, \phi_{nk} \rangle = \tilde{h}_{k-2j}, \qquad \langle \tilde{\psi}_{n-1,j}, \phi_{nk} \rangle = \tilde{g}_{k-2j}.$$

B.8.1. Convolution Implementation

The decomposition step can be written as two discrete convolutions, of computation time $\mathcal{O}(N\log_2 N)$ using the same improvement as the FFT algorithm. These convolutions are

$$((-)\tilde{\boldsymbol{h}} * \boldsymbol{s}_n)_j = \sum_k \tilde{h}_{-(j-k)} s_{nk}, \qquad ((-)\tilde{\boldsymbol{g}} * \boldsymbol{s}_n)_j = \sum_k \tilde{g}_{-(j-k)} s_{nk}, \tag{B.24a}$$

which are followed by down-sampling to determine $\boldsymbol{s}_{n-1}$ and $\boldsymbol{d}_{n-1}$ (assume computation time of $\mathcal{O}(1)$):

$$\boldsymbol{s}_{n-1} = (\downarrow 2)((-)\tilde{\boldsymbol{h}} * \boldsymbol{s}_n), \qquad \boldsymbol{d}_{n-1} = (\downarrow 2)((-)\tilde{\boldsymbol{g}} * \boldsymbol{s}_n). \tag{B.24b}$$

This is only one step of the algorithm, in practice these steps often repeated several times:

$$\begin{aligned} \boldsymbol{s}_n &\to \boldsymbol{s}_{n-1}, \boldsymbol{d}_{n-1} \\ \boldsymbol{s}_{n-1} &\to \boldsymbol{s}_{n-2}, \boldsymbol{d}_{n-2} \\ &\vdots \\ \boldsymbol{s}_{\ell+1} &\to \boldsymbol{s}_\ell, \boldsymbol{d}_\ell. \end{aligned}$$

Because in every step, the length of the components $\boldsymbol{s}_{n-1}$, $\boldsymbol{d}_{n-1}$ is half the length of the components $\boldsymbol{s}_n$, $\boldsymbol{d}_n$, the algorithm has to compute $\mathcal{O}(N) + \mathcal{O}(N/2) + \mathcal{O}(N/4) + \ldots = \mathcal{O}(N)$ convolutions. This results in $\mathcal{O}(N^2 \log_2 N)$ arithmetic operations to determine the discrete wavelet transform of a signal. The reconstruction of the signal from the DWT is opposite to the decomposition: first upsampling, followed by two convolutions:

$$\boldsymbol{s}_n = \boldsymbol{h}^* * (\uparrow 2)\boldsymbol{s}_{n-1} + \boldsymbol{g}^* * (\uparrow 2)\boldsymbol{d}_{n-1}. \tag{B.24c}$$

B.8.2. Programming the Routine

When we start with a signal $\boldsymbol{s}_n$ of length N, the first step produces $\boldsymbol{s}_{n-1}$ and $\boldsymbol{d}_{n-1}$, which are both of length $N/2$. These signals are most of the time stored in the same place as the original signal $\boldsymbol{s}_n$. So the output of the DWT routine after several steps becomes then

$$\begin{bmatrix} \boldsymbol{s}_\ell \\ \boldsymbol{d}_\ell \\ \boldsymbol{d}_{\ell+1} \\ \vdots \\ \boldsymbol{d}_{n-1} \end{bmatrix}.$$

This vector can be stored in the same space as $\boldsymbol{s}_n$ with which the routine started. This representation results in an ugly programmable routine. The *matrix formulation* of the DWT results in a more appealing matrix-vector product notation.

Both the decomposition as the reconstruction can be implemented as infinite matrix-vector products [28]. Here $(\boldsymbol{sd})_n = \left[\ldots, s_{n,-1}, d_{n,-1}, s_{n,0}, d_{n,0}, s_{n,1}, d_{n,1}, \ldots\right]^\mathsf{T}$, such that the decomposition step can be written as

$$(\boldsymbol{sd})_{n-1} = \tilde{L}\boldsymbol{s}_n, \qquad \text{with } \tilde{L} = \begin{bmatrix} \cdots & \cdots & \cdots & & \\ \cdots & \tilde{L}_0 & \tilde{L}_1 & \cdots & \\ & \cdots & \tilde{L}_0 & \tilde{L}_1 & \cdots \\ & & \cdots & \cdots & \cdots \end{bmatrix}, \qquad \text{for } \tilde{L}_k = \begin{bmatrix} \tilde{h}_{2k} & \tilde{h}_{2k+1} \\ \tilde{g}_{2k} & \tilde{g}_{2k+1} \end{bmatrix}. \tag{B.25}$$

The reconstruction step can thus be written as

$$\boldsymbol{s}_n = L^*(\boldsymbol{sd})_{n-1},$$

where the perfect reconstruction condition is expressed as $L^*\tilde{L} = I$. The finite, and therefore applicable versions will be derived when the boundaries are discussed.

B.9. Filter Formulation

The filter formulation of this algorithm will be discussed shortly for it is widely used [40, 42, 54]. In the algorithm the decomposition is given by a convolution and a down-sampling. The recomposition is given as a up sampling step follow by a convolution with the same signal. These steps are shown in Figure B.5. From these figures it is clear that both filters $g[n]$ and $h[n]$ have different properties. The filter $g[n]$ is a high pass filter, whereas the filter $h[n]$ is a low pass filter. The down-sampled low pass filter output is then treated as an input for the next stage, passing through the same analyzing filters. From this follows that admissible wavelets are either high pass or band pass filters [42]. This process can be repeated until the desired number of stages is achieved. An example for three stages is found in Figure B.6. In the recomposition it is clear why only the most coarse smooth part and all fine details are saved. By omitting the finest details, a signal can for instance be compressed. The representation in Figure B.6 is known as the dyadic implementation. The recomposition filters are known as *interpolating filters*. If wavelet packets are used, not only the smooth part is fed into the decomposition again, but also the detail parts are decomposed. If not all detail parts are decomposed, this can lead to interesting distributions of the time-frequency plane.They are almost nowhere used to display data, but have different applications in mostly compression and noise reduction [42].

Wavelets can be designed from this filter perspective, where $h[n]$ can be seen as high pass filter and $g[n]$ as a low pass filter. This design perspective will not be addressed much in this thesis. However, note that the choice of filter $h[n]$ has impact on the vanishing moments, the regularity and the decay of the accompanied wavelet. The choice of the coefficients of $h[n]$ that lead to maximum regularity differs from the choice of a maximum number of vanishing moments [14]. The filter implementation of the DWT algorithm is also known as the Fast Wavelet Transform (FWT) and was first proposed by Mallat in 1988. It finds it strength in using the Fourier transform of the signals and the convolution property (6) [37]. This will be elaborated further in Section B.12.

B.10. Pre- and Post-processing

As mentioned in the begin of Section B.7, the data, mostly in the form of a signal $s(2^{-n}k)$, has to be converted to the coefficients s_{nk} from (B.22). Keinert [28] discusses a few options to find the coefficients s_{nk} (assume the signal $s(t)$ is real for simplification):

- Use for the coefficients their exact values: $s_{nk} = \int_{-\infty}^{\infty} s(t)\tilde{\phi}_{nk}(t)\,\mathrm{d}t$. This is only feasible for continuous signals $s(t)$.
- For discrete signals, for instance the trapezoidal rule can be used: $s_{nk} \approx 2^{-n/2}\sum_{\ell} s(2^{-n}\ell)\tilde{\phi}(\ell-k)\,\mathrm{d}t$. It is important to note that the point values of $\tilde{\phi}$ at the integer points are known. Higher order quadrature rules can be used too. The trapezoidal rule is one of the many quadrature rules, in general form written as [58]
$$\int_{t_1}^{t_2} f(t)\,\mathrm{d}t \approx \sum_{k=1}^{K} w_k f(v_k),$$
where K is the number of quadrature points, w_k the weights and v_k the quadrature points in $[t_1, t_2]$. The Gaussian rules are a special type of these quadrature rules, where the integration points and weights are chosen such that the highest order of accuracy is reached for a particular number of integration points v_k.
- Keinert [28] suggests to use $s_{nk} \approx s(2^{-n}k)$. Both Walnut [59] and Keinert [28] refer to the book of Strang and Nguyen [52], where this assumption is called a *wavelet crime*. However, Keinert [28] shows that for smooth s (at least two times differentiable) the truncation error is smaller than the coefficients by a factor of order 2^{-n}.

(a) One step decomposition

(b) One step reconstruction

Figure B.5: Filter formulation of the DWT algorithm.

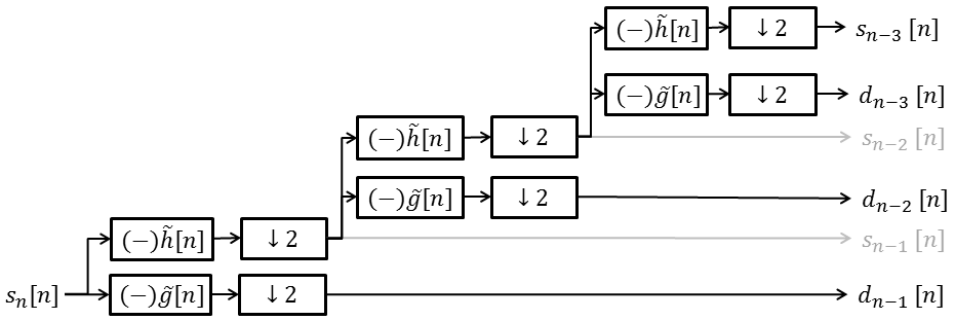

(a) Three steps decomposition

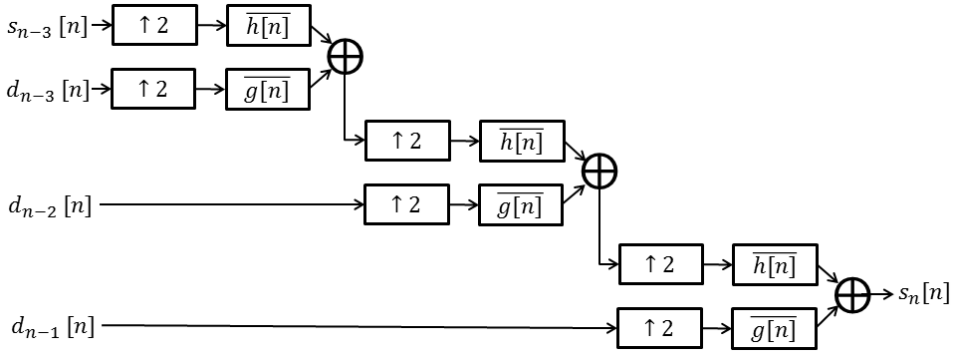

(b) Three steps reconstruction

Figure B.6: Filter formulation of the algorithm for a three step algorithm

Post-processing is the above described process in reverse: the conversion from s_{nk} to $s(t)$. There are two main approaches for post-processing:

- Adding up scaling function expansions in between sampling points to retrieve the continuous signal $s(t)$. Because many scaling functions are not smooth, this might lead to a non continuous reconstruction [28].
- The alternative is finding intermediate points using interpolation.
- Other approaches from papers or books, a start point is given by Keinert [28].

B.11. Boundaries: Different Approaches

In Section B.8 the infinite approach of the algorithm and the corresponding implementation (B.25) has been discussed. Of course this infinite approach is not implementable, therefore boundaries are introduced to abbreviate the infinite approach to a finite implementation. As for the infinite length DWT the finite length algorithm will be assumed linear, where the form of $\tilde{L}_n$ is changed to:

$$(\boldsymbol{sd})_{n-1} = \tilde{L}_n \boldsymbol{s}_n, \qquad \text{with } \tilde{L}_n = \begin{bmatrix} \tilde{L}_b & & \oslash \\ & \tilde{L}_i & \\ \oslash & & \tilde{L}_e \end{bmatrix}. \tag{B.26}$$

Here the subscript b, i and e stand for begin, interior and end. In the begin and end parts of the matrix, the boundaries will be handled. Generally the size of L_b and L_e are small with respect to the size of L_n and they both remain constant at all levels. The interior $\tilde{L}_i$ is a segment of the infinite matrix $\tilde{L}$ from (B.25). This part makes up the most of the matrix, approximately doubling in size when going from n to $n+1$. For the IDWT to exist, the matrix $\tilde{L}_n$ has to be invertible. In the orthogonal case $L_n^{-1} = L_n^*$, for the bi-orthogonal case the 'inverse' L_n^* has an analogous structure, being

$$L_n^* = \begin{bmatrix} \tilde{L}_b^* & & \oslash \\ & \tilde{L}_i^* & \\ \oslash & & \tilde{L}_e^* \end{bmatrix}.$$

There are three main ways to implement boundaries [28]. These boundary methods often do require some preprocessing. The choice for a specific method is data dependent. This will be discussed in the following enumeration. If one has non-periodic, non-symmetric data, and the boundary function approach is too hard, Keinert [28] advises to use linear extension for it is easy to implement and does not introduce artificial jumps in the data. For signals with enough zeros at the begin and end of the signal, the boundary handling is irrelevant.

- **The data extension approach**. This method extends the signal across the boundaries, such that each extended coefficient is a linear combination of known coefficients. The resulting $\tilde{L}_n$ can be singular, though most of the times it is not. The inverse L_n^* might not have the correct form such that reconstruction is possible. In this method several extension methods, known as modes in Matlab and Python:
  - Periodic extension: the signal is assumed to be periodic, so the h- and g-coefficients disappearing on the left side of the matrix appear at the right and vice versa. This extension always works, preserving orthogonality and approximation $\mathcal{O}(h)$. Matlab and Python also know an extension method called periodization [40, 54]. Periodization is virtually the same as periodic extension„ however, it ensures the smallest length wavelet decomposition. When the data is not truly periodic, the jump at the boundary leads to large d-coefficients [28].
  - Zero extension, also known as zero padding is done by truncating the infinite matrix $\tilde{L}$. The non-existing infinite part of the signal is observed as 0's. This also introduces jumps, as the periodic extension, and this method does not preserve orthogonality or approximation orders [28].
  - Symmetric extension mirrors the data in the endpoints, resulting in the coefficients in $\tilde{L}$ that disappear at the ends, get mirrored back. There are three ways of reflection: whole-sample symmetry, half-sample symmetry and antisymmetric reflection (only useful in the case $s_0 = 0$). If the data extension type matches the type of symmetry of the scaling function, the finite DWT will be equivalent to an infinite DWT [28].
  - Extrapolation does not conserve the orthogonality condition. Constant extrapolation leads to approximation $\mathcal{O}(2^{-n})$, linear approximation (also known as smooth-padding [54]) to order $\mathcal{O}(2^{-2n})$ [28].
- **The matrix completion approach** guarantees $\tilde{L}_n L_n^* = I$, approaching the problem from a linear algebra view. The downside is that this approach generally does not conserve approximation order.
- **The boundary function approach** is the most time-consuming approach, preserving both orthogonality and approximation order. This approach introduces special functions at the boundaries of the interval which, unlike ϕ_0, do not extend over the border. The decomposition and reconstruction algorithm have to be worked out newly. The hardest part is to derive boundary wavelets which have the same number of vanishing moments as the original [37].
- Instead of assuming the periodicity of the signal, **periodic wavelets** can be used. Wavelets that cross one border of the domain are made periodic [37]. These wavelets create high amplitude wavelet coefficients in the neighborhood of the borders of the domain and do not have vanishing moments. The method is mathematically the same as extending the data periodically [37].

DWT decomposition An example of a DWT decomposition: the signal at the bottom is decomposed four times. Note that the length of the detail coefficient vector is half the length of its predecessor and that the resulting smooth part and the fourth detail coefficients vector have the same length. The coefficients on the right have been translated to their contribution to the signal (left). The sum of the contributions results in the original signal. The error is negligible: in the order of 10^{-15} (see Figure B.7c)

B.12. Formulations

Till now we have seen the so-called matrix notation of the DWT. This notation is very convenient for those used to linear algebra. There are two different formulations of the DWT. The first is the *modulation formulation*, which is a way of looking at the DWT from Fourier analysis. This way is not implementable, but this is useful in the creation of new wavelets bases, for instance by using the *lifting* method [28].The *polyphase*

formulation arranges the calculation of the DWT in such a way that convolutions are used without wasting computations. The direct implementation of the DWT in terms of the convolutions throws away the half of the computed values in the downscaling step. This is very regrettable, therefore the polyphase formulation uses convolutions without wasting computations [28].

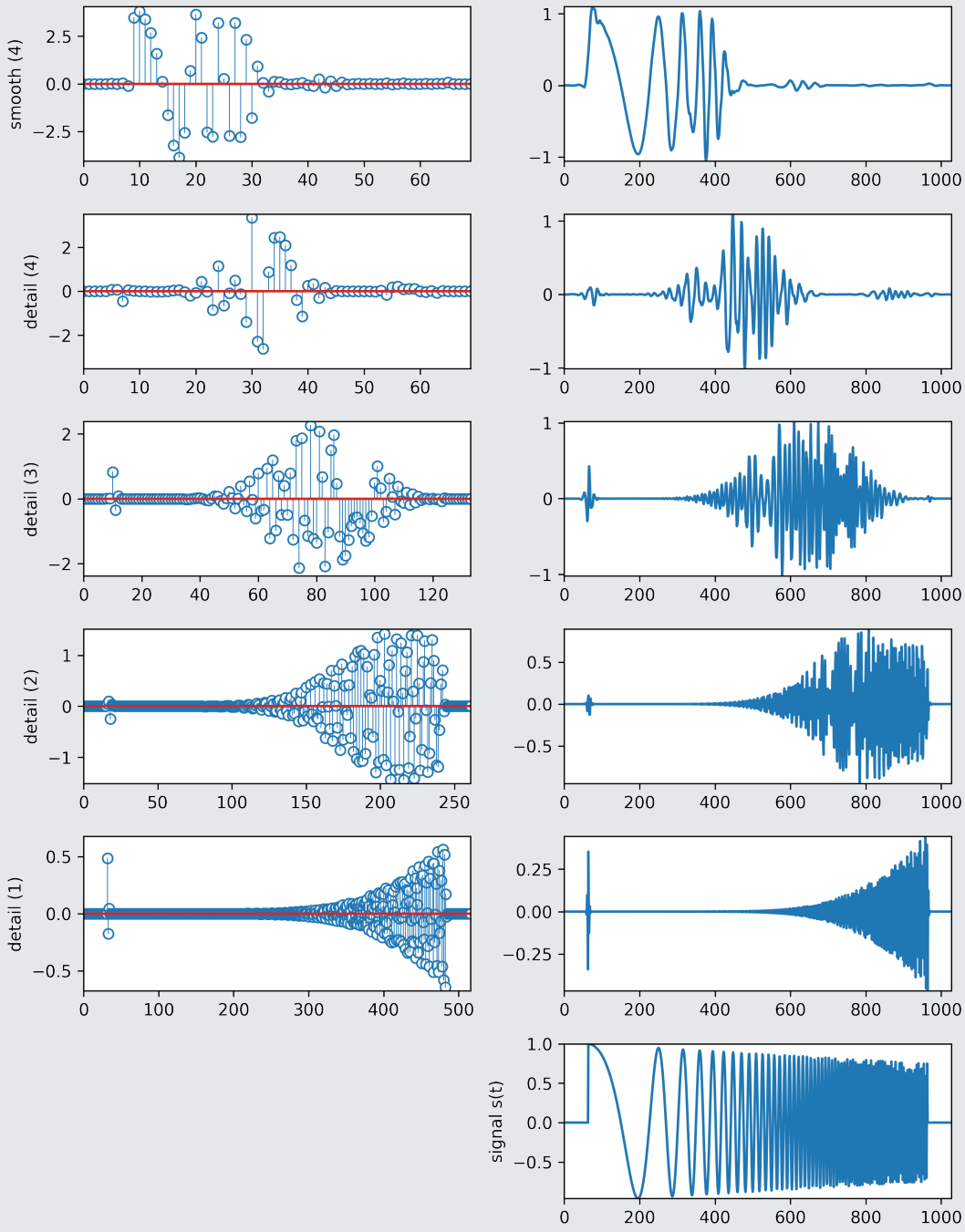

(a) An example of a DWT decomposition: the signal at the bottom is decomposed four times using the DWT algorithm. On the right the coefficients are translated to their contribution to the signal.

Figure B.7: Figures with Example B.6.

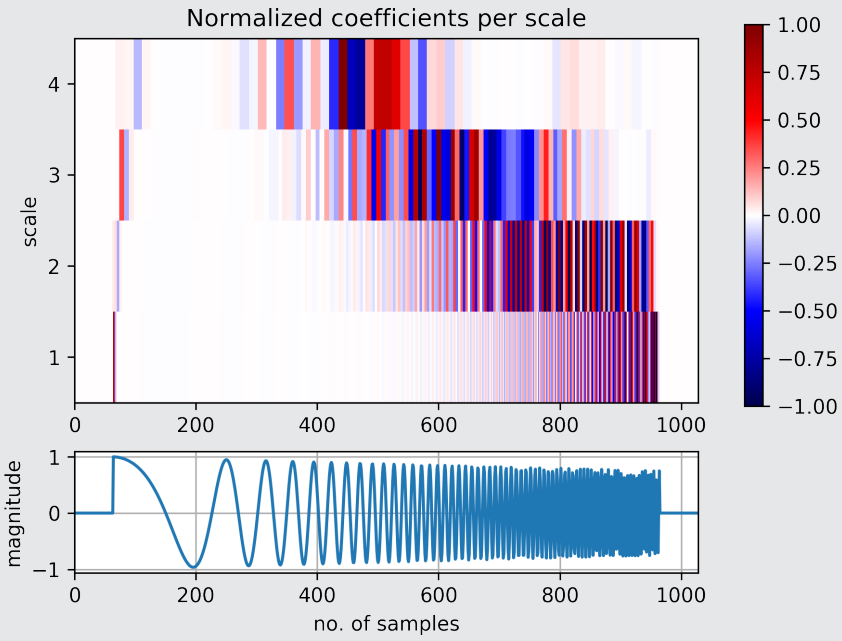

(b) The detail coefficients from (a) depicted differently.

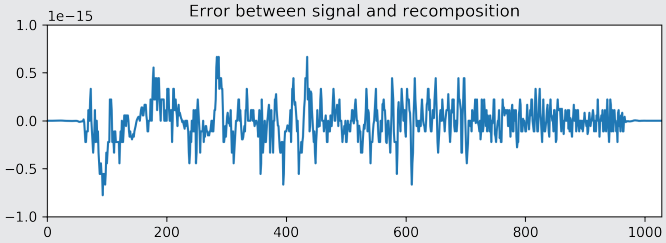

(c) The error between the reconstruction and the original signal from Example B.6, in numerical terms is the error 0.

Figure B.7: Figures with Example B.6.

B.12.1. Modulation Formulation

Here we use the symbol formulation. For the discrete sequence $\boldsymbol{a} = \{a_k\}$ the symbol is defined as $a(\omega) = \sum_k a_k e^{-ik\omega}$. Remember that $c = a * b$, then $c(\omega) = a(\omega)b(\omega)$. Down- and up-sampling are also defined for the Fourier domain as

$$(\downarrow 2)a(\omega) = \frac{1}{2}\left[a(\omega/2) + a(\omega/2+\pi)\right],$$
$$(\uparrow 2)a(\omega) = a(2\omega).$$

The full DWT algorithm in terms of the symbols is the modulation formulation. The original signal is $s_n(\omega)$, then the decomposition in s_{n-1} and d_{n-1} becomes

$$s_{n-1}(2\omega) = \frac{1}{\sqrt{2}}\left[\tilde{h}(\omega)s_n(\omega) + \tilde{h}(\omega+\pi)s_n(\omega+\pi)\right],$$
$$d_{n-1}(2\omega) = \frac{1}{\sqrt{2}}\left[\tilde{g}(\omega)s_n(\omega) + \tilde{g}(\omega+\pi)s_n(\omega+\pi)\right].$$

In this we recognise the convolution step from (B.24a) and the sampling step from (B.24b). The reconstruction is the same as (B.24c):

$$s_n(\omega) = \sqrt{2}[h(\omega)^* s_{n-1}(2\omega) + g(\omega)^* d_{n-1}(2\omega)].$$

This formulation can also be given in the matrix form. For the decomposition equation as

$$\begin{bmatrix} s_{n-1}(2\omega) \\ d_{n-1}(2\omega) \end{bmatrix} = \tilde{M} \cdot \frac{1}{2\sqrt{2}} \begin{bmatrix} s_n(\omega) \\ s_n(\omega+\pi) \end{bmatrix}, \qquad \text{with } M(\omega) = \begin{bmatrix} h(\omega) & h(\omega+\pi) \\ g(\omega) & g(\omega+\pi) \end{bmatrix}. \tag{B.27}$$

This matrix M is called the *modulation matrix*. For the reconstruction equation a redundant statement has to be added, which is the second row of the matrix formulation:

$$\begin{bmatrix} s_n(\omega) \\ s_n(\omega+\pi) \end{bmatrix} = M^* \cdot \sqrt{2} \begin{bmatrix} s_{n-1}(2\omega) \\ d_{n-1}(2\omega) \end{bmatrix}.$$

From these expressions another bi-orthogonality condition can be derived: $M(\omega)^* \tilde{M}(\omega) = I$. Note again that for the orthogonal MRA case, the tildes can be eliminated. The condition $M(\omega)^* M(\omega) = I$ is then called *paraunitary*.

B.12.2. Polyphase Formulation

The polyphase formulation begins by splitting the signal and the recursion coefficients into odd and even phases. The notation used for the even and odd phases $\boldsymbol{a}_0$ and $\boldsymbol{a}_1$ of a sequence $\boldsymbol{a} = \{a_k\}$ is defined by $a_{0,k} = a_{2k}$ and $a_{1,k} = a_{2k+1}$. Using this notation, the convolution (B.24a) to find $\boldsymbol{s}_{n-1}$ can be written as [28]

$$\boldsymbol{s}_{n-1} = (-)\tilde{\boldsymbol{h}}_0 * \boldsymbol{s}_{n,0} + (-)\tilde{\boldsymbol{h}}_1 * \boldsymbol{s}_{n,1}.$$

The odd and even phases are computed separately and finally recombined. Note that the number of floating point operations is unchanged from the direct implementation.

The polyphase symbols of the sequence $\boldsymbol{a}$ are given by

$$a_0(\omega) = \sum_k a_{0,k} e^{-ik\omega} = \sum_k a_{2k} e^{-ik\omega}, \qquad a_1(\omega) = \sum_k a_{1,k} e^{-ik\omega} = \sum_k a_{2k+1} e^{-ik\omega}.$$

Then the decomposition of the signal $\boldsymbol{s}$ can be written as

$$\begin{bmatrix} s_{n-1}(\omega) \\ d_{n-1}(\omega) \end{bmatrix} = \tilde{P} \begin{bmatrix} s_{n,0}(\omega) \\ s_{n,1}(\omega) \end{bmatrix} \qquad \text{with } P(\omega) = \begin{bmatrix} h_0(\omega) & h_1(\omega) \\ g_0(\omega) & g_1(\omega) \end{bmatrix}.$$

Where $P(\omega)$ is called the *polyphase matrix*. As for the modulation approach, the tildes can be dropped when an orthogonal MRA is used. The reconstruction step then is

$$\begin{bmatrix} s_{n,0}(\omega) \\ s_{n,1}(\omega) \end{bmatrix} = P^* \begin{bmatrix} s_{n-1}(\omega) \\ d_{n-1}(\omega) \end{bmatrix}.$$

The bi-orthogonality condition in this formulation becomes $P(\omega)^* \tilde{P}(\omega) = I$. For the orthogonal MRA the polyphase matrix is paraunitary, as for the modulation formulation.

B.12.3. Multi-wavelets and Wavelet Packets

Wavelet analysis knows two extensions which are really common in modern research: multi-wavelets and wavelet packets. These will be briefly be addressed. Remember the definition of the scaling function ϕ via the recursion relation (B.1), and its application in the refinement equation (B.7). Generalizations of this equation lead to all kind of other constructions [28, 42, 49]: wavelet packets, multivariate wavelets, ridgelets, curvelets, vaguelettes and much more. This theory is out of the scope of this thesis, but will be explained in a few sentences. The multi-wavelet theory is more complicated than the wavelet theory. The general idea is the replacement of the scaling function $\phi(t)$ by a function vector $\boldsymbol{\phi}(t)$ (in **bold**), known as a *multiscale function*

$$\boldsymbol{\phi}(t) = \begin{bmatrix} \phi_1(t) \\ \vdots \\ \phi_r(t) \end{bmatrix}.$$

In the refinement equation (B.7) the recursion coefficients will become $r \times r$ matrices H_k:

$$\boldsymbol{\phi}(t) = \sqrt{m} \sum_k H_k \boldsymbol{\phi}(mt - k).$$

Also note the addition of the *dilation factor m*. In the MRA theory discussed so far, the factor $m = 2$ was used. The whole derivation can be done using a factor m, which adds some complexity to the notation and is therefore skipped. The factor $m = 2$ is also well suitable for computer implementation. The advantage of multi-wavelets is their short support, coupled with high smoothness and high approximation orders. In addition they can be both symmetric and orthogonal, in contrary to the 'normal' wavelets. The disadvantages are the complexity of the theory and the requirement of pre- and post-proccesing steps in the algorithm, which takes more computation time [28].

A wavelet packet choses different decomposition [49]. The spaces W_n are "split" again in two orthogonal subspaces. The basis functions for these subspaces, are constructed from both the refinable function as the wavelet. This approach leads to a redundant representation of the input data, and is best known by its use in the *FBI Fingerprint Compression Specification* [49]. The time-frequency plane distribution changes from a 'regular' grid such as in Figure 2.1 but can be something like Figure B.8, still the boxes have the same area by the Heisenbergs restriction. These techniques are not discussed further in this thesis.

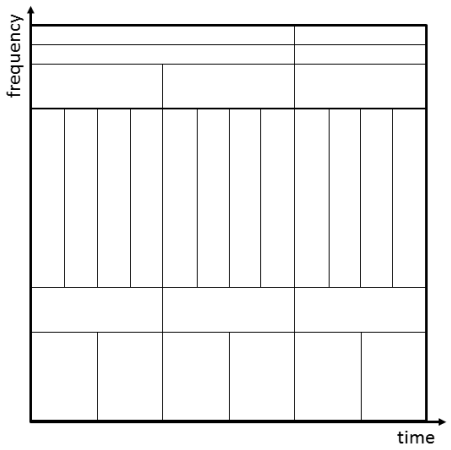

Figure B.8: Example of the distribution of the time-frequency plane by wavelet packets.

C

Wavelets

In this appendix an overview of important wavelet characteristics (Section C.1) and the most common wavelets is presented. These wavelets are summarised in Figure 2.3 and 2.5. Two commonly used numerical packages provide an extensive toolbox to apply wavelet transformations, including a lot of wavelets [40, 54]. When the wavelets characteristics originate from a toolbox, this is cited as [TB]. The continuous wavelets are discussed in Section C.2 and the discrete in Section C.3.

C.1. Wavelet Characteristics

In Appendix 2 the formal definition of a wavelet is given by (2.20). The discrete approach of the definition of a wavelet is presented in Section B.2. These wavelets do have the same characteristics. But what characteristics do make a wavelet a good wavelet? Sweldens [53] gives a very general description of wavelets to start with: "Wavelets are building blocks that can quickly decorrelate data." This sentence contains the three main characteristics of a wavelets. A wavelet is a *building block*, the first characteristic, for a general function or time signal. This is consistent with the MRA approach: the mathematical description of a basis fits this building block description.

The second characteristic is the *power to decorrelate*. This has not been addressed much yet, but the main message is that we can get an accurate approximation of the original signal $x(t)$ by only using a small fraction of the wavelet coefficients. Therefore the wavelet in a way has to resemble the data we want to represent, this leads to three core properties [53]:

- A wavelet has to have compact support to ensure localization in time;
- a wavelet has to be smooth, which results in decay towards high frequencies, to also have localization in frequency. This localization in frequency is referred to as selectivity;
- and a wavelet has to have vanishing moments, which results in decay toward low frequencies.

The last characteristic is hidden in the word *quickly*. Sweldens [53] decribes that we want to switch between the original representation and the wavelet representation of some data in a time proportional to the size of the data. This characteristic of course is very important to ensure the applicability of wavelets. At last there is a choice between orthogonal and bi-orthogonal wavelets, this is further elaborated in Section B.5.

C.1.1. Vanishing Moments

In the last section three core properties have been discussed. The last one was the property of 'having vanishing moments'. This subsection will shine some light on these moments. The name moment comes from the probabilistic idea of a moment generating function. For a random variable, the n^{th} derivative, evaluated at 0 gives the n^{th} moment of this variable [47] . The best known moments are the first moment (expected value) and the second moment (expected value of the square of the random variable).

One way to differentiate various wavelet is by their vanishing moments. In wavelet theory the moments are a number to estimate the rate of decay of a wavelet $\psi(t)$ [31]. The rate of decay for a general function $f(t)$

can be estimated by the formal integral

$$\int_{-\infty}^{\infty} t^k f(t)\ \mathrm{d}t.$$

Here the parameter k indicates the rate of decay. If we for example consider the function $f(t) = \cos t/t^2$, then we know that the integral converges to 0 for $k = 0$ and $k = 1$. For $k = 2$ this integral converges to π. For a general wavelet $\psi(t)$ we say it has p *vanishing moments* if [31]

$$\int_{-\infty}^{\infty} t^k \psi(t)\ \mathrm{d}t = 0 \qquad \text{for } 0 \leq k < p \in \mathbb{N}. \tag{C.1}$$

This leads to descriptions of moments for both discrete and continuous wavelets. The continuous moments μ_k and ν_k are defined by the integral (C.1) as

$$\mu_k = \int_{-\infty}^{\infty} t^k \phi(t)\ \mathrm{d}t, \qquad \nu_k = \int_{-\infty}^{\infty} t^k \psi(t)\ \mathrm{d}t.$$

In the Fourier domain, this can be checked by evaluating the transform of the derivatives of the functions. A function has p vanishing moments if the first $p-1$ derivatives of its Fourier transform are zero at $\omega = 0$ [31]. This leads to the analogous expression [28]:

$$\mu_k = 2\pi i^k \frac{\mathrm{d}^k \Phi}{\mathrm{d}\omega^k}(0), \qquad \nu_k = 2\pi i^k \frac{\mathrm{d}^k \Psi}{\mathrm{d}\omega^k}(0).$$

Note that the continuous moment μ_0 is not determined for the refinement equation [28], it depends on the scaling of ϕ. μ_0 can be picked arbitrarily for any given ϕ, but for a bi-orthogonal pair the following relationship has to hold: $\tilde{\mu}_0^* \cdot \mu_0 = 1$. However, when μ_0 has been chosen, all other continuous moments are uniquely defined.

The definition of the moments are clear. A moment is called vanishing if it is equal to 0. The advantage of the vanishing moments is the possibility to write the wavelet as a low pass filter. This simplifies the wavelet design process [31]. The higher the number of vanishing moments, the more complex a wavelet is and therefore it is more accurate in the representation of a complex signal. The disadvantage of a high number of vanishing moments is that it results in a longer support. As the number of vanishing moments increases, polynomials up to that order will not be identified by the wavelet.

C.1.2. Localization and Selectivity

So a wavelet with one vanishing moment, $p = 1$, cannot identify constant signals, but it does identify linear, quadratic, etc. signals. In an analysis with a wavelet with two vanishing moments, linear signals cannot be identified anymore. In the Fourier transform, for each analyzing function one frequency is addressed. In the wavelet transform a range of frequencies is encompassed in one analyzing function $\psi(t)$. So to analyse a lower range of frequencies, you need to be more *selective*, earlier referred to as 'localization in frequency'. However, if we link this to the uncertainty principle, we note that the more selective a wavelet is, the less compact support it has. This links the selectivity of the wavelet to its number of vanishing moments.

C.1.3. Regularity and decay

The last related aspect of wavelets is its *regularity*. Wavelet with low regularity create jagged representations of the signal which is analysed, wavelets with high regularity result in smoother representation of the functions. The more vanishing moments a wavelet has, the higher the regularity of the wavelet. However, the regularity of a wavelet increases linearly with the support width [14]. The application of the wavelet analysis lets us assess wavelet for different properties. Compact supported orthonormal wavelets are suitable for sparse representations of large matrices. Therefore the number of vanishing moments is far more important than the regularity [14]. For compression, smoothness is important to observe as little of the compression as possible, placing high regularity over number of vanishing moments [14].

C.2. Continuous Wavelets

A summary of the most used continuous wavelets is presented in Table C.1. Thereafter they are addressed more elaborately. At last two examples of the Morlet wavelet are presented, because of their extensive use in time-frequency analysis. Continuous wavelets are defined by functions, not by filters. However, most of them do have a filter implementation as well. Often the filter has to be truncated to become finite. There is also a differentiation in *analytic* or *complex* and *real* wavelets [37, 55]. Analytic wavelets often are wavelets of which their Fourier transforms are zero for negative frequencies:

$$\Psi(\omega) = 0 \ \forall \omega < 0.$$

Therefore an analytic wavelet has to be complex, but it can be characterised by its real part only [37]. The advantage of the use of an analytic wavelet is that they can measure time evolution of frequency transients by separating amplitude and phase components: it is better adapted to capturing oscillatory behaviour in time series [55]. Real wavelets often are used to detect sharp signal transitions.

- The **Complex Morlet** wavelet is described as a complex wave $e^{i2\pi\omega_0 t}$ within the Gaussian envelope $e^{-t^2/2}$. The term in font of the expression ensures unit energy. It complies to the admissibility conditions of a wavelet for $\omega_0 \geq 6$. Often $\omega_0 = 6$ is chosen in time-frequency analysis [55]. However, in Demonstration 3.10 is concluded that a Morlet 60 wavelet is much better applicable for separating waves.
- The **Morlet** wavelet is the real part of the complex Morlet wavelet [42]. The example given in Table C.1 is used in the Mathworks Toolbox [TB]. The complex Morlet is sometimes referred to as "Morlet" as well.
- The **(derivative of) Gaussian** wavelet family is a set of wavelets, derived from the derivatives of the Gaussian function, e^{-t^2}. This function can be derived infinitely many times, therefore there are a lot of Gaussian wavelets. The best known is the Mexican Hat wavelet, which is described next. The Mexican Hat wavelet is an example of a nice wavelet, with compact support and mean value zero [42]. Not all derivatives lead to wavelet with these nice characteristics. For a n-times differentiated Gaussian, the number of vanishing moments is n too. Moreover, if n is even the wavelet is symmetric, for odd n it is anti symmetric.

Table C.1: A summary of most common continuous wavelets. The 'present in literature' parameters and functions concerning these wavelets are presented here. They are summarised in Figure 2.3.

Name	Wavelet $\psi(t)$	$\mathcal{F}\{\psi\}(\omega) = \Psi(\omega)$	e-folding time τ_a	Equivalent wavelength λ_ψ
Complex Morlet [42, 55]	$\pi^{-1/4} e^{-i\omega_0 t} e^{-t^2/2}$	$\pi^{-1/4} H(\omega) e^{-(\omega-\omega_0)^2/2}$	$\sqrt{2}$	$\dfrac{4\pi}{\omega_0 + \sqrt{2+\omega_0^2}}$
Morlet [42]	$e^{t^2/2}\cos(5t)$	-	$\sqrt{2}$	–
Paul, order m [55]	$\dfrac{2^m i^m m!}{\sqrt{\pi(2m)!}}(1-it)^{-(m+1)}$	$\dfrac{2^m}{\sqrt{m(2m-1)!}} H(\omega)\omega^m e^{-\omega}$	$1/\sqrt{2}$	$\dfrac{2\pi}{\sqrt{m+1/2}}$
(Derivative of) Gaussian, order m [55]	$\dfrac{(-1)^{m+1}}{\sqrt{\Gamma(m+1/2)}} \dfrac{\mathrm{d}^m}{\mathrm{d}t^m}\left(e^{-t^2/2}\right)$	$\dfrac{-i^m}{\sqrt{\Gamma(m+1/2)}} \omega^m e^{-\omega^2/2}$	$\sqrt{2}$	$\dfrac{2\pi}{\sqrt{m+1/2}}$
Complex (Derivative of) Gaussian, order m [23]	$C \cdot \dfrac{\mathrm{d}^m}{\mathrm{d}t^m}\left(e^{-i\omega_0 t} e^{-t^2/2}\right)$	-	-	idem
Complex Shannon, order m [43]	$\sqrt{f_b}\left(\mathrm{sinc}\left(\dfrac{f_b t}{m}\right)\right)^m e^{i\omega_0 t}$	-	-	-
Shannon [42]	$\mathrm{sinc}\left(\dfrac{t}{2}\right)\cos\left(\dfrac{3\pi t}{2}\right)$	-	-	-
Meyer [13]	-	see (C.4)	-	-

- The **Mexican hat** wavelet is probably the best known continuous wavelet. It is defined by [42]:

$$\psi_{\text{mexh}}(t) = K(1-t^2)e^{-(t^2/2)}, \qquad K = \frac{2}{\sqrt{3}\pi^{1/4}}. \tag{C.2}$$

  The factor K normalises the Mexican hat wavelet. If $K = 1$ the wavelet is known as the unnormalised Mexican hat [42]. The wavelet is named after its shape, however, it is originally known as the **Ricker** wavelet. It is the second derivative of Gaussian wavelet and it is specifically well *localised* in time and has a *zero mean value* [42]. The support $[-5,5]$ can be used in a finite filter approximation. Note that this support is much larger than its support based on its e-folding time: $[-\sqrt{2},\sqrt{2}]$.

- The **complex (derivative of) Gaussian** wavelet family, also known as the **Hermitian** or **Gabor** wavelet family, has the same properties as the Gaussian wavelet family, the only difference is that this is a complex wavelet. It is made complex by multiplying the Gaussian window with a complex exponential function $e^{-i\omega_0 t}$. The C in the formula from Table C.1 is the normalising term.

- The **complex Shannon** wavelet is defined by a set of complex waveform within a sinc() function envelope [43], where

$$\text{sinc}(t) = \frac{\sin(\pi t)}{\pi t}. \tag{C.3}$$

  It has integer order m, a bandwidth parameter f_b controlling the width of the main lobe of the sinc() function and wavelet centre frequency ω_0. The centre frequency also determines the number of oscillations within the main lobe. The imaginairy part of the complex Shannon wavelet is shifted $\pi/4$ from the real part. This wavelet has *infinite* support and is therefore not much used.

- The **Shannon** wavelet as defined in Table C.1 is *real* and *symmetric* but does not have a finite support [42]„ however, it is infinitely differentiable and $\Psi(\omega)$ is zero in the neighbourhood of $\omega = 0$, as are all its derivatives [37]. We may conclude that it has infinitely many vanishing moments. It is therefore not a good wavelet to apply wavelet analysis with [42]. The Shannon wavelet is a specific case of the spline wavelets [37].

> *The Morlet, Gaussian and Shannon wavelets are also known as* crude *wavelets* [TB]. *These wavelets only have minimal properties. Their downsides are that the scaling function $\phi(t)$ does not exist, the analysis is not orthogonal or bi-orthogonal and $\psi(t)$ is not of compact support. Therefore reconstruction is not insured and there are no fast algorithms to do calculations with. These wavelets are only useful for a (complex) continuous decomposition. Good properties are the symmetry and explicit declaration of the wavelet $\psi(t)$* [TB]. *Complex wavelet can have a spectrum for which $\Psi(\omega)|_{\omega<0} = 0$, such that a wavelet transform for only positive frequencies is possible.*

- The **Paul** wavelet is a well localised mother wavelet, like the Morlet, and Gaussian wavelet. It can be used for the same applications, however, often one of the others is used.

- The **Meyer** wavelet is a *symmetric* and *orthogonal* wavelet invented by Meyer in 1990 [14]. It is a *band-limited* wavelet, limited to $2\pi/3 \le |\omega| \le 8\pi/3$, which results in an *infinite support* in the time domain [42]. Its amplitude in time decays rapidly, making it suitable for wavelet analysis. The Meyer scaling function satisfies [14]

$$\Phi(\omega) = \begin{cases} \dfrac{1}{\sqrt{2\pi}} e^{i\omega/2} \sin\left[\dfrac{\pi}{2}\nu\left(\dfrac{3}{2\pi}|\omega|-1\right)\right] & \text{for } \dfrac{2\pi}{3} \le |\omega| \le \dfrac{4\pi}{3}, \\ \dfrac{1}{\sqrt{2\pi}} e^{i\omega/2} \cos\left[\dfrac{\pi}{2}\nu\left(\dfrac{3}{4\pi}|\omega|-1\right)\right] & \text{for } \dfrac{4\pi}{3} \le |\omega| \le \dfrac{8\pi}{3}, \\ 0 & \text{elsewhere.} \end{cases} \tag{C.4}$$

  where

$$\nu(x) = \begin{cases} 0 & x \le 0, \\ \sin^2\left(\dfrac{\pi}{2}x\right) & 0 \le x \le 1, \\ 1 & x \ge 1. \end{cases}$$

The Meyer wavelet has infinite vanishing moments [37]. The Meyer wavelet is known as an infinitely regular wavelet [TB]. It can be applied in both continuous and discrete wavelet analysis. Its filter implementation, however, is not a finite impulse response filter. The analysis of the pair ψ_{Meyer} and ϕ_{Meyer} is orthogonal. Both functions are infinitely differentiable and have compact support. The symmetry and infinite regularity are its most important properties. The difficulty of this wavelet lies within the filter implementation: there is no fast algorithm available for the filter is of infinite impulse response.

C.3. Discrete Wavelets

Discrete wavelets are derived from the MRA approach which are easily implemented on a computer for they possess easy implementable filters. The most used ones were are all designed before 1992, a lot of them by Daubechies [14]. This section starts with an itemisation of these most used discrete wavelets, followed by an overview of the wavelets available in the PyWavelets [54] package inTable C.2. After that the five wavelets that were compared in Appendix 4 are presented.

- **The Haar wavelet** has been discussed extensively in examples in this chapter. Named after its inventor Alfred Haar who laid the foundation of multi resolution analysis in 1910 [6].
- **Daubechies wavelets** are wavelets designed by Ingrid Daubechies [13]. They are called by their number of *vanishing moments* p„ however, sometimes they are referred to as $2p$, which is consistent with the filter length of the particular Daubechies wavelet. So the Daubechies 2 wavelet has two vanishing moments, and a filter length of four and therefore sometimes referred to as Daubechies 4. In this thesis the number of vanishing moments is leading. Note that de Daubechies 1 wavelet is the same as the Haar wavelet. The Daubechies wavelets are *orthogonal*, have a *support* of $[0, 2p-1]$ [28] and are asymmetric [TB].
- **Coiflets**, just like the Daubechies wavelets, are *orthogonal* wavelets. These are also designed by Ingrid Daubechies on request of Ronald Coifman [14]. They are designed such that not only the wavelet, but also the scaling function has a number of vanishing moments. The advantage of Coiflets is for smooth signals $s(t)$, the scaling function expansion coefficients s_{nk} are very close to $s(2^{-n}k)$ [28], such that preprocessing can be omitted. This results in *near symmetric* wavelets, which are all *orthogonal*. Narasimhan et al. [42] notes that some Coiflets have no zeros at $\omega = \pi$, which results in a *non smooth* wavelet, with possibly high frequency components. The error of the reconstructed signal therefore will be relatively large. There are again infinitely many Coiflets, numbered with n, with a number of vanishing moments $p = 2n$. The support of the wavelet is $[0, 6n-1]$ and their filters are of length $6n$ [TB].

> *All above mentioned wavelets are* orthogonal *and* compactly supported. *These wavelet all have an orthogonal analysis, with an existing compactly supported $\psi(t)$ and $\phi(t)$. Their $\psi(t)$ has a known number of vanishing moments and their finite impulse response filter description is very clear. These properties make them suitable for both continuous and discrete wavelet transformation, with applicability of the fast wavelet transform algorithm. The main difficulty using these wavelets is their poor regularity* [TB].

- **Symmlets** are an adaptation of the Daubechies wavelets. They are an answer of Daubechies to the request from engineers for *linear phase* filters. Such linear filters are symmetric around $b \in \mathbb{Z}$. Note that therefore the Haar wavelet is not symmetric, although its coefficients are symmetric. If a filter is not symmetric, its deviation from symmetry is judged by how much its phase deviates from a linear function. These symmetrised Daubechies wavelets are close to symmetric, but not completely symmetric [14]. This characteristic caused the wavelets of this family to be *bi-orthogonal*. Again these wavelets are numbered by their number of vanishing moments.
- **Cohen wavelets**, also known as Cohen-Daubechies-Feauveau wavelets are scalar *bi-orthogonal* wavelets derived from the Daubechies wavelet using the lifting factor technique. In both MATLAB and Python these wavelets are known as the **bi-orthogonal** wavelets [40, 54]. Again a lot of them can be made, the vanishing moments p and $\tilde{p}$ of the wavelet and dual wavelet function are restricted by $p + \tilde{p} = 2k$ for $k \in \mathbb{Z}$. They are symmetric around 0 if p is even and around $1/2$ for p odd [28, 42]. The supports of these wavelets differs for the decomposition and reconstruction step (respectively ψ and $\tilde{\psi}$), they are

$[0,2p+1]$ and $[0,2\tilde{p}+1]$. The filter lengths differ a lot by choice of p and $\tilde{p}$, but is limited by $\max\{p,\tilde{p}\}+2$ [TB]. Note that the Cohen(1,1) wavelet is the Haar wavelet.

- **Spline** wavelets [TB], also known as **Battle-Lemarié** wavelets [37] are computed from spline MRA. The Fourier transform of the wavelet is chosen a block B-spline, leading to a band limiting finite impulse response. The wavelet $\psi(t)$ has $p = m+1$ vanishing moments if its Fourier transform is made up of splines of order m. The resulting wavelet ψ has an exponential decay. They are again referred to with their number of vanishing moments p. In relation with the Meyer wavelet, they are less regular, but they decay faster [37]. For p even we have ψ symmetric about 1/2, and for p odd it is antisymmetric around the same point. The spline wavelet of order 1 is again the Haar wavelet. The choice of such a spline MRA can lead to both *orthogonal* and *bi-orthogonal* wavelet bases [37, TB].

> *The Symmlets, Cohen and spline wavelets are part of the* bi-orthogonal and compactly supported wavelet pairs [TB]. *They have in common that that $\psi(t)$, $\tilde{\psi}(t)$, $\phi(t)$ and $\tilde{\phi}(t)$ are compactly supported. They have a known number of vanishing moments and are regular. These wavelet are applicable in both continuous and discrete analysis, and again the FWT algorithm is applicable. The wavelets have symmetry with finite impulse response filters, have desirable properties for decomposition and reconstruction and nice allocation is possible. The main downside is the loss of orthogonality* [TB].

- The **Discrete Meyer** wavelet is the finite filter approximation of the Meyer wavelet [60]. It remains *orthogonal* and *symmetric*. By the truncation it is the finite impulse response implementation of the Meyer wavelet. Technically this thus is a *discrete* wavelet.

> *The Meyer wavelet is known as an* infinitely regular wavelet [TB]. *It can be applied in both continuous and discrete wavelet analysis. Its filter implementation, however, is not a finite impulse response filter. The analysis of the pair ψ_{Meyer} and ϕ_{Meyer} is orthogonal. Both functions are infinitely differentiable and have compact support. The symmetry and infinite regularity are its most important properties. The difficulty of this wavelet lies within the filter implementation: there is no fast algorithm available for the filter is of infinite impulse response.*

Table C.2: An overview of the FWT applicable wavelets available in the PyWavelets package [54]. x is the number of vanishing moments, if specified. For more information about these characteristics, please have a look at Appendix B.

Wavelet family	**Filter length**	**Orth.**	**Biorth.**	**Sym.**	**Extra information**
Haar	2	Yes	No	No	Same as Daubechies 1 wavelet Discontinuous: little number of applications
Daubechies x	$2x$	Yes	Yes	No	$x \geq 1$
Symmlet x	$2x$	Yes	Yes	Near	$x \geq 2$ Derived from Daubechies wavelet to be near symmetric
Coiflet x	$6x$	Yes	Yes	Near	$x \geq 1$ Derived from Daubechies wavelet, scaling functions have vanishing moments
Bi-orthogonal	≥ 6	No	Yes	Yes	Also known as Spline wavelet. Exception: bi orthogonal 1.1 wavelet is the Haar wavelet
Reverse bi orthogonal	≥ 6	No	Yes	Yes	Dual set of the bi-orthogonal wavelets
Discrete Meyer	62	Yes	Yes	Yes	finite impulse response filter approximation of Meyer wavelet

C.3.1. Five Discrete Wavelets and Their Spectra

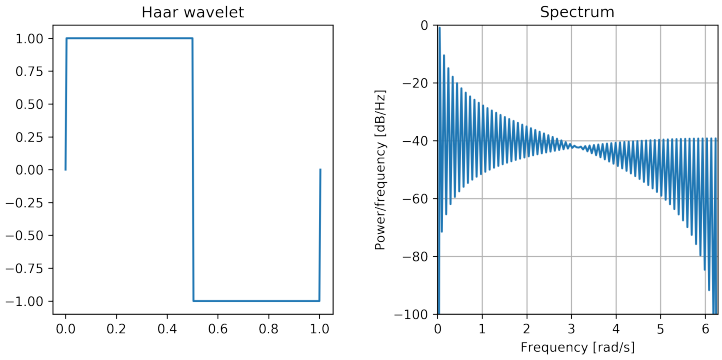

Figure C.1: The Haar wavelet

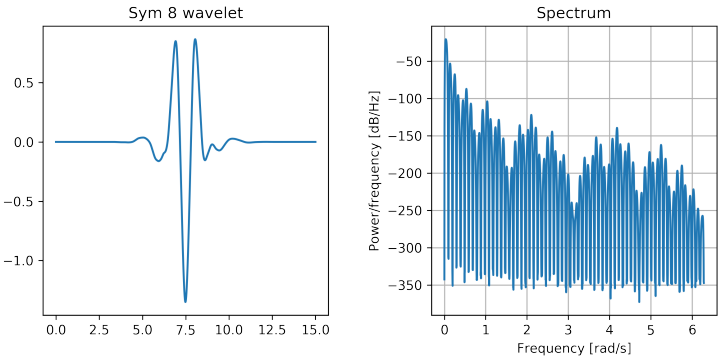

Figure C.2: The Symmlet 8 wavelet

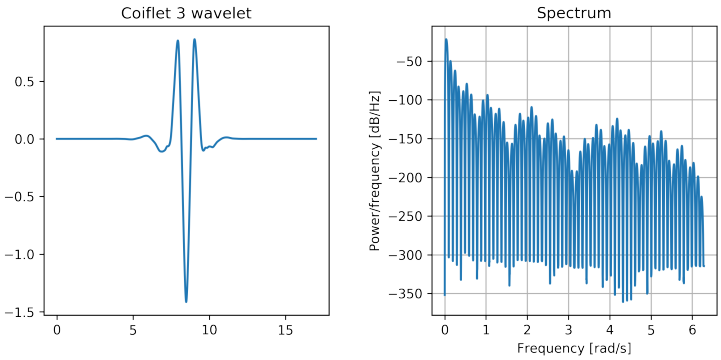

Figure C.3: The Coiflet 3 wavelet

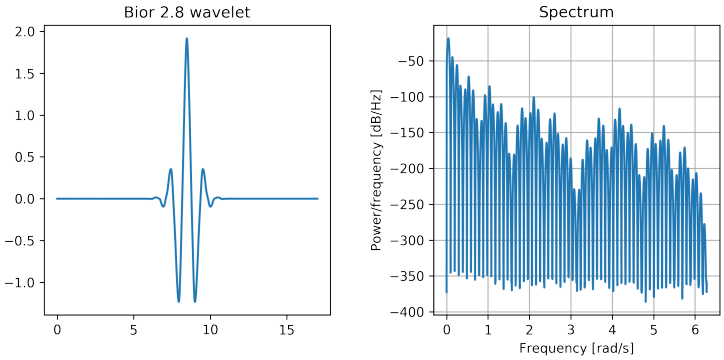

Figure C.4: The Bi-orthogonal 2.8 wavelet

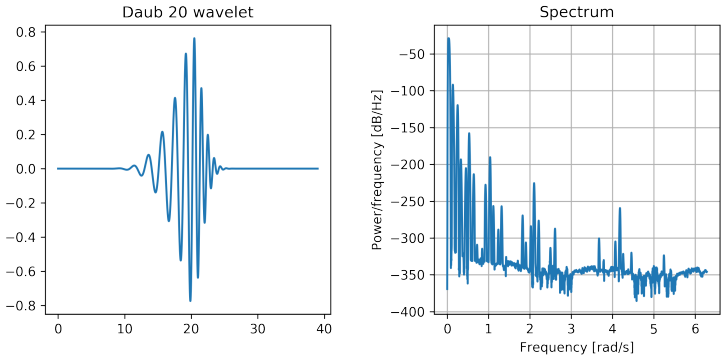

Figure C.5: The Daubechies 20 wavelet

D

Separating Incident and Reflected Waves

This appendix provides some extra background regarding the separation of incident and reflected waves and presents the results of the comparison of the Fourier and wavelet coefficient based solutions. The first section starts with a little background regarding the wave number, followed by the full derivation of the separated waves for two gauges, based on the work of Ma et al. [34]. In Section D.3 the results are presented which are discussed in Section 3.2.4. Section D.3.1 shortly addresses the information that is presented in these results.

D.1. Wave Number

The wave number k is measure of the spatial frequency of a wave. It is defined as cycles per unit distance, i.e. its unit is rad/m. It is based on linear wave theory, where it is assumed that the amplitude of the wave is small compared to the wave length and water depth [24]. For free harmonic wave the relationship between the radian frequency ω and the wave number k is given by the so-called dispersion equation [24]:

$$\omega^2 = gk\tanh(kd), \tag{D.1}$$

for any arbitrary depth d [m] and gravitational acceleration g [m/s^2]. The gravitational acceleration on earth is approximately 9.81 m/s^2. Because this relationship is an implicit expression in terms of the wave number, an iterating process is used to calculate the wave number. An example of such a process is given by Holthuijsen [24].

The dispersion relation is often simplified for deep and shallow water. In deep water $kd \to \infty$ and therefore $\tanh(kd) \to 1$, then the dispersion relationship approaches

$$\omega = \sqrt{gk_0}, \tag{D.2}$$

where k_0 is the deep-water wave number. In very shallow water $kd \to 0$ and therefore $\tanh(kd) \to kd$, then the dispersion relationship approaches

$$\omega = k\sqrt{gd}. \tag{D.3}$$

D.2. Derivation for Two Gauges

In Section 3.2 the analytic solution to the separated incident and reflected wave based on two gauges is addressed shortly. In this section, the whole derivation is given. Assume there are two gauges in the channel, one on a distance of x_1 from the wave maker and the second one at a distance $x_2 > x_1$. Define $x_2 - x_1 = \Delta x$. The situation is depicted in Figure 3.6. The surface elevation as recorded at point x_1 is:

$$\eta(x_1,t) = W_I\cos(\omega t - kx_1 + \theta_I) + W_R\cos(\omega t + kx_1 + \theta_R) \tag{D.4a}$$

and so at x_2 we find the following expression:

$$\begin{aligned}\eta(x_2,t) &= W_I\cos(\omega t - kx_2 + \theta_I) + W_R\cos(\omega t + kx_2 + \theta_R) \\ &= W_I\cos(\omega t - kx_1 - k\Delta x + \theta_I) + W_R\cos(\omega t + kx_1 + k\Delta x + \theta_R).\end{aligned} \tag{D.4b}$$

Reconstructing the incident and reflected waves through these equations directly is hard, therefore their analytic forms are being used:

$$\zeta(x_1,t) = W_I e^{i(\omega t - kx_1 + \theta_I)} + W_R e^{i(\omega t + kx_1 + \theta_R)} \text{ and} \tag{D.5a}$$

$$\begin{aligned}\zeta(x_2,t) &= W_I e^{i(\omega t - kx_2 + \theta_I)} + W_R e^{i(\omega t + kx_2 + \theta_R)} \\ & W_I e^{i(\omega t - kx_1 - k\Delta x + \theta_I)} + W_R e^{i(\omega t + kx_2 + k\Delta x + \theta_R)} \\ &= W_I e^{i(\omega t - kx_1 + \theta_I)} e^{-ik\Delta x} + W_R e^{i(\omega t + kx_2 + \theta_R)} e^{ik\Delta x}.\end{aligned} \tag{D.5b}$$

Note that the real part of $\zeta(x_1,t)$ is $\eta(x_1,t)$ and the same holds for $\zeta(x_2,t)$ and $\eta(x_2,t)$. In general the wave number k and the distance between the two gauges, Δx, is known. Using the exponential form of the sine function,

$$\sin(x) = \frac{e^{ix} - e^{-ix}}{2i}, \tag{D.6}$$

the analytic form of the incident and reflected waves at point x_1 can be obtained as follows.

$$\begin{aligned}\zeta(x_1,t)e^{ik\Delta x} - \zeta(x_2,t) = \quad & W_I e^{i(\omega t - kx_1 + \theta_I)} e^{ik\Delta x} + W_R e^{i(\omega t + kx_1 + \theta_R)} e^{ik\Delta x} \\ & - W_I e^{i(\omega t - kx_1 + \theta_I)} e^{-ik\Delta x} - W_R e^{i(\omega t + kx_2 + \theta_R)} e^{ik\Delta x} \\ = {} & W_I e^{i(\omega t - kx_1 + \theta_I)} e^{ik\Delta x} - W_I e^{i(\omega t - kx_1 + \theta_i)} e^{-ik\Delta x} \\ = {} & W_I e^{i(\omega t - kx_1 + \theta_I)} \left(e^{ik\Delta x} - e^{-ik\Delta x} \right)\end{aligned}$$

Divide this result by $2i \cdot \sin(ik\Delta x)$ to find:

$$a_I e^{i(\omega t - kx_1 + \theta_i)} = \frac{\zeta(x_1,t)e^{ik\Delta x} - \zeta(x_2,t)}{2i\sin(k\Delta x)}. \tag{D.7a}$$

In the same manner the analytic expression of the reflected wave is found as:

$$a_R e^{i(\omega t + kx_1 + \theta_R)} = \frac{\zeta(x_1,t)e^{-ik\Delta x} - \zeta(x_2,t)}{-2i\sin(k\Delta x)}. \tag{D.7b}$$

The real parts of the solutions will result in the incident and reflected wave at point x_1.

D.3. Results

D.3.1. Reading the Results

In the following section the results for separating incident and reflected waves are presented. These results are a comparison between the separation based on Fourier coefficients [63] and the separation based on wavelet coefficients as presented in this thesis Section 3.2. The results start with a number of settings, such as the kind of signal, the wavelet, the distances of the used gauges etc. This is followed by a table (without borders) which shows different RMSE's:

Reconstruction The difference between the original signal and the signal transformed back and forth, i.e.

$$\begin{aligned} &\textit{Fourier} \quad x(t) - \mathcal{F}^{-1}\{\mathcal{F}\{x\}\}(t) \\ &\textit{Wavelet} \quad x(t) - \mathcal{W}^{-1}\{\mathcal{W}\{x\}\}(t) \end{aligned}$$

Sum The difference between the sum of the recovered incident and reflected wave and the original signal, this is the RMSE of the residuals defined in equation 3.19.

Incident The difference between the reconstructed and the original incident wave.

Reflected Idem for the reflected wave.

Then there is a table that contains measures that are often used in coastal engineering, which are compared with respect to the 'original' ones, based on the numerical incident and reflected waves.

Ref.cff. Short for reflection coefficient, defined by

$$\sqrt{\frac{m_{0\text{reflected}}}{m_{0\text{incident}}}}; \tag{D.8}$$

m0_in m_0 of the incident wave, defined by equation D.9;

m0_ref m_0 of the reflected wave.

The Moment of the Wave Spectrum

The moment m_n is defined as the n^{th} order moment of the variance density spectrum. The zeroth order moment is equal to the variance of the surface elevation $x(t)$ [24], i.e.

$$m_0 = \text{Var}(x(t)). \tag{D.9}$$

Figures

Finally a number of figures are presented. The first row of figures shows the incident waves; i.e. the original one, the recovered ones and the difference between the recovered and the incident. The second row shows the same figures for the reflected waves. In the last row the different spectra can be compared. Note that the energy density on the left y-axis is scaled logarithmically. On the right y-axis the reflection coefficient per frequency is shown, which is defined by the energy density of the reflected wave divided by the energy density of the incident wave (per frequency).

Signal	90 waves from JONSWAP spectrum with f in [0.3,2]		
Wavelet	Morlet	Parameter	6
Sampling freq	25	Duration	480.0 sec = 8.0 min
Determined at gauge	11.0		
Using gauges	[11. 12.]		
with distances	[0. 1.]		
Wavenumber	dispersion	with water depth	-1
Noise	no	Weights	no
No of steps CWT	200		
p_min	8.000667E-02	p_max	4E+00
Error CWT reconstruction and original			1.062284E-02
Error CWT reconstruction and sum			4.540368E-17
Error CWT reconstruction incident and original incident			1.407499E-02
Error CWT reconstruction reflected and original reflected			1.105085E-02

	Original	Wavelet filtering	% difference
Reflection coeff	4.989225E-01	5.085815E-01	1.93595454481
m0_incident	5.672494E-03	7.398267E-03	30.4235262141
m0_reflected	1.412018E-03	1.913599E-03	35.5222882748

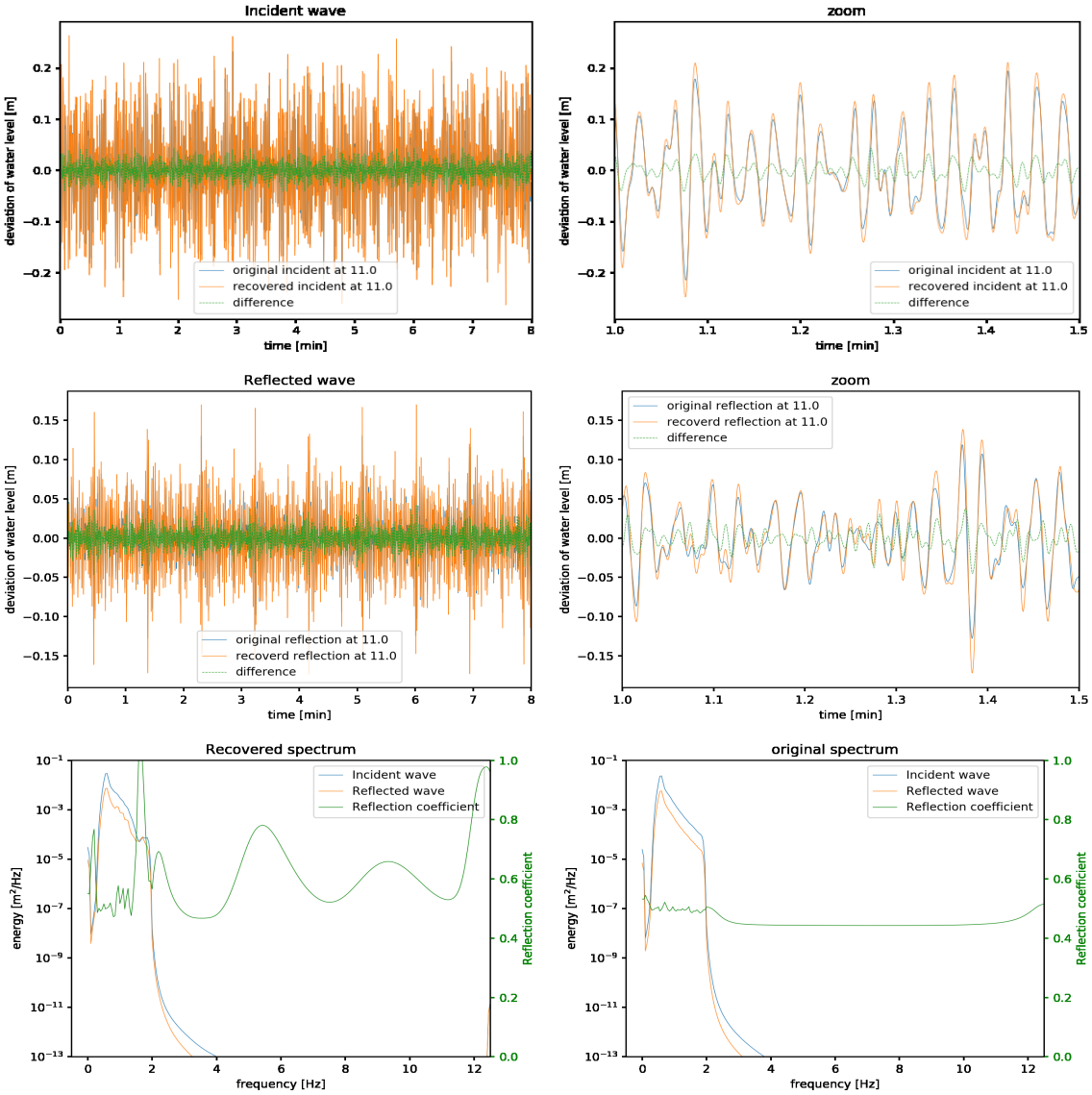

Figure D.1: Verification of error study by Ma et al. [34]. Water depth: 1 meter shallow water.

Signal	200 waves from JONSWAP spectrum with f in [0.01,fs/2]		
Wavelet	Morlet	Parameter	60.0
Sampling freq	12	Duration	480.0 sec = 8.0 min
Determined at gauge			39.382
Using gauges			[39.382 40.1]
Wavenumber	dispersion	with water depth	1
Noise	no	Weights	no
No of steps CWT			200
Determinant limit			0
p_min	1.666956E-01	p_max	1.777215E+01

RMSE	Fourier	Wavelet
reconstruction	1.714063E-16	1.03757E-03
sum	2.02122E-14	3.626032E-16
incident	1.282526E-01	1.398801E-02
reflected	1.282526E-01	1.397111E-02

	Original	Fourier	% diff	Wavelet	% diff
Ref.cff.	5.013296E-01	8.994054E-01	79.4	5.272067E-01	5.16
m0_in	5.5754E-03	2.209132E-02	296.23	5.878451E-03	5.44
m0_ref	1.401273E-03	1.787033E-02	1175.29	1.633897E-03	16.6

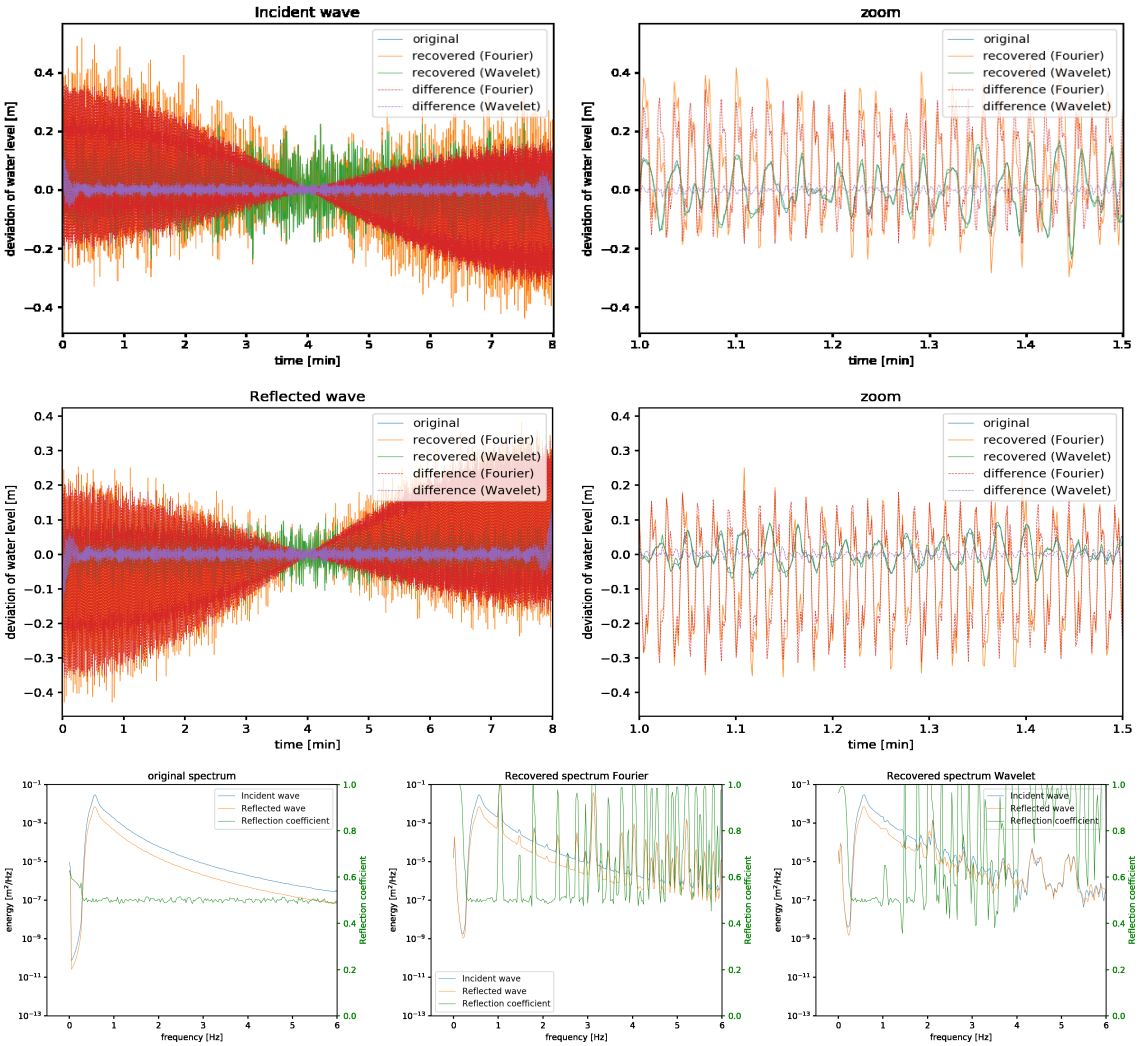

Figure D.2: Separating waves using 2 gauges

Signal	200 waves from JONSWAP spectrum with f in [0.01,fs/2]		
Wavelet	Morlet	Parameter	60.0
Sampling freq	12	Duration	480.0 sec = 8.0 min
Determined at gauge	39.382		
Using gauges	[39.382 40.1]		
Wavenumber	equal	with water depth	1
Noise	no	Weights	no
No of steps CWT	200		
Determinant limit	0.0		
p_min	1.666956E-01	p_max	1.777215E+01

RMSE	Fourier	Wavelet
reconstruction	1.945462E-16	1.156294E-03
sum	2.731964E-17	6.464717E-17
incident	3.507527E-02	1.398079E-03
reflected	3.507528E-02	1.211011E-03

	Original	Fourier	% diff	Wavelet	% diff
Ref.cff.	5.017083E-01	1E+00	99.32	5.016081E-01	-0.02
m0_in	5.599747E-03	2.274359E-03	-59.38	5.725979E-03	2.25
m0_ref	1.409519E-03	2.274359E-03	61.36	1.440717E-03	2.21

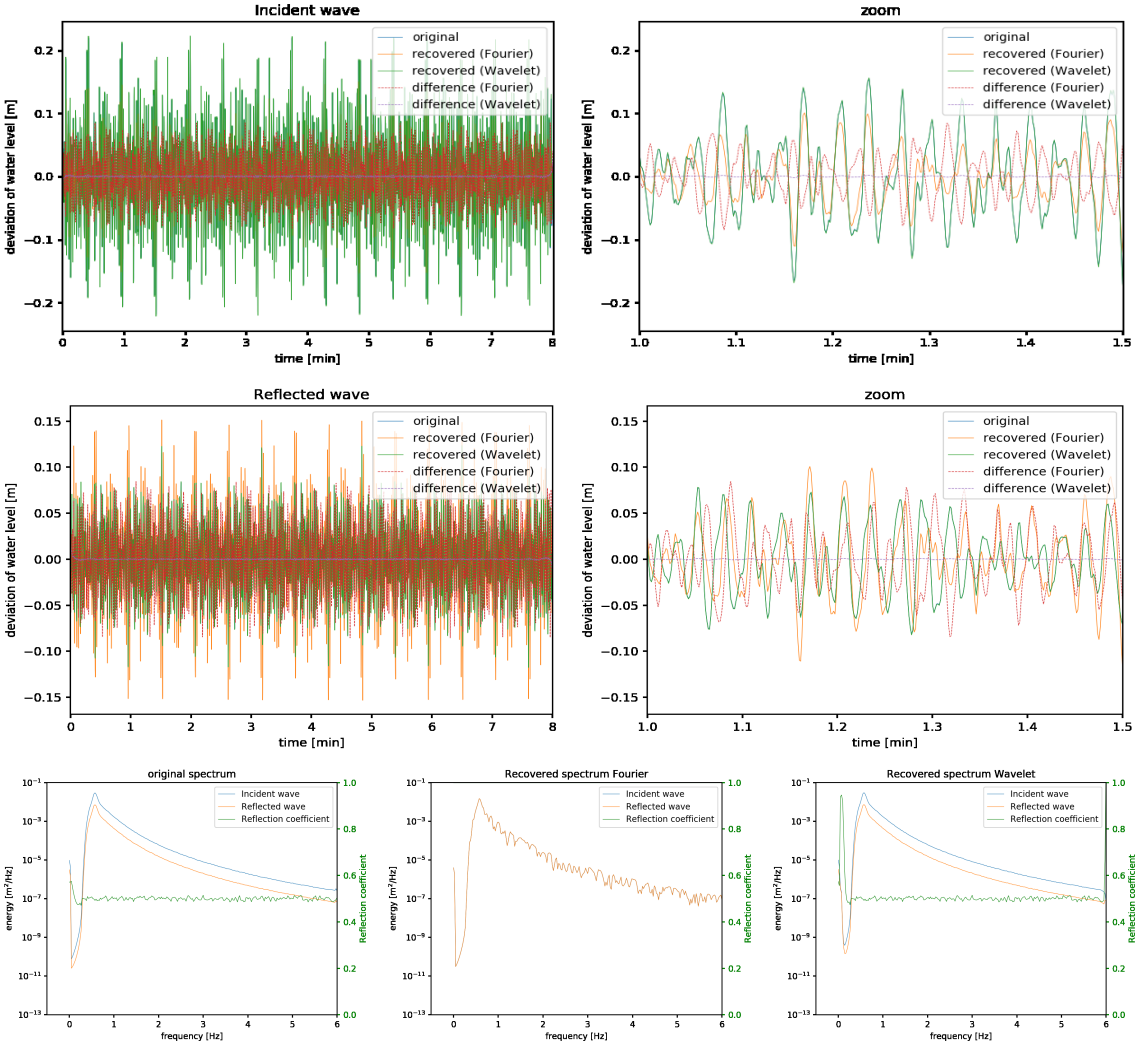

Figure D.3: Separating waves using 2 gauges, using an equal wave number for all frequencies. The Fourier algorithm was disables in this example.

Signal	200 waves from JONSWAP spectrum with f in [0.01,fs/2]		
Wavelet	Morlet	Parameter	60.0
Sampling freq	12	Duration	480.0 sec = 8.0 min
Determined at gauge			39.382
Using gauges			[39.382 39.83 40.1]
Wavenumber	dispersion	with water depth	1
Noise	no	Weights	no
No of steps CWT			200
Determinant limit			0
p_min	1.666956E-01	p_max	1.777215E+01

RMSE	Fourier	Wavelet
reconstruction	1.793458E-16	1.045626E-03
sum	1.579025E-03	1.701242E-03
incident	1.585319E-02	3.387655E-03
reflected	1.572349E-02	2.58678E-03

	Original	Fourier	% diff	Wavelet	% diff
Ref.cff.	5.029976E-01	5.335495E-01	6.07	5.039578E-01	0.19
m0_in	5.598901E-03	5.844593E-03	4.39	5.716851E-03	2.11
m0_ref	1.416559E-03	1.66381E-03	17.45	1.451928E-03	2.5

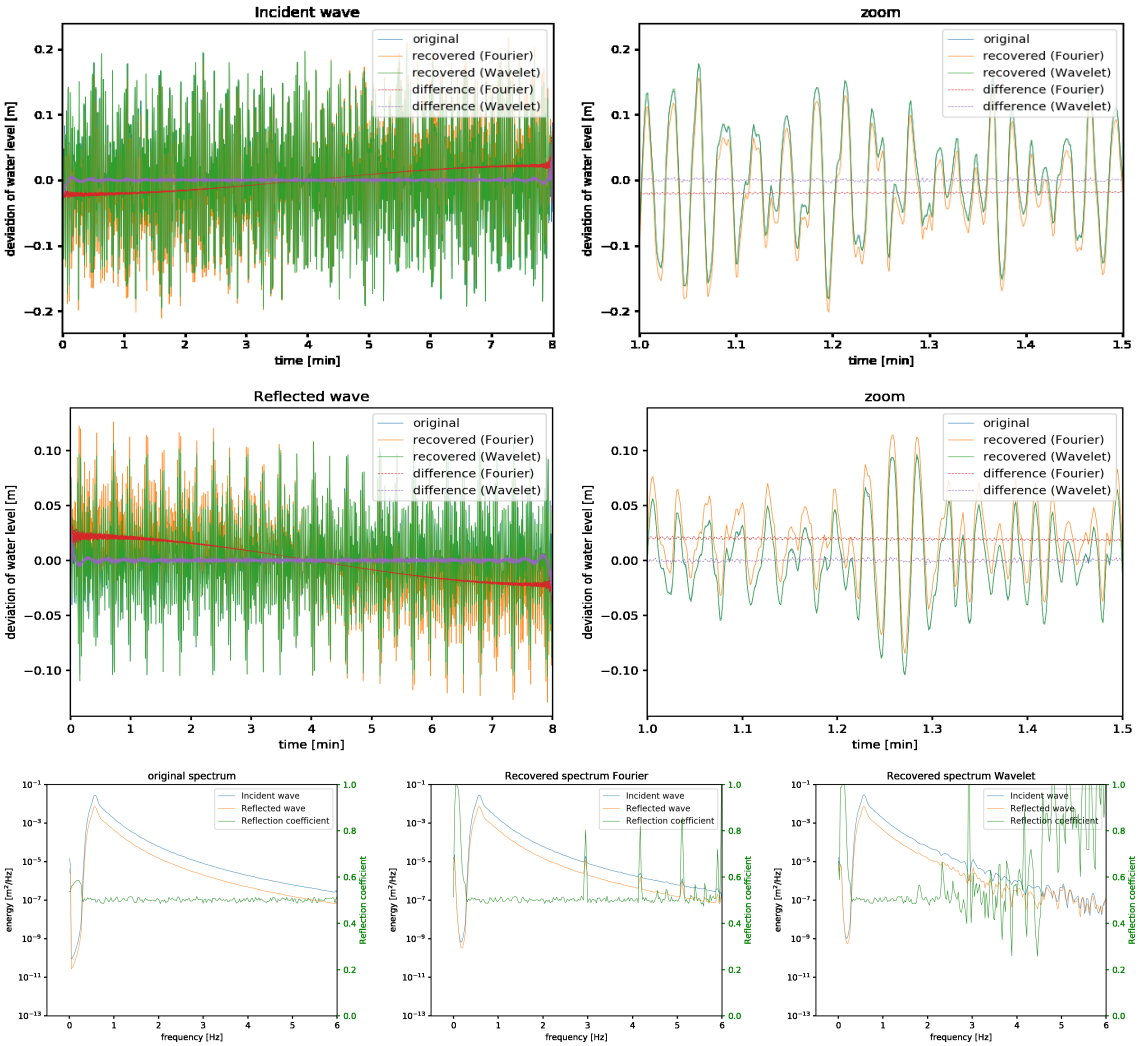

Figure D.4: Separating waves using 3 gauges

Signal	200 waves from JONSWAP spectrum with f in [0.01,fs/2]		
Wavelet	Morlet	Parameter	60.0
Sampling freq	12	Duration	480.0 sec = 8.0 min
Determined at gauge		35.742	
Using gauges		[35.742 38.726 39.382 39.83 40.:	
Wavenumber	dispersion	with water depth	1
Noise	no	Weights	no
No of steps CWT		200	
Determinant limit		0	
p_min	1.666956E-01	p_max	1.777215E+01

RMSE	Fourier	Wavelet
reconstruction	1.513282E-16	9.131862E-04
sum	4.853375E-03	7.743863E-03
incident	7.782599E-03	9.207705E-03
reflected	6.376457E-03	5.471597E-03

	Original	Fourier	% diff	Wavelet	% diff
Ref.cff.	5.024461E-01	5.051175E-01	0.53	5.006965E-01	-0.35
m0_in	5.612317E-03	5.646311E-03	0.61	5.364472E-03	-4.42
m0_ref	1.416841E-03	1.440621E-03	1.68	1.344857E-03	-5.08

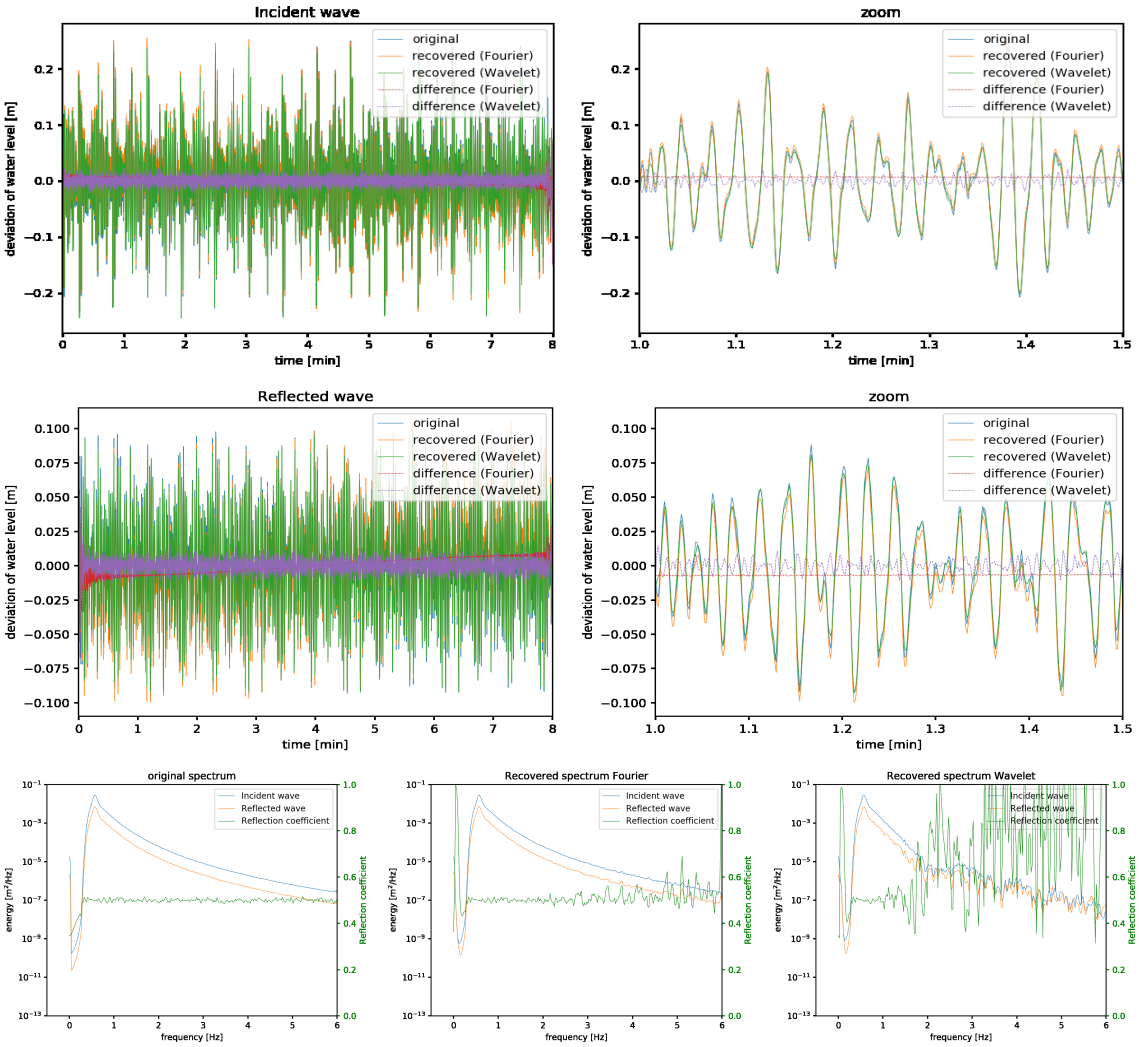

Figure D.5: Separating waves using 5 gauges

Signal	200 waves from JONSWAP spectrum with f in [0.01,fs/2]		
Wavelet	Morlet	Parameter	60.0
Sampling freq	12	Duration	480.0 sec = 8.0 min
Determined at gauge			39.382
Using gauges			[39.382 40.1]
Wavenumber	dispersion	with water depth	1
Noise	no	Weights	no
No of steps CWT			200
Determinant limit			0.1
p_min	1.666956E-01	p_max	1.777215E+01

RMSE	Fourier	Wavelet
reconstruction	1.714063E-16	1.03757E-03
sum	1.396335E-02	1.158056E-02
incident	1.234553E-02	1.150164E-02
reflected	7.85703E-03	7.384558E-03

	Original	Fourier	% diff	Wavelet	% diff
Ref.cff.	5.013296E-01	5.064333E-01	1.02	5.065781E-01	1.05
m0_in	5.5754E-03	5.457513E-03	-2.11	5.554474E-03	-0.38
m0_ref	1.401273E-03	1.399714E-03	-0.11	1.425397E-03	1.72

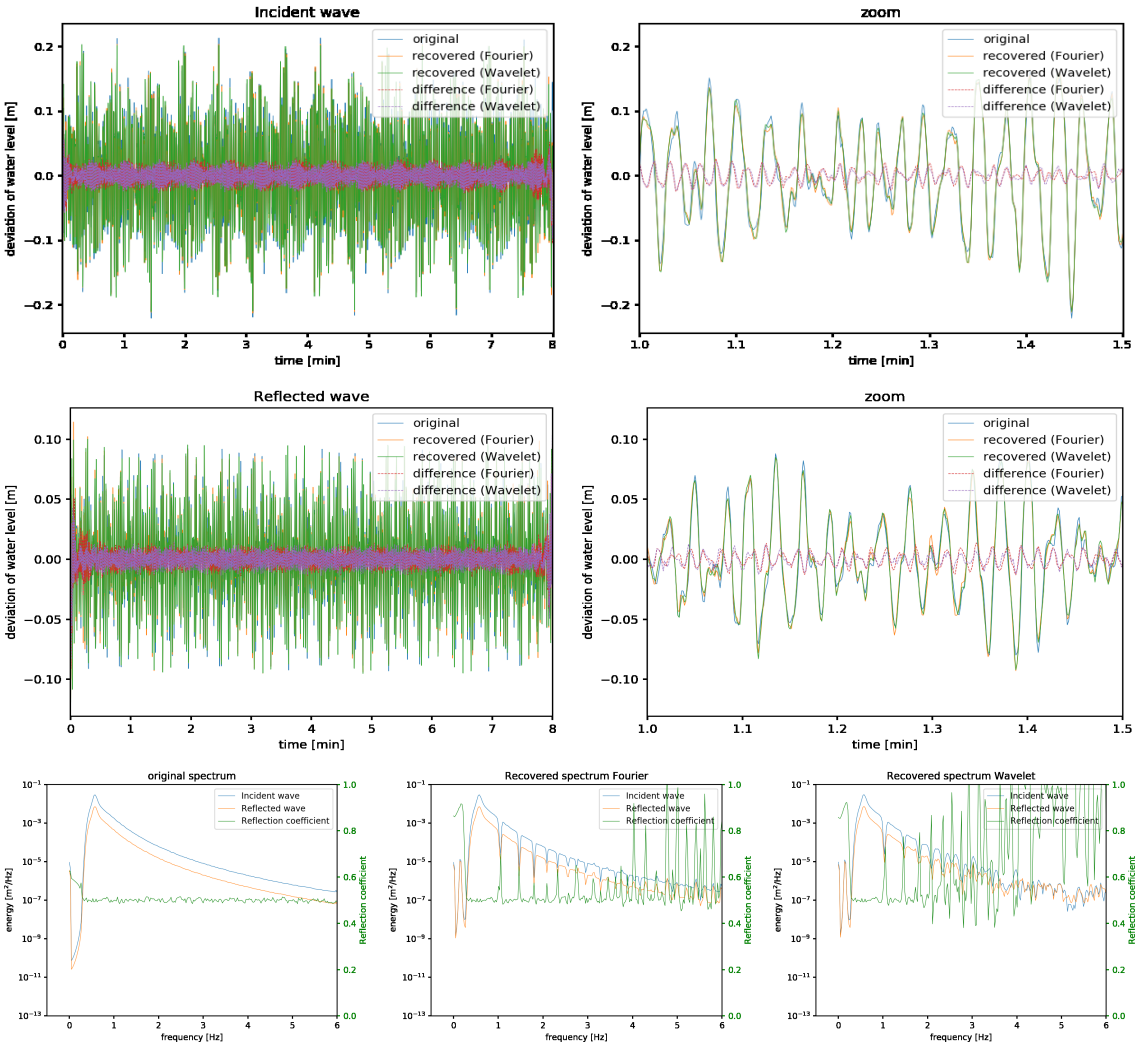

Figure D.6: Separating waves using 2 gauges, a determinant limiter of 0.1 has been added.

Signal	200 waves from JONSWAP spectrum with f in [0.01,fs/2]		
Wavelet	Morlet	Parameter	60.0
Sampling freq	12	Duration	480.0 sec = 8.0 min
Determined at gauge			39.382
Using gauges			[39.382 39.83 40.1]
Wavenumber	dispersion	with water depth	1
Noise	no	Weights	no
No of steps CWT			200
Determinant limit			0.1
p_min	1.666956E-01	p_max	1.777215E+01

RMSE	Fourier	Wavelet
reconstruction	1.793458E-16	1.045626E-03
sum	1.679487E-03	1.731344E-03
incident	2.721639E-03	3.003698E-03
reflected	1.829881E-03	2.110095E-03

	Original	Fourier	% diff	Wavelet	% diff
Ref.cff.	5.029976E-01	5.034707E-01	0.09	5.03642E-01	0.13
m0_in	5.598901E-03	5.599655E-03	0.01	5.714215E-03	2.06
m0_ref	1.416559E-03	1.419416E-03	0.2	1.44944E-03	2.32

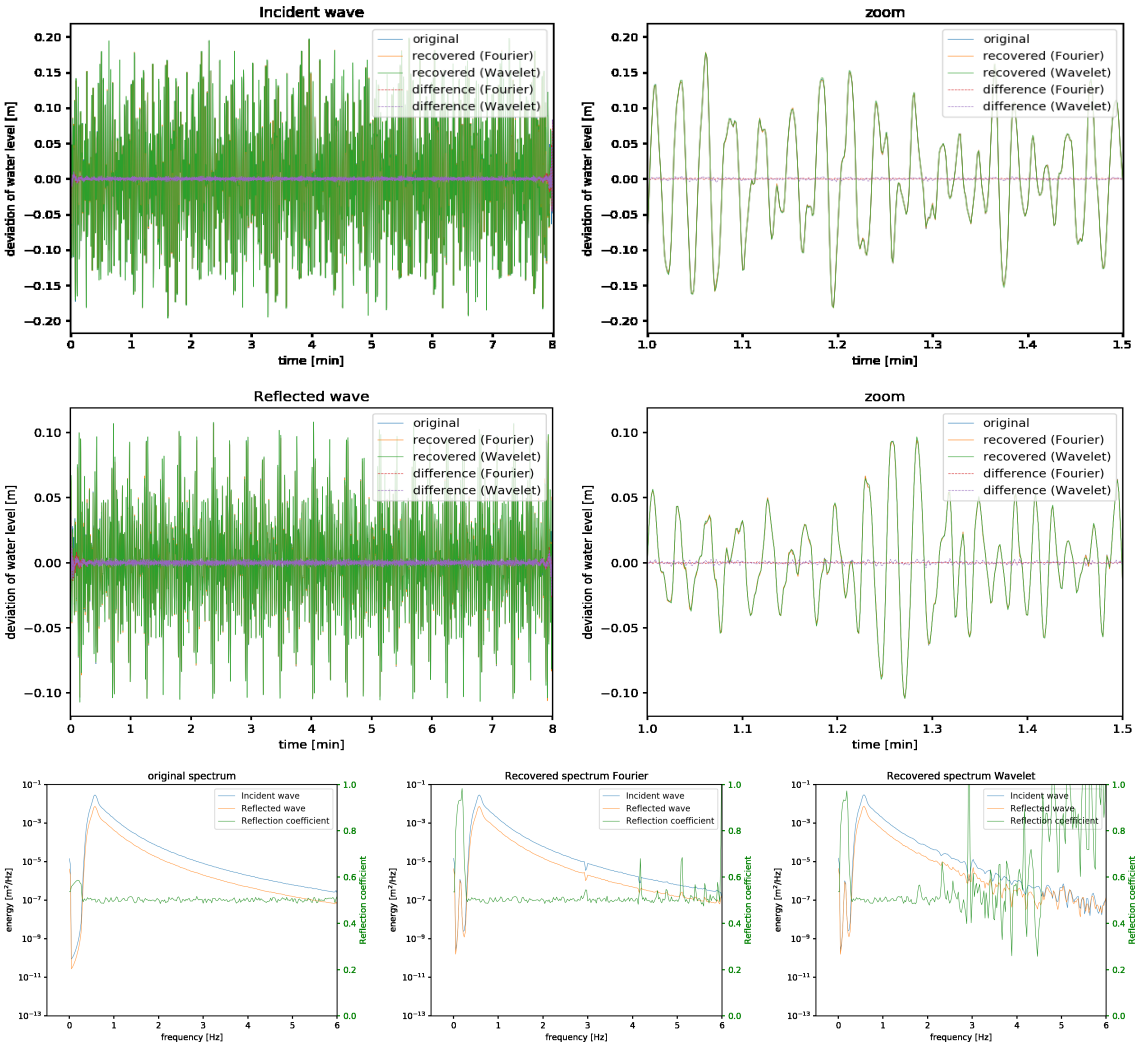

Figure D.7: Separating waves using 3 gauges, a determinant limiter of 0.1 has been added.

Signal	200 waves from JONSWAP spectrum with f in [0.01,fs/2]		
Wavelet	Morlet	Parameter	60.0
Sampling freq	12	Duration	480.0 sec = 8.0 min
Determined at gauge			35.742
Using gauges			[35.742 38.726 39.382 39.83 40.:
Wavenumber	dispersion	with water depth	1
Noise	no	Weights	no
No of steps CWT			200
Determinant limit			0.1
p_min	1.666956E-01	p_max	1.777215E+01

RMSE	Fourier	Wavelet
reconstruction	1.513282E-16	9.131862E-04
sum	4.853573E-03	7.743863E-03
incident	5.62117E-03	9.207705E-03
reflected	3.411883E-03	5.471597E-03

	Original	Fourier	% diff	Wavelet	% diff
Ref.cff.	5.024461E-01	5.012945E-01	-0.23	5.006965E-01	-0.35
m0_in	5.612317E-03	5.617279E-03	0.09	5.364472E-03	-4.42
m0_ref	1.416841E-03	1.411601E-03	-0.37	1.344857E-03	-5.08

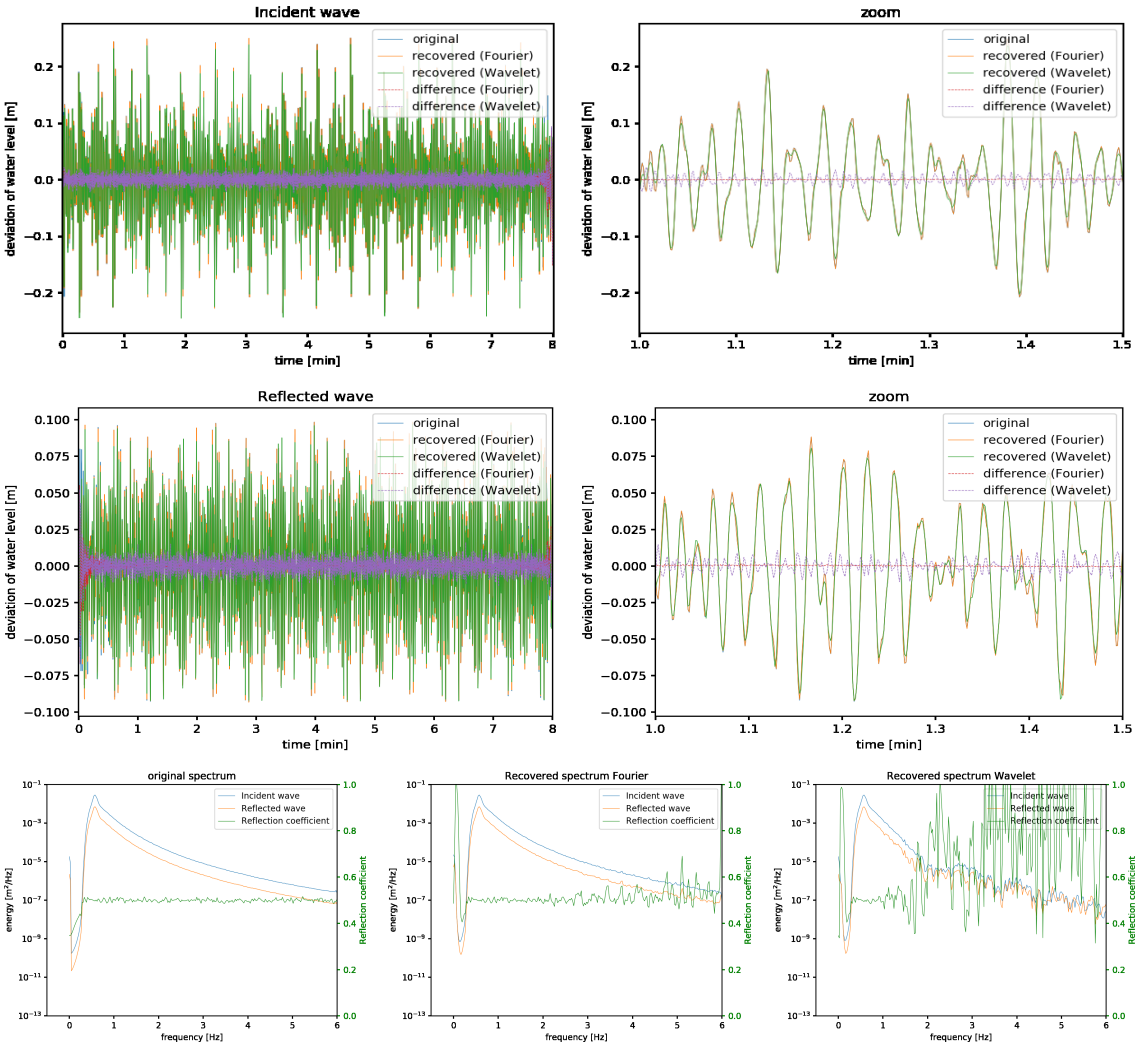

Figure D.8: Separating waves using 5 gauges, a determinant limiter of 0.1 has been added.

Signal	200 waves from JONSWAP spectrum with f in [0.01,fs/2]		
Wavelet	Morlet	Parameter	6.0
Sampling freq	12	Duration	480.0 sec = 8.0 min
Determined at gauge			39.382
Using gauges			[39.382 40.1]
Wavenumber	dispersion	with water depth	1
Noise	no	Weights	no
No of steps CWT			200
Determinant limit			0
p_min	1.666956E-01	p_max	1.753438E+02

RMSE	Fourier	Wavelet
reconstruction	1.754694E-16	8.094903E-03
sum	4.151245E-14	2.427245E-15
incident	1.864212E-01	9.062197E-02
reflected	1.864213E-01	9.219416E-02

	Original	Fourier	% diff	Wavelet	% diff
Ref.cff.	5.039467E-01	9.472165E-01	87.96	9.468592E-01	87.89
m0_in	5.55159E-03	4.028092E-02	625.57	9.806519E-03	76.64
m0_ref	1.409894E-03	3.614081E-02	2463.37	8.791959E-03	523.59

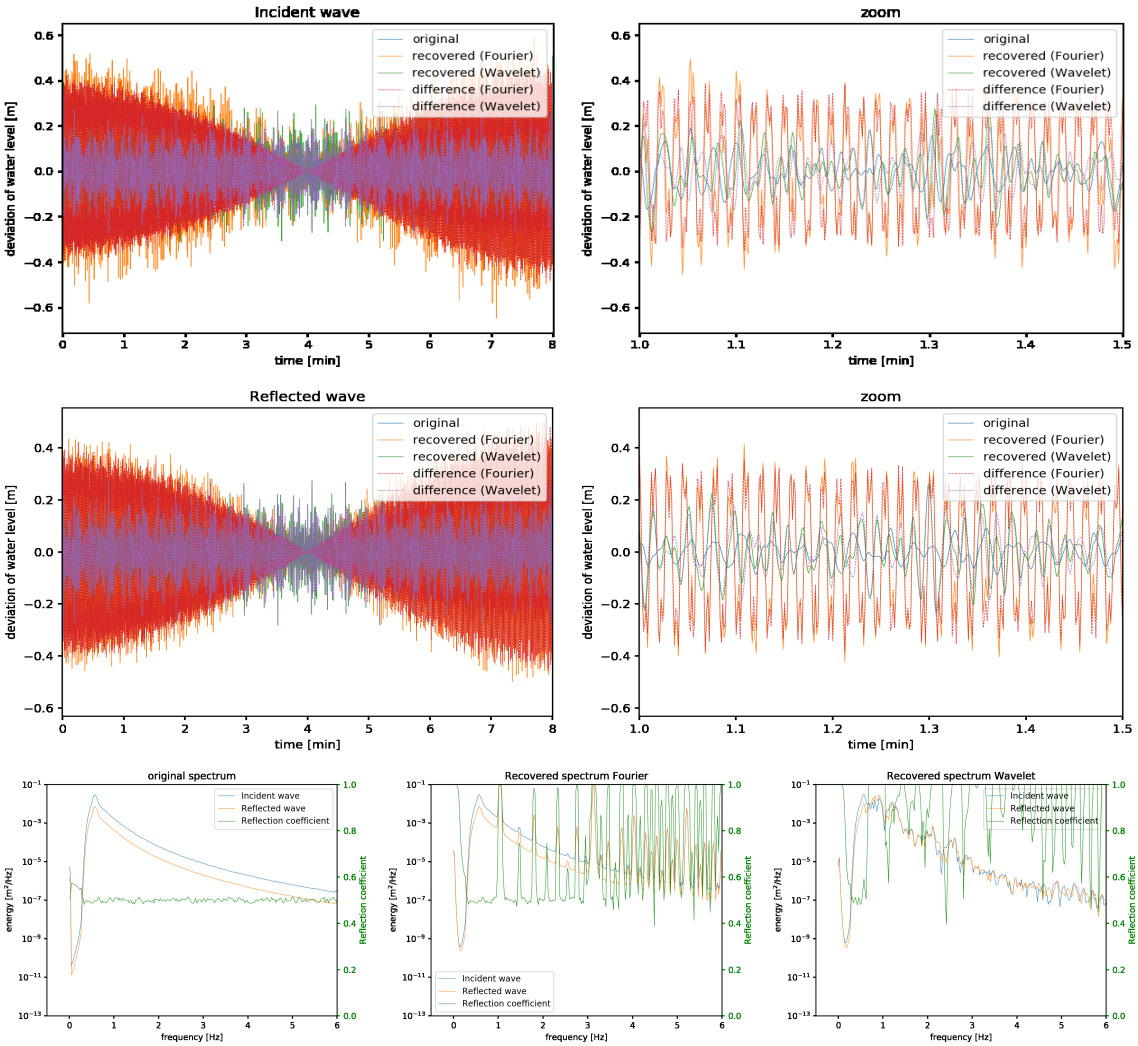

Figure D.9: Separating waves using 2 gauges, the Morlet 6 wavelet is used.

Signal	200 waves from JONSWAP spectrum with f in [0.01,fs/2]		
Wavelet	Morlet	Parameter	6.0
Sampling freq	12	Duration	480.0 sec = 8.0 min
Determined at gauge			35.742
Using gauges			[35.742 38.726 39.382 39.83 40.:
Wavenumber	dispersion	with water depth	1
Noise	no	Weights	no
No of steps CWT			200
Determinant limit			0
p_min	1.666956E-01	p_max	1.753438E+02

RMSE	Fourier	Wavelet
reconstruction	1.49919E-16	7.131343E-03
sum	6.033238E-03	4.20067E-02
incident	8.564489E-03	4.358948E-02
reflected	5.884976E-03	2.517018E-02

	Original	Fourier	% diff	Wavelet	% diff
Ref.cff.	4.997987E-01	5.058063E-01	1.2	5.687812E-01	13.8
m0_in	5.631724E-03	5.615814E-03	-0.28	1.328323E-03	-76.41
m0_ref	1.406798E-03	1.43675E-03	2.13	4.297284E-04	-69.45

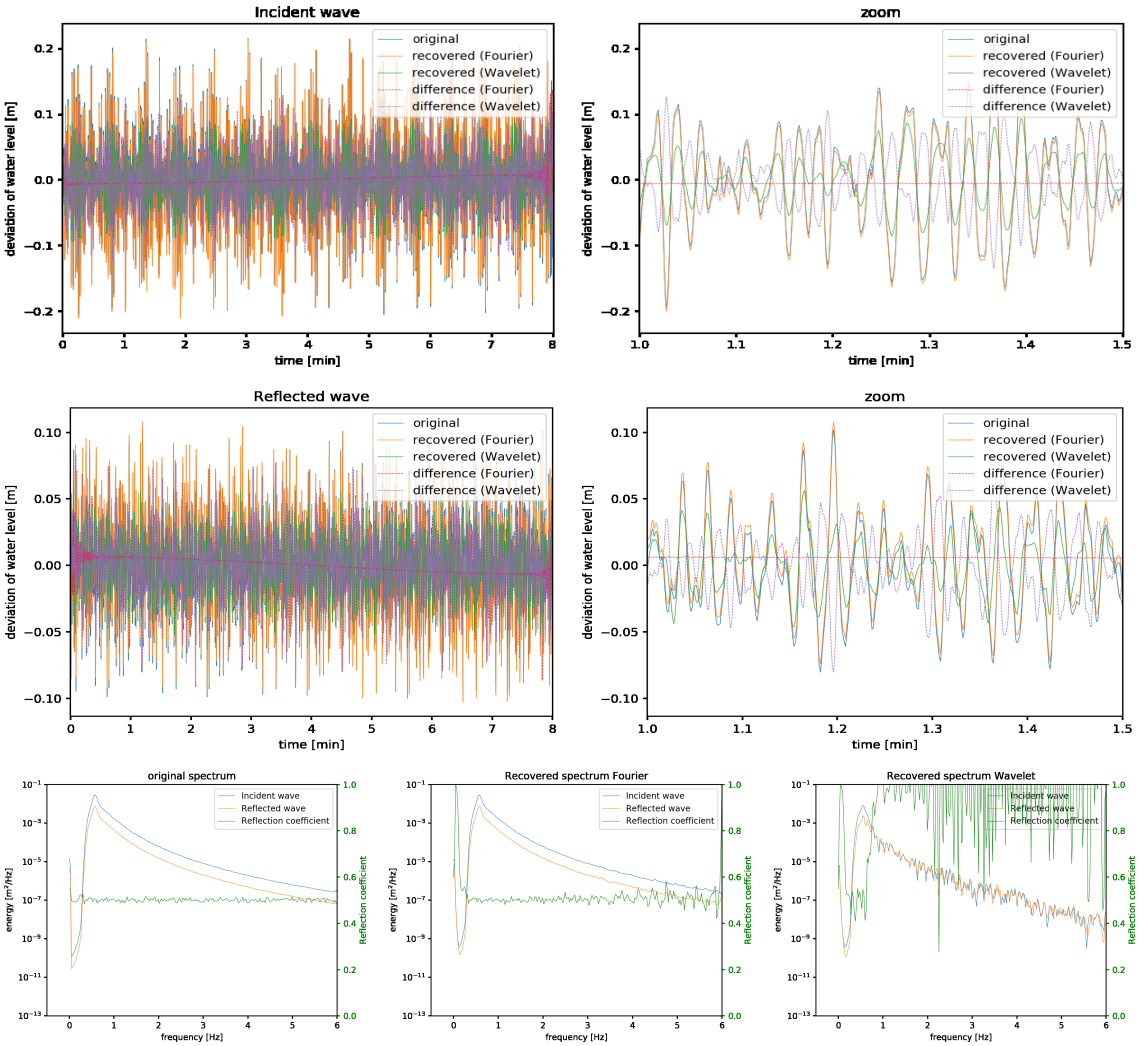

Figure D.10: Separating waves using 2 gauges, the Morlet 6 wavelet is used.

Signal	200 waves from JONSWAP spectrum with f in [0.01,fs/2]		
Wavelet	Morlet	Parameter	6.0
Sampling freq	12	Duration	480.0 sec = 8.0 min
Determined at gauge	39.382		
Using gauges	[39.382 40.1]		
Wavenumber	equal	with water depth	1
Noise	no	Weights	no
No of steps CWT	200		
Determinant limit	0.0		
p_min	1.666956E-01	p_max	1.753438E+02

RMSE	Fourier	Wavelet
reconstruction	1.690193E-16	7.587509E-03
sum	2.633091E-17	7.19489E-17
incident	4.182334E-02	7.042717E-03
reflected	4.182334E-02	3.89677E-03

	Original	Fourier	% diff	Wavelet	% diff
Ref.cff.	4.967628E-01	1E+00	101.3	4.966376E-01	-0.03
m0_in	5.678219E-03	1.790534E-03	-68.47	6.737207E-03	18.65
m0_ref	1.401233E-03	1.790534E-03	27.78	1.661724E-03	18.59

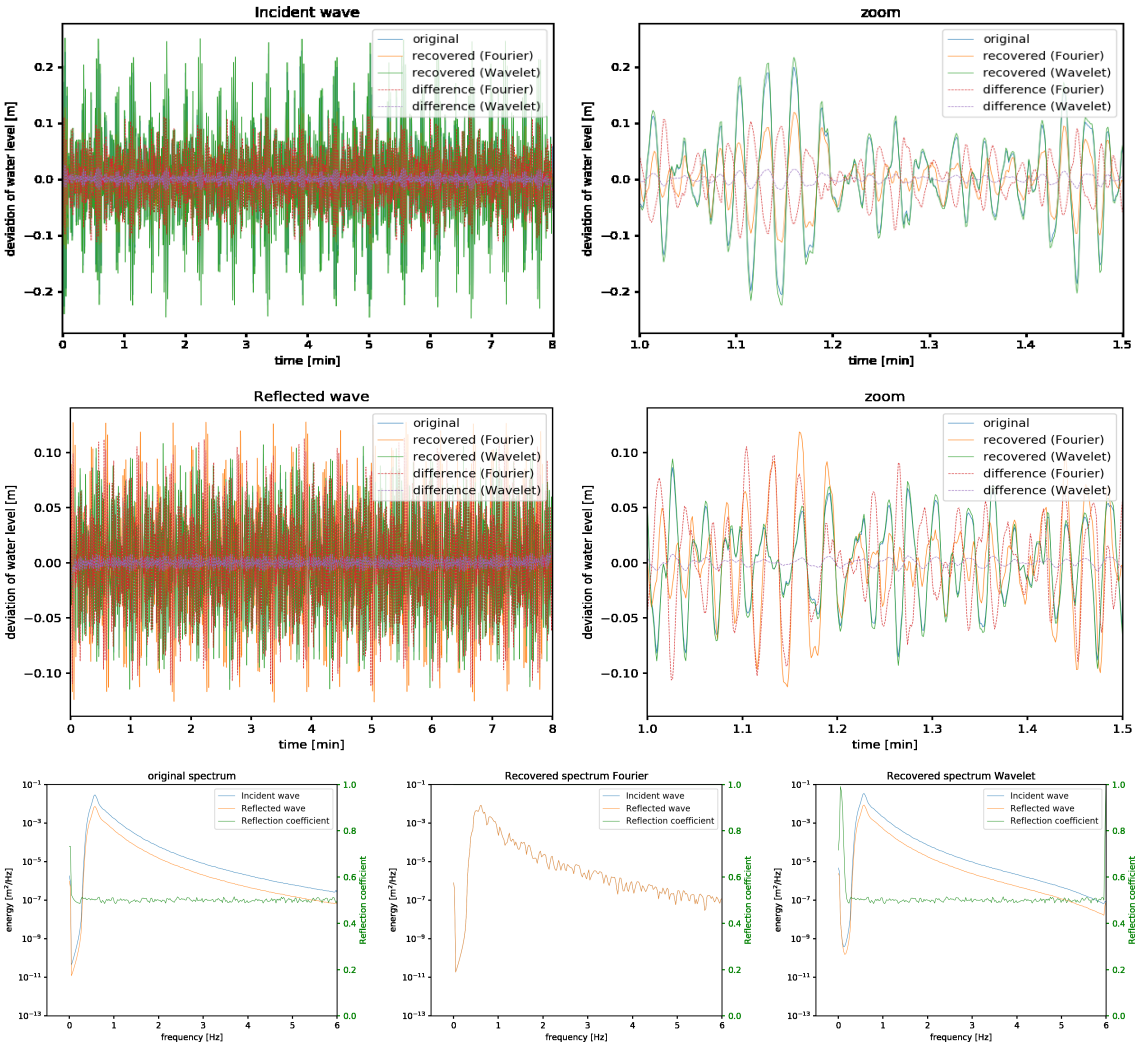

Figure D.11: Separating waves using 2 gauges, using the same wave number for all frequencies and the Morlet 6 wavelet.

Signal	200 waves from JONSWAP spectrum with f in [0.01,fs/2]		
Wavelet	Morlet	Parameter	60.0
Sampling freq	12	Duration	480.0 sec = 8.0 min
Determined at gauge	35.742		
Using gauges	[35.742 38.726 39.382 39.83 40.1]		
Wavenumber	disperion	with water depth	1
Noise	no	Weights	no
No of steps CWT	20		
Determinant limit	0.0		
p_min	1.666956E-01	p_max	1.777215E+01

RMSE	Fourier	Wavelet
reconstruction	1.513282E-16	1.242043E-01
sum	4.853375E-03	2.701533E-02
incident	7.782599E-03	1.107794E-01
reflected	6.376457E-03	5.617696E-02

	Original	Fourier	% diff	Wavelet	% diff
Ref.cff.	5.024461E-01	5.051175E-01	0.53	5.028802E-01	0.09
m0_in	5.612317E-03	5.646311E-03	0.61	1.537792E-02	174.0
m0_ref	1.416841E-03	1.440621E-03	1.68	3.888897E-03	174.48

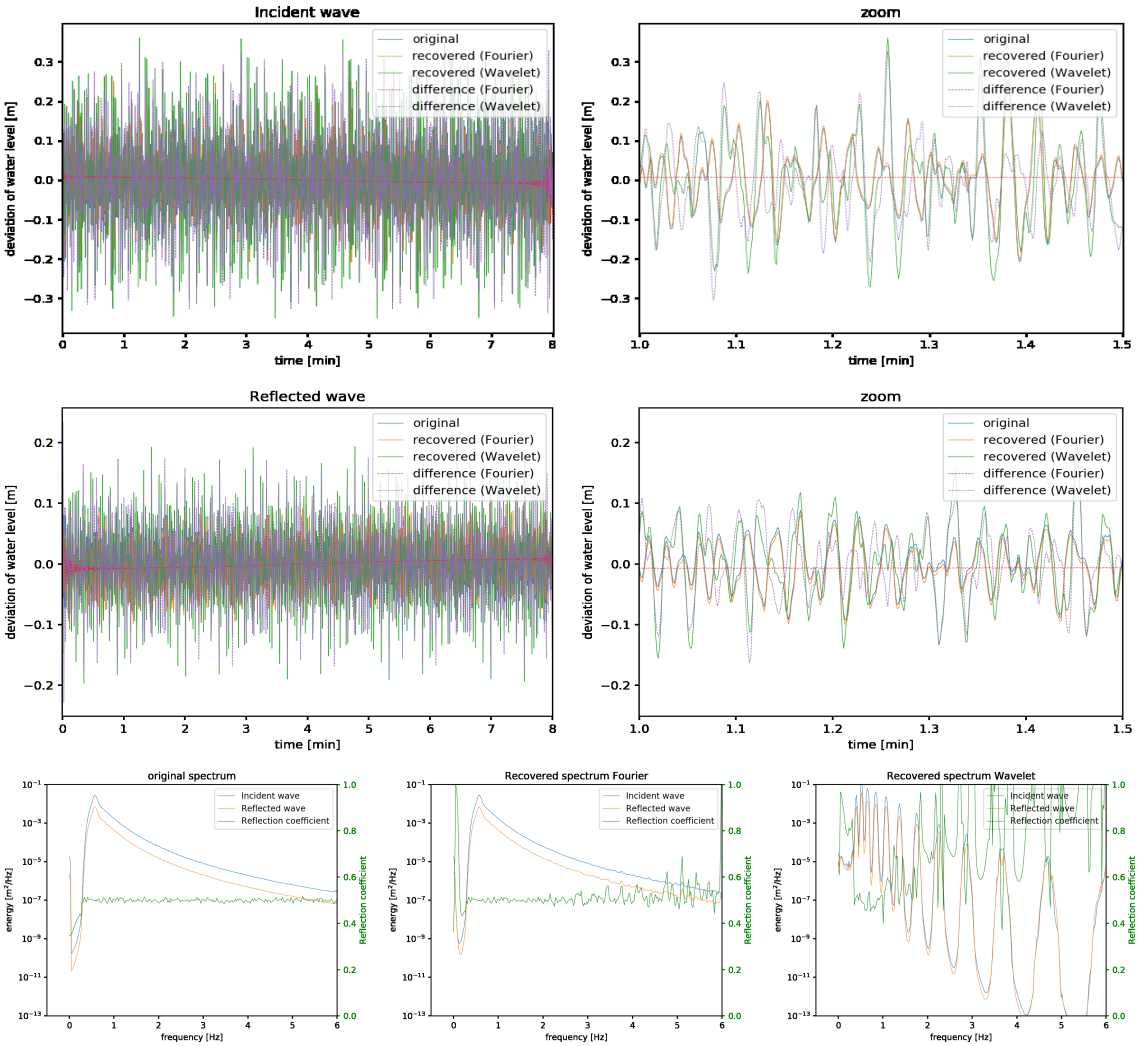

Figure D.12: Separating waves using 5 gauges, using too little scales; 20 scales.

Signal	200 waves from JONSWAP spectrum with f in [0.01,fs/2]		
Wavelet	Morlet	Parameter	60.0
Sampling freq	12	Duration	480.0 sec = 8.0 min
Determined at gauge	35.742		
Using gauges	[35.742 38.726 39.382 39.83 40.1]		
Wavenumber	dispersion	with water depth	1
Noise	no	Weights	no
No of steps CWT	1000		
Determinant limit	0.0		
p_min	1.666956E-01	p_max	1.777215E+01

RMSE	Fourier	Wavelet
reconstruction	1.501484E-16	1.25802E-03
sum	3.788041E-03	7.06129E-03
incident	6.930915E-03	8.285033E-03
reflected	6.054826E-03	4.931244E-03

	Original	Fourier	% diff	Wavelet	% diff
Ref.cff.	4.991929E-01	5.040241E-01	0.97	5.006313E-01	0.29
m0_in	5.572451E-03	5.582134E-03	0.17	5.347351E-03	-4.04
m0_ref	1.388619E-03	1.418087E-03	2.12	1.340216E-03	-3.49

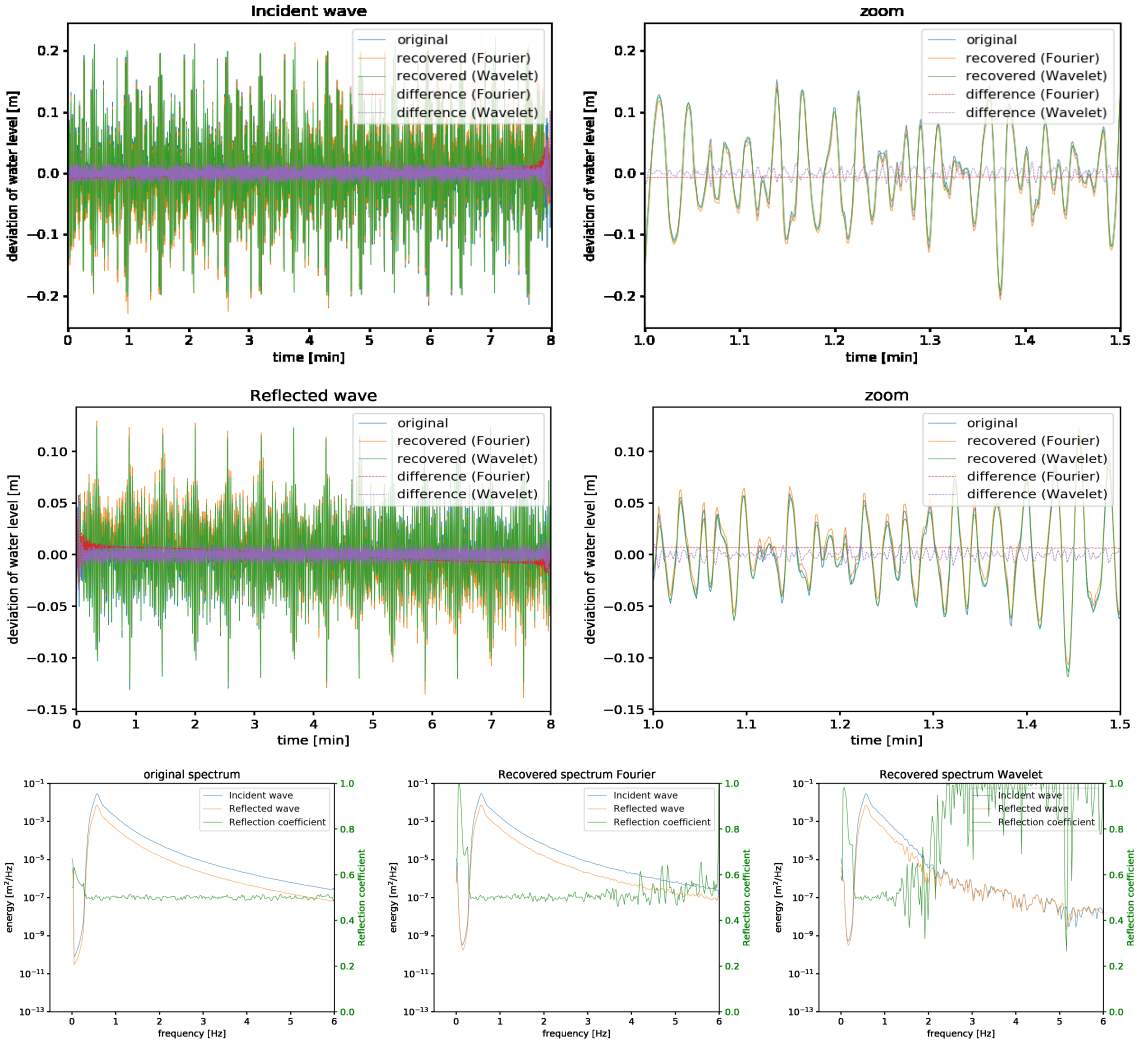

Figure D.13: Separating waves using 5 gauges, using many scales; 1000 scales.

Signal	200 waves from JONSWAP spectrum with f in [0.01,fs/2]		
Wavelet	Morlet	Parameter	60.0
Sampling freq	12	Duration	480.0 sec = 8.0 min
Determined at gauge			39.382
Using gauges			[39.382 40.1]
Wavenumber	dispersion	with water depth	1
Noise	no	Weights	no
No of steps CWT			200
Determinant limit			0.5
p_min	1.666956E-01	p_max	1.777215E+01

RMSE	Fourier	Wavelet
reconstruction	1.714063E-16	1.03757E-03
sum	2.151178E-02	1.977146E-02
incident	1.806545E-02	1.676688E-02
reflected	9.452914E-03	8.831368E-03

	Original	Fourier	% diff	Wavelet	% diff
Ref.cff.	5.013296E-01	5.039098E-01	0.51	5.046765E-01	0.67
m0_in	5.5754E-03	5.254034E-03	-5.76	5.343346E-03	-4.16
m0_ref	1.401273E-03	1.334131E-03	-4.79	1.360941E-03	-2.88

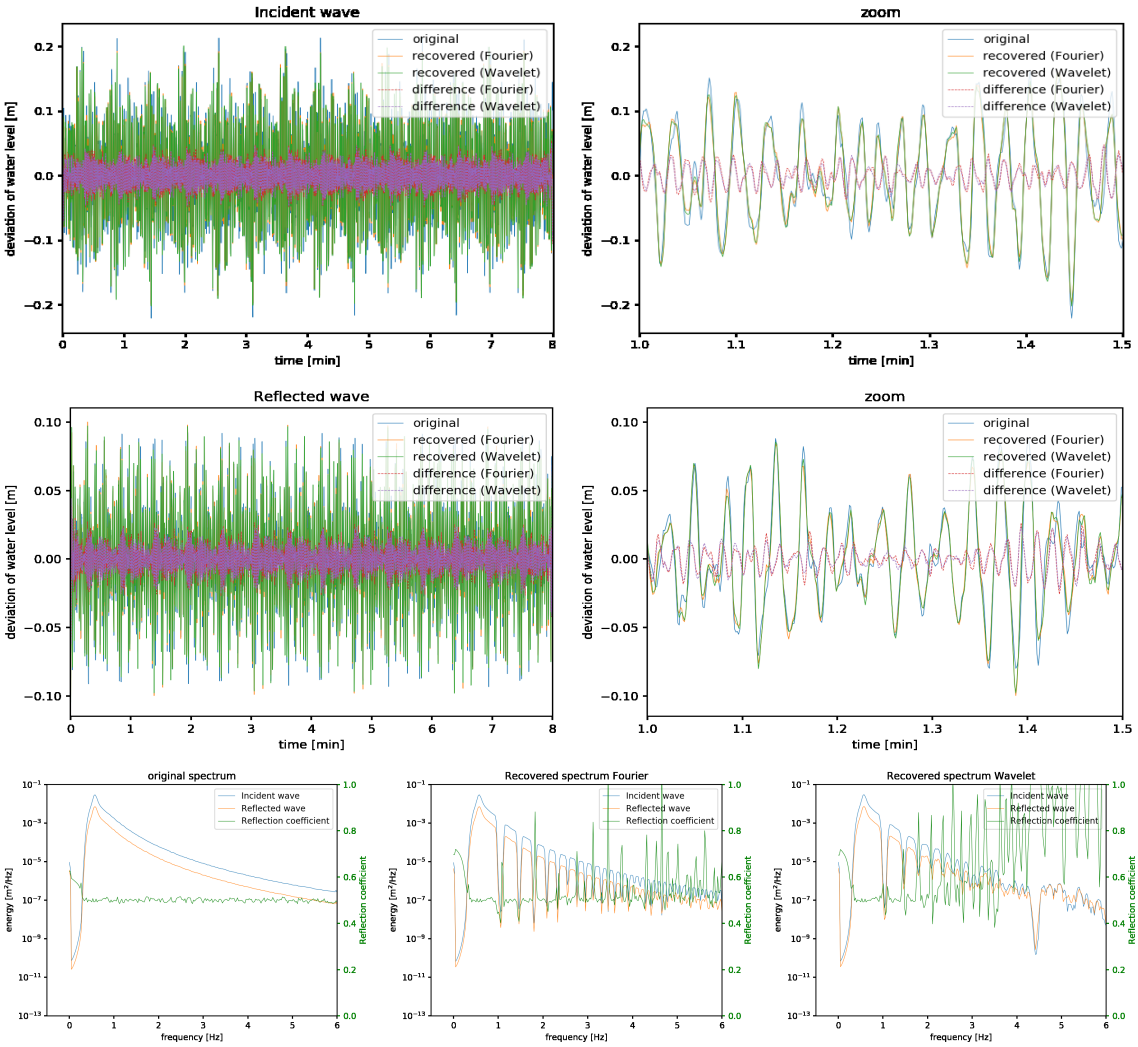

Figure D.14: Separating waves using 2 gauges, a determinant limiter of 0.5 has been added.

Signal	200 waves from JONSWAP spectrum with f in [0.01,fs/2]		
Wavelet	Morlet	Parameter	60.0
Sampling freq	12	Duration	480.0 sec = 8.0 min
Determined at gauge			39.382
Using gauges			[39.382 39.83 40.1]
Wavenumber	dispersion	with water depth	1
Noise	no	Weights	zelt
No of steps CWT			200
Determinant limit			0
p_min	1.666956E-01	p_max	1.777215E+01

RMSE	Fourier	Wavelet
reconstruction	1.378247E-16	8.438111E-04
sum	1.177983E-03	1.331431E-03
incident	1.005492E-02	2.675956E-03
reflected	1.005925E-02	2.519676E-03

	Original	Fourier	% diff	Wavelet	% diff
Ref.cff.	4.989154E-01	5.117766E-01	2.58	4.996177E-01	0.14
m0_in	5.698587E-03	5.801439E-03	1.8	5.821553E-03	2.16
m0_ref	1.418473E-03	1.519486E-03	7.12	1.453164E-03	2.45

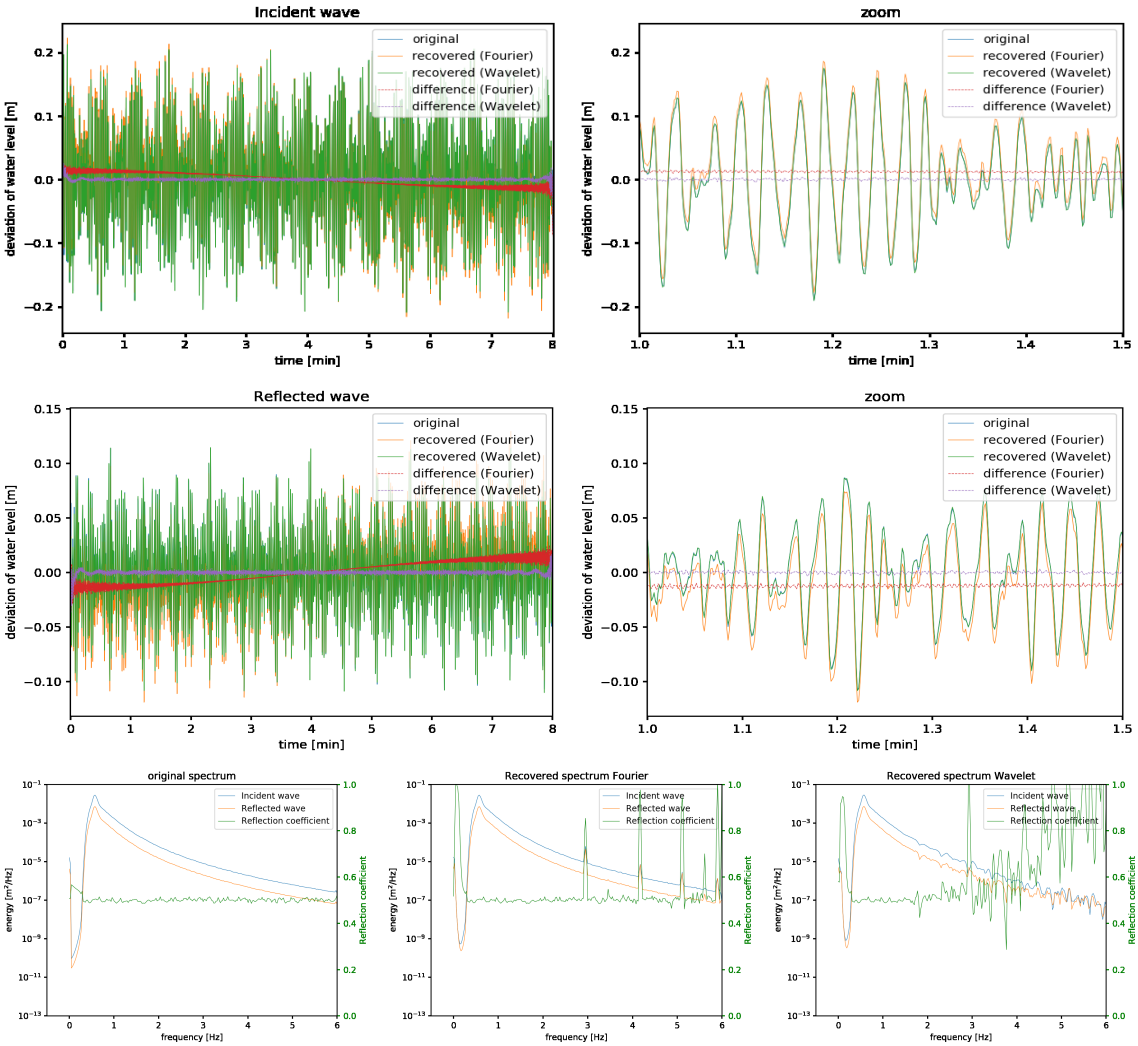

Figure D.15: Separating waves using 3 gauges, added the weightings described in equation 3.20.

Signal	200 waves from JONSWAP spectrum with f in [0.01,fs/2], refl.cff changes		
Wavelet	Morlet	Parameter	60.0
Sampling freq	12	Duration	480.0 sec = 8.0 min
Determined at gauge	35.742		
Using gauges	[35.742 38.726 39.382 39.83 40.1]		
Wavenumber	disperion	with water depth	1
Noise	no	Weights	no
No of steps CWT	200		
Determinant limit	0.0		
p_min	1.666956E-01	p_max	1.777215E+01

RMSE	Fourier	Wavelet
reconstruction	1.845117E-16	2.893224E-03
sum	4.703134E-03	8.699147E-03
incident	6.176124E-03	9.499821E-03
reflected	3.143778E-03	6.266618E-03

	Original	Fourier	% diff	Wavelet	% diff
Ref.cff.	7.092311E-01	7.118718E-01	0.37	7.121914E-01	0.42
m0_in	5.593476E-03	5.568218E-03	-0.45	5.324922E-03	-4.8
m0_ref	2.813567E-03	2.821758E-03	0.29	2.700888E-03	-4.0

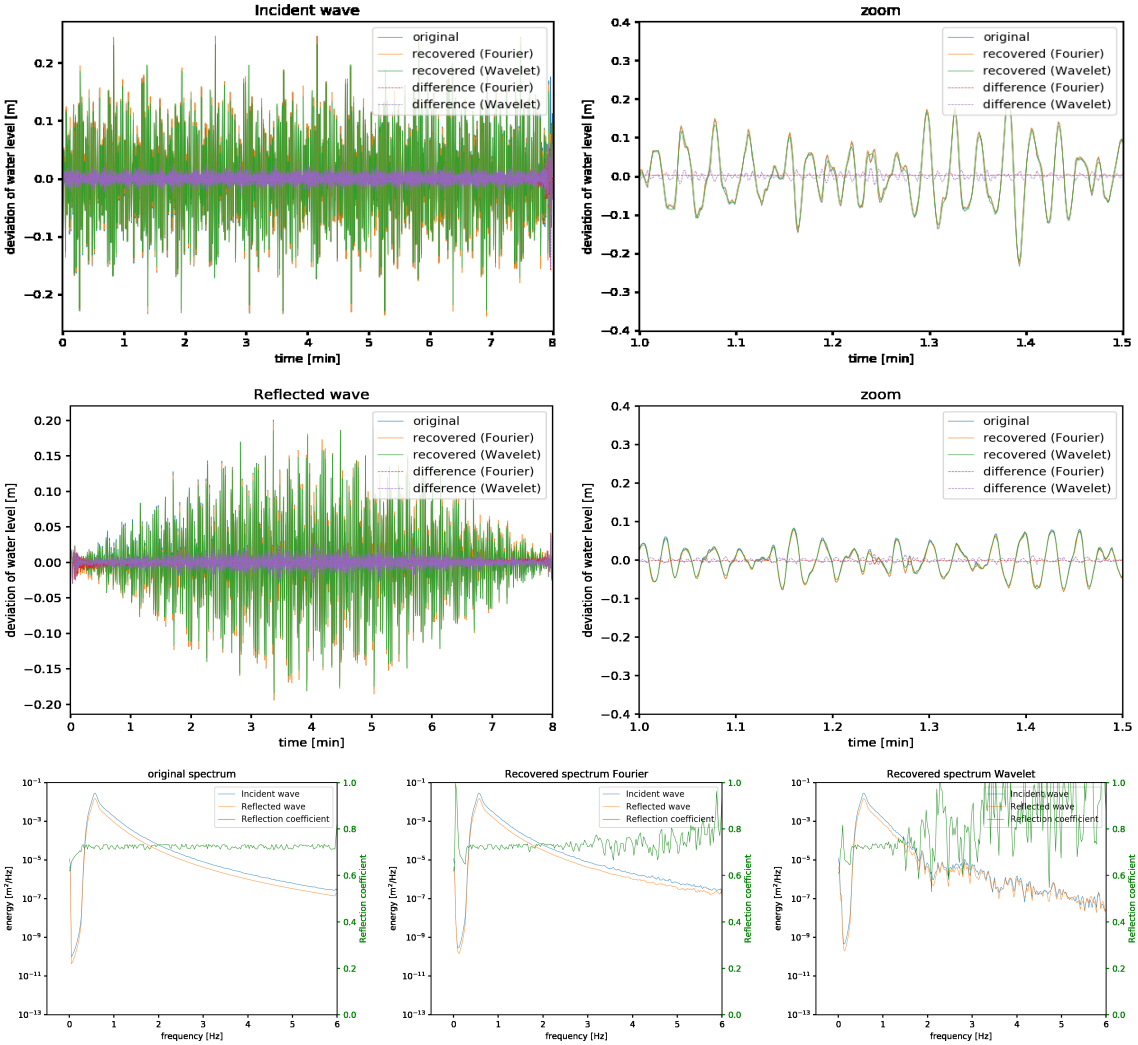

Figure D.16: Separating waves using 5 gauges, reflection coefficient changes over time; following a half a sine over the entire interval.

Signal	200 waves from JONSWAP spectrum with f in [0.01,fs/2], slope in signal		
Wavelet	Morlet	Parameter	60.0
Sampling freq	12	Duration	480.0 sec = 8.0 min
Determined at gauge	35.742		
Using gauges	[35.742 38.726 39.382 39.83 40.1]		
Wavenumber	disperion	with water depth	1
Noise	no	Weights	no
No of steps CWT	200		
Determinant limit	0.0		
p_min	1.666956E-01	p_max	1.777215E+01

RMSE	Fourier	Wavelet
reconstruction	2.729379E-16	1.448473E-01
sum	1.749256E-02	2.389889E-02
incident	7.997851E-02	1.546532E-02
reflected	6.664183E-02	1.266747E-02

	Original	Fourier	% diff	Wavelet	% diff
Ref.cff.	5.016754E-01	7.03346E-01	40.2	5.185117E-01	3.36
m0_in	5.627654E-03	1.17803E-02	109.33	5.518058E-03	-1.95
m0_ref	1.416358E-03	5.827664E-03	311.45	1.483554E-03	4.74

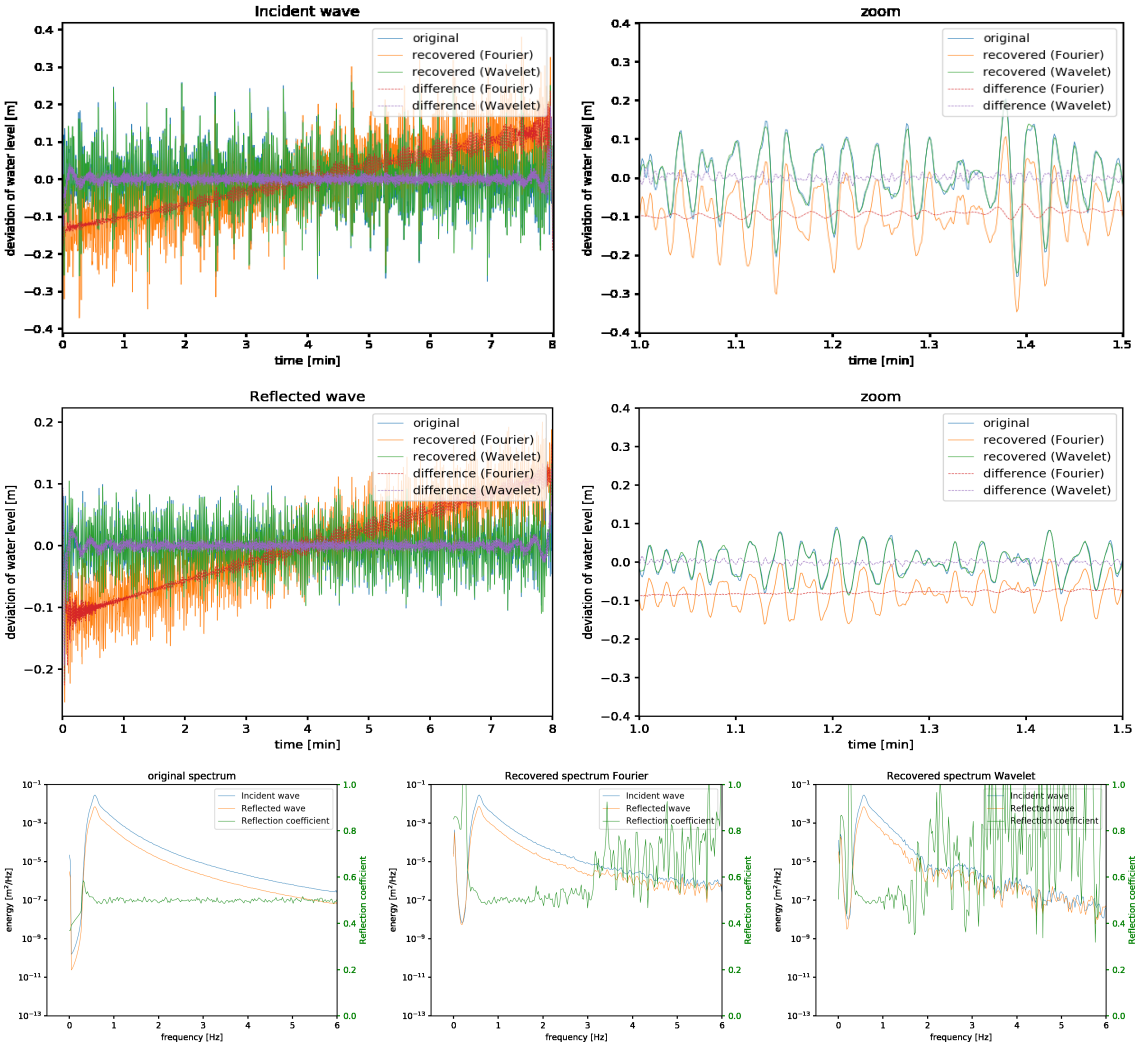

Figure D.17: Separating waves using 5 gauges, slope added to the signal. Increase of water level of 0.5 meter in 8 minutes. The sum of the wavelet separated incident and reflected wave is not close to the original signal because the slope is not present in the separated waves.

Signal	200 waves from JONSWAP spectrum with f in [0.01,fs/2], non stationary reflec		
Wavelet	Morlet	Parameter	60.0
Sampling freq	12	Duration	480.0 sec = 8.0 min
Determined at gauge	35.742		
Using gauges	[35.742 38.726 39.382 39.83 40.1]		
Wavenumber	disperion	with water depth	1
Noise	no	Weights	no
No of steps CWT	200		
Determinant limit	0.0		
p_min	1.666956E-01	p_max	1.777215E+01

RMSE	Fourier	Wavelet
reconstruction	6.919914E-16	4.038558E-01
sum	4.705659E-02	4.721172E-02
incident	1.216143E-01	2.353307E-01
reflected	1.217744E-01	2.353185E-01

	Original	Fourier	% diff	Wavelet	% diff
Ref.cff.	9.527674E-01	9.554861E-01	0.29	7.129344E-01	-25.17
m0_in	4.91902E-02	5.000326E-02	1.65	8.91487E-03	-81.88
m0_ref	4.465318E-02	4.565066E-02	2.23	4.531209E-03	-89.85

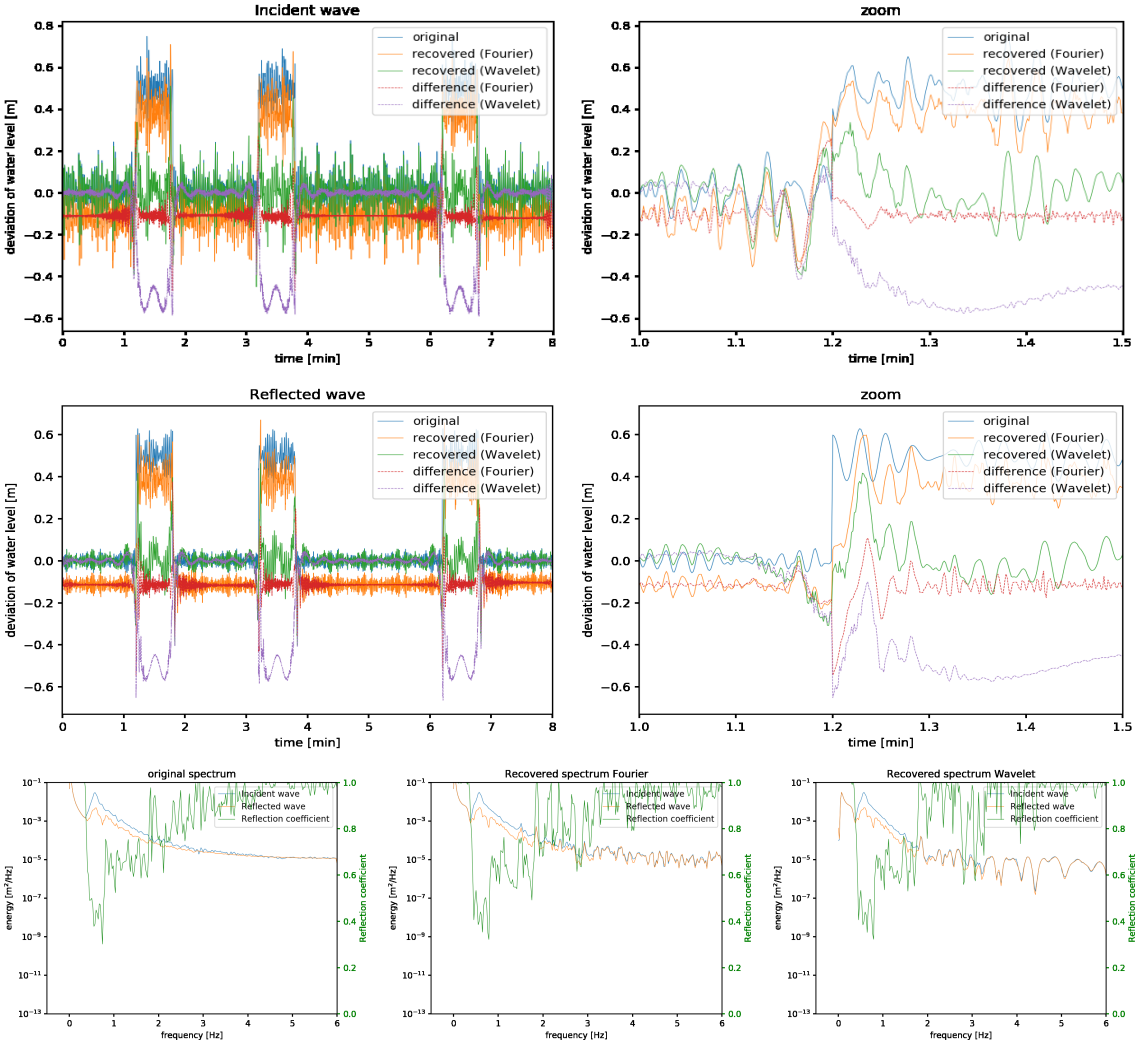

Figure D.18: Separating waves using 5 gauges, jumps added to signal.

Signal	200 waves from JONSWAP spectrum with f in [0.01,fs/2]		
Wavelet	Morlet	Parameter	60.0
Sampling freq	12	Duration	480.0 sec = 8.0 min
Determined at gauge	39.382		
Using gauges	[39.382 39.83 40.1]		
Wavenumber	disperion	with water depth	1
Noise	var/0.1	Weights	no
No of steps CWT	200		
Determinant limit	0.1		
p_min	1.666956E-01	p_max	1.777215E+01

RMSE	Fourier	Wavelet
reconstruction	1.987186E-16	5.914581E-03
sum	3.293101E-02	2.78428E-02
incident	4.85699E-02	4.050161E-02
reflected	4.840732E-02	4.030858E-02

	Original	Fourier	% diff	Wavelet	% diff
Ref.cff.	5.011157E-01	6.76284E-01	34.96	6.337757E-01	26.47
m0_in	5.622184E-03	8.077011E-03	43.66	7.472823E-03	32.92
m0_ref	1.411826E-03	3.694102E-03	161.65	3.001621E-03	112.61

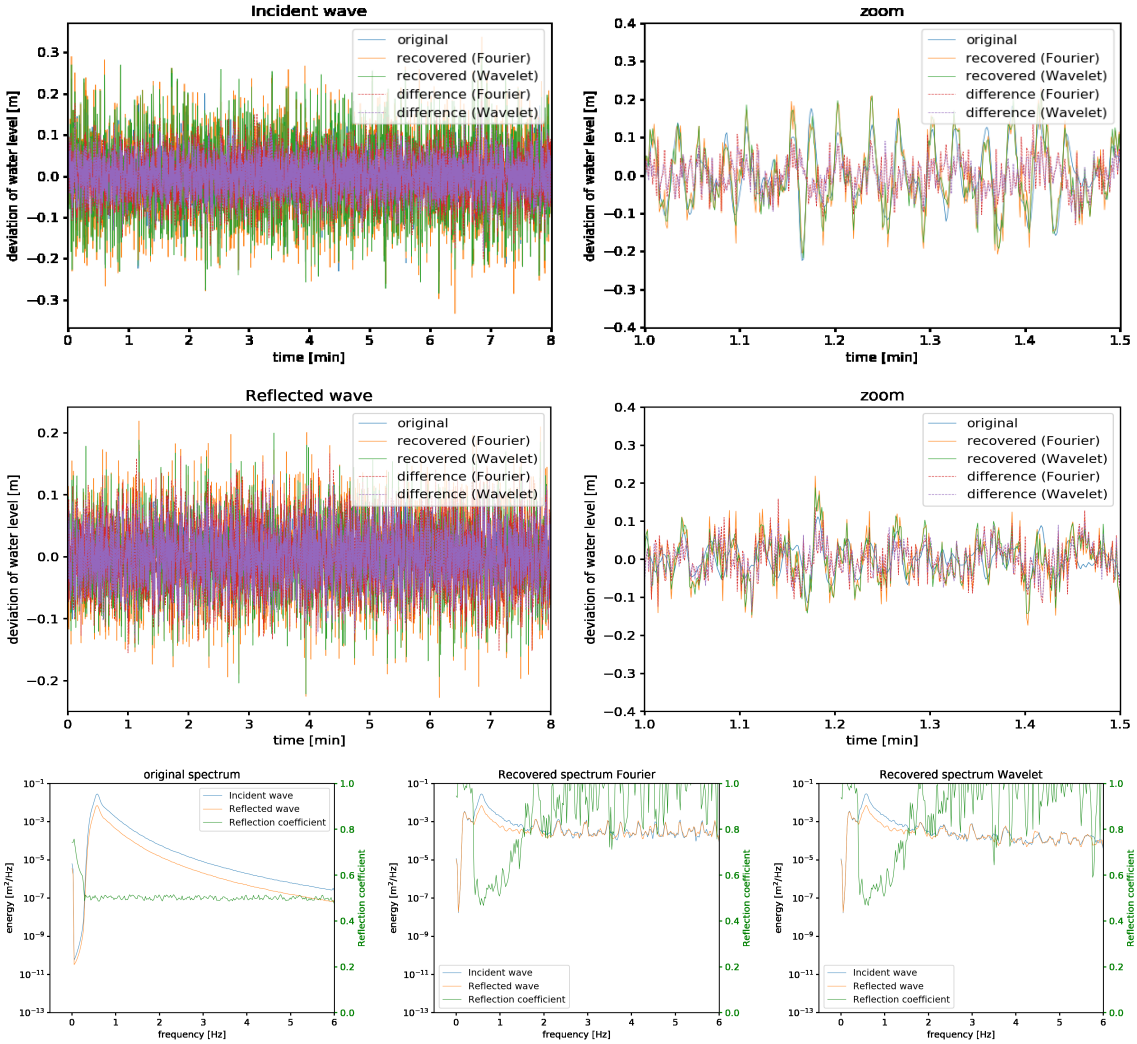

Figure D.19: Separating waves using 3 gauges, noise added to the signal of 10 times the incident wave power. Solved using a determinant limiter of 0.1.

Signal	200 waves from JONSWAP spectrum with f in [0.01,fs/2]		
Wavelet	Morlet	Parameter	60.0
Sampling freq	12	Duration	480.0 sec = 8.0 min
Determined at gauge	35.742		
Using gauges	[35.742 38.726 39.382 39.83 40.1]		
Wavenumber	disperion	with water depth	1
Noise	var/0.1	Weights	no
No of steps CWT	200		
Determinant limit	0.1		
p_min	1.666956E-01	p_max	1.777215E+01

RMSE	Fourier	Wavelet
reconstruction	2.147517E-16	8.35714E-03
sum	4.258662E-02	3.904357E-02
incident	3.093711E-02	2.371355E-02
reflected	3.099383E-02	2.300432E-02

	Original	Fourier	% diff	Wavelet	% diff
Ref.cff.	5.016262E-01	6.05833E-01	20.77	5.699105E-01	13.61
m0_in	5.564055E-03	6.380366E-03	14.67	5.700034E-03	2.44
m0_ref	1.400077E-03	2.341809E-03	67.26	1.851359E-03	32.23

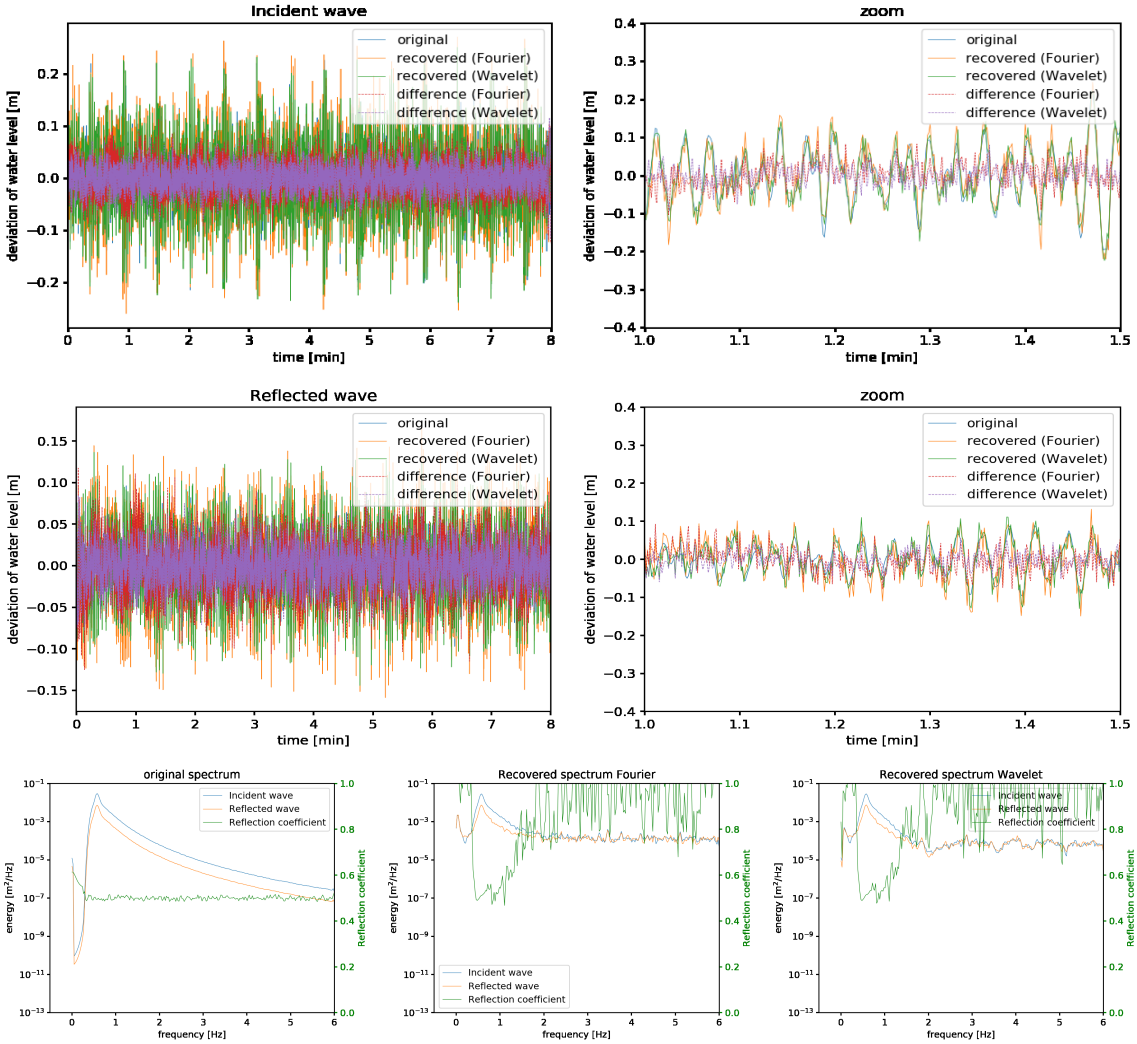

Figure D.20: Separating waves using 5 gauges, noise added to the signal of 10 times the incident wave power. Solved using a determinant limiter of 0.1.

E

Filter results

E.1. Denoising

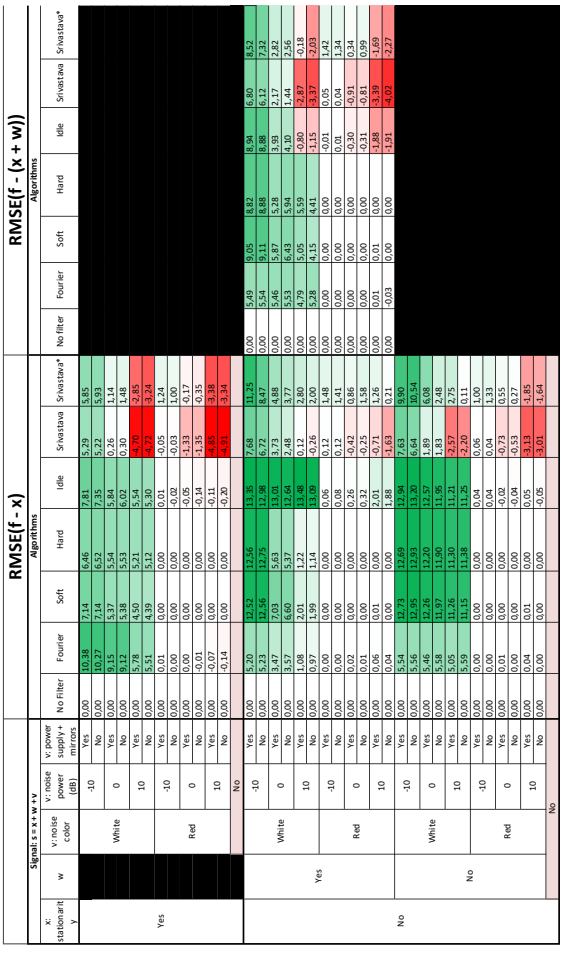

Figure E.1: The increase of SNR for the different filter methods. 'Idle' is the algorithm based on a signal free period, Srivastava* is the Srivastava algorithm with the adjusted peak-to-sum ratio.

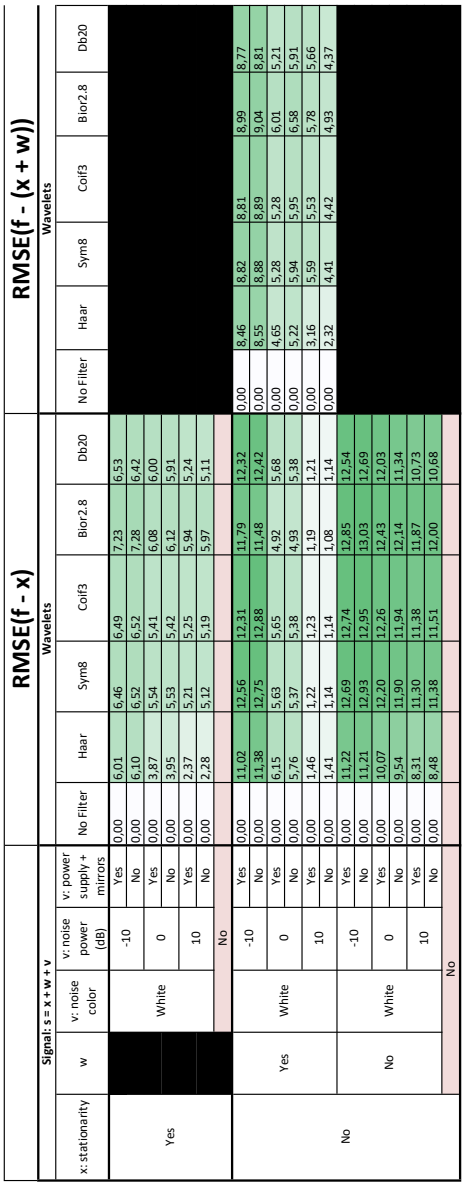

Signal: s = x + w + v				RMSE(f - x)							RMSE(f - (x + w))						
				Wavelets							Wavelets						
x: stationarity	w	v: noise color	v: noise power (dB)	v: power supply + mirrors	No Filter	Haar	Sym8	Coif3	Bior2.8	Db20	No Filter	Haar	Sym8	Coif3	Bior2.8	Db20
Yes		White	-10	Yes	0,00	6,01	6,46	6,49	7,23	6,53						
				No	0,00	6,10	6,52	6,52	7,28	6,42						
			0	Yes	0,00	3,87	5,54	5,41	6,08	6,00						
				No	0,00	3,95	5,53	5,42	6,12	5,91						
			10	Yes	0,00	2,37	5,21	5,25	5,94	5,24						
				No	0,00	2,28	5,12	5,19	5,97	5,11						
No			No								0,00	8,46	8,82	8,81	8,99	8,77
	Yes	White	-10	Yes	0,00	11,02	12,56	12,31	11,79	12,32	0,00	8,55	8,88	8,89	9,04	8,81
				No	0,00	11,38	12,75	12,88	11,48	12,42	0,00	4,65	5,94	5,28	6,01	5,21
			0	Yes	0,00	6,15	5,63	5,65	4,92	5,68	0,00	5,22	5,95	5,28	6,58	5,91
				No	0,00	5,76	5,37	5,38	4,93	5,38	0,00	3,16	5,53	5,53	5,78	5,66
			10	Yes	0,00	1,46	1,22	1,23	1,19	1,21	0,00	2,32	4,41	4,42	4,93	4,37
				No	0,00	1,41	1,14	1,14	1,08	1,14	0,00					
	No	White	-10	Yes	0,00	11,22	12,69	12,74	12,85	12,54						
				No	0,00	11,21	12,93	12,95	13,03	12,69						
			0	Yes	0,00	10,07	12,20	12,26	12,43	12,03						
				No	0,00	9,54	11,90	11,94	12,14	11,34						
			10	Yes	0,00	8,31	11,30	11,38	11,87	10,73						
				No	0,00	8,48	11,38	11,51	12,00	10,68						
			No													

Figure E.2: The increase of SNR for for the different wavelets in hard thresholding for the white noise cases

E.2. Examples of Other Filters

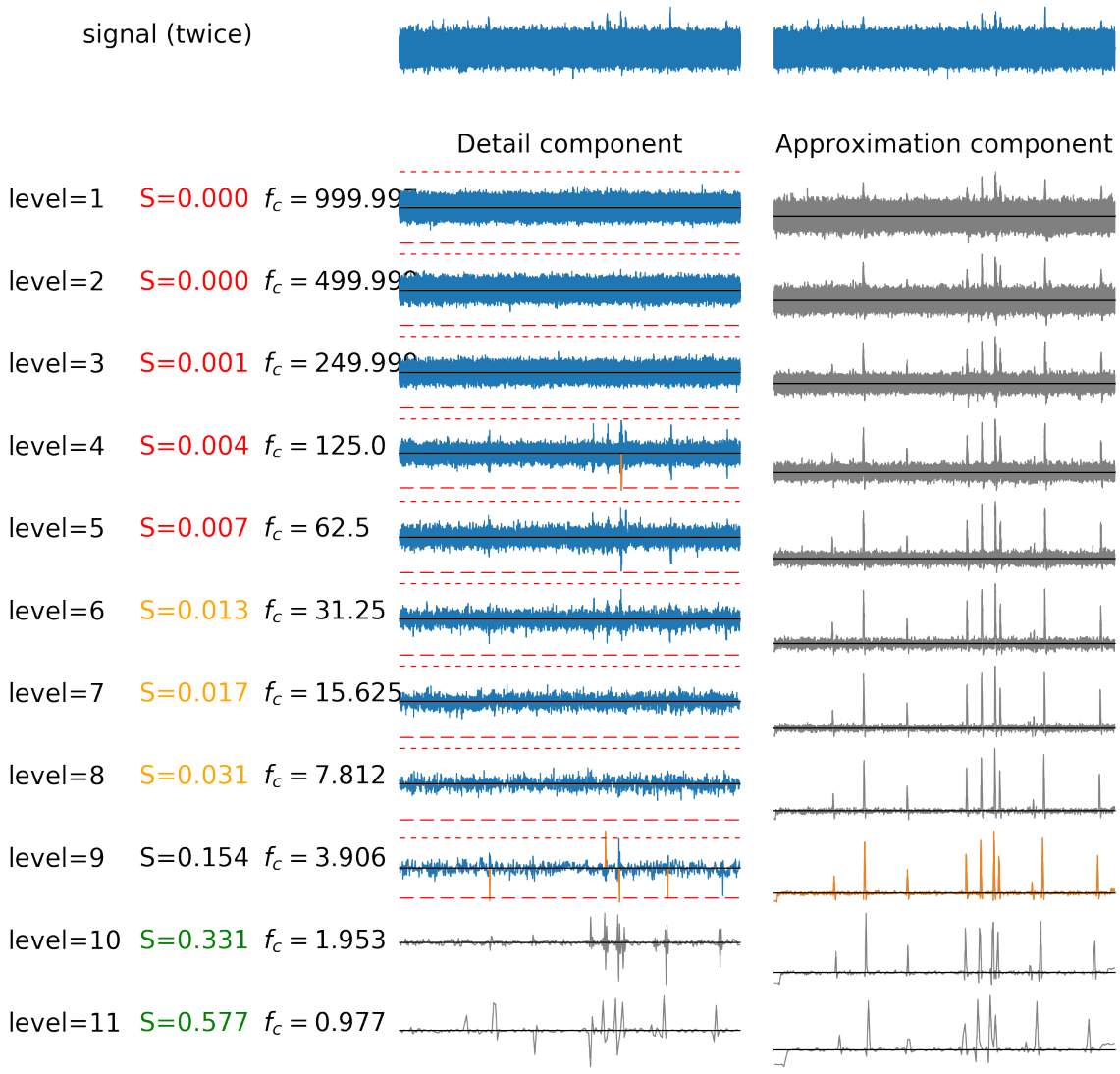

Figure E.3: The approximation and detail coefficients and their thresholds, based on the hard thresholding methods. The colours correspond with the colours in Figure 3e) of the original file. The *S* denotes the peak-to-sum ratio (or sparsity) of the detail coefficients at that level.

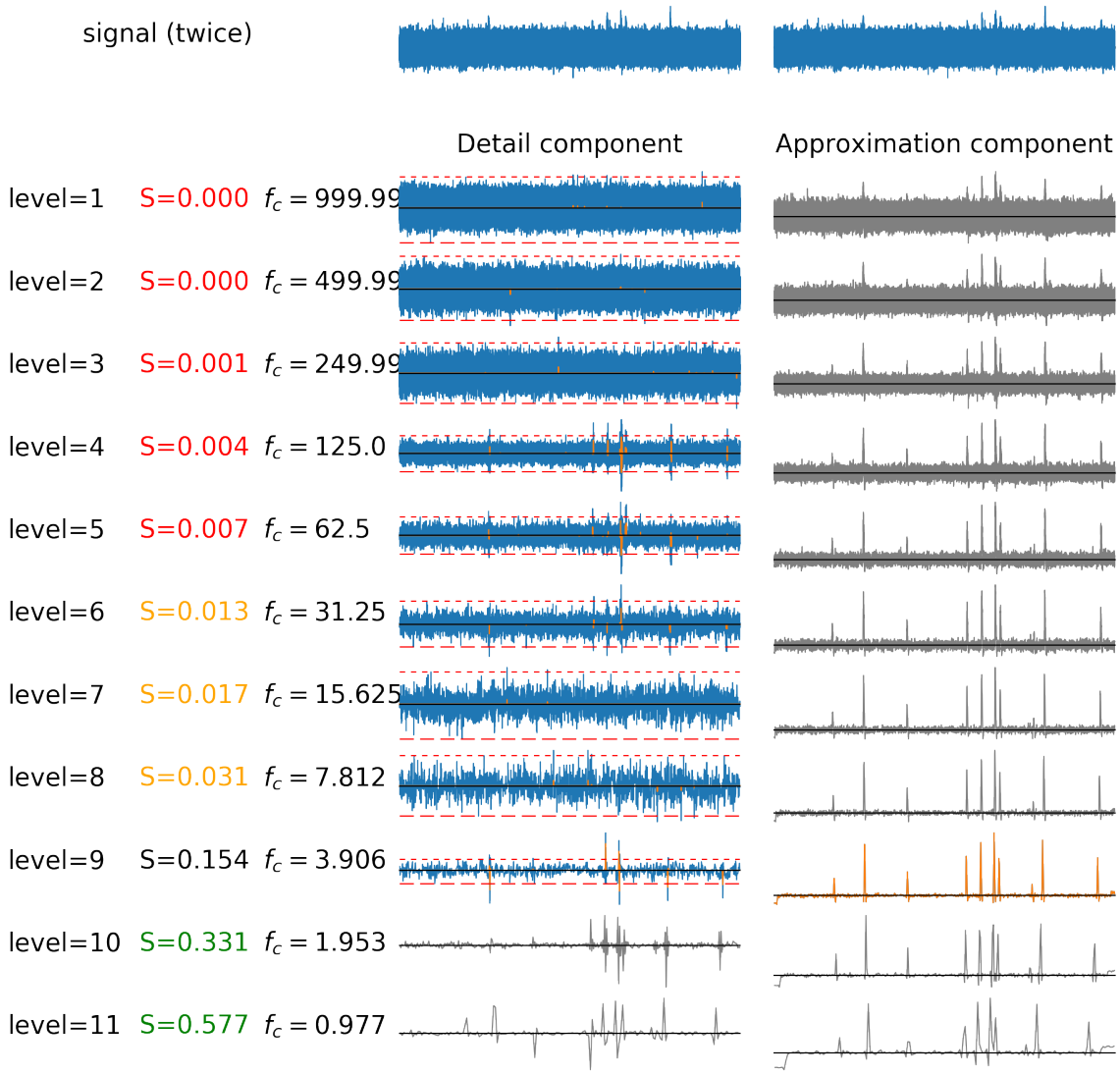

Figure E.4: The approximation and detail coefficients and their thresholds, based on the first 30 seconds being signal free. The colours correspond with the colours in Figure 3e) of the original file. The *S* denotes the peak-to-sum ratio (or sparsity) of the detail coefficients at that level.

E.3. Comparison of Wavelets in Filtering

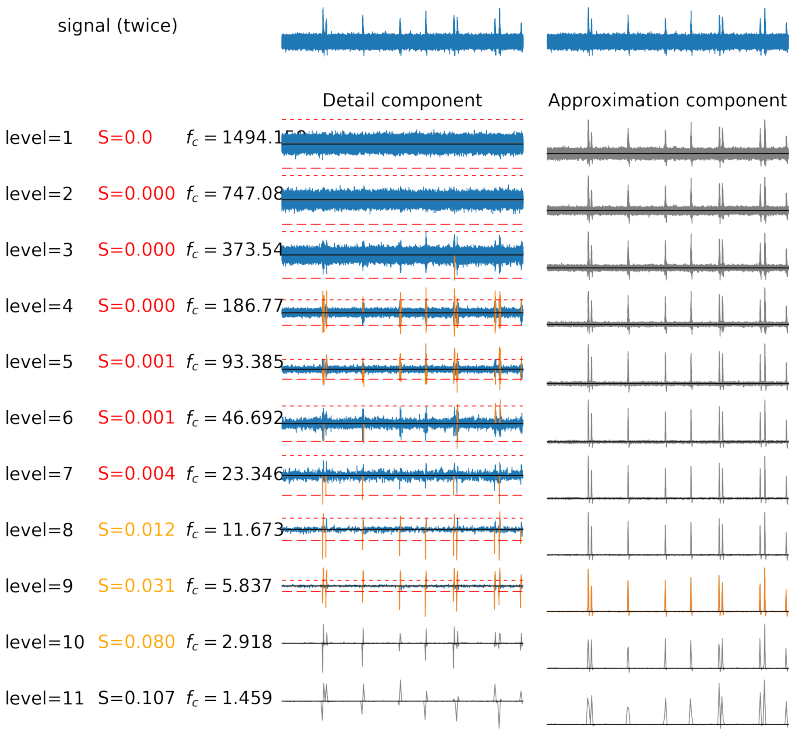

Figure E.5: The hard filtering algorithm applied with the Haar wavelet for the non-stationary signal with w and a SNR of 0 dB.

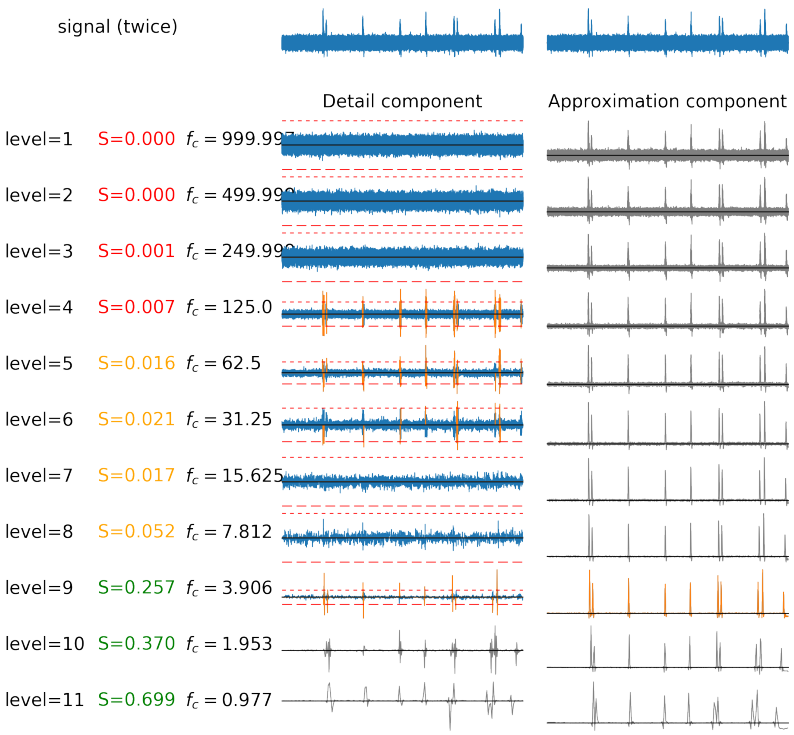

Figure E.6: The hard filtering algorithm applied with the Symlet 8 wavelet for the non-stationary signal with w and a SNR of 0 dB.

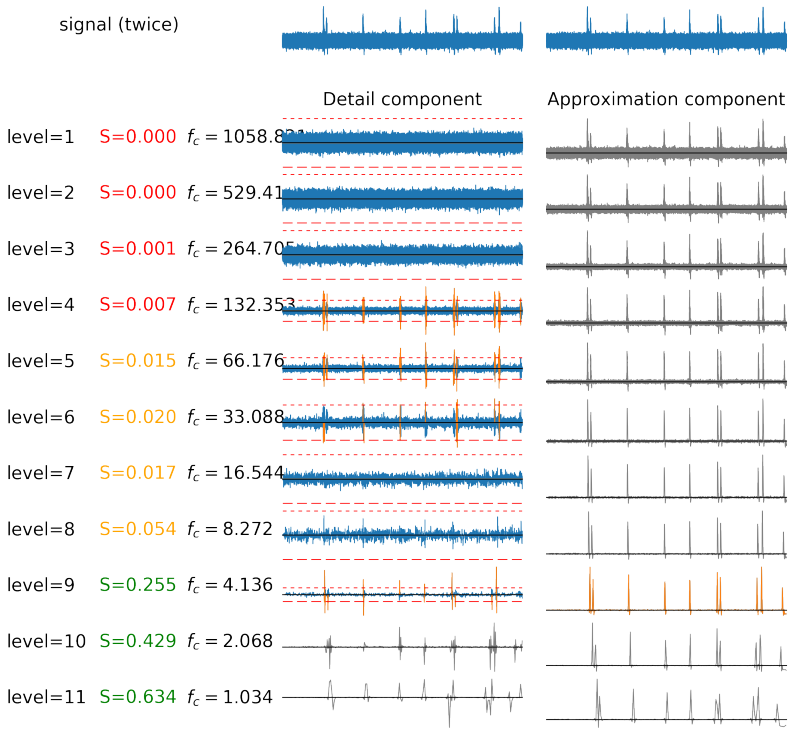

Figure E.7: The hard filtering algorithm applied with the Coiflet 3 wavelet for the non-stationary signal with w and a SNR of 0 dB.

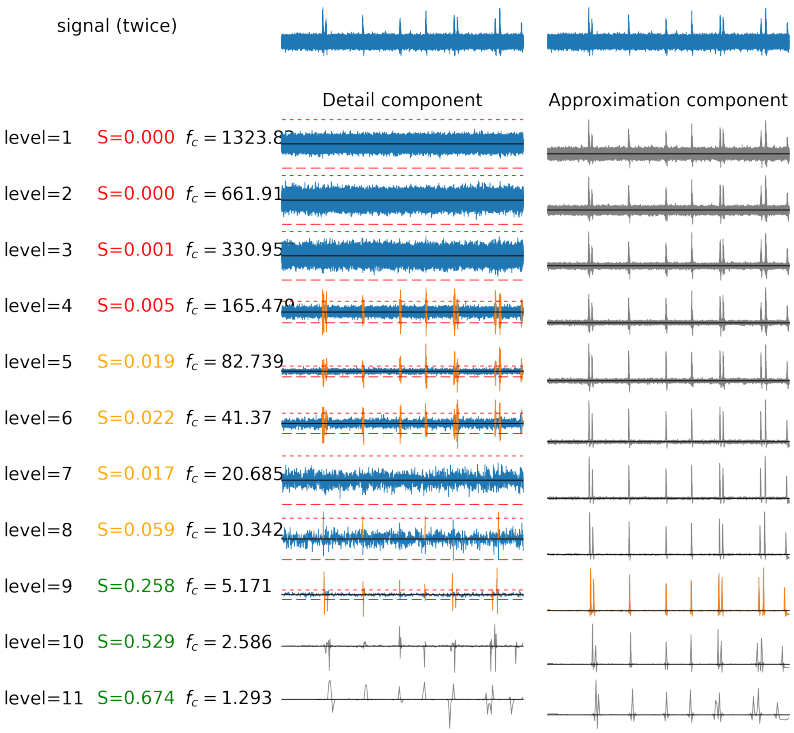

Figure E.8: The hard filtering algorithm applied with the Biorthogonal 2.8 wavelet for the non-stationary signal with w and a SNR of 0 dB.

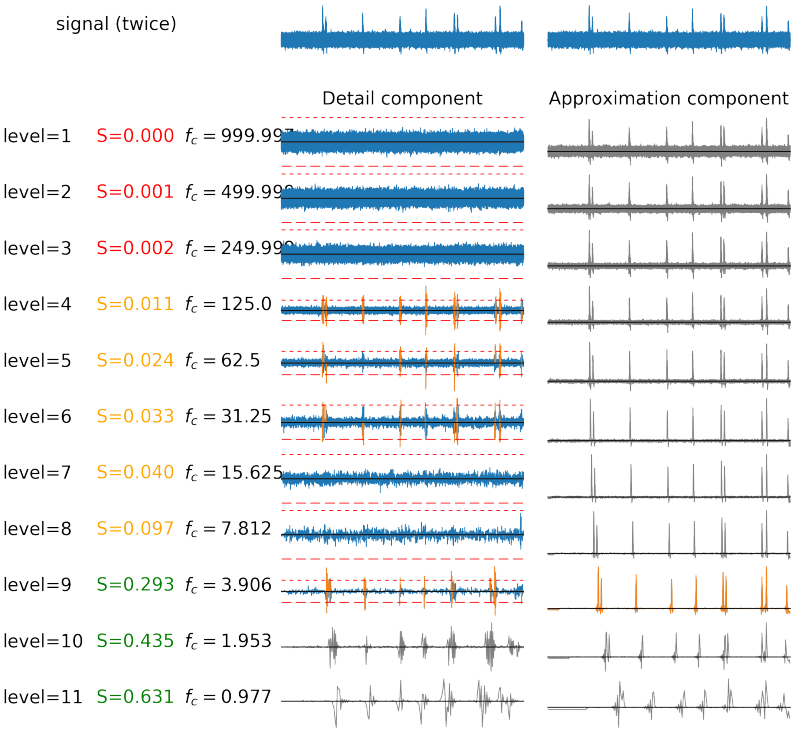

Figure E.9: The hard filtering algorithm applied with the Daubechies 20 wavelet for the non-stationary signal with w and a SNR of 0 dB.

E.4. Periodic Signal Extension

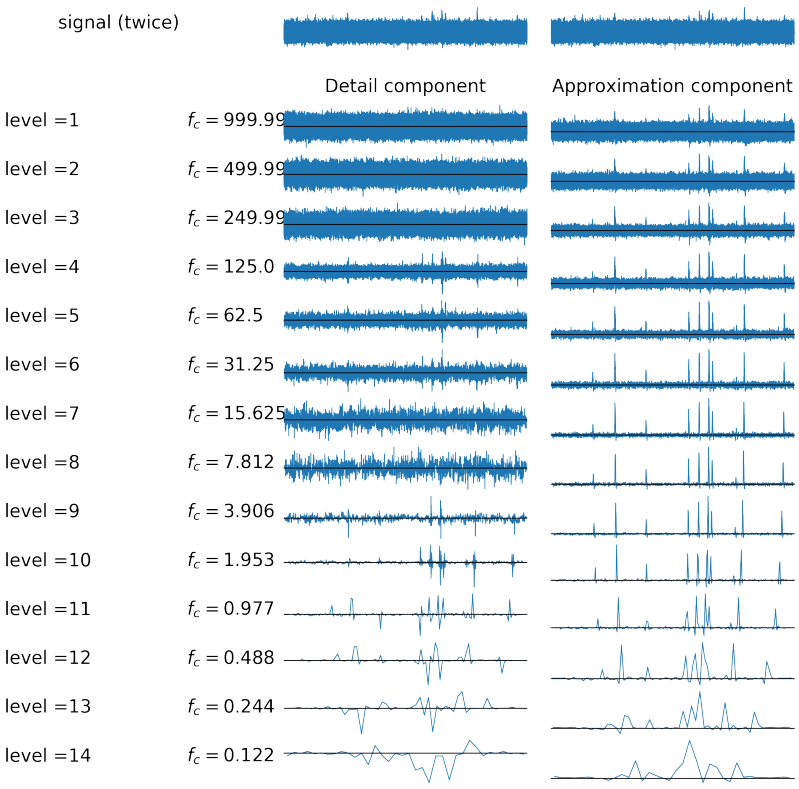

Figure E.10: Figure 5 from original, now using periodic signal extension instead of symmetric signal extension.

E.5. Signals

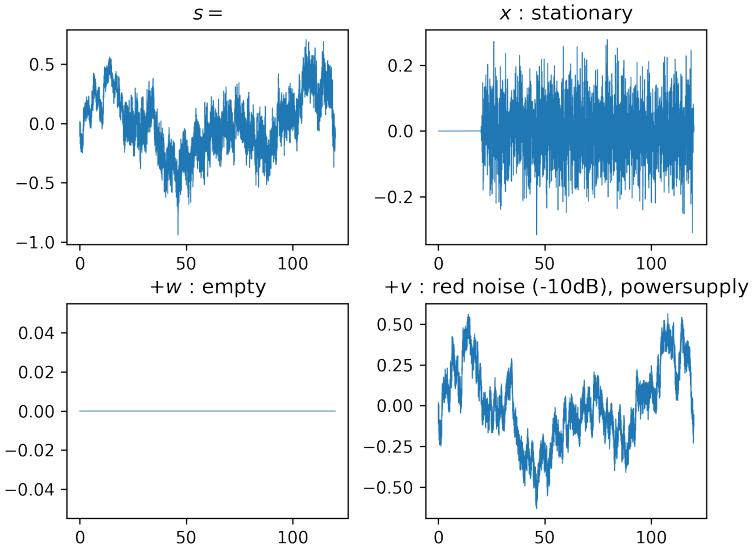

Figure E.11: non-stationary signal, with red noise.

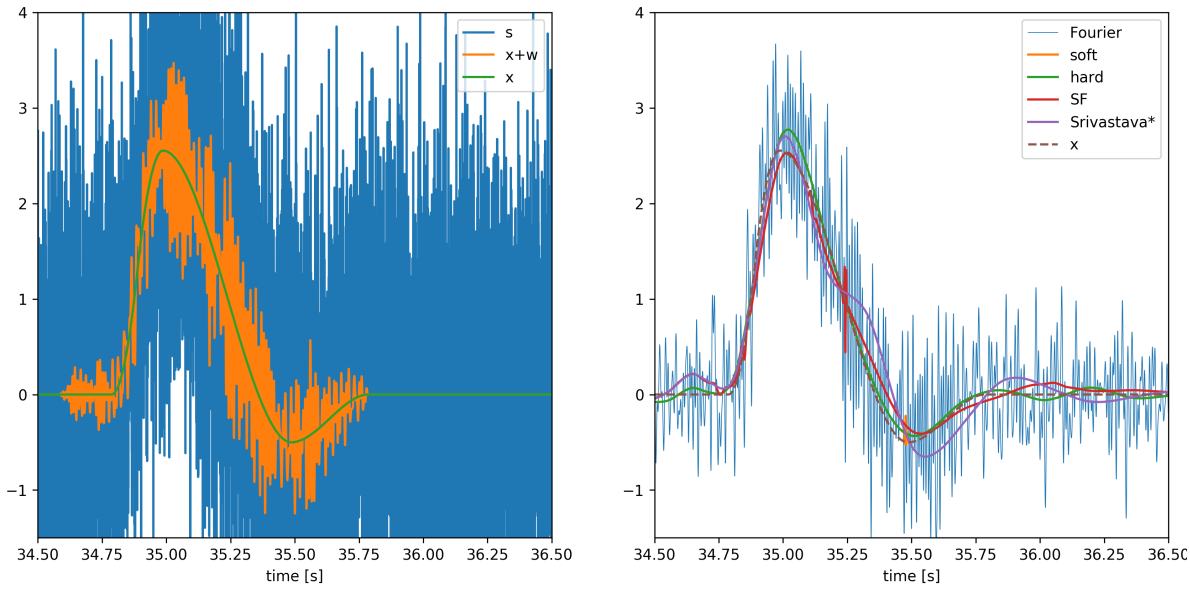

Figure E.12: A peak in the non-stationary noise case, with SNR=-10 dB, measurement noise and power supply noise. On the left the original signals, on the right the filtered results.

F

Added Value Wavelet Analysis

This appendix supports the result in Appendix 5. The signals used to compare the different techniques are presented in the first section of this chapter. In the second section some supporting figures are shown.

F.1. Signals

F.1.1. Westerschelde

This set of measurements comes from the Westerschelde, a river in the Netherlands. This are the values over the year 2016, from the gauge at Walsoorden. This data is made available via *https://waterberichtgeving.rws.nl/water-en-weer/dataleveringen*. A plot of the data is presented in Figure 5.1. The water level is sampled with a sampling interval of 15 minutes.

F.1.2. WL657585e

This measurement is conducted in the Scheldt flume at the Deltares facilities. The mean water level of this 144 minutes experiment is raised by 20 cm and lowered again, to mimic tidal behaviour. The three water level measurement points are set up at distances of 35.92, 36.47 and 36.69 meter from the wave maker, sampling with a frequency of 25 Hz. The wave conditions imposed by the wave maker are based on a JONSWAP spectrum, with a peak at about 0.5 Hz. The signal and the mean water level are shown in Figure F.1.

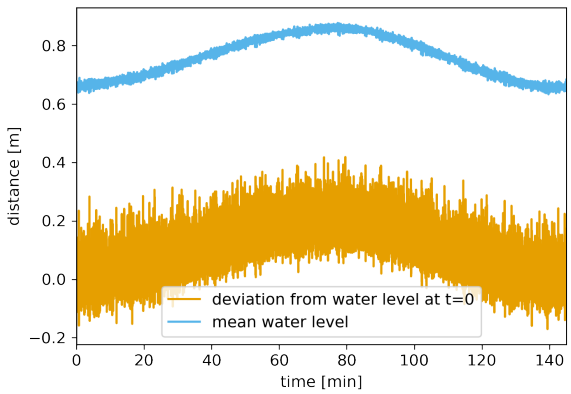

Figure F.1: Water level measurement from data set WL657585e

F.1.3. A3W1T304

This measurement is conducted in the Scheldt flume as well. The deviation of the mean water level (70 cm) is measured at a number of gauges in the flume, set up at distances as presented in Table 3.2, forces and pressures at the structure of the end of the channel are measured as well. The sampling frequency is 3 kHz. Both time and frequency content of a force and a pressure signal are depicted in Figure F.2.

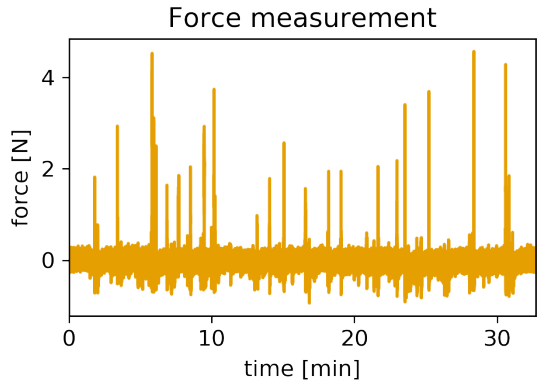

(a) Force measurement

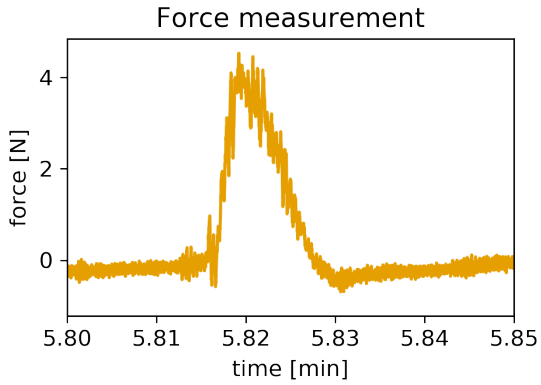

(b) Zoom of force measurement

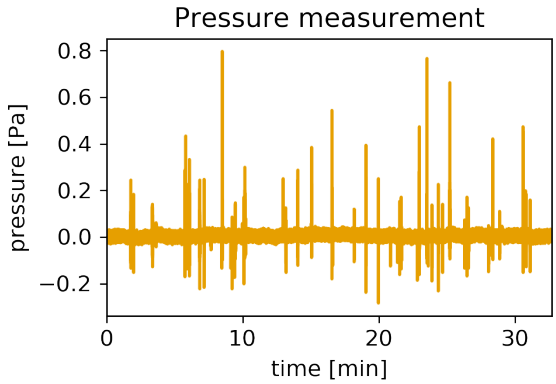

(c) Pressure measurement

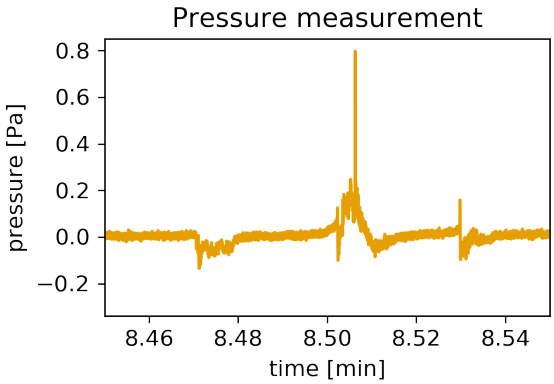

(d) Zoom of pressure measurement

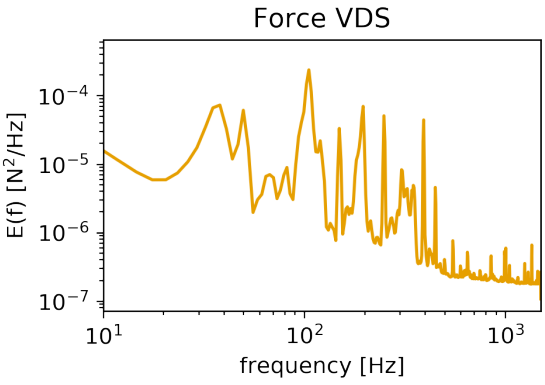

(e) Variance density spectrum force measurement

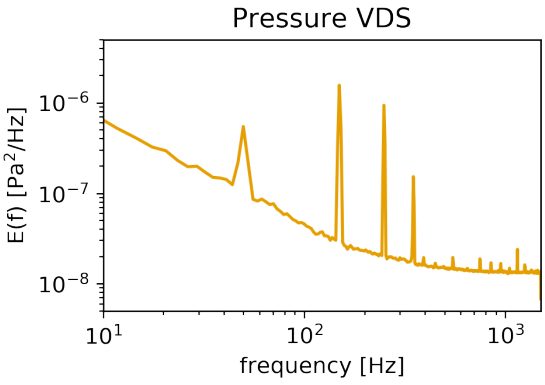

(f) Variance density spectrum pressure measurement

Figure F.2: Signals from data set A3W1T304

F.2. Figures

F.2.1. Separating Waves

Signal	WL657585e		
Wavelet	Morlet	Parameter	60
Sampling freq	20.0	Duration	8699.95 sec = 144.999166(
Determined at gauge	35.92		
Using gauges	[35.92 36.47 36.69]		
Wavenumber	dispersion	with water depth	[0.6602 0.6618 0.6616 ...,
No of steps CWT	150		
Determinant limit	0.1		
p_min	1E-01	p_max	3.220643E+02

	Fourier	Wavelet
RMSE reconstruction	2.676379E-16	1.200836E-01
sum	1.201751E-01	1.292706E-02

	Fourier	Wavelet
Ref.cff.	2.553696E-01	2.562337E-01
m0_in.	2.883003E-03	3.009569E-03
m0_ref	1.880111E-04	1.975953E-04

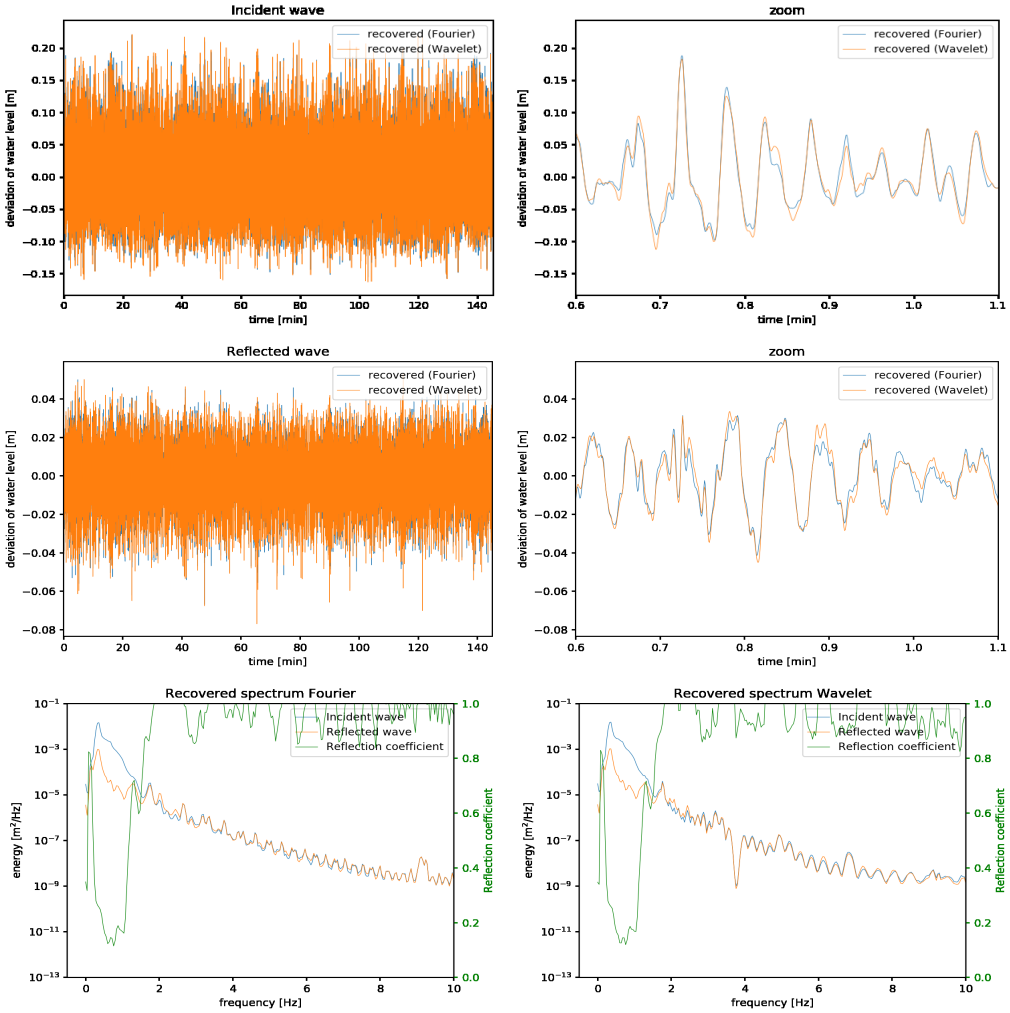

Figure F.3: Separating waves for non-stationary signal from coastal engineering, determinant limiter 0.1 (Morlet 60 wavelet)

Signal	WL657585e_250steps		
Wavelet	Morlet	Parameter	60
Sampling freq	20.0	Duration	8699.95 sec = 144.999166
Determined at gauge	35.92		
Using gauges	[35.92 36.47 36.69]		
Wavenumber	dispersion	with water depth	[0.6602 0.6618 0.6616 ...,
No of steps CWT	300		
Determinant limit	0		
p_min	1E-01	p_max	3.220643E+02

RMSE	Fourier	Wavelet
reconstruction	2.676379E-16	1.19493E-01
sum	5.083595E-03	5.025583E-03

	Fourier	Wavelet
Ref.cff.	9.991147E-01	4.26688E-01
m0_in.	2.789107E+01	3.348221E-03
m0_ref	2.784171E+01	6.09586E-04

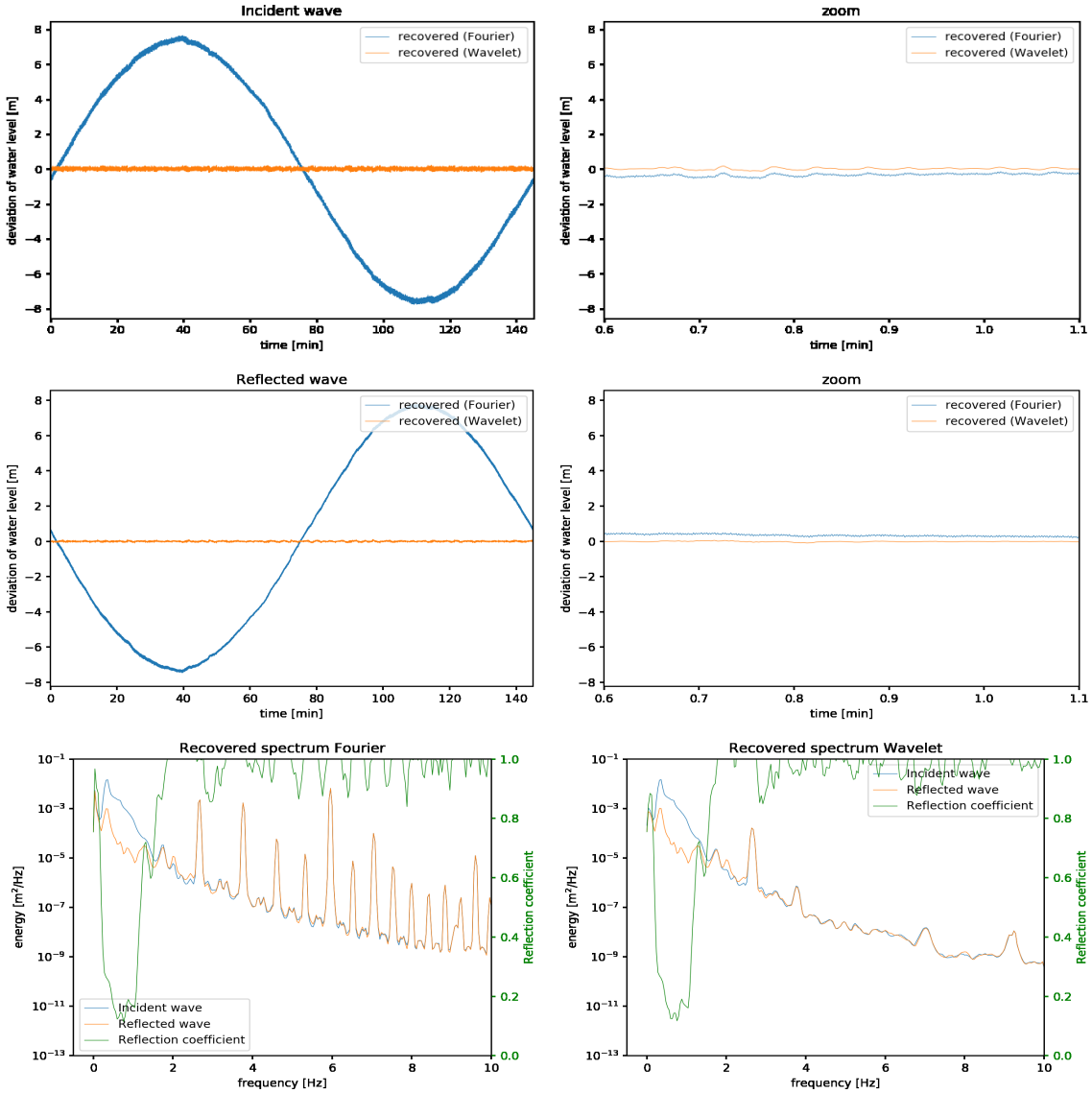

Figure F.4: Separating waves for non-stationary signal from coastal engineering, without determinant limiter. (Morlet 60 wavelet)

Signal	WL657585e_250steps		
Wavelet	Morlet	Parameter	60
Sampling freq	20.0	Duration	8699.95 sec = 144.999166
Determined at gauge	35.92		
Using gauges	[35.92 36.47 36.69]		
Wavenumber	dispersion	with water depth	[0.6602 0.6618 0.6616 ...,
No of steps CWT	300		
Determinant limit	0		
p_min	1E-01	p_max	1E+01

RMSE	Fourier	Wavelet
reconstruction	2.676379E-16	1.200272E-01
sum	1.201393E-01	5.084425E-03

	Fourier	Wavelet
Ref.cff.	4.962071E-01	2.627414E-01
m0_in.	3.579397E-03	2.973176E-03
m0_ref	8.813242E-04	2.052475E-04

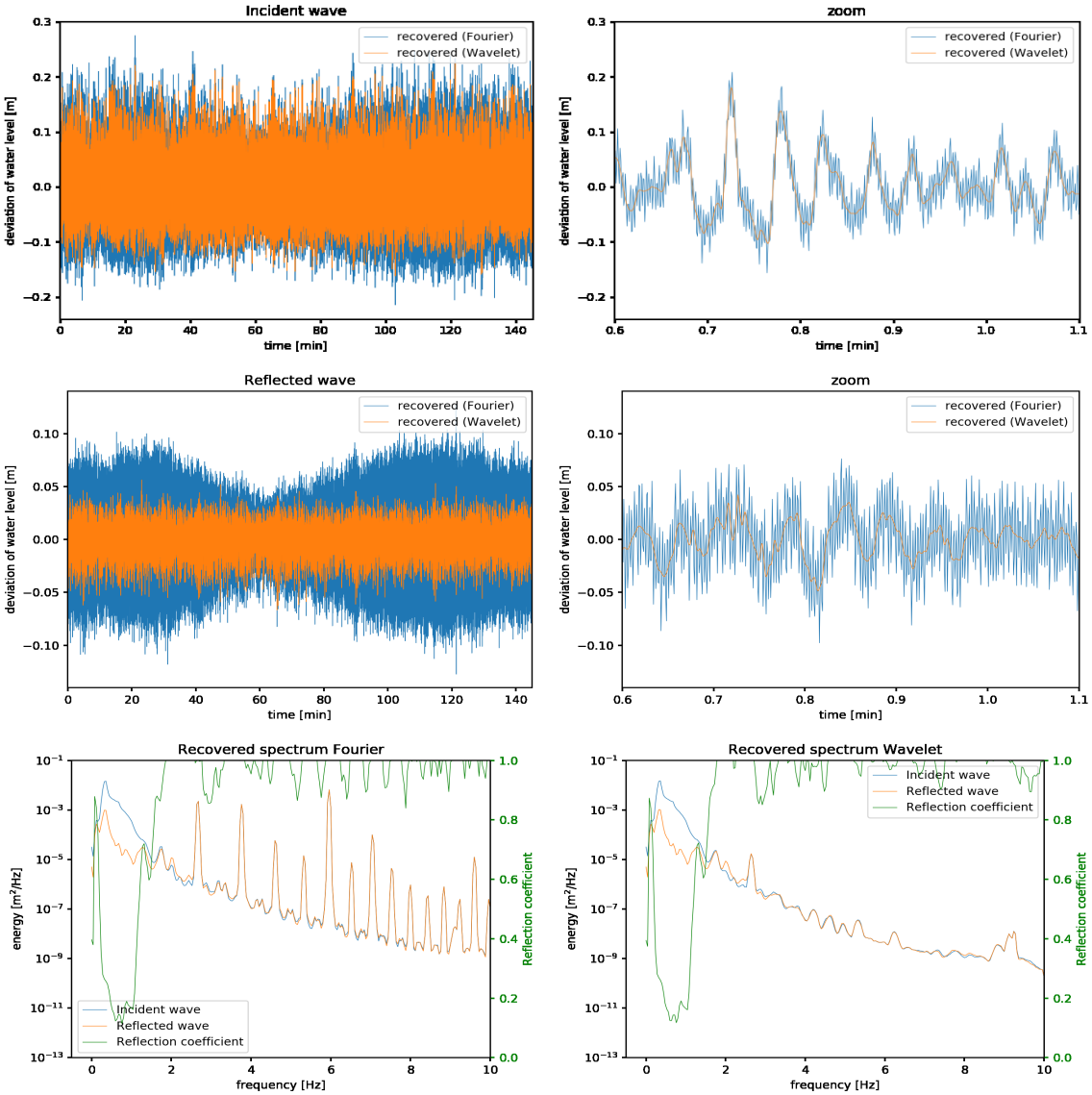

Figure F.5: Separating waves for non-stationary signal from coastal engineering, without determinant limiter. Maximum period of 10 seconds imposed. (Morlet 60 wavelet)

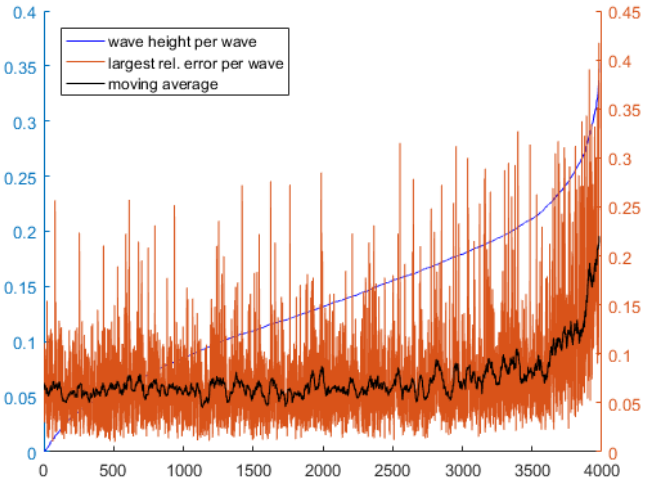

Figure F.6: The almost 4000 waves and the corresponding residuals sorted on wave height

F.2.2. Filters

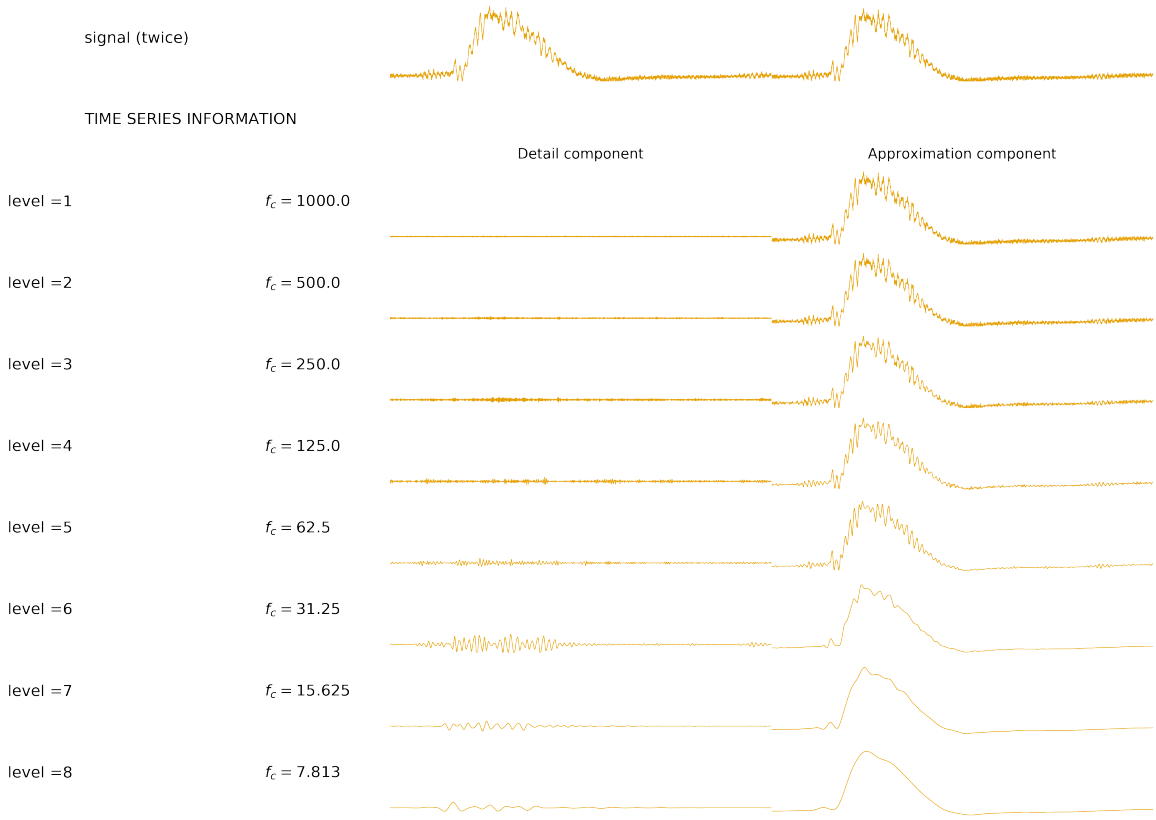

Figure F.7: The approximation and detail levels transformed to signals for force measurement. Note that the resonance frequency on the peak is mostly contained in detail level 6 and 7. (Discrete Wavelet Decomposition using the Symmlets 8 wavelet, upto level 8)

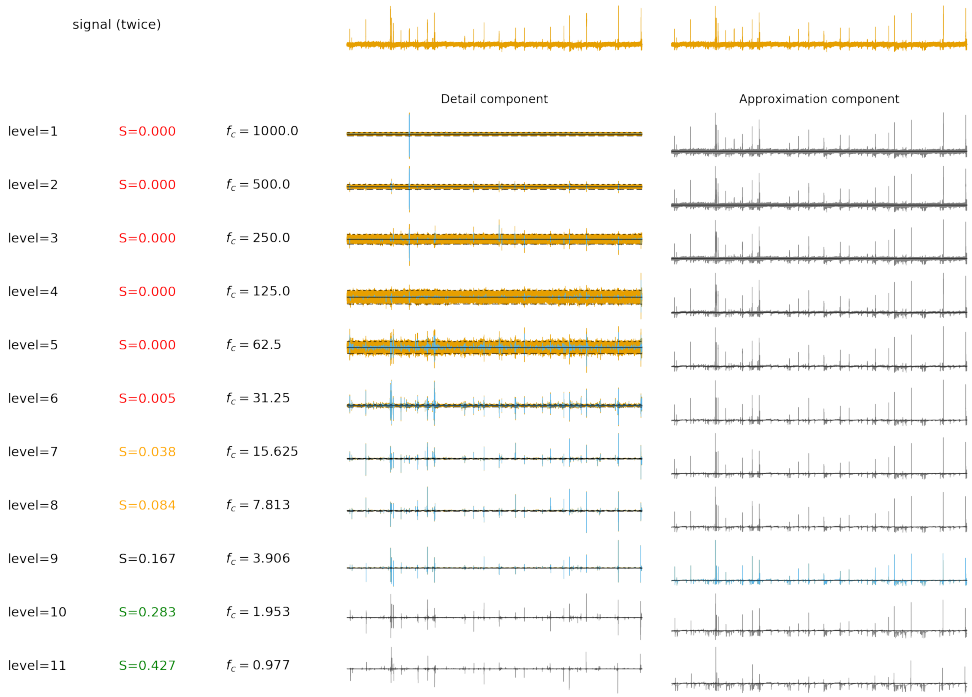

Figure F.8: Discrete wavelet filter based on noise in first 10 seconds of signal. (Discrete Wavelet Decomposition using the Symmlets 8 wavelet, upto level 11)

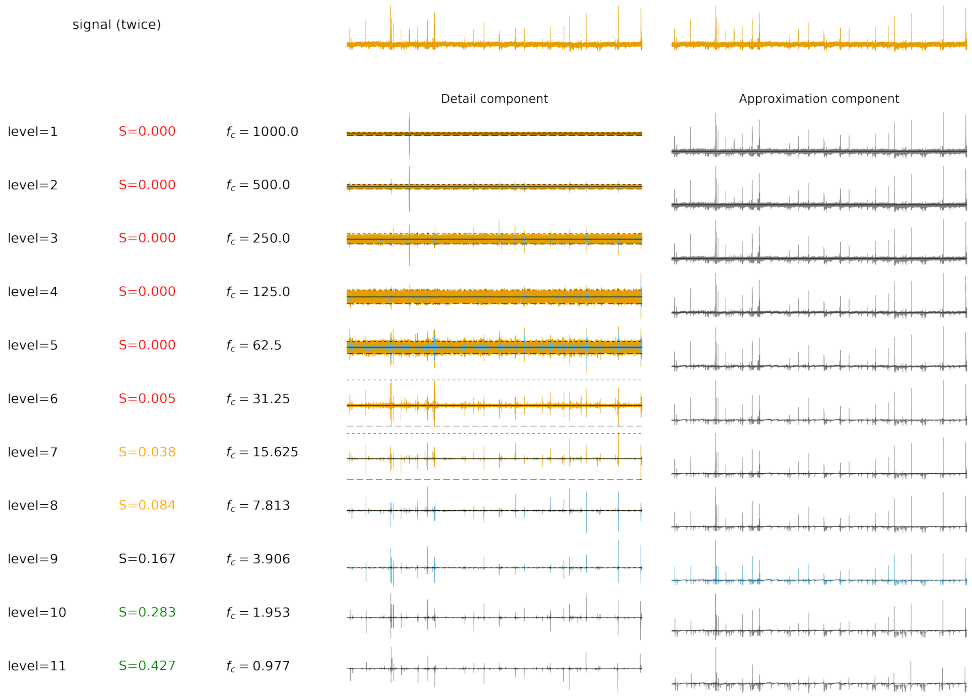

Figure F.9: Discrete wavelet filter based on noise in first 10 seconds of signal. Detail level 6 and 7 are filtered out (see Figure F.7). (Discrete Wavelet Decomposition using the Symmlets 8 wavelet, upto level 11)

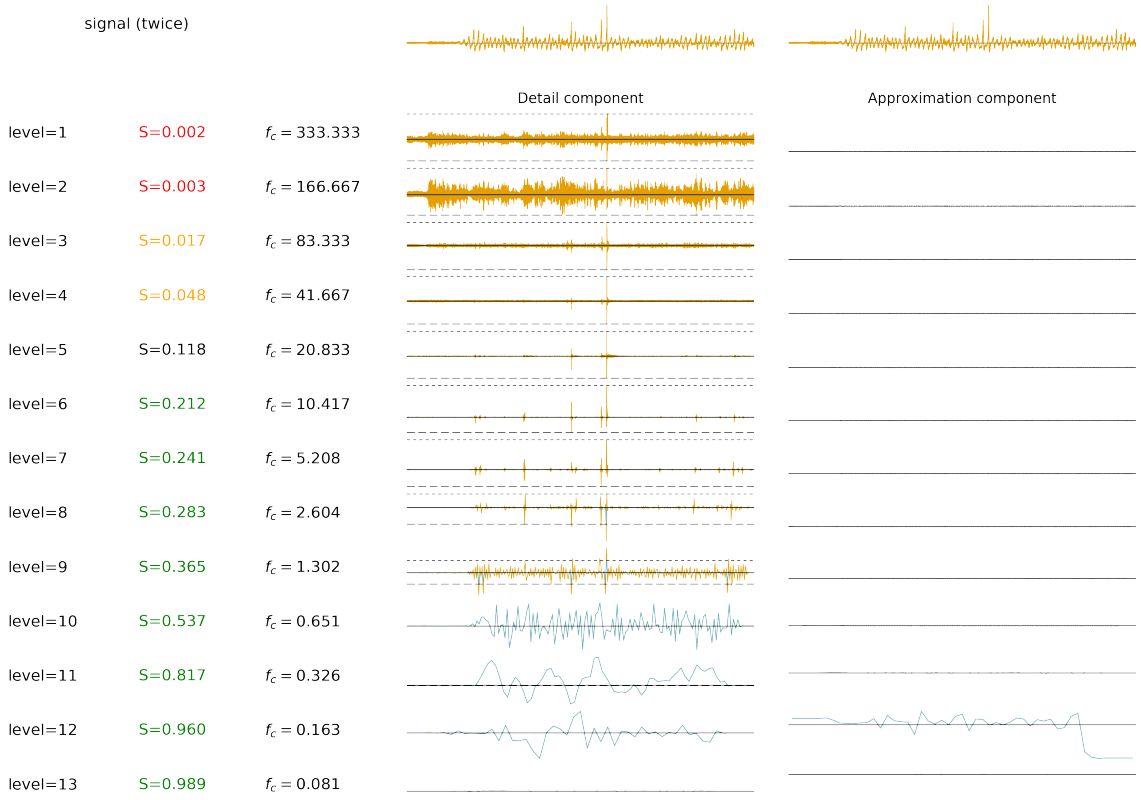

Figure F.10: Discrete wavelet filter to filter transient for signal presented in Figure 5.7a. (Discrete Wavelet Decomposition using the Symmlets 8 wavelet, upto level 9)

G

Fourier Transforms

G.1. Continuous Fourier Transforms

Property	**Time signal** $f(t)$	**Fourier transform** $\mathcal{F}\{f\}(\omega) = F(\omega)$	
Linearity	$c_1 f_1(t) + c_2 f_2(t)$	$c_1 F_1(\omega) + c_2 F_2(\omega)$	(G.1)
Translation	$f(t-h)$	$e^{-i\omega h} F(\omega)$	(G.2)
Modulation	$e^{i\xi t} f(t)$	$F(\omega - \xi)$	(G.3)
Scaling	$f\left(\frac{t}{a}\right)$	$\lvert a \rvert F(a\omega)$	(G.4)
Convolution	$f_1 * f_2(t)$	$F_1(\omega) F_2(\omega)$	(G.5)
Multiplication	$f_1 f_2(t)$	$\frac{1}{2\pi} F_1 * F_2(\omega)$	(G.6)
Inversion	$F(t)$	$f(-\omega)$	(G.7)
Time differentiation	$\frac{\mathrm{d}f(t)}{\mathrm{d}t}$	$i\omega F(\omega)$	(G.8)

G.1.1. Functions

Time signal $f(t)$	**Fourier transform** $\mathcal{F}\{f\}(\omega)$	
$\delta(t-\tau)$	$e^{-i\tau\omega}$	(G.9)
$H(t)$	$\frac{1}{2}\left(\delta(\omega) - \frac{i}{\pi\omega}\right)$	(G.10)

MSc Thesis Assignment

MSc-thesis assignment

Wavelets

Figure 1 Example of obtaining ware field information near trunk of a breakwater

The FBI uses wavelet techniques for image compression of digital fingerprints to save storage space. In geophysics wavelets are being used to analyse seismic signals for detecting e.g. earthquakes and oil layers. In finance the wavelet is used to analyse stock markets due to their dynamic and non-linear nature. These are just a few examples to highlight the applicability of the wavelet techniques.

The same techniques are potentially very interesting for Deltares as coastal engineers have to deal with complex time dependent physical processes as for example illustrated in the figures included.

Figure 2 Example of measuring wave field

To improve the understanding of these physical processes associated with waves, wave structure interaction, stability of structures or the influence on morphology various measurements techniques like time sampling, lasers scanning, photography are employed to capture instant information on wave conditions, forces, currents, erosion and accretion for further detailed analysis.

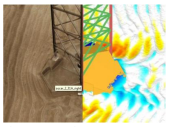

Figure 3 Example Stereophotography

This assignment is related to the part of detailed analysis of time series containing the time evolution of wave heights, forces, etc. Currently, the analysis is performed through Fourier analysis combined with filtering techniques to remove e.g. noise. However, the Fourier analysis has its limitations.

The purpose of this assignment is to look into the added value of applying existing wavelets and the related techniques compared to Fourier type of analysis.

The question is: can we improve our analysis by employing wavelet instead of Fourier technique? To answer this question, the following tasks have been defined for this assignment.

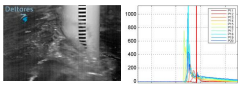

Figure 4 Example wave impact on a pile and measured pressure

Tasks

1. Provide a summary/overview on how wavelets are being used in other fields of expertise, including background information on the mathematical aspects of wavelets.
2. Verify the added value of wavelets by comparing results obtained through wavelet techniques with Fourier analysis by using different type of measured of time series (e.g. pressure due to wave impact, wave height, etc.) which representative for Deltares. Important aspects related to this task are:
    a. Use wavelets to detect and filter different components (e.g. noise) from the signal by using for example thresholding methods.
    b. Use wavelets to detect, if possible, the influence of wave basin characteristics on measured signals.
    c. Use wavelets to detect non-stationary properties in a signal, which is not possible by using standard Fourier analysis.
3. Research the sensitivity of wavelet specific parameters, e.g. type of wavelet, on the output of a wavelet analysis, including using statistical techniques to be able to interpret results.
4. Make wavelet analysis accessible in projects through scripts on top of an existing wavelet toolbox (yet to be selected). One important aspect for this task is the presentation of results.

Requirements

- Programming skills in either Matlab and/or Python.

This assignment is your chance to start a new era in coastal engineering with respect to time series analysis and also create added value to your own skills as wavelets are used in various fields of expertise. The only difference is jargon as the mathematics stays the same! If you are interested, please contact me.

Indication start date: After August 2016

Company: Deltares

Name : Jan Kramer

Email address: jan.kramer@deltares.nl

Figure H.1: The MSc thesis proposal as subjected by Deltares via *http://ta.twi.tudelft.nl/nw/users/vuik/numanal/rooij.html*.